Supporting Information

Dual Role of Doubly Reduced Arylboranes as Dihydrogen- and Hydride-Transfer Catalysts

Esther von Grotthuss, Sven E. Prey, Michael Bolte, Hans-Wolfram Lerner, and Matthias Wagner*

Table of contents:

1. Experimental details and characterization data

General considerations. All reactions, manipulations, and analyses were carried out in an argon-filled glovebox or by applying standard Schlenk techniques under a nitrogen atmosphere. Toluene, Et_2O, and THF were dried over Na/benzophenone; THF-d_8 was dried over Na-K alloy without benzophenone. Prior to use, the solvents were distilled from the drying agent; THF and THF-d_8 were degassed by applying three freeze-pump-thaw cycles.

NMR spectra were recorded at 298 K using the following spectrometers: Bruker DPX-250, Avance-300, Avance-400, or Avance-500.

Chemical shifts are referenced to (residual) solvent signals ($^1H/^{13}C\{^1H\}$; THF-d_8: δ = 3.58/67.21 ppm[1]) or external $BF_3{\cdot}Et_2O$ (^{11}B; $^{11}B\{^1H\}$). Abbreviations: s = singlet, d = doublet, t = triplet, q = quartet, sept = septet, m = multiplet, br = broad, n.o. = not observed, n.r. = not resolved.

Numbering schemes for symmetrically substituted (left) and unsymmetrically substituted (right) DBA cores are as follows:

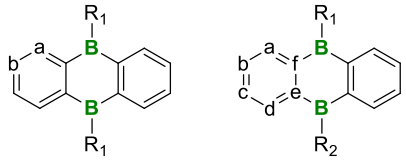

The compounds 9,10-dibromo-DBA,[2] **1**,[3] **2**,[4] **3**,[3] **4**,[6,7] **9**,[5] Li_2[**1**],[4,8] Li_2[**2**],[4] K_2[**1**],[4] Li_2[**4**],[7] Na_2[**4**],[7] Li_2[**1**-H_2],[4] Li_2[**2**-H_2],[4] and K_2[**1**-H_2][4] were synthesized according to literature procedures.

Cyclic voltammetry (CV) measurements were performed in a glovebox at room temperature in a one-chamber, three-electrode cell using an EG&G Princeton Applied Research 263A potentiostat. A platinum disk electrode (2.00 mm diameter) was used as the working electrode with a platinum wire counter electrode and a silver wire reference electrode, which was coated with AgCl by immersion into HCl/HNO_3 (3:1). Prior to measurements, the solvent THF was dried with Na-K alloy. [*n*Bu_4N][PF_6] was employed as the supporting electrolyte (0.1 mol L^{-1}). All potential values were referenced against the FcH/FcH^+ redox couple (FcH = ferrocene; $E_{1/2}$ = 0 V). Scan rates were varied between 100 and 400 mV s^{-1}.

High-resolution mass spectra were measured in positive mode using a Thermo Fisher Scientific MALDI LTQ Orbitrap XL and α-cyano-4-hydroxycinnamic acid or 4-chloro-α-cyanocinnamic acid as the matrix. Exact masses were calculated based on the predominant combination of natural isotopes.

1.1 Synthesis of the DBA derivatives

General procedure for the synthesis of symmetrically substituted DBA-derivatives:

The freshly prepared Grignard reagent aryl-MgBr or alkyl-MgBr (1.888 mmol, 2.1 equiv) in Et_2O (15 mL) was added dropwise with stirring over 15 min to a cooled (–78 °C) solution of 9,10-dibromo-DBA (300 mg, 0.899 mmol, 1.0 equiv) in toluene (25 mL). The reaction mixture was slowly allowed to warm to room temperature and stirred overnight. All volatiles were removed under reduced pressure, the residue was extracted with toluene (3 × 10 mL) and the combined extracts were filtered over a glass frit (G4) covered with Celite (1 cm; pre-dried at 120 °C for several days). After the removal of all volatiles in a dynamic vacuum, the symmetrically substituted DBA derivatives were obtained as pale yellow to ocher solids. See Table S1 for the obtained yields.

The ethyl derivative **5** was sufficiently volatile to grow X-ray quality crystals by sublimation (110 °C/10^{-3} mbar). X-ray quality crystals of **8** were obtained by gas-phase diffusion of *n*-hexane into its toluene solution.

Table S1. Overview of the DBA derivatives obtained via the described method. (*) Yield not determined because compound was not pure.

DBA derivative	reagent		yield	
		mL	mg	%
5	1-bromoethane	0.14	150	72
6	2-bromopropane	0.18	–	(*)
7	4-bromotoluene	0.22	246	77
8	5-bromo-*m*-xylene	0.26	224	65

General procedure for DBA reduction with lithium granules:

In a glovebox, lithium granules (10 mg, 1.44 mmol) were added at room temperature to a stirred solution of the respective neutral DBA (**1**-**5** and **7**-**9**; 0.050 mmol) in THF-d_8 (0.5 mL), whereupon the reaction mixture immediately adopted a red color. After 30 min, the solution was separated from residual lithium metal with a syringe and used without further treatment. NMR analysis revealed a quantitative conversion to the respective dianion in all cases.

X-ray quality crystals of $[Li(thf)_2]_2$[**7**] were grown by slow evaporation of its THF-d_8 solution.

General procedure for DBA reduction with elemental sodium:

In a glovebox, sodium metal (10 mg, 0.435 mmol) was added at room temperature to a stirred solution of the respective neutral DBA (**1**, **2**, **4**, and **7**; 0.050 mmol) in THF-d_8 (0.5 mL), whereupon the reaction mixture immediately adopted a pink color and turned dark green within 30 min. After 60 min, the solution was separated from residual sodium metal with a syringe and used without further treatment. NMR analysis revealed a quantitative conversion to the respective dianion in all cases.

X-ray quality crystals of $[Na_2(thf)_3]$[**1**] were grown by slow evaporation of its THF-d_8 solution.

General procedure for DBA reduction with KC_8:

In a glovebox, KC_8 (27 mg, 0.200 mmol) was added at room temperature to a stirred solution of the respective neutral DBA (**1** and **4**-**8**; 0.050 mmol) in THF (1 mL), whereupon the reaction mixture immediately adopted a pink color and turned dark green within 30 min. After 60 min, the solution was separated from residual KC_8 and graphite by filtration (G4 glass frit), the solvent was removed from the filtrate under reduced pressure, and the residue dissolved in THF-d_8. NMR analysis showed exclusively the resonances of the respective dianion in all cases.

Red X-ray quality crystals of $[K_2(thf)_4][$**1**$]$ and $[K(thf)]_2[$**7**$]$ were grown by slow evaporation of their THF solutions.

Note: The compound $K_2[$**4**$]$ was previously prepared by Siebert et al., who observed a red color, both for the solid material and its THF solutions. However, they also mentioned broad and purely resolved NMR spectra containing more resonances than expected.[9]

General procedure for the measurement of H_2-addition kinetics:

H_2 activation reactions were carried out in flame-sealed NMR tubes. The experimental setup was as follows: An NMR tube connected to a Schlenk line was charged with a THF-d_8 solution (0.5 mL) of the respective doubly reduced 9,10-dihydro-9,10-diboraanthracene (approx. 0.050 mmol $[$**A**$]^{2-}$; preparation as described above). The solution was frozen with liquid nitrogen, the system was evacuated, and then H_2 (purity grade 5.0) was filled in through a condensation trap cooled with liquid nitrogen (to remove traces of H_2O). The content of the NMR tube was allowed to unfreeze whereby H_2 dissolved in the THF-d_8.[10] During the entire process, the system remained connected to the H_2 cylinder and a mercury bubbler to release the overpressure.

The mixture was frozen again, the partial pressure of H_2 was adjusted such that it remained slightly below 1 atm, and the NMR tube was flame-sealed. CAUTION: Care must be taken not to generate a leak in the glass wall. However, given the small amount of H_2 present in the NMR tube, we found that the hazard of an oxyhydrogen explosion was low even in the event of a leakage.

The sealed NMR samples were kept at either 50 or 100 °C (*cf.* Table S2) and the progress of the H_2-activation reaction was monitored by ^{1}H NMR spectroscopy in regular steps (*cf.* Figure 1). The spectra were recorded at ambient temperature, at which the activation reaction does not proceed further.[4] The conversion rates of H_2-addition in dependence of the boron-bonded substituent and the counter cation are summarized in Table S2 and Figures 1 and 4.

Table S2. Time (in hours) required until the individual H_2-addition reactions reached a dynamic equilibrium or were completed (see also Figures 1 and 4).

$[\mathbf{A}]^{2-}$ derivative	M = Li *T* = 100 °C	M = Na *T* = 100 °C	M = Na *T* = 50 °C	M = K *T* = 50 °C
$[\mathbf{1}]^{2-}$	86	21	183	12
$[\mathbf{2}]^{2-}$	48	93	-	-
$[\mathbf{4}]^{2-}$	264	14	76	3
$[\mathbf{5}]^{2-}$	480	-	-	8
$[\mathbf{7}]^{2-}$	640	21	129	13
$[\mathbf{8}]^{2-}$	480	-	-	11

X-ray quality crystals of $[Na][Na(thf)_2(18\text{-c-}6)][Na(thf)_2]_2(n\text{-hexane})[\mathbf{7}\text{-}H_2]_2$, $[K(18\text{-c-}6)]_2[\mathbf{1}\text{-}H_2]$, and $[K]_2[K(18\text{-c-}6)][K(18\text{-c-}6)(thf)_2][\mathbf{7}\text{-}H_2]_2$ were obtained by gas-phase diffusion of *n*-hexane into their THF-d_8/18-crown-6 (18-c-6) solutions.

X-ray quality crystals of $[K][K(thf)]_3[\mathbf{4}\text{-}H_2]_2$ were obtained by gas-phase diffusion of *n*-hexane into its THF-d_8 solution.

1.2 Spectroscopic data for the DBA derivatives

NMR data in THF-d_8 for the neutral DBA derivatives:

5

^{1}H NMR (500.2 MHz, THF-d_8): δ = 7.88–7.86 (m, 4H; H-a), 7.33–7.31 (m, 4H; H-b), 1.54 (q, ^3J(H,H) = 7.7 Hz, 4H; CH_2CH$_3$), 0.69 (t, ^3J(H,H) = 7.7 Hz, 6H; CH$_2$CH_3).

^{11}B NMR (160.5 MHz, THF-d_8): δ = 40.3 ($h_{1/2}$ = 500 Hz).

^{13}C{^{1}H} NMR (125.8 MHz, THF-d_8): δ = 151.4 (BC), 133.5 (C-a), 129.0 (C-b), 14.3 (*C*H$_2$CH$_3$), 10.3 (CH$_2$*C*H$_3$).

^{1}H NMR data in C_6D_6 are in accordance with the literature.[11]

^{1}H NMR (500.2 MHz, C_6D_6): δ = 8.04–8.02 (m, 4H; C_6H_4), 7.36–7.34 (m, 4H; C_6H_4), 1.92 (q, ^3J(H,H) = 8.3 Hz, 4H; CH_2CH$_3$), 1.10 (t, ^3J(H,H) = 8.3 Hz, 6H; CH$_2$CH_3).

6

^{1}H NMR (250.1 MHz, C_6D_6): δ = 8.02–7.99 (m, 4H; C_6H_4), 7.31–7.27 (m, 4H; C_6H_4), 2.46 (sept, ^3J(H,H) = 7.4 Hz, 2H; C*H*(CH$_3$)$_2$), 1.33 (t, ^3J(H,H) = 7.4 Hz, 12H; CH(C$_3$)$_2$).

Note: The compound could not be purified. Further NMR data were therefore not recorded.

7

^{1}H NMR (500.2 MHz, THF-d_8): δ = 7.65–7.63 (m, 4H; H-a), 7.35 (d, ^3J(H,H) = 7.7 Hz, 4H; Tol-H-*o*), 7.25–7.23 (m, 4H; H-b), 7.13 (d, ^3J(H,H) = 7.7 Hz, 4H; Tol-H-*m*), 2.34 (s, 6H; Tol-CH$_3$-*p*).

^{11}B NMR (160.5 MHz, THF-d_8): δ = 36.3 ($h_{1/2}$ = 670 Hz).

^{13}C{^{1}H} NMR (125.8 MHz, THF-d_8): δ = 152.4 (BC), 145.4 (Tol-C-*i*), 137.3 (C-a), 136.5 (Tol-C-*p*), 134.0 (Tol-C-*o*), 129.3 (C-b), 128.6 (Tol-C-*m*), 21.0 (Tol-CH$_3$-*p*).

8

^{1}H NMR (500.2 MHz, THF-d_8): δ = 7.64–7.62 (m, 4H; H-a), 7.25–7.23 (m, 4H; H-b), 7.07 (s, 4H; Xyl-H-*o*), 6.90 (s, 2H; Xyl-H-*p*), 2.30 (s, 12H; Xyl-CH$_3$-*m*).

^{11}B NMR (160.5 MHz, THF-d_8): δ = 38.1 ($h_{1/2}$ = 830 Hz).

^{13}C{^{1}H} NMR (125.8 MHz, THF-d_8): δ = 151.7 (BC), 148.3 (Xyl-C-*i*), 137.2 (C-a), 136.2 (Xyl-C-*m*), 131.0 (Xyl-C-*o*), 129.1 (C-b), 128.5 (Xyl-C-*p*), 21.6 (Xyl-CH$_3$-*m*).

NMR data in THF-d_8 for Li_2[A] salts:

Li_2[3]

^{1}H NMR (500.2 MHz, THF-d_8): δ = 8.45–8.43 (m, 4H; H-a), 7.10–7.07 (d, ^3J(H,H) = 18.1 Hz, 2H; CH=CH), 6.66–6.64 (m, 4H; H-b), 6.11–6.08 (d, ^3J(H,H) = 18.1 Hz, 2H; CH=CH), 1.24 (s, 18H; CH_3)

^{11}B NMR (160.5 MHz, THF-d_8): δ = 21.6 ($h_{1/2}$ = 390 Hz).

^{13}C{^{1}H} NMR (125.8 MHz, THF-d_8): δ = 148.4 (CH=CH), 136.4 (C-a), 131.9 (br; CH=CH), 118.4 (C-b), 34.9 ($C(CH_3)_3$), 30.6 ($C(CH_3)_3$); n.o. (BC).

Li_2[5]

^{1}H NMR (500.2 MHz, THF-d_8): δ = 8.29–8.27 (m, 4H; H-a), 6.67–6.65 (m, 4H; H-b), 1.98 (q, ^3J(H,H) = 7.9 Hz, 4H; CH_2CH_3), 1.32 (t, ^3J(H,H) = 7.9 Hz, 6H; CH_2CH_3).

^{11}B NMR (160.5 MHz, THF-d_8): δ = 25.7 ($h_{1/2}$ = 420 Hz).

^{13}C{^{1}H} NMR (125.8 MHz, THF-d_8): δ = 135.3 (C-a), 134.1 (BC), 117.8 (C-b), 16.9 (CH_2CH_3), 8.7 (CH_2CH_3).

Li_2[7]

^{1}H NMR (500.2 MHz, THF-d_8): δ = 8.12–8.10 (m, 4H; H-a), 7.58 (d, ^3J(H,H) = 7.6 Hz, 4H; Tol-H-*o*), 7.14 (d, ^3J(H,H) = 7.6 Hz, 4H; Tol-H-*m*), 6.59–6.57 (m, 4H; H-b), 2.40 (s, 6H; Tol-CH_3-*p*).

^{11}B NMR (160.5 MHz, THF-d_8): δ = 26.8 ($h_{1/2}$ = 570 Hz).

^{13}C{^{1}H} NMR (125.8 MHz, THF-d_8): δ = 149.8 (Tol-C-*i*), 137.2 (Tol-C-*o*), 136.9 (C-a), 134.8 (BC), 132.7 (Tol-C-*p*), 128.3 (Tol-C-*m*), 118.8 (C-b), 21.1 (Tol-CH_3-*p*).

Li_2[8]

^{1}H NMR (500.2 MHz, THF-d_8): δ = 8.10–8.08 (m, 4H; H-a), 7.30 (s, 4H; Xyl-H-*o*), 6.79 (s, 2H; Xyl-H-*p*), 6.58–6.56 (m, 4H; H-b), 2.35 (s, 12H; Xyl-CH_3-*m*).

^{11}B NMR (160.5 MHz, THF-d_8): δ = 26.0 ($h_{1/2}$ = 540 Hz).

^{13}C{^{1}H} NMR (125.8 MHz, THF-d_8): δ = 153.4 (Xyl-C-*i*), 137.0 (C-a), 135.6 (Xyl-C-*m*), 135.2 (Xyl-C-*o*), 134.7 (BC), 125.9 (Xyl-C-*p*), 118.7 (C-b), 21.6 (Xyl-CH_3-*m*).

NMR data in THF-d_8 for Na_2[A] salts:

Na_2[1]

$^1H\{^{11}B\}$ NMR (300.0 MHz, THF-d_8): δ = 8.07–8.04 (m, 4H; H-a), 6.47–6.44 (m, 4H; H-b), 5.47 (br, 2H; BH).

^{11}B NMR (96.3 MHz, THF-d_8): δ = 20.3 ($h_{1/2}$ = 510 Hz).

$^{13}C\{^1H\}$ NMR (75.4 MHz, THF-d_8): δ = 143.0 (BC), 139.8 (C-a), 115.9 (C-b).

Na_2[2]

^1H NMR (500.2 MHz, THF-d_8): δ = 8.50–8.48 (m, 4H; H-a), 6.60–6.58 (m, 4H; H-b), 1.40 (s, 18H; CH_3).

^{11}B NMR (160.5 MHz, THF-d_8): δ = 16.6 ($h_{1/2}$ = 410 Hz).

$^{13}C\{^1H\}$ NMR (125.8 MHz, THF-d_8): δ = 141.2 (BC), 137.1 (C-a), 116.5 (C-b), 114.4 (C≡*C*C(CH_3)$_3$), 95.8 (*C*≡CC(CH_3)$_3$), 33.1 (C(*C*H$_3$)$_3$), 29.5 (*C*(CH_3)$_3$).

Na_2[7]

^1H NMR (500.2 MHz, THF-d_8): δ = 8.29–8.27 (m, 4H; H-a), 7.62 (d, ^3J(H,H) = 7.6 Hz, 4H; Tol-H-*o*), 7.05 (d, ^3J(H,H) = 7.6 Hz, 4H; Tol-H-*m*), 6.49–6.47 (m, 4H; H-b), 2.36 (s, 6H; Tol-CH_3-*p*).

^{11}B NMR (160.5 MHz, THF-d_8): δ = 27.8 ($h_{1/2}$ = 620 Hz).

$^{13}C\{^1H\}$ NMR (125.8 MHz, THF-d_8): δ = 151.7 (Tol-C-*i*), 137.4 (Tol-C-*o*), 136.6 (C-a), 136.2 (BC), 130.7 (Tol-C-*p*), 127.2 (Tol-C-*m*), 116.2 (C-b), 21.4 (Tol-CH_3-*p*).

NMR data in THF-d_8 for K_2[A] salts:

K_2[4]

^{1}H NMR (300.0 MHz, THF-d_8): δ = 8.22–8.19 (m, 4H; H-a), 6.47–6.44 (m, 4H; H-b), 1.22 (s, 6H; CH_3).

^{11}B NMR (96.3 MHz, THF-d_8): δ = 23.6 ($h_{1/2}$ = 550 Hz).

^{13}C{^{1}H} NMR (75.4 MHz, THF-d_8): δ = 139.2 (BC), 135.1 (C-a), 113.9 (C-b), –0.1 (CH_3).

K_2[5]

^{1}H NMR (500.2 MHz, THF-d_8): δ = 8.28–8.26 (m, 4H; H-a), 6.47–6.45 (m, 4H; H-b), 1.96 (q, ^3J(H,H) = 7.7 Hz, 4H; CH_2CH$_3$), 1.22 (t, ^3J(H,H) = 7.7 Hz, 6H; CH$_2$CH_3).

^{11}B NMR (160.5 MHz, THF-d_8): δ = 27.0 ($h_{1/2}$ = 450 Hz).

^{13}C{^{1}H} NMR (125.8 MHz, THF-d_8): δ = 138.8 (BC), 135.2 (C-a), 114.6 (C-b), 16.2 (CH$_2$*C*H$_3$), 9.5 (*C*H$_2$CH$_3$).

K_2[7]

^{1}H NMR (500.2 MHz, THF-d_8): δ = 8.20–8.18 (m, 4H; H-a), 7.56 (d, ^3J(H,H) = 7.6 Hz, 4H; Tol-H-*o*), 7.04 (d, ^3J(H,H) = 7.6 Hz, 4H; Tol-H-*m*), 6.43–6.41 (m, 4H; H-b), 2.35 (s, 6H; Tol-CH$_3$-*p*).

^{11}B NMR (160.5 MHz, THF-d_8): δ = 27.7 ($h_{1/2}$ = 400 Hz).

^{13}C{^{1}H} NMR (125.8 MHz, THF-d_8): δ = 153.3 (Tol-C-*i*), 139.0 (BC), 137.4 (Tol-C-*o*), 136.5 (C-a), 130.8 (Tol-C-*p*), 127.6 (Tol-C-*m*), 115.8 (C-b), 21.2 (Tol-CH$_3$-*p*).

K_2[8]

^{1}H NMR (400.1 MHz, THF-d_8): δ = 8.19–8.17 (m, 4H; H-a), 7.30 (s, 4H; Xyl-H-*o*), 6.66 (s, 2H; Xyl-H-*p*), 6.43–6.40 (m, 4H; H-b), 2.32 (s, 12H; Xyl-CH$_3$-*m*).

^{11}B NMR (128.4 MHz, THF-d_8): δ = 28.8 ($h_{1/2}$ = 630 Hz).

^{13}C{^{1}H} NMR (100.6 MHz, THF-d_8): δ = 156.2* (Xyl-C-*i*), 138.5* (BC), 136.2 (C-a), 135.0 (Xyl-C-*o*), 134.2 (Xyl-C-*m*), 124.0 (Xyl-C-*p*), 115.4 (C-b), 22.0 (Xyl-CH$_3$-*m*). *detectable only in the ^{13}C/^{1}H HMBC spectrum

NMR data in THF-d_8 for Li_2[A-H_2] salts:

Li_2[4-H_2]

^{1}H NMR (300.0 MHz, THF-d_8): δ = 7.36–7.33 (m, 4H; H-a), 6.64–6.61 (m, 4H; H-b), 1.74 (n.r., 2H; BH), 0.21 (m, 6H; CH_3).

^{11}B NMR (96.3 MHz, THF-d_8): δ = –20.0 (d, ^1J(B,H) = 59.1 Hz).

^{13}C{^{1}H} NMR (125.8 MHz, THF-d_8): δ = 164.6 (BC), 130.0 (C-a), 121.4 (C-b), 5.1 (CH_3).

Li_2[5-H_2]

^{1}H{^{11}B} NMR (300.0 MHz, THF-d_8): δ = 7.39–7.36 (m, 4H; H-a), 6.63–6.60 (m, 4H; H-b), 1.61 (s, 2H; BH), 1.04–0.94 (m, 10H; CH_2CH_3).

^{11}B NMR (96.3 MHz, THF-d_8): δ = –17.9 (d, ^1J(B,H) = 57.1 Hz).

^{13}C{^{1}H} NMR (75.4 MHz, THF-d_8): δ = 163.9* (BC), 130.8 (C-a), 121.5 (C-b), 14.1 (CH_2CH_3), 11.7** (CH_2CH_3). *detectable only in the ^{13}C/^{1}H HMBC spectrum, **detectable only in the ^{13}C/^{1}H HSQC spectrum

Li_2[7-H_2]

^{1}H NMR (400.1 MHz, THF-d_8): δ = 7.33 (d, ^3J(H,H) = 7.5 Hz, 4H; Tol-H-*o*), 6.87–6.84 (m, 8H; Tol-H-*m*, H-a), 6.46–6.44 (m, 4H; H-b), 2.61 (n.r., 2H; BH), 2.28 (s, 6H; Tol-CH_3-*p*).

^{11}B NMR (128.4 MHz, THF-d_8): δ = –9.9 (d, ^1J(B,H) = 60.1 Hz).

^{13}C{^{1}H} NMR (100.6 MHz, THF-d_8): δ = 138.3 (Tol-C-*o*), 133.3 (C-a), 130.1 (Tol-C-*p*), 127.2 (Tol-C-*m*), 121.7 (C-b), 21.2 (Tol-CH_3-*p*); n.o. (BC, Tol-C-*i*).

Li_2[8-H_2]

^{1}H NMR (500.2 MHz, THF-d_8): δ = 7.08 (s, 4H; Xyl-H-*o*), 6.88–6.86 (m, 4H; H-a), 6.52 (s, 2H; Xyl-H-*p*), 6.46–6.44 (m, 4H; H-b), 2.61 (n.r., 2H; BH), 2.21 (s, 12H; Xyl-CH_3-*m*).

^{11}B NMR (160.5 MHz, THF-d_8): δ = –12.3 (d, ^1J(B,H) = 58.8 Hz).

^{13}C{^{1}H} NMR (125.8 MHz, THF-d_8): δ = 165.8 (Xyl-C-*i*), 162.6 (BC), 136.4 (Xyl-C-*o*), 133.8 (Xyl-C-*m*), 133.6 (C-a), 124.1 (Xyl-C-*p*), 121.6 (C-b), 21.7 (Xyl-CH_3-*m*).

NMR data in THF-d_8 for Na_2[A-H_2] salts:

A color code is used in order to distinguish the NMR resonances of the *cis* (red) and *trans* (blue) stereoisomers of the respective H_2 addition product. A black color is used if *cis*/*trans*-signals are overlapping.

Na_2[1-H_2]

^{1}H NMR (500.2 MHz, THF-d_8): δ = 7.35 (n.r., 4H; H-a), 6.68–6.66 (m, 4H; H-b), 2.5 (q, ^1J(B,H) = 77.3 Hz, 4H; BH).

^{11}B NMR (160.5 MHz, THF-d_8): δ = –19.8 (t, ^1J(B,H) = 77.3 Hz).

^{13}C{^{1}H} NMR (125.8 MHz, THF-d_8): δ = 161.5 (BC), 135.1 (C-a), 122.6 (C-b).

Na_2[2-H_2]

^{1}H NMR (500.2 MHz, THF-d_8): δ = 7.82–7.80 (m, 4H; H-a), 6.79–6.77 (m, 4H; H-b), 2.17 (q, ^1J(B,H) = 72.4 Hz, 2H; BH), 1.33 (s, 18H; CH_3).

^{11}B NMR (96.3 MHz, THF-d_8): δ = –23.6 (d, ^1J(B,H) = 72.4 Hz).

^{13}C{^{1}H} NMR (125.8 MHz, THF-d_8): δ = 159.9 (BC), 131.1 (C-a), 122.6 (C-b), 33.3 (C(CH$_3$)$_3$), 28.9 (C(CH$_3$)$_3$); n.o. $C{\equiv}C$.

Na_2[4-H_2]

^{1}H{^{11}B} NMR (500.2 MHz, THF-d_8): δ = 7.49–7.47 (m, 4H; H-a), 7.45–7.43 (m, 4H; H-a), 6.78–6.75 (m, 4H; H-b/4H; H-b), 2.52 (br, 2H; BH), 1.91 (br, 2H; B), 0.24 (br, 6H; CH_3), 0.05 (m, 6H; CH_3).

^{11}B NMR (160.5 MHz, THF-d_8): δ = –18.5 (d, ^1J(B,H) = 70.8 Hz), –19.8 (d, ^1J(B,H) = 69.0 Hz).

^{13}C{^{1}H} NMR (125.8 MHz, THF-d_8): δ = 165.6 (BC), 163.0* (BC), 135.1 (C-a), 130.9 (C-a), 123.2 (C-b), 122.7 (C-b), 11.5 (CH_3), 4.8 (CH_3). *detectable only in the ^{13}C/^{1}H HMBC spectrum

Note: The *cis*:*trans* integral ratio was approx. 4:1.

Na_2[7-H_2]

^{1}H{^{11}B} NMR (500.2 MHz, THF-d_8): δ = 7.36–7.35 (m, 4H; Tol-H-*o*), 7.31–7.29 (m, 4H; H-a), 7.23–7.21 (m, 4H; Tol-H-*o*), 7.03–7.01 (m, 4H; H-a), 6.94–6.93 (m, 4H; Tol-H-*m*), 6.80–6.78 (m, 4H; Tol-H-*m*), 6.75–6.73 (m, 4H; H-b), 6.61–6.59 (m, 4H; H-b), 3.09 (s, 1.5H; BH), 2.69 (s, 2H; BH), 2.30 (s, 6H; Tol-CH_3-*p*), 2.19 (s, 4.5H; Tol-CH_3-*p*).

^{11}B NMR (160.5 MHz, THF-d_8): δ = –11.2 (d, ^1J(B,H) = 67.4 Hz), –11.6 (d, ^1J(B,H) = 69.1 Hz).

^{13}C{^{1}H} NMR (125.8 MHz, THF-d_8): δ = 164.4 (BC), 162.9 (BC), 161.4 (Tol-C-*i*), 138.0 (Tol-C-*o*), 136.2 (Tol-C-*o*), 135.2 (C-a), 133.2 (C-a), 131.0 (Tol-C-*p*), 130.8 (Tol-C-*p*), 127.8 (Tol-C-*m*), 123.2 (C-b), 122.2 (C-b), 21.1 (Tol-CH_3-*p*), 20.9 (Tol-CH_3-*p*).

Note: The *cis*:*trans* integral ratio was approx. 4:3.

NMR data in THF-d_8 for Na_2[A-H_2] salts:

A color code is used in order to distinguish the NMR resonances of the *cis* (red) and *trans* (blue) stereoisomers of the respective H_2 addition product. A black color is used if *cis*/*trans*-signals are overlapping.

K_2[4-H_2]

$^1H\{^{11}B\}$ NMR (500.2 MHz, THF-d_8): δ = 7.39–7.38 (m, 4H; H-a), 7.35–7.33 (m, 4H; H-a), 6.72–6.68 (m, 4H; H-b/ 4H; H-b), 2.57 (s, 2H; BH), 1.88 (s, 2H; BH), 0.12 (m, 6H; CH_3), 0.02 (m, 6H; CH_3).

^{11}B NMR (160.5 MHz, THF-d_8): δ = –16.4 (d, ^1J(B,H) = 71.3 Hz), –17.9 (d, ^1J(B,H) = 69.0 Hz).

$^{13}C\{^1H\}$ NMR (125.8 MHz, THF-d_8): δ = 167.0 (BC), 165.1 (BC), 133.8 (C-a), 129.8 (C-a), 122.3 (C-b), 122.2 (C-b), 10.2 (CH_3), 4.8 (CH_3).

Note: The *cis*:*trans* integral ratio was approx. 8:1.

K_2[5-H_2]

$^1H\{^{11}B\}$ NMR (500.2 MHz, THF-d_8): δ = 7.41–7.38 (m, 4H; H-a/4H; H-a), 6.74–6.72 (m, 4H; H-b), 6.71–6.69 (m, 4H; H-b), 2.32 (br, 2H; BH), 1.82 (br, 2H; B), 1.05 (t, ^3J(H,H) = 7.4 Hz, 6H; CH_2CH_3), 0.92–0.85 (m, 4H; CH_2CH_3/6H; CH_2CH_3), 0.60–0.54 (m, 4H; CH_2CH_3).

^{11}B NMR (160.5 MHz, THF-d_8): δ = –12.7 (d, ^1J(B,H) = 71.1 Hz), –14.5 (d, ^1J(B,H) = 66.7 Hz).

$^{13}C\{^1H\}$ NMR (125.8 MHz, THF-d_8): δ = 167.5 (BC), 133.1 (C-a), 130.8 (C-a), 122.4 (C-b), 122.3 (C-b), 16.9*(CH_2CH), 14.4 (CH_2CH_3), 14.3 (CH_2CH_3), 12.8* (CH_2CH_3); n.o. (BC). *detectable only in the $^{13}C/^1H$ HSQC spectrum

Note: The *cis*:*trans* integral ratio was approx. 2:1.

K_2[7-H_2]

$^1H\{^{11}B\}$ NMR (500.2 MHz, THF-d_8): δ = 7.37–7.35 (m, 4H; Tol-H-*o*), 7.25–7.24 (m, 4H; H-a), 7.23–7.21 (m, 4H; Tol-H-*o*), 7.10–7.08 (m, 4H; H-a), 6.91–6.89 (m, 4H; Tol-H-*m*), 6.78–6.76 (m, 4H; Tol-H-*m*), 6.70–6.68 (m, 4H; H-b), 6.61–6.59 (m, 4H; H-b), 3.22 (br, 2H; BH), 3.00 (br, 2H; BH), 2.26 (s, 6H; Tol-CH_3-*p*), 2.18 (s, 6H; Tol-CH_3-*p*).

^{11}B NMR (160.5 MHz, THF-d_8): δ = –11.5 (d, ^1J(B,H) = 81.2 Hz), –12.0 (d, ^1J(B,H) = 77.9 Hz).

$^{13}C\{^1H\}$ NMR (125.8 MHz, THF-d_8): δ = 162.8* (Ph-C-*i*), 162.6* (Ph-C-*i*), 165.9* (BC), 165.2* (BC), 137.5 (Tol-C-*o*), 136.7 (Tol-C-*o*), 134.1 (C-a), 133.6 (C-a), 130.7 (Tol-C-*p*), 130.4 (Tol-C-*p*), 127.9 (Tol-C-*m*), 127.6 (Tol-C-*m*), 122.8 (C-b), 122.5 (C-b), 21.1 (Tol-CH_3-*p*), 20.9 (Tol-CH_3-*p*). *detectable only in the $^{13}C/^1H$ HMBC spectrum

Note: The *cis*:*trans* integral ratio was approx. 2:1.

K_2[8-H_2]

$^{1}H\{^{11}B\}$ NMR (500.2 MHz, THF-d_8): δ = 7.26–7.25 (m, 4H; H-a), 7.18–7.16 (m, 4H; H-a), 7.10 (s, 4H; Xyl-H-*o*), 6.97 (s, 4H; Xyl-H-*o*), 6.71–6.69 (m, 4H; H-b), 6.65–6.63 (m, 4H; H-b), 6.51 (s, 2H; Xyl-H-*p*), 6.44 (s, 2H; Xyl-H-*p*), 3.20 (br, 2H; BH), 3.01 (br, 2H; BH), 2.19 (s, 12H; Xyl-CH_3-*m*), 2.13 (s, 12H; Xyl-CH_3-*m*).

^{11}B NMR (160.5 MHz, THF-d_8): δ = –10.1 (d, ^{1}J(B,H) = 73.2 Hz), –10.6 (d, ^{1}J(B,H) = 68.9 Hz).

$^{13}C\{^{1}H\}$ NMR (125.8 MHz, THF-d_8): δ = 165.6* (Xyl-C-*i*), 165.3* (BC), 164.8* (BC), 135.0 (Xyl-C-*o*), 134.4 (Xyl-C-*o*), 134.3 (Xyl-C-*m*), 133.7 (C-a), 133.3 (C-a), 124.1 (Xyl-C-*p*), 123.9 (Xyl-C-*p*), 122.4 (C-b), 122.2 (C-b), 21.9 (Xyl-CH_3-*m*), 21.8 (Xyl-CH_3-*m*). *detectable only in the $^{13}C/^{1}H$ HMBC spectrum

Note: The *cis*:*trans* integral ratio was approx. 1:1.

2. Additional data regarding the isomerization of DBA derivatives of the type M_2[A-H_2]

In line with the ^{1}H NMR spectra (Figure 6) of K_2[**4**-H_2] and K_2[**7**-H_2], the ^{11}B NMR spectra in Figure S1 show different ratios of the respective *cis* (■) and *trans* (▲) isomers.

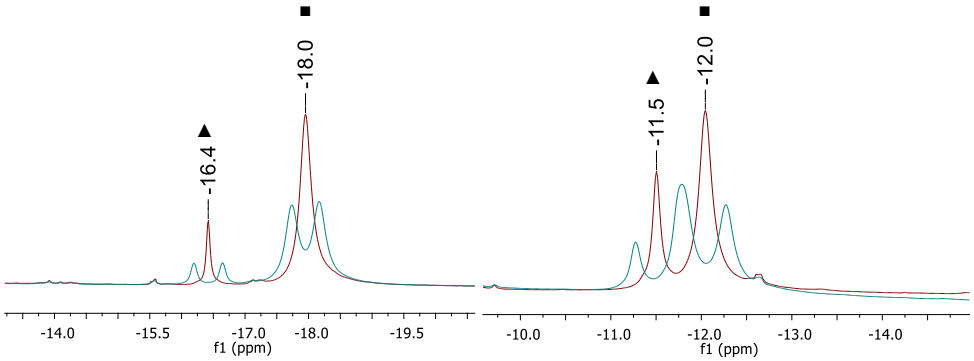

Figure S1. Comparison of the ^{11}B NMR (blue) and ^{11}B{^{1}H} NMR (red) spectra (160.5 MHz, THF-d_8) of K_2[**4**-H_2] (left) and K_2[**7**-H_2] (right); resonances of the *cis* (■) and the *trans* isomer (▲).

During H_2 activation experiments, the appearance of two compounds (*cis* and *trans* isomer of M_2[**A**-H_2]; M = Na, K; only exception: R = C≡C*t*Bu) was observed. According to the postulated concerted mechanism of the H_2 addition, H_2 approaches the DBA core from one side so that initially the *cis* isomer is formed.[4] At the elevated temperatures applied, a subsequent isomerization takes place and the *trans* isomer is generated. In the case of Na_2[**7**-H_2], we succeeded in the selective crystallization of *cis*-[Na][Na(thf)$_2$(18-c-6)][Na(thf)$_2$]$_2$(*n*-hexane)[**7**-H_2]$_2$ (confirmed by X-ray analysis). NMR spectra recorded on these single crystals allowed us to unequivocally confirm the chemical shift values of the *cis* isomer (Figure S2a). With time, also this sample showed the slow formation of a second species – the *trans* isomer – even at room temperature (Figure S2b). The isomerization is accelerated at elevated temperatures (Figure S2c).

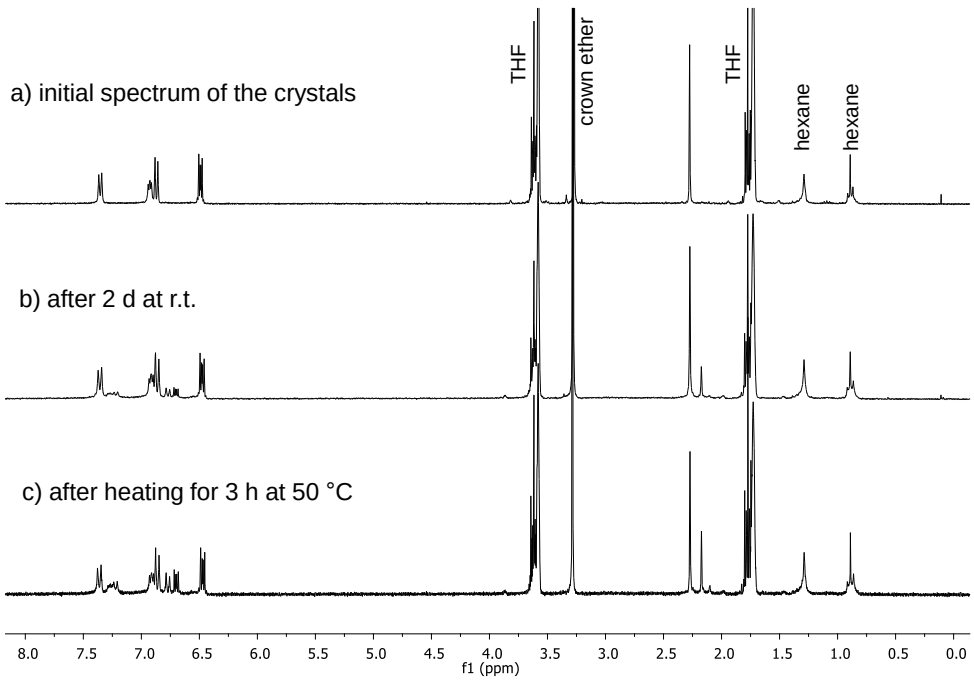

Figure S2. ^{1}H NMR spectra (THF-d_8) of re-dissolved single crystals of *cis*-[Na][Na(thf)$_2$(18-c-6)][Na(thf)$_2$]$_2$(*n*-hexane)[**7**-H$_2$]$_2$: a) spectrum recorded immediately after sample preparation (300.0 MHz), b) spectrum recorded after storage of the sample at room temperature for 2 d (250.1 MHz; resonances of the *trans* isomer start to appear), c) spectrum recorded after storage of the sample at 50 °C for 3 h (250.1 MHz; the amount of the *trans* isomer has almost doubled. Note: after storage of the NMR tube at room temperature for several months, the amount of *cis* isomer increased again at the expense of the *trans* isomer. This points toward a temperature-dependent dynamic isomerization equilibrium).

In order to further proof the existence of *cis*/*trans* isomers, K$_2$[**7**-H$_2$] was also synthesized via a non-concerted route by using a 1M THF solution of K[HBEt$_3$] instead of H$_2$. K[HBEt$_3$] readily reacts with **7** (0.050 mmol) in a 2:1 stoichiometry (THF-d_8, 0.5 mL). In Figure S3, the ^{1}H NMR spectra of both reaction mixtures are shown for comparison. In each case, two isomers are formed. However, the *cis*/*trans* ratios differ significantly depending on the hydride source, which is in line with the assumption of a concerted *vs*. non-concerted mechanism.

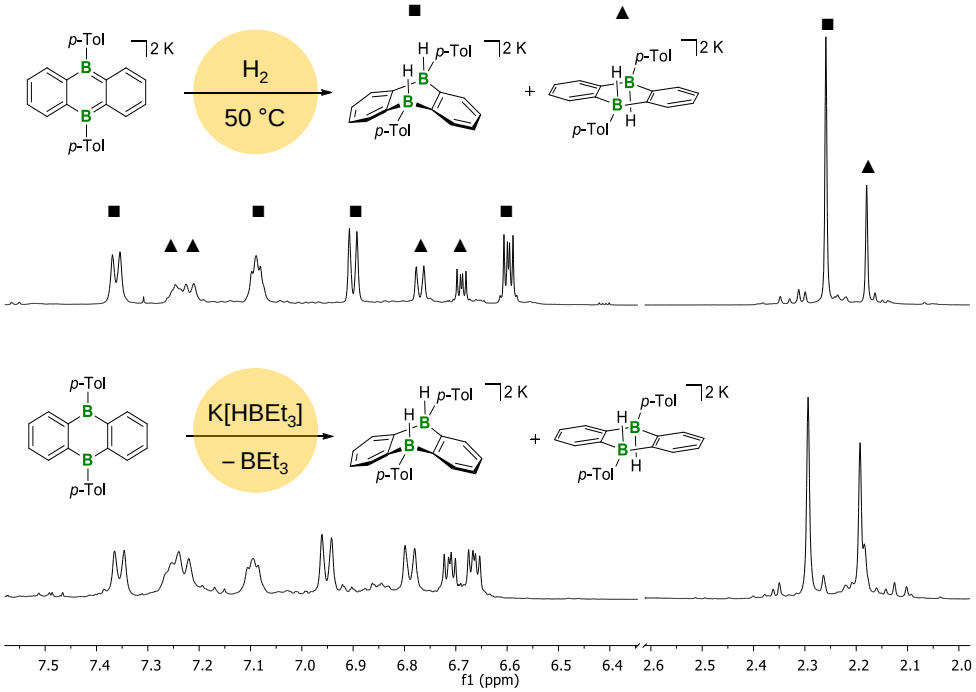

Figure S3. Comparison of the ^{1}H NMR spectra of the reaction mixtures of K_2[**7**] with H_2 (top: 500.2 MHz, THF-d_8) and **7** with K[HBEt$_3$] (bottom: 400.1 MHz, THF-d_8).

3. Hydrogenation reactions using $[A]^{2-}$ derivatives

3.1 General procedures and characterization data

General procedure for the hydrogenation of Ph(H)C=N*t*Bu with 37 mol% of the respective M_2[A] in an NMR tube:

Neat, dry *N*-benzylidene-*tert*-butylamine (10 µL, 9.1 mg, 56.2 µmol) was added to the respective freshly reduced M_2[**A**] derivative (20.8 µmol) in THF-d_8 (0.5 mL) and the solution was transferred to an NMR tube. After the addition of H_2 following the procedure described in 1.1, the NMR tube was flame-sealed, and warmed to 100 °C. The progress of the reaction was monitored by ^{1}H NMR spectroscopy. The percent conversion to the hydrogenation product after 16 h is summarized in Table 1.

^{1}H NMR (300.0 MHz, THF-d_8): δ = 7.35–7.32 (m, 2H; C_6H_5), 7.25–7.20 (m, 2H; C_6H_5), 7.16–7.11 (m, 1H; C_6H_5), 3.72 (d, ^3J(H,H) = 7.6 Hz, 2H; CH_2), 1.14 (s, 9H; CH_3); n.o. (NH).

The NMR data are in accordance with those of a commercial sample of the amine $Ph(H)_2C$–N(H)*t*Bu measured in THF-d_8, except for the doublet multiplicity of the CH_2 resonance. Given that an independently prepared mixture of Li_2[**4**] and the commercial amine showed the same effect, the doublet for the CH_2 protons likely results from Li^+ coordination (this was also observed for the corresponding Na^+ salt).

Hydrogenation of Ph(H)C=N*t*Bu with 10 mol% of Li_2[4] in a steel autoclave:

In a glovebox, the glass inlet of a steel autoclave (100 mL/100 bar steel autoclave from *Roth*, model I) was charged with a solution of freshly prepared Li_2[**4**] (0.124 mmol) in THF (10 mL). Neat, dry *N*-benzylidene-*tert*-butylamine (200 mg, 1.24 mmol) was added, the autoclave was closed inside the glovebox, and an H_2 pressure of approx. 7 bar was applied under inert conditions outside the glovebox. The reaction mixture was stirred at 100 °C for 18 h, the cooled autoclave was opened under ambient atmosphere, and the conversion to $Ph(H)_2C$–N(H)*t*Bu determined to be quantitative by ^{1}H NMR spectroscopy. The amine was isolated after aqueous work-up: THF was removed under reduced pressure, the residue extracted with Et_2O, the extract washed with NaOH solution (0.1 M), and dried over $MgSO_4$. After evaporation of all volatiles *in vacuo*, a colorless oil of $Ph(H)_2C$–N(H)*t*Bu remained. Yield: 153 mg, 0.94 mmol, 76%.

^{1}H NMR (500.2 MHz, C_6D_6): δ = 7.38–7.37 (m, 2H; C_6H_5), 7.23–7.20 (m, 2H; C_6H_5), 7.14–7.11 (m, 1H; C_6H_5), 3.59 (s, 2H; CH_2), 1.01 (s, 9H; CH_3); n.o. (N*H*).

^{13}C{^{1}H} NMR (125.8 MHz, C_6D_6): δ = 142.4 (C_6H_5), 128.6 (C_6H_5), 128.5 (C_6H_5), 126.9 (C_6H_5), 50.4 ($C(CH_3)_3$), 47.4 (CH_2), 29.2 ($C(CH_3)_3$).

The NMR data in C_6D_6 are in accordance with the literature.[12]

HRMS: 164.14355 (found); 164.14338 (calc. as $[C_{11}H_{17}N_1+H]^+$).

General procedure for hydrogenation reactions using 37 mol% of Li_2[4] in an NMR tube:

The respective substrate (53.0 µmol) was added to freshly prepared Li_2[**4**] (19.6 µmol) in THF-d_8 (0.5 mL) and the resulting mixture was transferred to an NMR tube. After the addition of H_2 following the procedure described in 1.1, the NMR tube was flame-sealed and kept at 100 °C. The progress of the reaction was monitored by ^{1}H NMR spectroscopy.

1,1-Diphenylethylene → 1,1-diphenylethane

1,1-Diphenylethylene (9.6 mg, 9.4 µL) was quantitatively hydrogenated after 35 h.

^{1}H NMR (500.2 MHz, THF-d_8): δ = 7.24–7.10 (m, 10H; C_6H_5), 4.14 (q, ^3J(H,H) = 7.3 Hz, 1H; CH), 1.61 (d, ^3J(H,H) = 7.3 Hz, 3H; CH_3).

^{13}C{^{1}H} NMR (125.8 MHz, THF-d_8): δ = 147.7 (C_6H_5), 129.2 (C_6H_5), 128.5 (C_6H_5), 126.8 (C_6H_5), 45.4 (CH), 21.7 (CH_3).

HRMS: 221.08007 (found); 221.07271 (calc. as $[C_{14}H_{14}+K]^+$).

Anthracene → 9,10-dihydroanthracene

Anthracene (9.4 mg) was quantitatively hydrogenated after 35 h. Note: A solvent mixture of THF-d_8 (0.5 mL) and C_6D_6 (0.1 mL) was used in order to improve the solubility of anthracene.

^{1}H NMR (500.2 MHz, THF-d_8/C_6D_6): δ = 7.24–7.22 (m, 4H; CH), 7.14–7.12 (m, 4H; CH), 3.85 (s, 4H; CH_2).

^{13}C{^{1}H} NMR (125.8 MHz, THF-d_8/C_6D_6): δ = 137.9 (C), 128.2 (CH), 126.9 (CH), 36.3 (CH_2).

HRMS: 180.08830 (found); 180.09335 (calc. as $C_{14}H_{12}$).

The following substrates showed no reaction with Li_2[**4**]/H_2: 1-(1-piperidinyl)cyclohexene, 2,3-dimethyl-2-butene, cyclohexene, phenanthrene, naphthalene, 2-butyne, and bis-(trimethylsilyl)-acetylene.

3.2 Additional experimental data regarding the hydrogenation reactions

[4+2]-Cycloaddition reaction between Ph(H)C=N*t*Bu and Li_2[4]: In order to investigate the interaction between Ph(H)C=N*t*Bu and Li_2[**4**], a ^{1}H NMR temperature study was undertaken using an approx. equimolar mixture of both substrates in THF-d_8 (0.5 mL). Figure S4a shows that the [4+2]-cycloaddition product Li[**10**] forms to some extent already within 0.5 h at room temperature. After 2 d at room temperature, the conversion was almost complete as evidenced by NMR spectroscopy (Figure S4b) and a color change of the solution from deep red to pale red. A temperature rise, however, promotes the retro-Diels-Alder reaction and shifts the dynamic cycloaddition equilibrium back toward the starting materials (Figure S4c); in agreement with that the red color became more intense again.

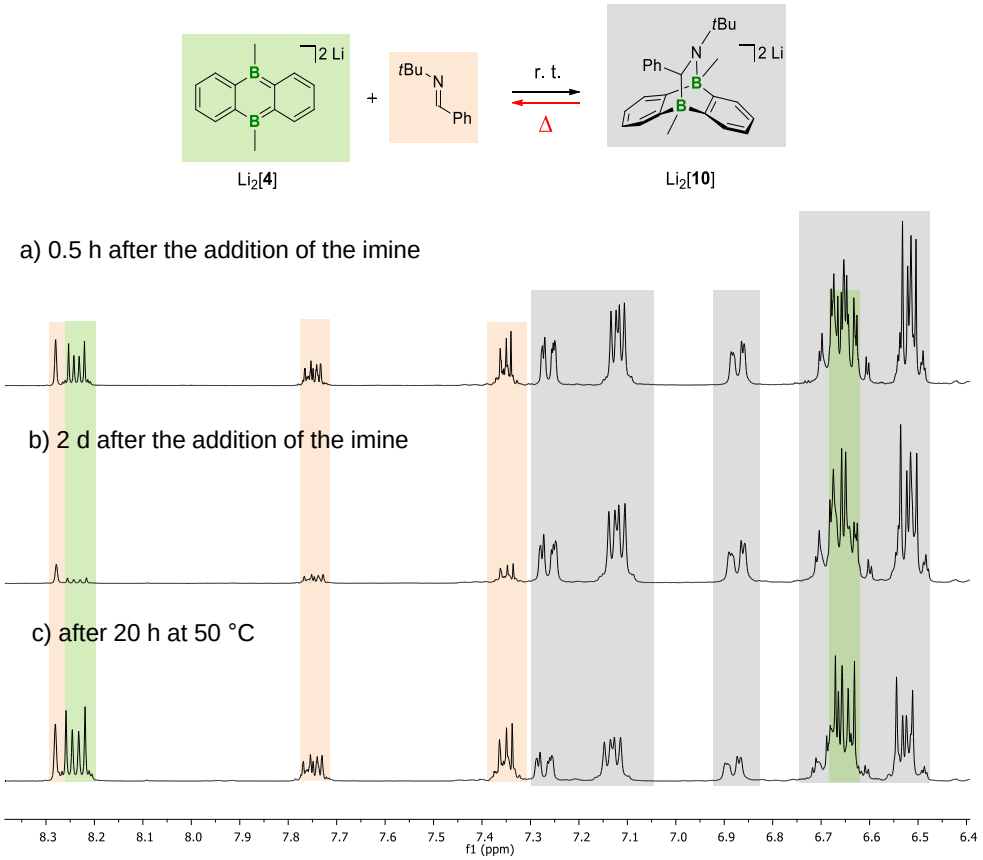

Figure S4. Comparison of the ^{1}H NMR spectra (250.1 MHz, THF-d_8) of the same sample of Li_2[**4**] a) 0.5 h after the addition of the imine Ph(H)C=N*t*Bu, b) 2 d after the addition of the imine Ph(H)C=N*t*Bu, and c) after 20 h at 50 °C (the spectrum was recorded immediately after the sample had been cooled to room temperature).

Li_2[10]

^{1}H NMR (500.2 MHz, THF-d_8): δ = 7.27–7.25 (m, 1H; C_6H_4), 7.12–7.10 (m, 2H; C_6H_4), 6.87–6.86 (m, 1H; C_6H_4), 6.70–6.64 (m, 3H; 1×C_6H_4 and 2×Ph), 6.65–6.61 (m, 1H; C_6H_4), 6.54–6.49 (m, 3H; 1×Ph and 2×C_6H_4), 6.00 (very br, 2H; Ph), 2.71 (s, 1H; CH), 0.80 (s, 9H; $C(CH_3)_3$), 0.63 (s, 3H; $NBCH_3$), –0.41 (s, 3H; $CBCH_3$).

^{11}B NMR (160.5 MHz, THF-d_8): δ = –10.5 (br; BN), –15.0 (s; BC).

^{13}C{^{1}H} NMR (125.8 MHz, THF-d_8): δ = 176.5 (very br; CB*C*), 171.3 (very br; CB*C*), 164.5 (br; NBC), 164.1 (Ph-*i*), 163.7 (br; NBC), 130.0 (C_6H_4), 126.4 (2×Ph), 126.3 (C_6H_4), 125.6 (C_6H_4), 124.2 (C_6H_4), 123.5 (C_6H_4), 120.7, 120.6, 120.4 (1×C_6H_4 and 2×C_6H_4), 120.1 (Ph), 69.8 (n.r.; CH), 58.9 (*C*$(CH_3)_3$), 32.8 (C(*C*$H_3)_3$), 8.7 ($NBCH_3$), 2.9 (n.r.; $CBCH_3$); n.o. (2×Ph).

Note: Resonances marked with a blue/red color belong to the same C_6H_4 spin system.

The attempt to grow single crystals of the addition product Li_2[**10**] from THF in the presence of 12-crown-4 resulted in the crystallization of the *N*-protonated salt [Li(12-c-4)$_2$]H[**10**](THF). The origin of the proton is not clear. We speculate that Li^+ coordination by the crown ether drastically increases the basicity of the tricyclic amine; the crown ether might also have contained traces of water as proton source.

[Li(12-c-4)$_2$]H[10](THF)

^{1}H NMR (500.2 MHz, THF-d_8): δ = 7.39–7.38 (m, 1H; C_6H_4), 7.33–7.30 (m, 2H; C_6H_4), 6.91 (br, 1H; Ph), 6.82–6.81 (m, 2H; C_6H_4 and Ph), 6.79–6.76 (m, 2H; C_6H_4), 6.73–6.72 (m, 1H; C_6H_4), 6.70–6.67 (m, 2H; C_6H_4 and Ph), 6.63 (br, 1H; Ph), 5.21 (br, 1H; Ph), 2.86 (d, ^3J(H,H) = 7.00 Hz, 1H; CH), 2.73 (d, ^3J(H,H) = 7.00 Hz, 1H; NH), 0.89 (s, 9H; $C(CH_3)_3$), 0.79 (s, 3H; $NBCH_3$), –0.29 (s, 3H; $CBCH_3$).

^{11}B NMR (160.5 MHz, THF-d_8): δ = –2.0 (br, BN), –14.7 (s, BC).

^{13}C{^{1}H} NMR (125.8 MHz, THF-d_8): δ = 170.5 (very br; CB*C*), 167.7 (very br; CB*C*), 160.5 (br; NBC), 159.0 (br; NBC), 153.3 (Ph-*i*), 129.5 (C_6H_4), 128.7 (br; Ph), 128.1 (C_6H_4), 127.2 (br; Ph), 126.5 (C_6H_4 and Ph), 126.4 (C_6H_4), 123.3 (C_6H_4), 123.1 (C_6H_4), 122.3 (2×Ph), 121.6 (C_6H_4), 121.5 (C_6H_4), 68.0 (CH), 61.5 (*C*$(CH_3)_3$), 30.4 (C(*C*$H_3)_3$), 7.6 (br; $NBCH_3$), 2.4 (very br; $CBCH_3$).

[4+2]-Cycloaddition products of other substrates

The imine Ph(H)C=N*t*Bu is not the only substrate that undergoes a formal [4+2] cycloaddtion with Li_2[**4**].

1,1'-Diphenylethylene and Li_2[4]

Neat 1,1'-diphenylethylene (13 µL, 13 mg, 74 µmol) was added at room temperature to Li_2[**4**], freshly prepared from **4** (15 mg, 74 µmol) and excess lithium granules, in THF-d_8 (0.5 mL; see 1.1). The mixture was transferred to an NMR tube and the tube was flame-sealed. NMR spectroscopy revealed the immediate and quantitative consumption of the starting materials and the selective formation of a cycloadduct.

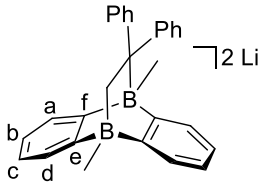

^{1}H NMR (500.2 MHz, THF-d_8): δ = 7.30 (n.r., 2H; H-d), 7.14–7.13 (m, 2H; H-a), 6.75–6.73 (m, 4H; Ph-H-*o*), 6.61–6.58 (m, 2H; H-c), 6.53–6.50 (m, 6H; Ph-H-*m* and H-b), 6.38–6.35 (m, 2H; Ph-H-*p*), 0.81–0.80 (n.r., 2H; CH_2), 0.19 (s, 3H; $CBCH_3$), 0.18 (n.r., 3H; CH_2BCH_3).

^{11}B NMR (160.5 MHz, THF-d_8): δ = −11.7 (s; BC), −15.4 (s; BCH_2).

^{13}C{^{1}H} NMR (125.8 MHz, THF-d_8): δ = 171.7 (q, ^1J(B,C) = 44 Hz; C-e), 169.5 (n.r.; C-f), 165.0 (Ph-C-*i*), 131.6 (Ph-C-*o*), 129.7 (C-a), 126.8 (C-d), 124.6 (Ph-C-*m*), 120.9 (C-b), 120.8 (C-c), 118.9 (Ph-C-*p*), 51.5 (q, ^1J(B,C) = 37 Hz; CH_2), 4.6 (q, ^1J(B,C) = 45 Hz; CH_2BCH_3), 2.1 (n.r.; $CBCH_3$); n.o. (CPh_2).

Ethylene and Li_2[4]

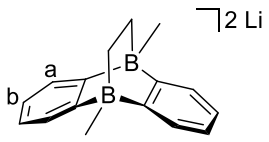

Li_2[**11**]

An NMR tube, charged with a solution of freshly prepared Li_2[**4**] (74 µmol) in THF-d_8 (0.5 mL; see 1.1), was connected to a Schlenk line. The solution was frozen with liquid nitrogen, the system evacuated, and ethylene (1 atm; quality grade > 99.95% GC) was filled in. The content of the NMR tube was allowed to warm to room temperature and the excess pressure released through a Hg bubbler. After 10 min, the reaction mixture was frozen again, the NMR tube was evacuated and flame-sealed. After storage of the sample at room temperature for 3 h, NMR spectroscopy revealed the immediate and quantitative consumption of Li_2[**4**] and the selective formation of the cycloadduct Li_2[**11**]. X-ray-

quality crystals of [Li(12-c-4)(thf)][Li(12-c-4)][**11**] were obtained by gas-phase diffusion of *n*-hexane into a THF/12-crown-4 solution of Li_2[**11**].

^{1}H NMR (500.2 MHz, THF-d_8): δ = 7.28 (n.r., 4H; H-a), 6.60–6.59 (m, 4H; H-b), 0.15 (n.r., 6H; BCH_3), –0.30 (n.r., 4H; CH_2).

^{11}B NMR (160.5 MHz, THF-d_8): δ = –15.2.

^{13}C{^{1}H} NMR (125.8 MHz, THF-d_8): δ = 170.8–169.6 (m; BC), 127.2 (C-a), 120.6 (C-b), 25.2–24.4 (m; CH_2), 5.5–4.3 (m; BCH_3).

1,2-Diphenylacetylene and Li_2[4]

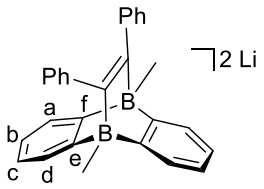

Neat 1,2-diphenylacetylene (13 mg, 74 µmol) was added at room temperature to Li_2[**4**], freshly prepared from **4** (15 mg, 74 µmol) and excess lithium granules in THF-d_8 (0.5 mL; see 1.1). The mixture was transferred to an NMR tube and the tube was flame-sealed. NMR spectroscopy revealed the immediate and quantitative consumption of 1,2-diphenylacetylene and the selective formation of an cycloadduct. X-ray-quality crystals of this cycloadduct were obtained by gas-phase diffusion of *n*-hexane into its THF/12-crown-4 solution. The structure is deposited with the CCDC and can be accessed via the following code: 1888739.

^{1}H NMR (500.2 MHz, THF-d_8): δ = 7.31–7.30 (m, 4H; H-a), 6.67–6.64 (m, 4H; Ph-H-*m*), 6.56–6.54 (m, 4H; Ph-H-*o*), 6.55–6.51 (m, 4H; H-b), 6.49–6.46 (m, 2H; Ph-H-*p*), 0.26 (s, 6H; BCH_3).

^{11}B NMR (160.5 MHz, THF-d_8): δ = –13.3 (s).

^{13}C{^{1}H} NMR (125.8 MHz, THF-d_8): δ = 170.9 (n.r.; BC), 168.5 (n.r.; C=C), 154.9 (Ph-C-*i*), 130.2 (Ph-C-*o*), 126.9 (C-a), 125.7 (Ph-C-*m*), 120.4 (Ph-C-*p*), 120.0 (C-b), 2.1 (n.r.; BCH_3).

Influence of the counter cation on the hydrogenation step

A comparison of Li_2[**4**] and Na_2[**4**] as catalysts for the hydrogenation of Ph(H)C=N*t*Bu reveals four distinct differences (Figure S5):

1. The cycloaddition product [**10**]$^{2-}$ of [**4**]$^{2-}$ and Ph(H)C=N*t*Bu is only observable with Li^+ as the counter cation (*cf.* Figures S5a *vs.* S5c). The strong Lewis acid Li^+ is likely required to promote cycloaddition by means of imine coordination.

2. Due to the reversibility of the cycloaddition process, the reaction mixture – after storage at 100 °C for 16 h – contains no Li_2[**10**] but exclusively Li_2[**4**] and amine $Ph(H)_2C–N(H)tBu$ (*cf.* Figure S5b).

3. Given that H_2 activation is much slower with Li_2[**4**] than with Na_2[**4**], the former reaction mixture contains mainly M_2[**4**] and only little M_2[**4**-H_2], whereas the opposite is true for the latter (after 16 h at 100 °C; *cf.* Figures S5b *vs.* S5d).

4. Hydrogenation of Ph(H)C=N*t*Bu occurs much faster using Li_2[**4**] than Na_2[**4**], even though the H_2-activation step is slower with the Li^+ than with the Na^+ salt.

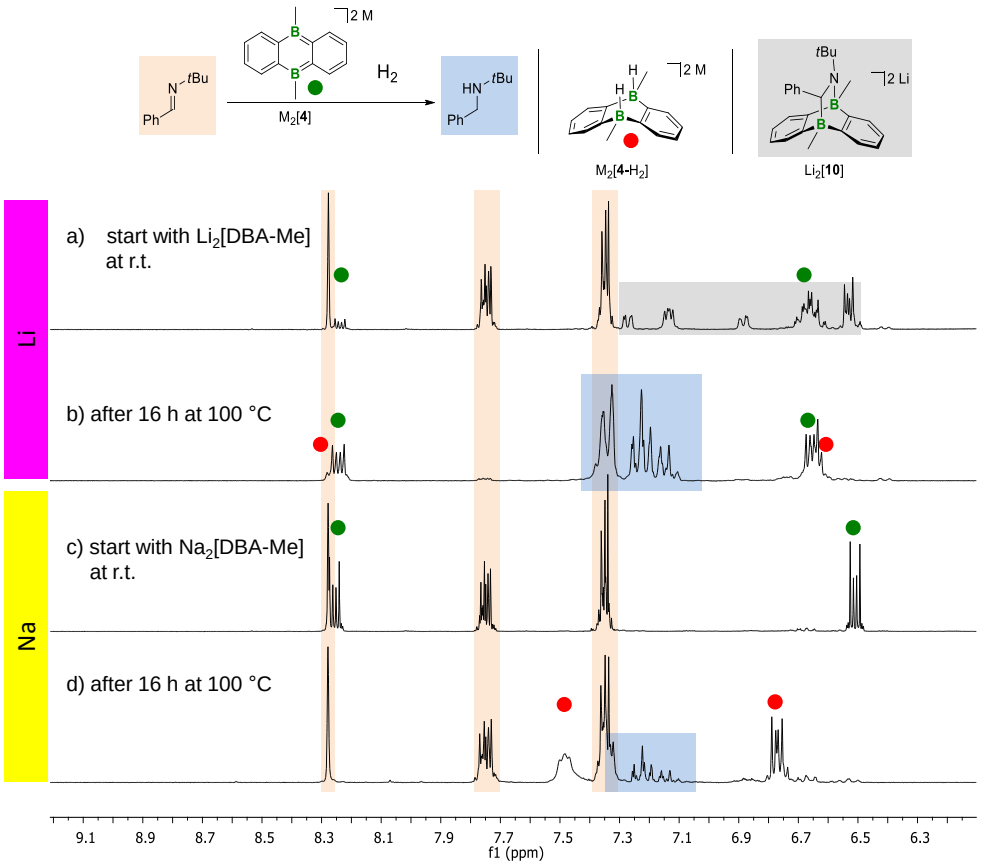

Figure S5. Comparison of the hydrogenation of Ph(H)C=N*t*Bu with Li_2[**4**] (a+b) or Na_2[**4**] (c+d) as the catalyst (THF-d_8). ^{1}H NMR spectra recorded on a mixture of Ph(H)C=N*t*Bu, Li_2[**4**], and excess H_2 immediately after sample preparation (a, 300.0 MHz) and after 16 h at 100 °C (b, 250.1 MHz). ^{1}H NMR spectra recorded on a mixture of Ph(H)C=N*t*Bu, Na_2[**4**], and excess H_2 immediately after sample preparation (a, 300.0 MHz) and after 16 h at 100 °C (b, 250.1 MHz).

4. Hydride-transfer reactions with Na_2[4-H_2]

It is conceivable that the hydride transfer from Na_2[**4**-H_2] to substrates R_nECl proceeds in a stepwise manner *via* an intermediate hydride monoadduct Na[**4**-H]. We therefore treated Na_2[**4**-H_2] with either 1 or 2 equiv Et_3SiCl.

4.1 Reaction of Na_2[4-H_2] with 1 equiv of Et_3SiCl

The reaction was performed at room temperature in THF-d_8 solution in an NMR tube: Na_2[**4**-H_2] (0.060 mmol), Et_3SiCl (10 µL, 9.0 mg, 0.060 mmol).

^{1}H NMR (500.2 MHz, THF-d_8): δ = 8.05 (n.r., 2H; C_6H_4), 7.75 (n.r., 2H; C_6H_4), 7.19 (n.r., 2H; C_6H_4), 7.01 (n.r., 2H; C_6H_4), 2.32 (q, ^1J(B,H) = 69.8 Hz, 1H; BH), 1.32 (s, 3H; Me), 0.01 (s, 3H; Me).
^{11}B NMR (160.5 MHz, THF-d_8): δ = 62.5 ($h_{1/2}$ = 820 Hz), −17.6 (d, ^1J(B,H) = 69.8 Hz).

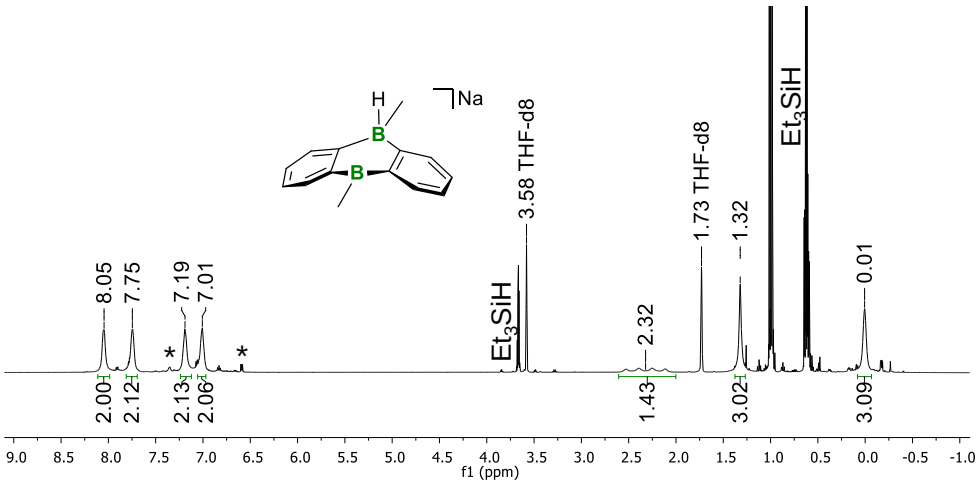

Figure S6. ^{1}H NMR spectrum of the reaction mixture Na_2[**4**-H_2]/1 Et_3SiCl (500.2 MHz, THF-d_8). Asterisks mark resonances of the starting material Na_2[**4**-H_2].

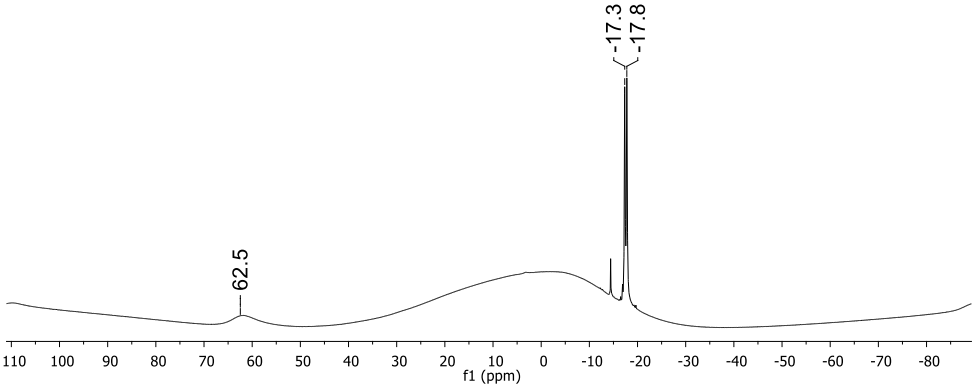

Figure S7. ^{11}B NMR spectrum of the reaction mixture Na_2[**4**-H_2]/1 Et_3SiCl (160.5 MHz, THF-d_8).

The structural motif of Na[**4**-H] with one tetracoordinated and one trigonal-planar boron atom is already known for other DBA derivatives (compare crystal structures with the following CSD codes: IBUTAC, IBUTEG, IBUTOQ, IBUVAE, XITREA, XITRIE, XITROK, XITRUQ, XITSAX, XUQHAS).

4.2 Reaction of Na_2[**4**-H_2] with 2 equiv of Et_3SiCl; perspectives for a catalytic cycle

The aimed-for accumulation of Et_3SiH over multiple catalytic cycles as described in the main text requires a stepwise procedure in order to avoid side reactions between Et_3SiCl and Na_2[**4**] or sodium metal.

1) Twofold reduction of **4** (as described in 1.1) using elemental sodium in THF-d_8.

Comment: The use of NMR tubes as reaction vessels limited the amount of Na_2[**4**] to 0.074 mmol because otherwise the available volume of H_2 is not sufficient to convert all of the starting material to Na_2[**4**-H_2].

2) Transfer of the THF-d_8 solution of Na_2[**4**] to an NMR tube and addition of H_2 following the procedure described in 1.1. Heating of the reaction mixture to 100 °C for 18 h so that no unreacted Na_2[**4**] remained.

3) Transfer of the resulting THF-d_8 solution of Na_2[**4**-H_2] to a new NMR tube and addition of 2 equiv of Et_3SiCl (24 µL, 22 mg, 0.143 mmol). The hydride-transfer reaction is completed within minutes and accompanied by the precipitation of NaCl (*cf.* Figure S10 for an X-ray powder diffractogram of the precipitate).

4) Repetition of the steps 1) – 3) in the presence of Et_3SiH, which has no effect on the reaction cascade. *Comment:* As a proof of concept, we have successfully repeated this protocol three times.

Et_3SiCl → Et_3SiH

^{1}H NMR (500.2 MHz, THF-d_8): δ = 3.66 (n.r., 1H; Et_3SiH), 0.99 (t, ^3J(H,H) = 7.9 Hz, 9H; $(H_3CH_2C)_3SiH$), 0.62 (dq, ^3J(H,H) = 7.9 Hz, ^3J(H,H) = 3.0 Hz, 6H; $(H_3CH_2C)_3SiH$).

^{29}Si NMR (99.4 MHz, THF-d_8): δ = 0.3 (d, ^1J(Si,H) = 178 Hz; Et_3SiH).

The ^{29}Si NMR shift is in accordance with the literature: δ = 0.2 (^1J(Si,H) = 179 Hz).[13]

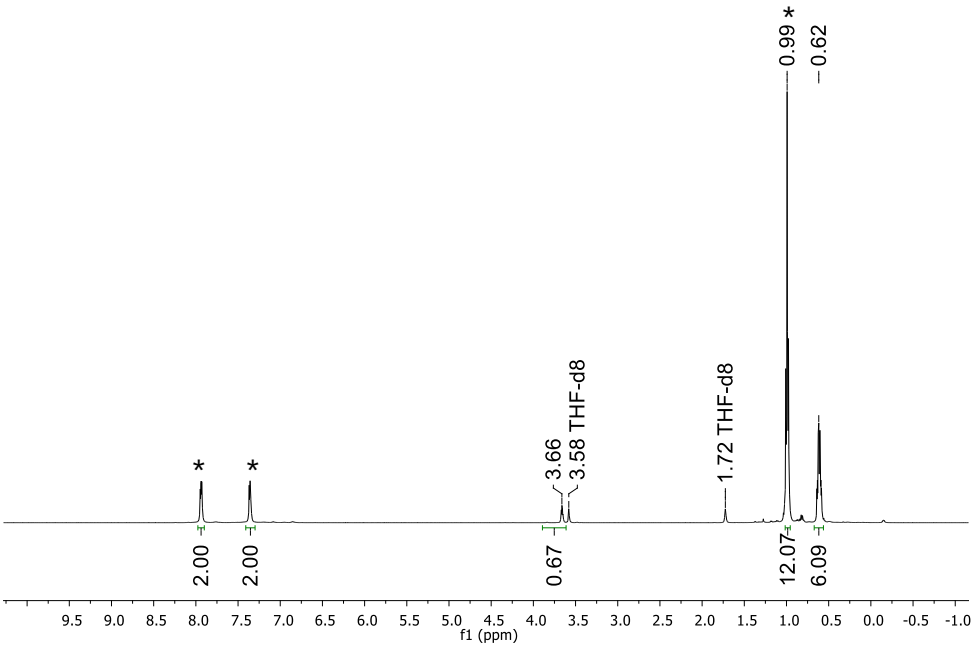

Figure S8. ^{1}H NMR spectrum (500.2 MHz, THF-d_8) recorded after the reaction between Na_2[**4**-H_2] and Et_3SiCl to give Et_3SiH and **4** (*).

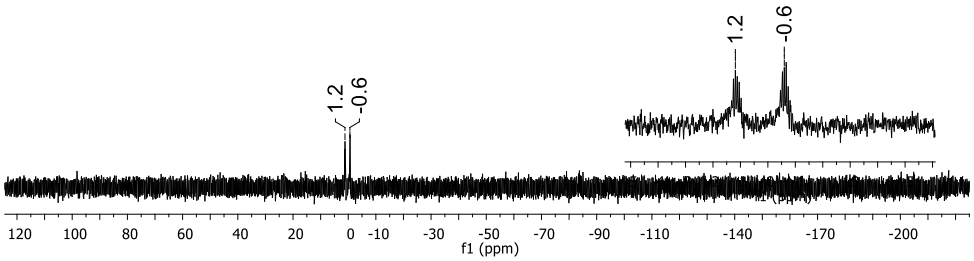

Figure S9. ^{29}Si NMR spectrum (99.4 MHz, THF-d_8) recorded after the reaction between Na_2[**4**-H_2] and Et_3SiCl to give Et_3SiH and **4**.

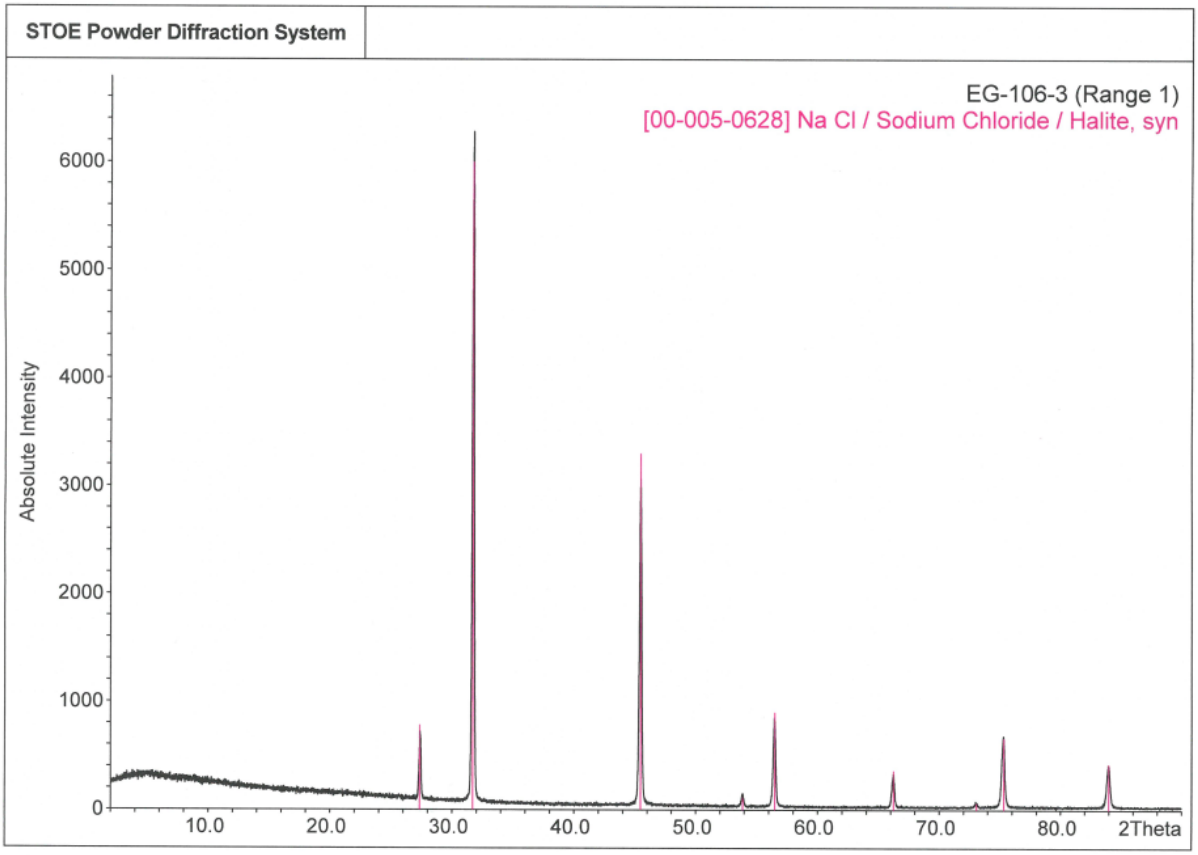

Figure S10. X-ray powder diffraction pattern of the NaCl precipitate from the reaction between Na_2[**4**-H_2] and Et_3SiCl (black: experiment, red: simulation).

In a second experiment, two cycles 1)-4) (see above) were conducted. A sealed glass capillary containing Me_4Si and THF-d_8 served as an internal reference in order to determine the yield of Et_3SiH. In Figure S11, the proton-integral value of the CH_2 groups of Et_3SiH are compared to the normalized integral value of the internal standard. As expected, the amount of Et_3SiH doubled from the first to the second cycle. The amount of the catalyst **4** remained unchanged, as proven by the integral ratios.
Comment: A perfectly equimolar stoichiometry between Na_2[**4**-H_2] and Et_3SiCl was not achieved in the 2nd cycle; the black square in Figure S11 indicates small amounts of still unreacted Et_3SiCl.

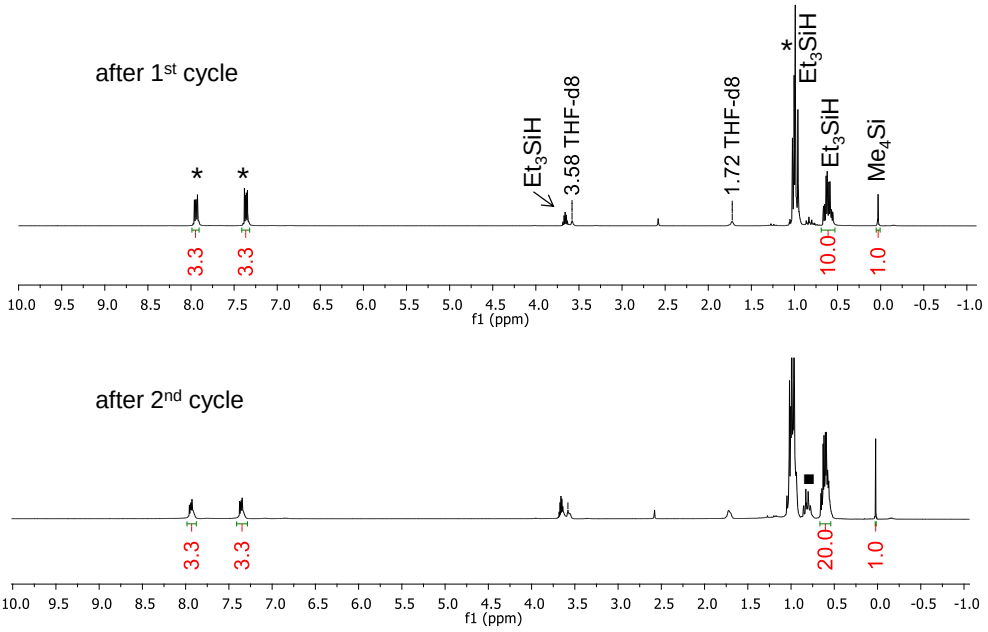

Figure S11. ^{1}H NMR spectra recorded on the reaction mixture Na_2[**4**-H_2]/Et_3SiCl (top: 250.1 MHz, bottom: 300.0 MHz; THF-d_8). Asterisks mark resonances of Na_2[**4**] and the black square indicates remaining Et_3SiCl.

4.3 Reaction between Et_3SiCl and Na_2[4]

As discussed in the main article, Et_3SiCl should not directly encounter the dianion Na_2[**4**] in order to avoid unwanted side reactions. In the following, this issue is assessed in more detail.

As shown in Figure S12, the cathodic peak potential for the reduction of Et_3SiCl amounts to E^{pc} = –1.3 V (*vs.* FcH/FcH^+) and is thus more anodic than $E_{1/2}$ of **4** (*cf.* Table S4). Na_2[**4**] should therefore be capable of reducing Et_3SiCl.

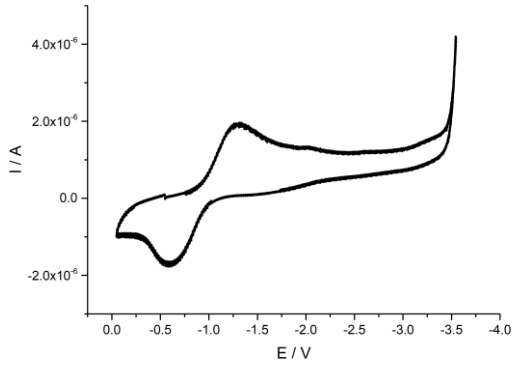

Figure S12. Cyclic voltammogram of Et_3SiCl in THF (*vs.* FcH/FcH^+, room temperature, supporting electrolyte: [*n*-Bu_4N][PF_6] (0.1 M), scan rate 200 mV s^{-1}).

An ^1H NMR spectrum recorded on a stoichiometric mixture of Na_2[**4**] and Et_3SiCl 15 min after sample preparation showed substantially broadened Na_2[**4**] resonances (Figure S13). This indicates an interaction between both components, but at this point no new resonances had emerged.

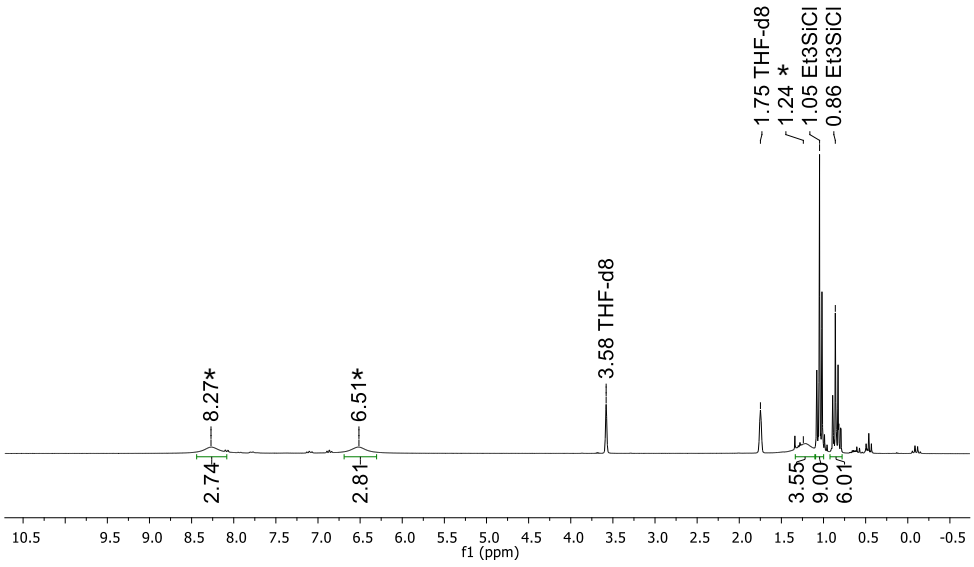

Figure S13. ^1H NMR spectrum (250.1 MHz, THF-d_8) recorded 15 min after the addition of Et_3SiCl to the solution of Na_2[**4**] (1:1). Asterisks mark the broadened resonances of Na_2[**4**].

After storage of the sample for 2 d at room temperature, a colorless precipitate had formed and NMR signals assignable to the silylborate [MeB-(oC$_6$H$_4$)$_2$-B(Me)SiEt$_3$]$^-$ had appeared (two stereoisomers with Et$_3$Si in axial or equatorial positions).

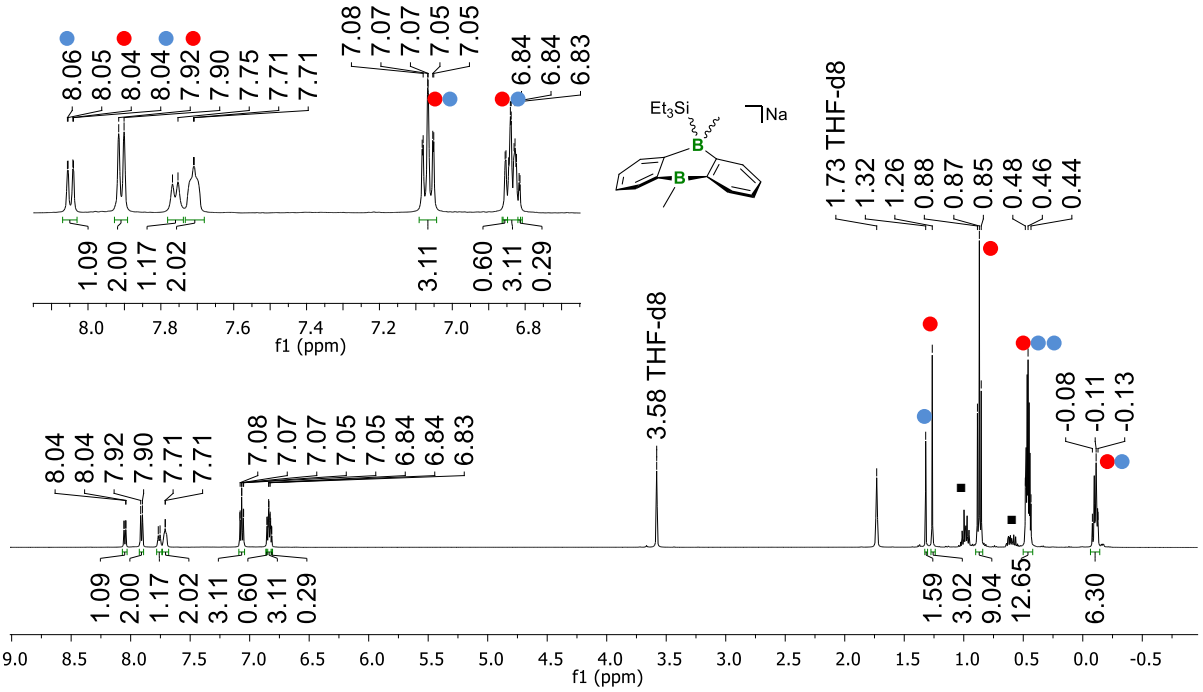

Figure S14. ^{1}H NMR spectrum (500.2 MHz, THF-d_8) recorded 2 d after the addition of Et$_3$SiCl to the solution of Na$_2$[**4**] (1:1). Red and blue dots indicate the resonances of the two stereoisomers of [MeB-(oC$_6$H$_4$)$_2$-B(Me)SiEt$_3$]$^-$; squares mark resonances of residual Et$_3$SiCl.

The NMR data below referring to the major component are colored in red, the one of the minor component in blue. Note: The major:minor integral ratio was approx. 2:1.

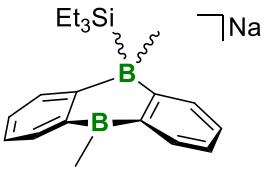

^{1}H NMR (500.2 MHz, THF-d_8): δ = 8.06–8.04 (m, 2H; H-d), 7.92–7.90 (m, 2H; H-d), 7.77–7.75 (m, 2H; H-a), 7.71 (n.r., 2H; H-a), 7.08–7.05 (m, 2H; H-b/2H; H-b), 6.85–6.83 (m, 2H; H-c), 6.84–6.81 (m, 2H; H-c), 1.32 (s, 3H; BC*H*$_3$), 1.26 (s, 3H; BC*H*$_3$), 0.87 (t, ^3J(H,H) = 7.9 Hz, 9H; CH$_2$C*H*$_3$), 0.48–0.44 (m, 6H+12H; C*H*$_2$CH$_3$, CH$_2$C*H*$_3$, SiBC*H*$_3$), –0.08–(–0.13) (m, 3H+6H; C*H*$_2$CH$_3$, SiBC*H*$_3$).

^{11}B NMR (96.3 MHz, THF-d_8): δ = 59.0 (br), –15.3, –16.6.

^{13}C{^{1}H} NMR (125.8 MHz, THF-d_8): δ = 182.8 (q, ^1J(C,B) = 48 Hz; C-f), 177.5 (q, ^1J(C,B) = 48 Hz; C-f), 145.0 (C-e), 144.2 (C-e), 134.8 (C-d), 134.1 (C-d), 132.8 (C-a), 132.2 (C-a), 128.7 (C-b), 127.3 (C-b), 120.7 (C-c), 119.3 (C-c), 14.1 (q, ^1J(C,B) = 41 Hz, SiBCH$_3$), 9.0 (CH$_2$*C*H$_3$), 7.0 (CH$_2$*C*H$_3$), 5.0 (*C*H$_2$CH$_3$), 4.9 (BCH$_3$), 4.9 (q, ^1J(C,B) = 43 Hz; SiBCH$_3$), 4.0 (BCH$_3$), 3.3 (*C*H$_2$CH$_3$).

^{29}Si NMR (99.4 MHz, THF-d_8): δ = 14.8, –2.6.

4.4 Reaction between $Na_2[4\text{-}H_2]$ and Me_2SiCl_2

The reaction between $Na_2[\mathbf{4}\text{-}H_2]$ and Me_2SiCl_2 (1:1; THF-d_8) resulted in the clean formation of **4** and Me_2SiH_2 (Figure S16a). If 2 equiv of Me_2SiCl_2 were employed, the primary product was not $Me_2Si(H)Cl$, but an equimolar mixture of Me_2SiH_2 and Me_2SiCl_2. Over several days, however, the free Lewis acid **4** catalyzes a comproportionation reaction furnishing $Me_2Si(H)Cl$ as the final product.

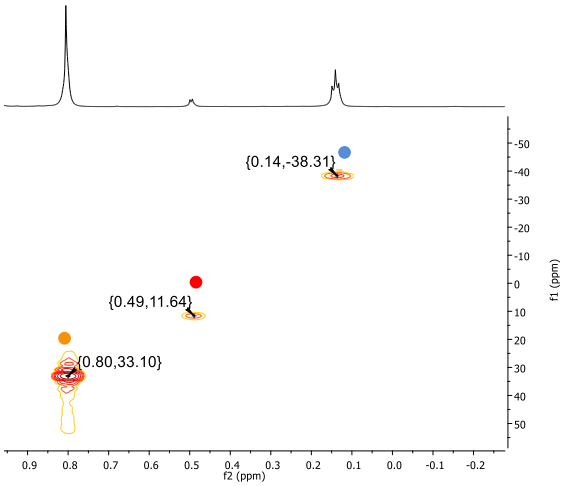

Figure S15. $^{29}Si/^{1}H$ HMBC-NMR spectrum of the reaction mixture $Na_2[\mathbf{4}\text{-}H_2]/Me_2SiCl_2$, recorded after the sample had been kept at room temperature for 5 h (500.2 MHz, THF-d_8). Orange: Me_2SiCl_2, red: $Me_2Si(H)Cl$, blue: Me_2SiH_2.

The conversion $Me_2SiCl_2 + Me_2SiH_2 \rightarrow 2\ Me_2Si(H)Cl$ can be accelerated by heating the sample to 120 °C and is almost quantitative after 16 h at this temperature (Figure S16b).

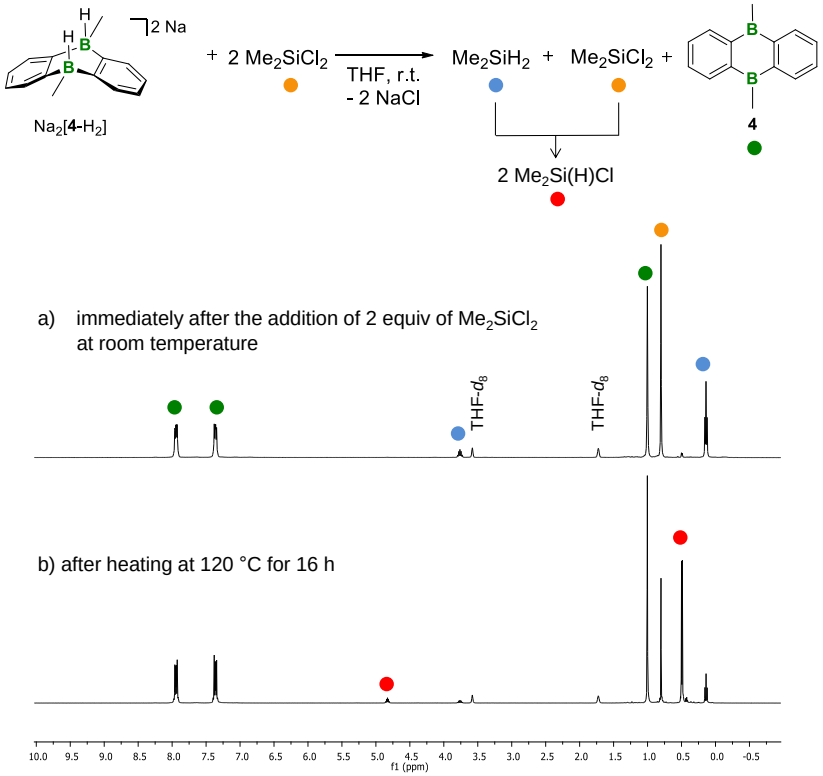

Figure S16. ^{1}H NMR spectra (250.1 MHz, THF-d_8) (a) of the reaction mixture $Na_2[\mathbf{4}\text{-}H_2]/2\ Me_2SiCl_2$ immediately after sample preparation and (b) after the sample had been kept at 120 °C for 16 h.

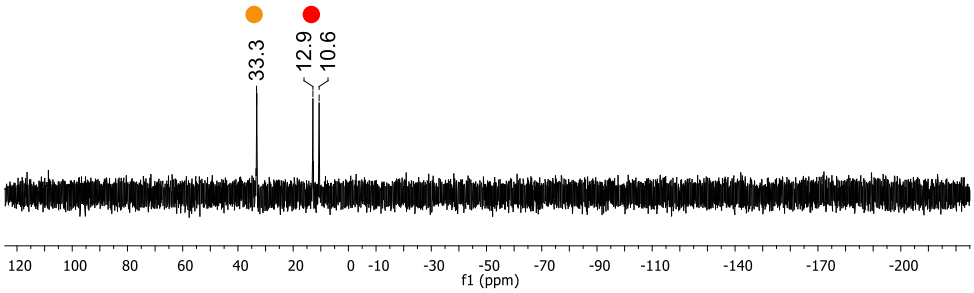

Figure S17. ^{29}Si NMR spectrum (99.4 MHz, THF-d_8) corresponding to sample (b) in Figure S16.

Published ^{29}Si NMR shifts for comparison:[13]
Me_2SiCl_2 $\delta = 32.0$
$Me_2Si(H)Cl$ $\delta = 11.1$
Me_2SiH_2 $\delta = -37.7$ (^1J(Si,H) = 179 Hz)

4.5 Substrate scope of the hydride-transfer reaction

General procedure

The respective substrate was added to an NMR tube containing M_2[**A**-H_2] (preparation described in 1.1) in THF-d_8 (0.5 mL). After mixing the components by shaking the NMR tube, the sample was flame-sealed. Table S3 summarizes the stoichiometries used in this screening process. Each reaction was accompanied by the formation of a colorless precipitate and complete within minutes (according to ^{1}H NMR spectroscopy). *Note*: Similar to the case of Me_2SiCl_2 (see above), we always observed the exclusive formation of exhaustively hydrogenated products, even if an excess of the halogenated substrate was used.

Table S3. [**A**]$^{2-}$ derivatives and substrates investigated for the hydride-transfer reaction.

DBA derivative			**substrate**				**product**
compound	*n* / mmol	equiv	compound	*n* / mmol	equiv	*V* / µL	
Li_2[**1**-H_2]	0.028	1	Me_3SiCl	0.056	2	7.1	Me_3SiH
K_2[**1**-H_2]	0.015	1	Me_3SiCl	0.030	2	3.8	Me_3SiH
Na_2[**4**-H_2]	0.050	1	Ph_2SiCl_2	0.050	1	10.5	Ph_2SiH_2
Na_2[**4**-H_2]	0.050	1	$SiCl_4$	0.025	0.5	2.9	SiH_4
Na_2[**4**-H_2]	0.050	1	$GeCl_4$	0.025	0.5	2.9	GeH_4
Na_2[**4**-H_2]	0.058	3	PCl_3	0.039	2	3.4	PH_3
Na_2[**4**-H_2]	0.050	1	EtBr	0.100	2	7.5	EtH

$Me_3SiCl \rightarrow Me_3SiH$

^{1}H NMR (500.2 MHz, THF-d_8): δ = 3.95 (m, 1H; $Me_3Si\mathit{H}$), 0.08 (d, ^3J(H,H) = 3.6 Hz, 9H; Me_3SiH).

^{29}Si-INEPT NMR (99.4 MHz, THF-d_8): δ = –17.1 (Me_3SiH).

The ^{29}Si NMR shift is in accordance with the literature: δ = –16.3.[13]

$Ph_2SiCl_2 \rightarrow Ph_2SiH_2$

^{1}H NMR (500.2 MHz, THF-d_8): δ = 7.41–7.33 (m, 10H; Ph_2SiH_2), 4.90 (s, 2H; $Ph_2Si\mathit{H}_2$).

^{29}Si NMR (99.4 MHz, THF-d_8): δ = –33.9 (t, ^1J(Si,H) = 199 Hz; Ph_2SiH_2).

The ^{29}Si NMR shift is in accordance with the literature: δ = –33.8 (^1J(Si,H) = 200 Hz).[13]

$SiCl_4 \rightarrow SiH_4$

^{1}H NMR (400.1 MHz, THF-d_8): δ = 3.18 (s; $Si\mathit{H}_4$).

The ^{1}H NMR shift is in accordance with the literature (THF-d_8): δ = 3.14.[14]

^{29}Si NMR (99.4 MHz, THF-d_8): δ = –96.3 (q, ^1J(Si,H) = 200 Hz; SiH_4).

The ^{29}Si NMR shift is in accordance with the literature: δ = –93.1 (^1J(Si,H) = 202 Hz).[13]

$GeCl_4 \rightarrow GeH_4$

^{1}H NMR (400.1 MHz, THF-d_8): δ = 3.14 (s; $Ge\mathit{H}_4$).

The ^{1}H NMR shift is in accordance with the literature (CCl_4): δ = 3.27.[15]

$PCl_3 \rightarrow PH_3$

^{1}H NMR (400.1 MHz, THF-d_8): δ = 1.76 (d, ^1J(P,H) = 186 Hz; $P\mathit{H}_3$).

The ^{1}H NMR shift is in accordance with the literature (acetonitrile): τ = 8.21 ($\triangleq$ δ = 1.79, ^1J(P,H) = 189 Hz).[16]

^{31}P{^{1}H} NMR (121.5 MHz, THF-d_8): δ = –247.4 (q, ^1J(P,H) = 186 Hz; PH_3).

The ^{31}P NMR shift is in accordance with the literature (THF): δ = –245.4.[17]

EtBr $\rightarrow$ C_2H_6

^{1}H NMR (500.2 MHz, THF-d_8): $\delta = 0.85$ (s; C_2H_6).

^{13}C{^{1}H} NMR (125.8 MHz, THF-d_8): $\delta = 6.4$ (C_2H_6).

The ^{1}H and ^{13}C{^{1}H} NMR shifts are in accordance with the literature.[1]

Procedure for the reduction of CO_2

An NMR tube, charged with a solution of Na_2[**4**-H_2] (0.059 mmol) in THF-d_8 (0.5 mL), was connected to a Schlenk line. The solution was frozen with liquid nitrogen, the system evacuated, and CO_2 (1 atm; quality grade 4.5) was filled in. The content of the NMR tube was allowed to warm to room temperature and the excess pressure released through a Hg bubbler. After 10 min, a precipitate had formed. The reaction mixture was frozen again, the NMR tube was evacuated, flame-sealed, and investigated by NMR spectroscopy. Afterwards, the liquid phase was discarded and the precipitate characterized by IR and NMR spectroscopy (in D_2O).

The mother liquor showed NMR signals assignable to a weak formate adduct.

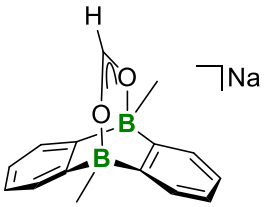

^{1}H NMR (500.2 MHz, THF-d_8): δ = 8.00 (s, 1H; HCOO), 7.79–7.77 (m, 4H; H-a), 7.17–7.15 (m, 4H; H-b), 0.72 (s, 6H; CH_3).

^{11}B NMR (160.5 MHz, THF-d_8): δ = 34.7 ($h_{1/2}$ = 750 Hz).

^{13}C{^{1}H} NMR (125.8 MHz, THF-d_8): δ = 171.6 (HCOO), 155.7 (BC), 133.5 (C-a), 127.6 (C-b), 9.4 (CH_3).

Note: Attempts at the crystallization of the formate adduct gave crystals of the free Lewis acid **4**.

NMR data of the precipitated sodium formate (*Note*: 1 equiv of Na_2[**4**-H_2] is sufficient to produce 2 equiv of sodium formate):

^{1}H NMR (500.2 MHz, D_2O): δ = 8.44 (HCOO).

^{13}C{^{1}H} NMR (125.8 MHz, D_2O): δ = 171.0 (HCOO).

The ^{13}C NMR shift is in accordance with the literature: 171.0 ppm.[18]

ATR-IR data of the precipitated sodium formate: 2830, 1587, 1363, 775 cm^{-1}.

Literature data (KBr): 2831, 1611, 1362, 775 cm^{-1}.[19]

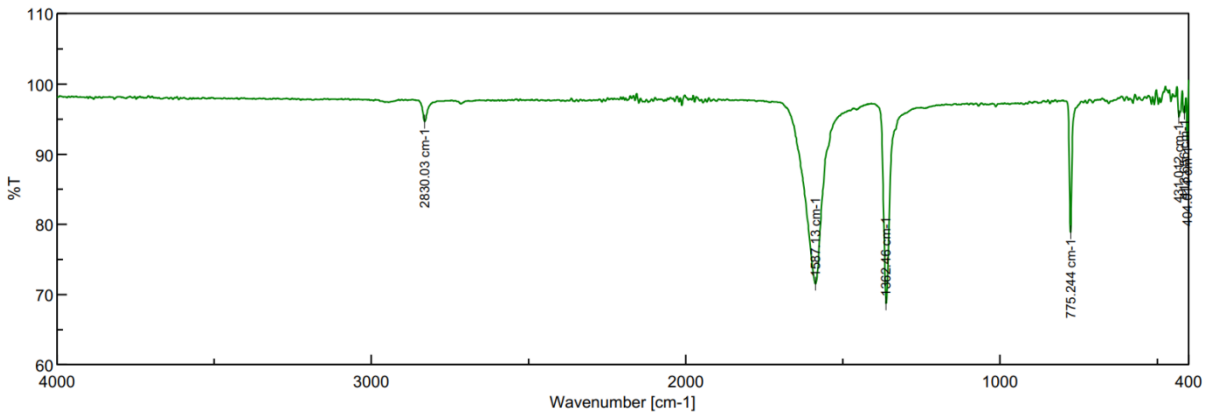

Figure S18. ATR-IR spectrum of the sodium formate obtained from the reaction between Na_2[**4**-H_2] and CO_2.

5. Cyclic voltammetry measurements

Table S4. Electrochemical data obtained by cyclic voltammetry (*vs.* FcH/FcH^+; red1 = first reduction event, red2 = second reduction event, pc = peak current).

DBA derivative	$E_{1/2}$, red1 (V)	$E_{1/2}$, red2 (V)	E^{pc}, red2 (V)
1	−2.08	–	−2.75
2	−1.66	−2.32	–
4	−2.02	–	−2.77
5	−2.01	–	−2.74
7	−1.80	–	−2.48
8	−1.90	–	−2.71

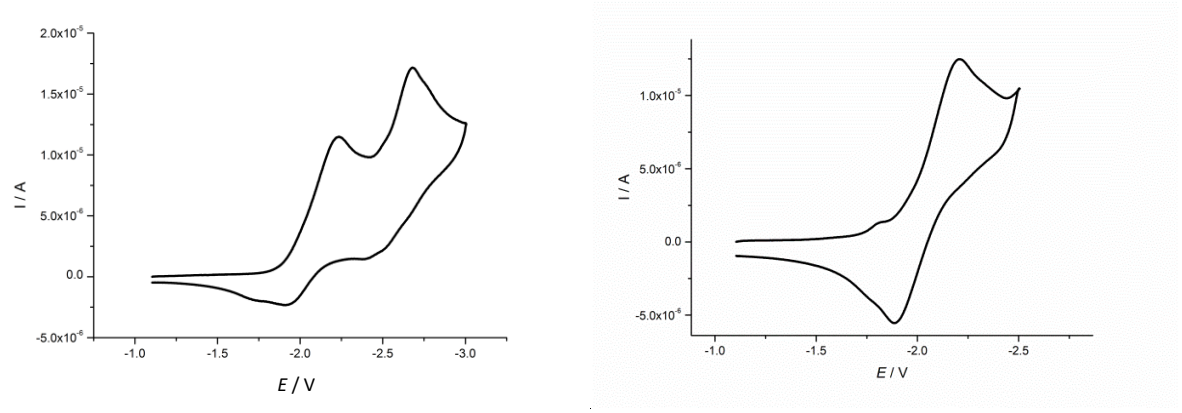

Figure S19. Cyclic voltammograms of **1** in THF (*vs.* FcH/FcH^+, room temperature, supporting electrolyte: [*n*-Bu_4N][PF_6] (0.1 M), scan rate 200 mV s^{-1}). Left: Full voltammogram; right: first redox event only.

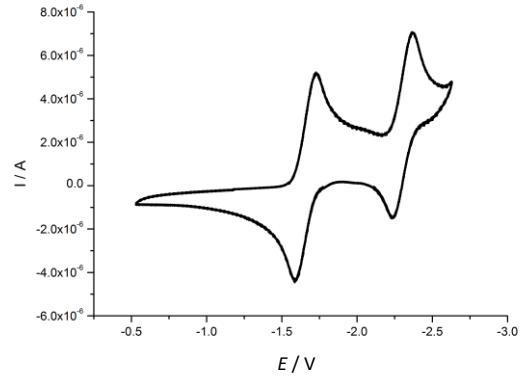

Figure S20. Cyclic voltammogram of **2** in THF (*vs.* FcH/FcH^+, room temperature, supporting electrolyte: [*n*-Bu_4N][PF_6] (0.1 M), scan rate 200 mV s^{-1}).

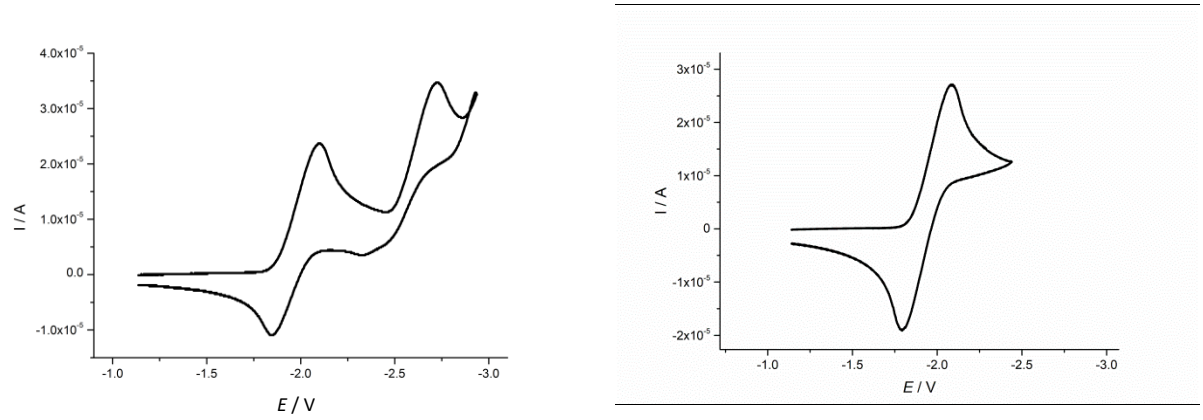

Figure S21. Cyclic voltammograms of **4** in THF (*vs.* FcH/FcH$^+$, room temperature, supporting electrolyte: [*n*-Bu$_4$N][PF$_6$] (0.1 M), scan rate 200 mV s^{-1}). Left: Full voltammogram; right: first redox event only.

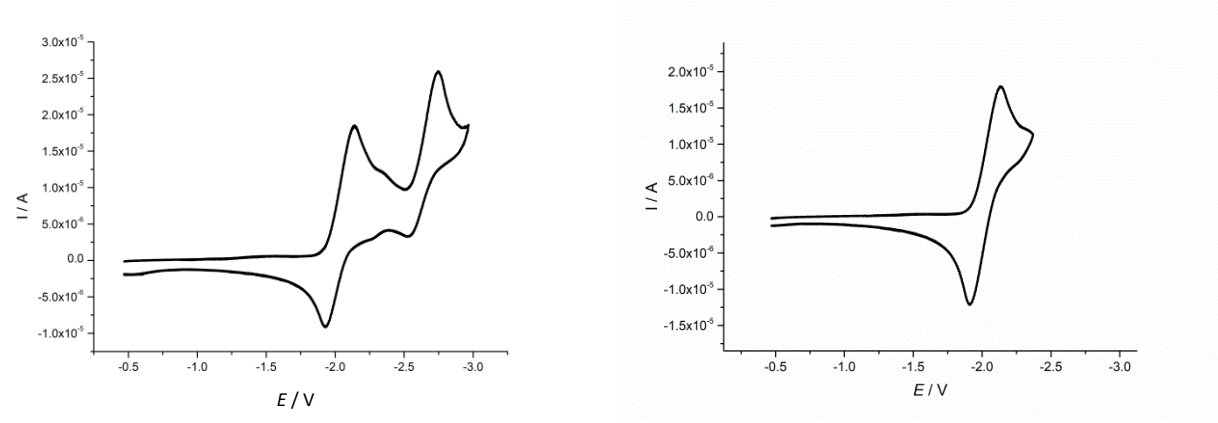

Figure S22. Cyclic voltammograms of **5** in THF (*vs.* FcH/FcH$^+$, room temperature, supporting electrolyte: [*n*-Bu$_4$N][PF$_6$] (0.1 M), scan rate 200 mV s^{-1}). Left: Full voltammogram; right: first redox event only.

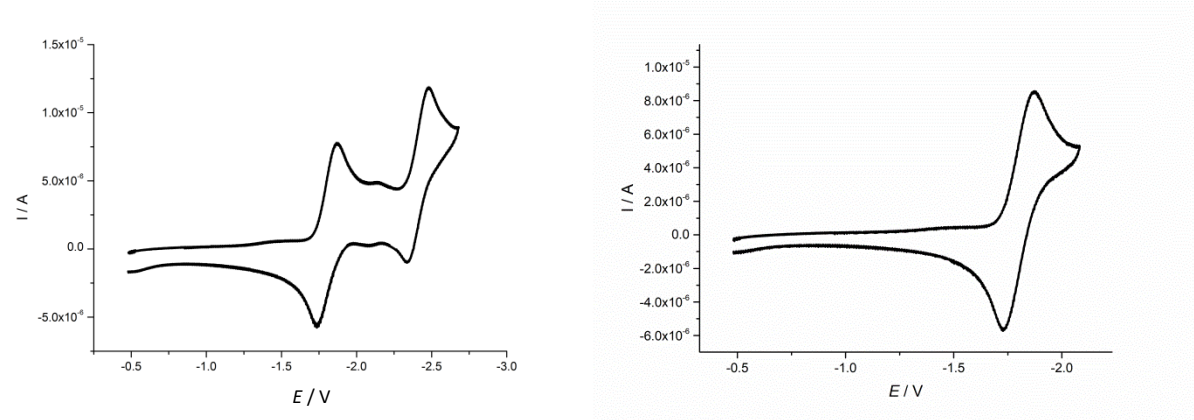

Figure S23. Cyclic voltammograms of **7** in THF (*vs.* FcH/FcH$^+$, room temperature, supporting electrolyte: [*n*-Bu$_4$N][PF$_6$] (0.1 M), scan rate 200 mV s^{-1}). Left: Full voltammogram; right: first redox event only.

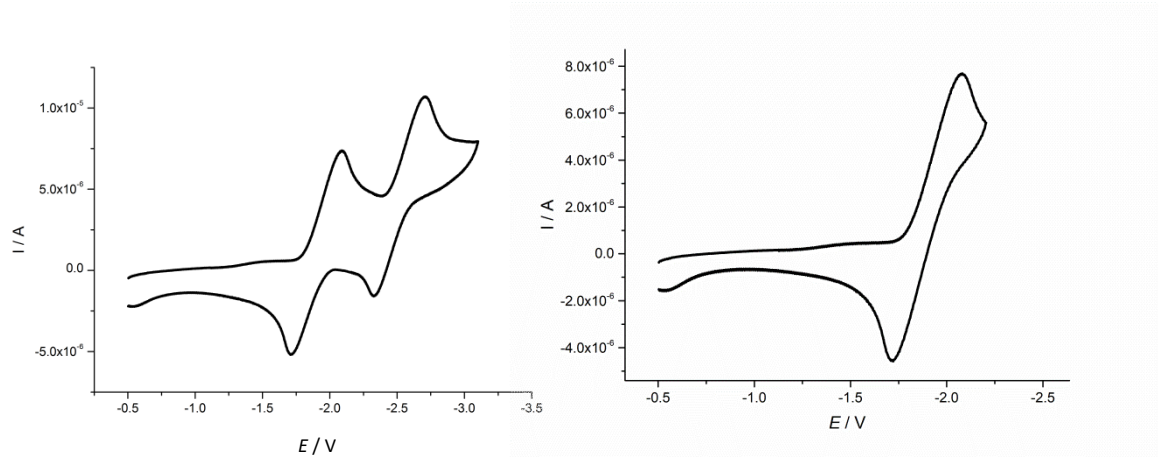

Figure S24. Cyclic voltammograms of **8** in THF (*vs.* FcH/FcH^+, room temperature, supporting electrolyte: [*n*-Bu_4N][PF_6] (0.1 M), scan rate 200 mV s^{-1}).

6. Computational details

Geometry optimizations and frequency calculations were carried out with the Gaussian 09 software package[20] using the B3LYP functional and the 6-31G* basis set in combination with the SMD solvation model[21] (to account for effects of the THF solvent). The stationary points were characterized as minima (no imaginary frequencies in the vibrational analysis).

Table S5. LUMO-energy values of **1**, **2**, **4**, **5**, **7**, **8**, and **9**, as estimated from cyclic voltammetry (E_{LUMO}^{CV}) or computed by DFT (E'_{LUMO}^{DFT}).

Cmpd	E_{LUMO}^{CV} / eV[a]	E'_{LUMO}^{DFT} / eV	E_{LUMO}^{DFT} / eV[b]
1	–2.72	–2.59	–3.12
2	–3.14	–2.59	–3.12
4	–2.78	–2.17	–2.70
5	–2.79	–2.26	–2.79
8	–2.90	–2.42	–2.95
7	–3.00	–2.43	–2.96
9	–2.96[c]	–2.43	–2.96

[a] E_{LUMO}^{CV} = –4.8 eV – $E_{1/2}^{Red1}$ (FcH/FcH^+ = –4.8 eV *vs.* vacuum level).[22]
[b] For better comparability with the E_{LUMO}^{CV} values, the computed LUMO energies (E'_{LUMO}^{DFT}) were scaled by addition of a constant value of –0.53 eV, which corresponds to the difference E_{LUMO}^{CV}(**9**) – E'_{LUMO}^{DFT}(**9**). Compound **9** was selected, because it does not coordinate THF ligands.
[c] Ref.[5].

The electrochemical and computed LUMO-energy levels are directly juxtaposed in Figure S25 for better comparison. We note a pleasingly good correlation, except for the case of **1**. THF ligation is an important perturbative factor only to the least hindered parent DBA, but negligible for its derivatives. In conclusion, cyclic voltammetry is a proper tool to evaluate electronic substituent effects provided that THF ligation is not an issue.

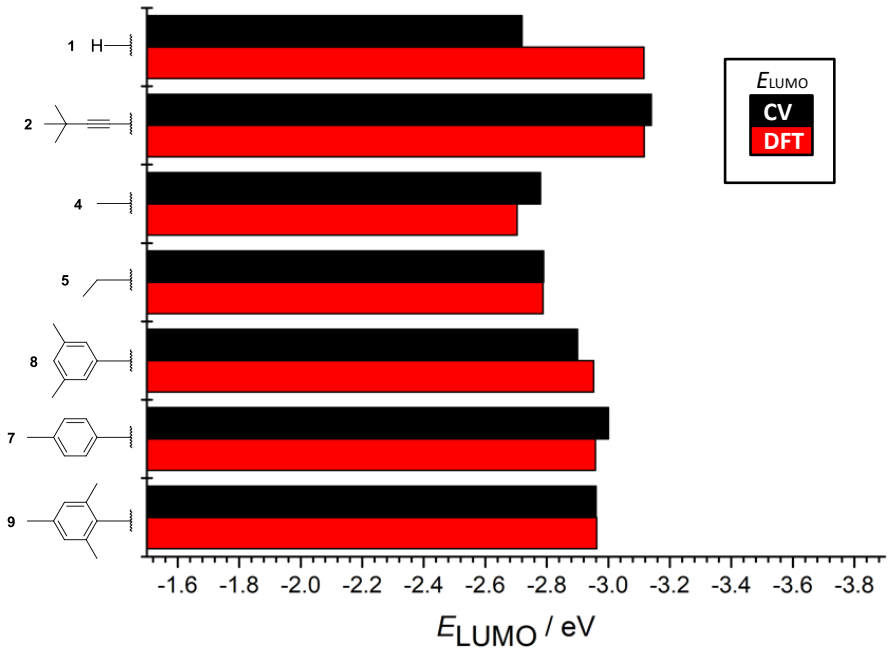

Figure S25. Comparison of the E_{LUMO}^{CV} and E_{LUMO}^{DFT} values of the compounds **1**, **2**, **4**, **5**, **7**, **8**, and **9** (data from Table S5).

1

B	0.000000	-1.482377	0.000291
C	-1.350470	-0.714609	0.000130
C	-2.578127	-1.394479	-0.000022
H	-2.587756	-2.482479	-0.000027
C	-3.792753	-0.697621	-0.000176
H	-4.734007	-1.241607	-0.000295
C	1.350470	-0.714609	0.000130
C	2.578127	-1.394478	-0.000022
H	2.587756	-2.482479	-0.000027
C	3.792753	-0.697621	-0.000176
B	0.000000	1.482377	0.000291
C	1.350470	0.714609	0.000131
H	4.734007	-1.241608	-0.000295
C	2.578127	1.394478	-0.000022
H	2.587756	2.482479	-0.000028
C	3.792753	0.697621	-0.000176
H	4.734007	1.241608	-0.000295
C	-1.350470	0.714609	0.000131
C	-2.578127	1.394479	-0.000022
H	-2.587756	2.482479	-0.000028
C	-3.792753	0.697621	-0.000176
H	-4.734007	1.241607	-0.000295
H	0.000000	2.683826	0.000005
H	0.000000	-2.683826	0.000000

2

B	1.496402	0.002296	-0.000736	B	-1.496401	-0.002293	0.000565
C	0.715583	-1.353161	-0.000545	C	-0.715581	1.353163	0.000339
C	-0.711417	-1.355375	0.000448	C	0.711419	1.355377	-0.000648
C	-1.386444	-2.587850	0.001024	C	1.386446	2.587852	-0.001239
H	-2.473677	-2.597848	0.001817	H	2.473679	2.597850	-0.002021
C	-0.691944	-3.800316	0.000576	C	0.691946	3.800318	-0.000821
H	-1.236861	-4.741167	0.001050	H	1.236863	4.741170	-0.001310
C	0.703923	-3.798127	-0.000551	C	-0.703920	3.798130	0.000300
H	1.251765	-4.737281	-0.000958	H	-1.251762	4.737284	0.000690
C	1.394532	-2.583458	-0.001108	C	-1.394530	2.583460	0.000881
H	2.481794	-2.589629	-0.002018	H	-2.481791	2.589632	0.001796
C	3.019298	0.004476	-0.000235	C	-3.019297	-0.004474	0.000204
C	4.241800	0.006545	0.001422	C	-4.241798	-0.006551	-0.001304
C	5.714036	0.005043	0.001595	C	-5.714037	-0.005044	-0.001362
C	6.212572	-0.561386	-1.349964	C	-6.212440	0.561086	1.350366
H	7.308927	-0.571539	-1.361204	H	-7.308794	0.571151	1.361739
H	5.856849	-1.585686	-1.504907	H	-5.856778	1.585386	1.505451
H	5.866036	0.052021	-2.188782	H	-5.865753	-0.052459	2.189018
C	6.238958	1.446874	0.189615	C	-6.238991	-1.446832	-0.189622
H	7.335563	1.448358	0.189418	H	-7.335596	-1.448296	-0.189326
H	5.895359	2.100474	-0.619695	H	-5.895327	-2.100604	0.619522
H	5.896763	1.870070	1.140405	H	-5.896893	-1.869842	-1.140530
C	6.218862	-0.890418	1.157954	H	-6.218971	0.890669	-1.157479
H	7.315274	-0.900795	1.164296	H	-7.315386	0.900989	-1.163766
H	5.874370	-0.515322	2.127870	H	-5.874506	0.515824	-2.127501
H	5.864910	-1.920780	1.044425	H	-5.865071	1.921022	-1.043715

4

B	-0.00000	-1.50656	-0.19526	C	-2.57172	1.38874	0.10268
C	1.34766	-0.71365	-0.04611	H	-2.59205	2.47587	0.09654
C	2.57167	-1.38875	0.10271	C	-3.77411	0.69751	0.27540
H	2.59203	-2.47587	0.09665	H	-4.70513	1.24442	0.40410
C	3.77408	-0.69750	0.27534	C	0.00001	3.07009	-0.43447
H	4.70511	-1.24441	0.40392	C	1.34765	0.71367	-0.04616
C	0.00014	-3.07008	-0.43445	C	2.57166	1.38879	0.10266
C	-1.34770	-0.71369	-0.04625	H	2.59199	2.47592	0.09656
C	-2.57172	-1.38879	0.10257	C	3.77407	0.69756	0.27531
H	-2.59211	-2.47590	0.09639	H	4.70510	1.24449	0.40386
C	-3.77411	-0.69756	0.27534	H	0.88463	3.43276	-0.97092
H	-4.70513	-1.24448	0.40396	H	0.00050	3.58513	0.54116
H	-0.88489	-3.43325	-0.96987	H	-0.88489	3.43301	-0.97028
B	-0.00004	1.50656	-0.19522	H	0.88462	-3.43269	-0.97118
C	-1.34771	0.71364	-0.04620	H	0.00117	-3.58495	0.54128

5

B	0.000178	-1.485283	0.312034	B	-0.000190	1.485289	-0.312048
C	-1.352272	-0.698977	0.149948	C	1.352261	0.698981	-0.149968
C	-1.352436	0.698602	-0.149954	C	1.352424	-0.698597	0.149938
C	-2.588209	1.355184	-0.290088	C	2.588197	-1.355179	0.290071
H	-2.612389	2.416721	-0.519827	H	2.612377	-2.416716	0.519812
C	-3.804015	0.681173	-0.144743	C	3.804003	-0.681170	0.144721
H	-4.742880	1.217862	-0.258286	H	4.742868	-1.217859	0.258264
C	-3.803857	-0.682183	0.144683	C	3.803845	0.682186	-0.144707
H	-4.742597	-1.219102	0.258165	H	4.742586	1.219104	-0.258191
C	-2.587880	-1.355887	0.290021	C	2.587869	1.355890	-0.290043
H	-2.611787	-2.417451	0.519691	H	2.611776	2.417454	-0.519713
C	0.000399	-3.053379	0.564144	C	-0.000412	3.053392	-0.564108
H	0.874594	-3.369033	1.148276	H	-0.874635	3.369074	-1.148183
H	-0.873943	-3.369380	1.147859	H	0.873902	3.369405	-1.147860
C	0.000819	-3.834727	-0.773958	C	-0.000750	3.834696	0.774019
H	0.000779	-4.918379	-0.600953	H	-0.000701	4.918354	0.601050
H	-0.881979	-3.597075	-1.379896	H	0.882076	3.597010	1.379903
H	0.883933	-3.597048	-1.379416	H	-0.883836	3.597012	1.379516

7

B	1.511976	-0.007032	-0.043171
B	-1.512000	-0.007115	-0.043285
C	0.715377	-1.359070	0.000295
C	-0.715308	-1.359118	0.000321
C	-1.386899	-2.589516	0.112805
H	-2.472212	-2.605771	0.143173
C	-0.696425	-3.802360	0.197928
H	-1.245387	-4.737518	0.277684
C	0.696730	-3.802307	0.197898
H	1.245768	-4.737421	0.277633
C	1.387089	-2.589402	0.112749
H	2.472408	-2.605531	0.143067
C	3.084852	-0.001261	-0.001491
C	3.861499	-0.671337	-0.967499
H	3.367444	-1.208921	-1.773939
C	5.257382	-0.654018	-0.930015
H	5.820857	-1.171214	-1.704090
C	5.945812	0.008714	0.094167
C	-3.084866	-0.001391	-0.001691
C	-3.861617	-0.671765	-0.967395
H	-3.367647	-1.209593	-1.773724
C	-5.257499	-0.654412	-0.929791
H	-5.821046	-1.171854	-1.703647
C	-5.945830	0.008727	0.094187
C	-7.454539	0.024184	0.147777
C	0.715027	1.342749	-0.120071
C	-0.715117	1.342701	-0.120211
C	-1.387385	2.569929	-0.259868
H	-2.472982	2.585483	-0.284596
C	-0.696718	3.779789	-0.380008
H	-1.245533	4.712627	-0.484243
C	0.696524	3.779839	-0.379855
H	1.245290	4.712721	-0.483954
C	1.387245	2.570021	-0.259603
H	2.472844	2.585632	-0.284129
C	3.792275	0.677274	1.014523
H	3.240742	1.210480	1.785955
C	5.184818	0.668516	1.071609
H	5.692003	1.188027	1.882713
C	-3.792211	0.677639	1.014079
H	-3.240594	1.211208	1.785199
C	-5.184739	0.668956	1.071276
H	-5.691859	1.188865	1.882167
H	-7.889395	-0.624682	-0.619434
H	-7.849697	1.036601	-0.009236
C	7.454530	0.024356	0.147440
H	7.849618	1.036280	-0.012986
H	7.889255	-0.626942	-0.617787
H	7.824386	-0.309507	1.124889
H	-7.824194	-0.312879	1.124224

8

B	1.511246	0.012423	0.018691
C	0.714043	-1.299098	0.346008
C	-0.716034	-1.298551	0.346144
C	-1.388814	-2.478899	0.708880
H	-2.474334	-2.488414	0.735536
C	-0.698358	-3.646826	1.047459
H	-1.247707	-4.545164	1.318607
C	0.694892	-3.647430	1.047010
H	1.243636	-4.546260	1.317753
C	1.386093	-2.480006	0.708244
H	2.471628	-2.490222	0.734487
C	3.085510	0.003391	-0.002015
C	3.836748	0.836081	0.848903
H	3.320404	1.504282	1.535839
C	5.238580	0.825734	0.853094
C	5.901321	-0.015278	-0.048436
H	6.990585	-0.020393	-0.068878
C	5.196982	-0.851620	-0.926054
C	3.798497	-0.841433	-0.877096
H	3.250563	-1.499282	-1.549166
C	6.017146	1.688649	1.818960
H	5.439346	2.565940	2.129720
H	6.957521	2.038803	1.378304
H	6.276492	1.131469	2.729857
C	5.938394	-1.746339	-1.892257
B	-1.512212	0.013394	0.017896
C	-0.715150	1.329867	-0.290001
C	0.715204	1.329576	-0.289013
C	1.387800	2.515366	-0.633568
H	2.473211	2.524525	-0.661957
C	0.697571	3.689210	-0.951391
H	1.247039	4.592079	-1.206809
C	-0.695649	3.689441	-0.952568
H	-1.244385	4.592481	-1.208953
C	-1.386774	2.515857	-0.635750
H	-2.472134	2.525272	-0.665916
C	-3.086568	0.005652	-0.003423
C	-3.800097	-0.843487	-0.875847
H	-3.251485	-1.503592	-1.545211
C	-5.197524	-0.856839	-0.921731
C	-5.902067	-0.020760	-0.042012
H	-6.991083	-0.031050	-0.056916
C	-5.239920	0.824291	0.854096
C	-3.836835	0.838208	0.846422
H	-3.320235	1.506942	1.533083
C	-5.938604	-1.743739	-1.895131
H	-5.270053	-2.480046	-2.353495
H	-6.754433	-2.287537	-1.403422
H	-6.389975	-1.157223	-2.706679
C	-6.011368	1.696575	1.817615
H	5.246123	-2.335008	-2.503129
H	6.598499	-2.446924	-1.364645
H	6.572598	-1.163727	-2.572768
H	-7.077610	1.722987	1.569185
H	-5.637510	2.727591	1.815052
H	-5.922005	1.327834	2.848327

9

B	-1.512270	0.001484	0.000339
B	1.512273	0.001508	-0.000283
C	-0.714362	1.351991	0.000195
C	0.714343	1.352002	-0.000142
C	1.389259	2.584729	-0.000384
H	2.476160	2.597570	-0.000751
C	0.697001	3.800182	-0.000236
H	1.244555	4.739469	-0.000433
C	-0.697058	3.800172	0.000167
H	-1.244626	4.739450	0.000305
C	-1.389296	2.584708	0.000376
H	-2.476198	2.597532	0.000747
C	-3.094965	0.001028	0.001134
C	-3.819759	-0.000668	-1.215310
C	-5.218599	-0.005332	-1.197271
H	-5.758206	-0.008401	-2.143522
C	-5.940486	-0.006864	0.002374
C	-7.451064	0.009044	-0.001405
C	3.094966	0.001078	-0.001135
C	3.817139	-0.001910	-1.216338
C	5.218239	-0.006653	-1.199150
H	5.757294	-0.011193	-2.145349
C	5.940486	-0.006864	-0.002433
C	7.451065	0.009032	0.001282
C	-0.714326	-1.349027	0.000207
C	0.714347	-1.349015	-0.000112
C	1.389286	-2.581746	-0.000290
H	2.476179	-2.594591	-0.000638
C	0.697064	-3.797209	-0.000101
H	1.244648	-4.736477	-0.000243
C	-0.696996	-3.797221	0.000270
H	-1.244563	-4.736498	0.000441
C	-1.389241	-2.581771	0.000411
H	-2.476134	-2.594642	0.000748
C	-3.817157	-0.001856	1.216314
C	-5.218268	-0.006583	1.199096
H	-5.757331	-0.011052	2.145290
C	3.819780	-0.000536	1.215288
C	5.218629	-0.005242	1.197216
H	5.758248	-0.008278	2.143460
C	-3.089312	-0.000566	-2.542044
H	-2.443447	0.880905	-2.647716
H	-3.790405	-0.000735	-3.383252
H	-2.442842	-0.881591	-2.647843
C	-3.087504	-0.003040	2.543549
H	-2.441386	-0.884323	2.649330
H	-3.789222	-0.003719	3.384244
H	-2.441572	0.878212	2.650640
C	3.089364	-0.000394	2.542032
H	2.443408	0.881015	2.647646
H	3.790472	-0.000428	3.383229
H	2.442978	-0.881474	2.647914
C	3.087434	-0.003135	-2.543545
H	3.789118	-0.003837	-3.384269
H	2.441495	0.878113	-2.650636
H	2.441314	-0.884423	-2.649273

H	-7.855848	-0.214470	0.991398	H	7.855816	-0.215630	-0.991277
H	-7.860973	-0.724484	-0.706421	H	7.860966	-0.723705	0.707120
H	-7.840807	0.991200	-0.302164	H	7.840836	0.991523	0.300903

7. Plots of the NMR spectra

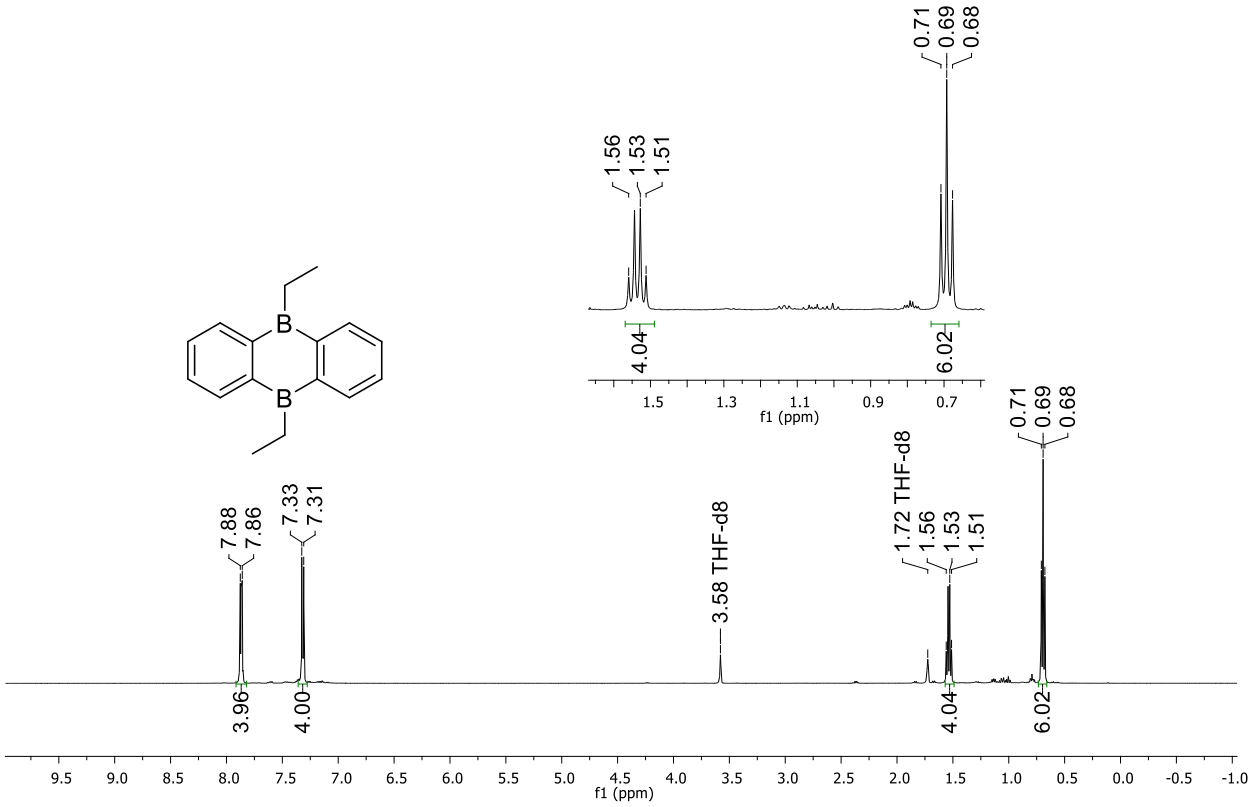

Figure S26. ^{1}H NMR spectrum of **5** (500.2 MHz, THF-d_8).

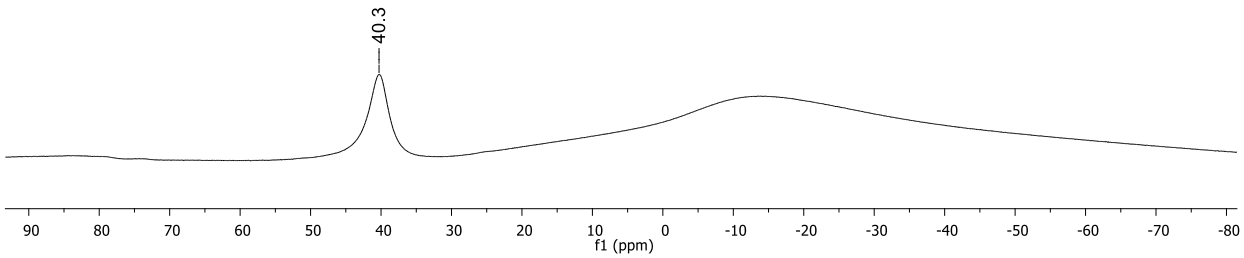

Figure S27. ^{11}B NMR spectrum of **5** (160.5 MHz, THF-d_8).

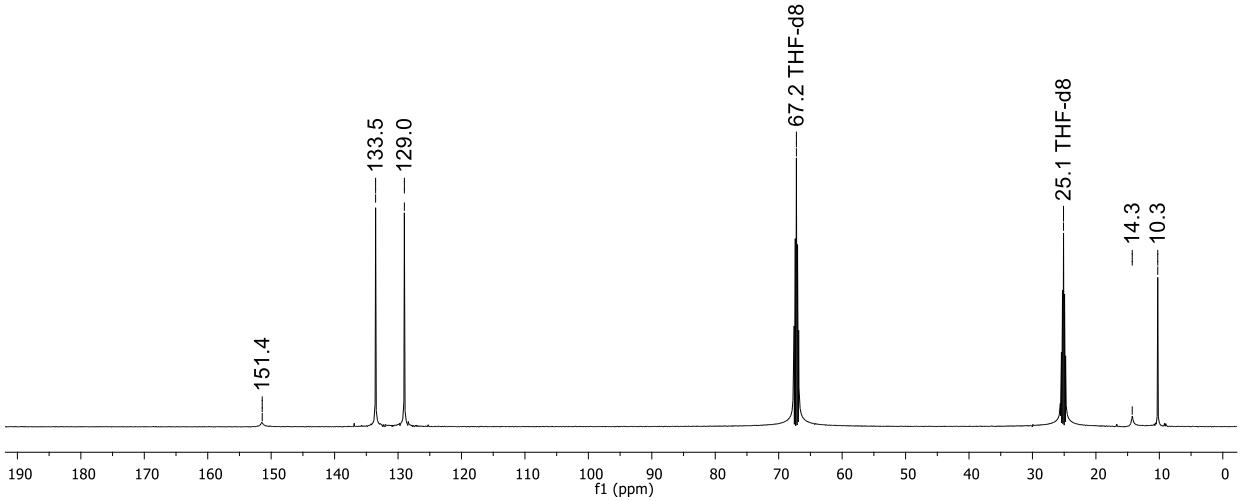

Figure S28. ^{13}C{^{1}H} NMR spectrum of **5** (125.8 MHz, THF-d_8).

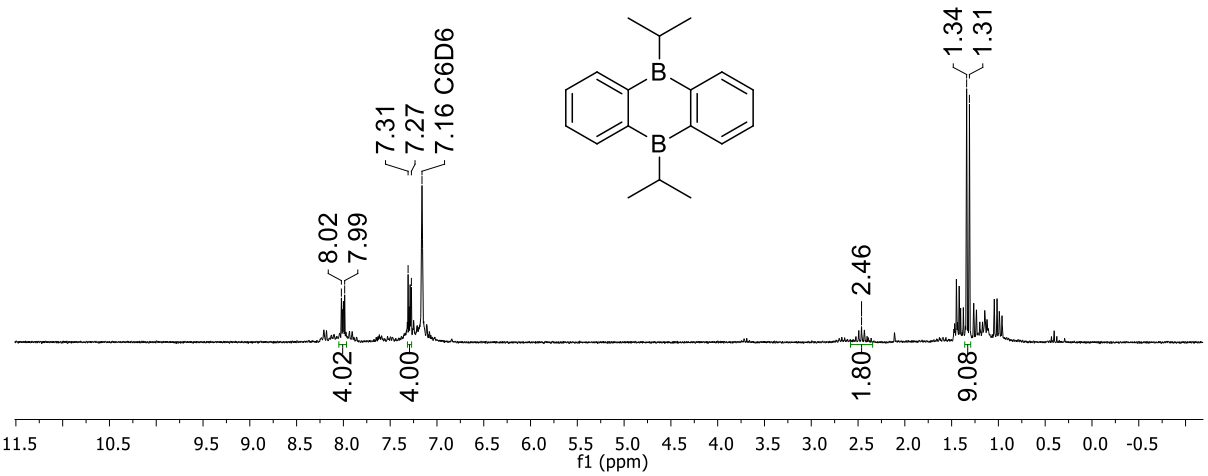

Figure S29. ^{1}H NMR spectrum of **6** (250.1 MHz, C_6D_6).

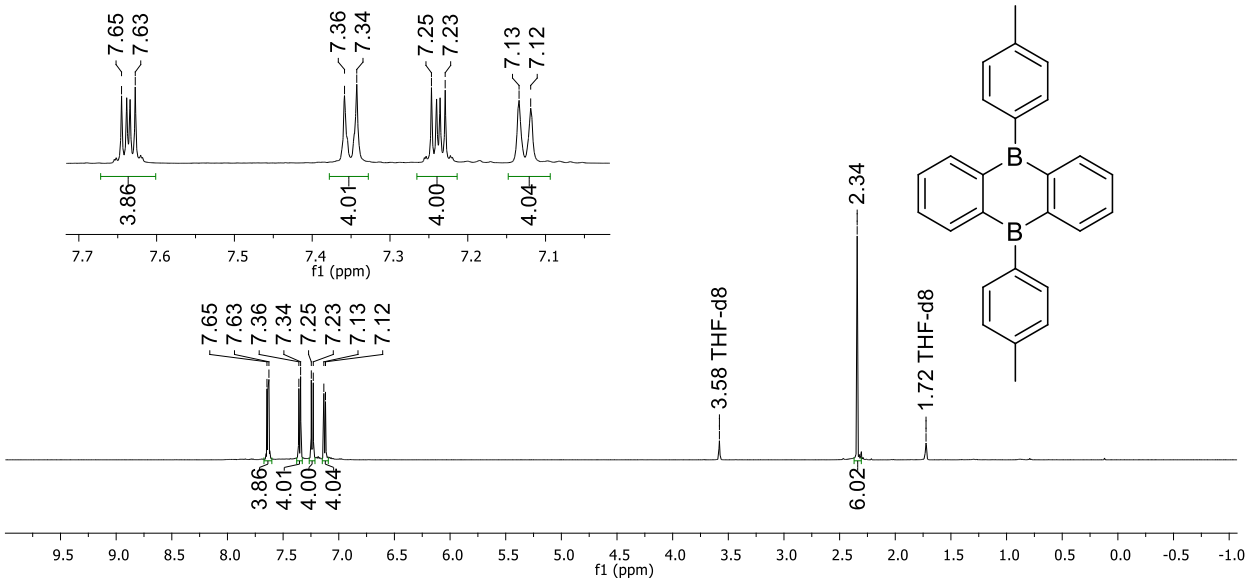

Figure S30. ^{1}H NMR spectrum of **7** (500.2 MHz, THF-d_8).

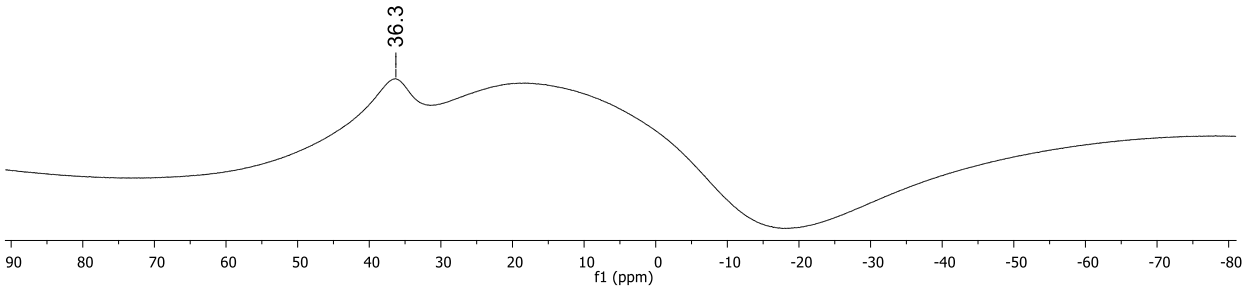

Figure S31. ^{11}B NMR spectrum of **7** (160.5 MHz, THF-d_8).

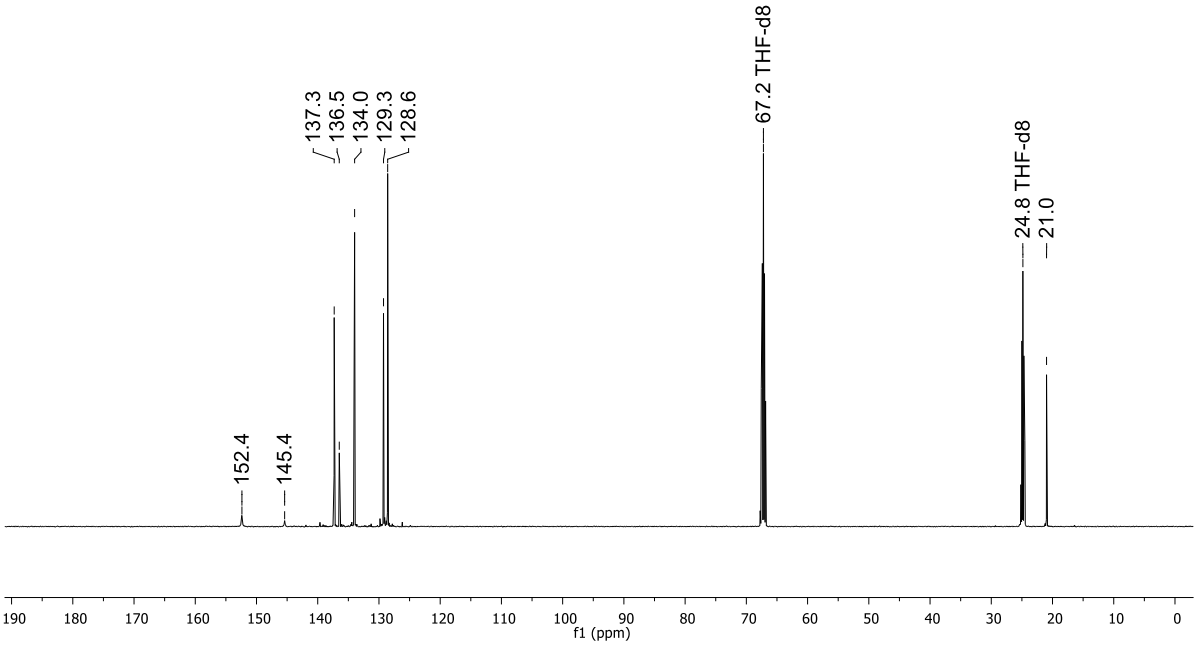

Figure S32. ^{13}C{^{1}H} NMR spectrum of **7** (125.8 MHz, THF-d_8).

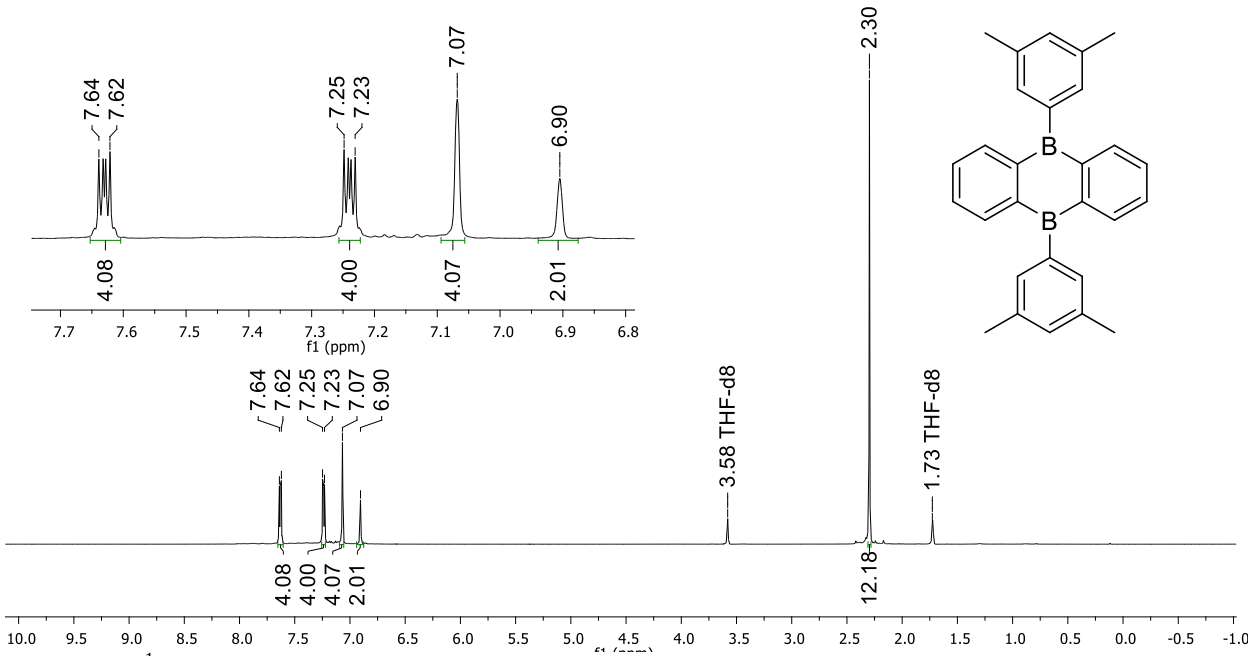

Figure S33. ^{1}H NMR spectrum of **8** (500.2 MHz, THF-d_8).

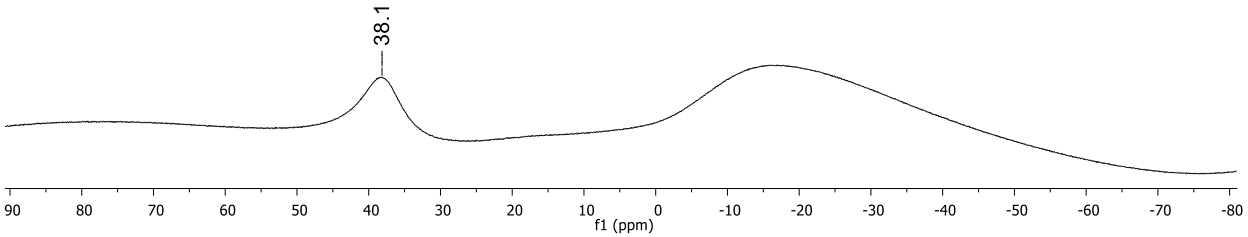

Figure S34. ^{11}B NMR spectrum of **8** (160.5 MHz, THF-d_8).

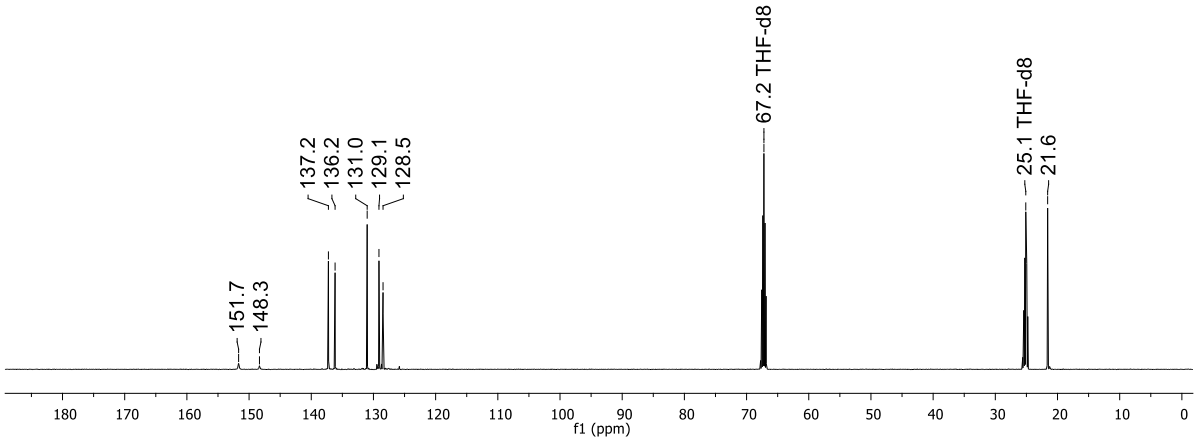

Figure S35. ^{13}C{^{1}H} NMR spectrum of **8** (125.8 MHz, THF-d_8).

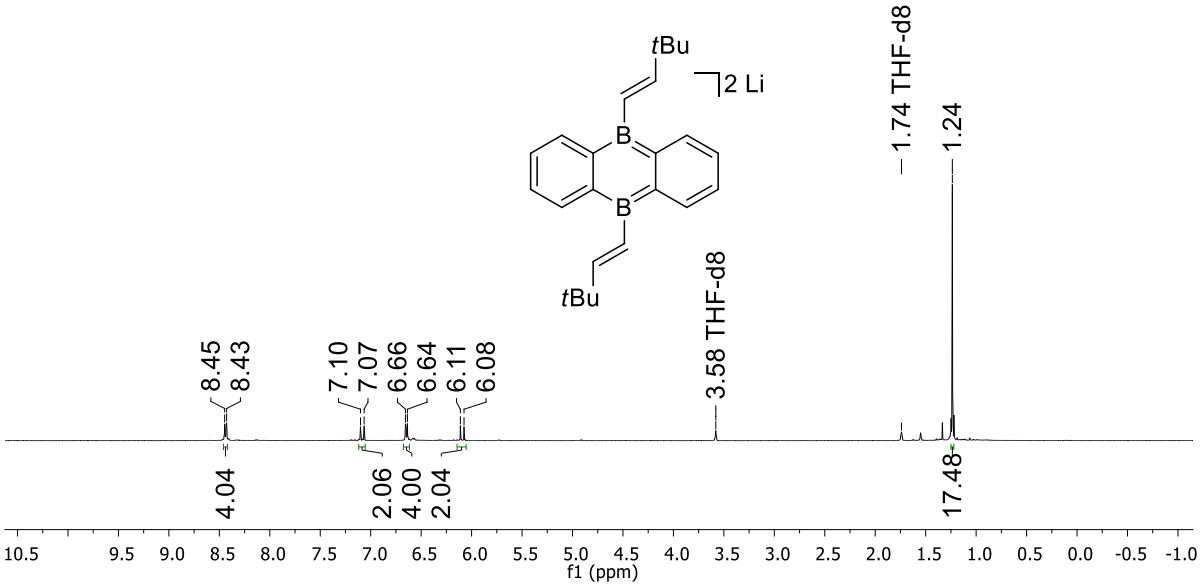

Figure S36. ^{1}H NMR spectrum of Li_2[**3**] (500.2 MHz, THF-d_8).

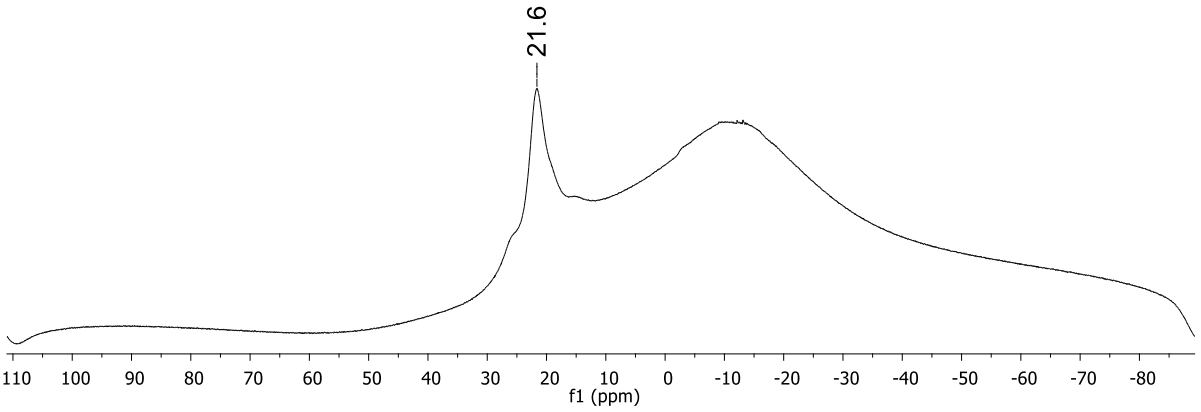

Figure S37. ^{11}B NMR spectrum of Li_2[**3**] (160.5 MHz, THF-d_8).

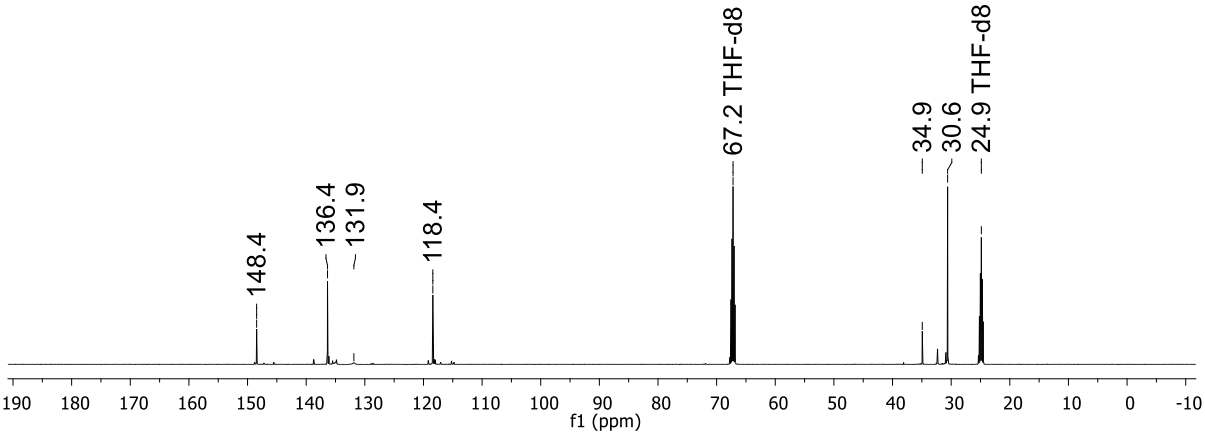

Figure S38. ^{13}C{^{1}H} NMR spectrum of Li_2[**3**] (125.8 MHz, THF-d_8).

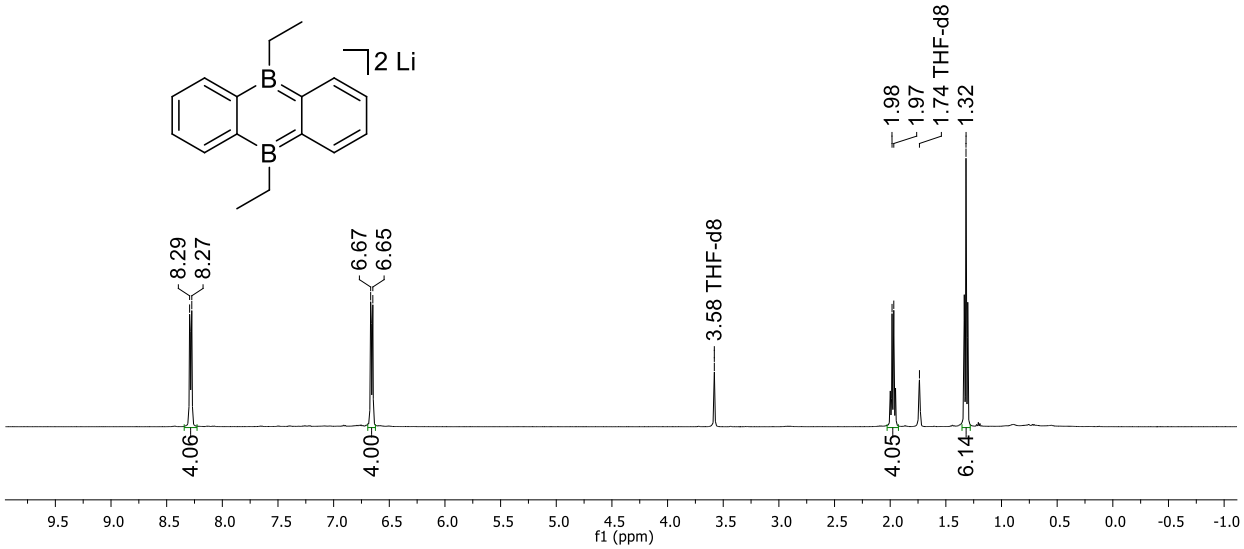

Figure S39. ^{1}H NMR spectrum of Li_2[**5**] (500.2 MHz, THF-d_8).

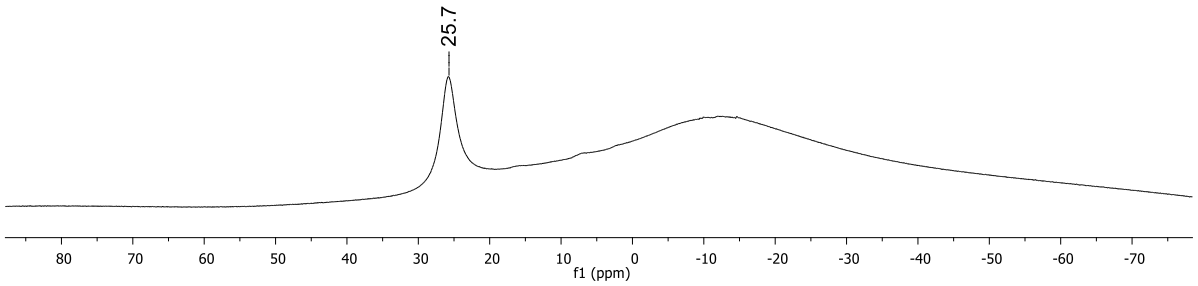

Figure S40. ^{11}B NMR spectrum of Li_2[**5**] (160.5 MHz, THF-d_8).

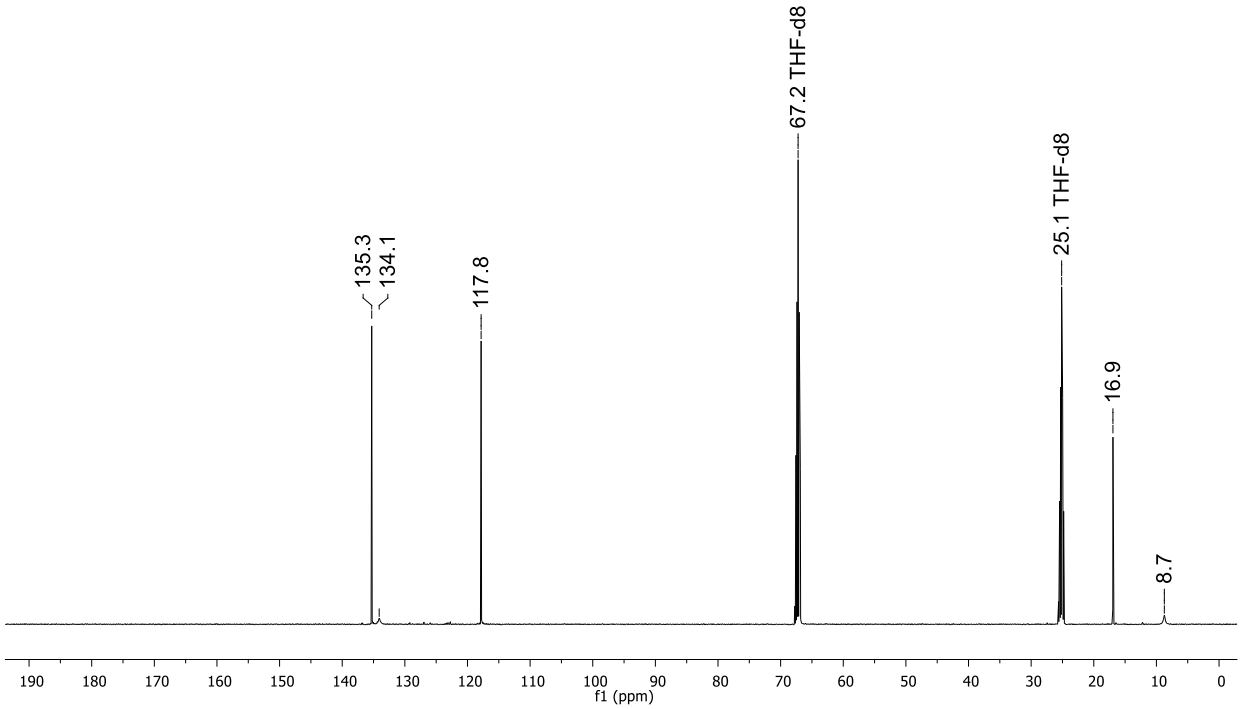

Figure S41. ^{13}C{^{1}H} NMR spectrum of Li_2[**5**] (125.8 MHz, THF-d_8).

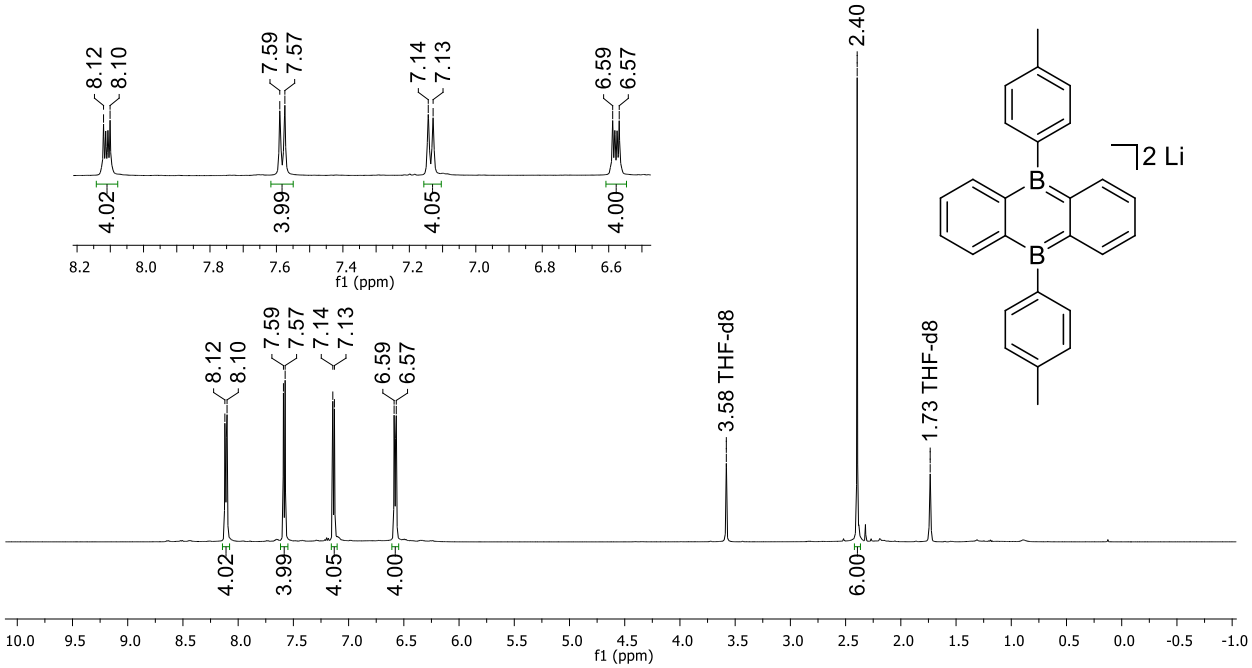

Figure S42. ^{1}H NMR spectrum of Li_2[**7**] (500.2 MHz, THF-d_8).

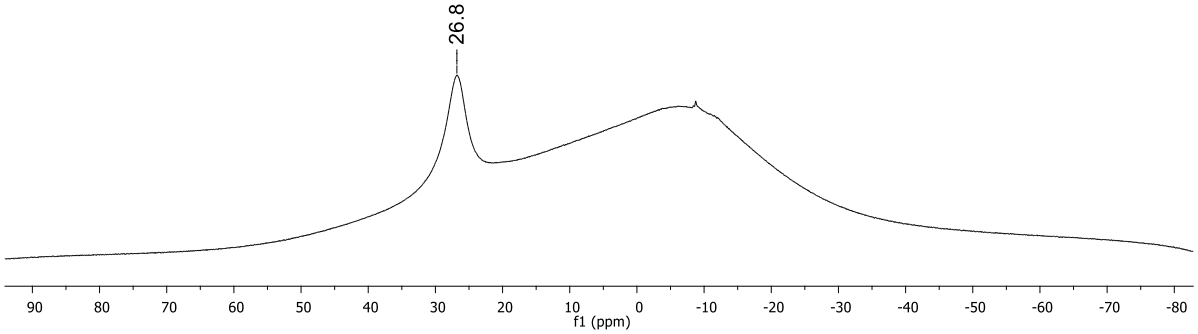

Figure S43. ^{11}B NMR spectrum of Li_2[**7**] (160.5 MHz, THF-d_8).

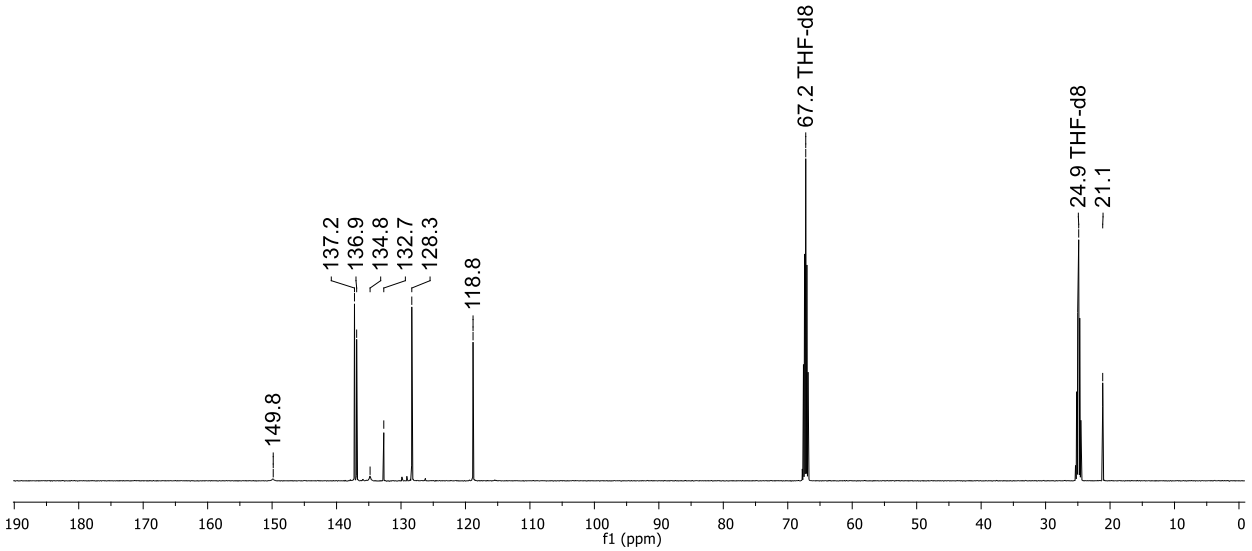

Figure S44. ^{13}C{^{1}H} NMR spectrum of Li_2[**7**] (125.8 MHz, THF-d_8).

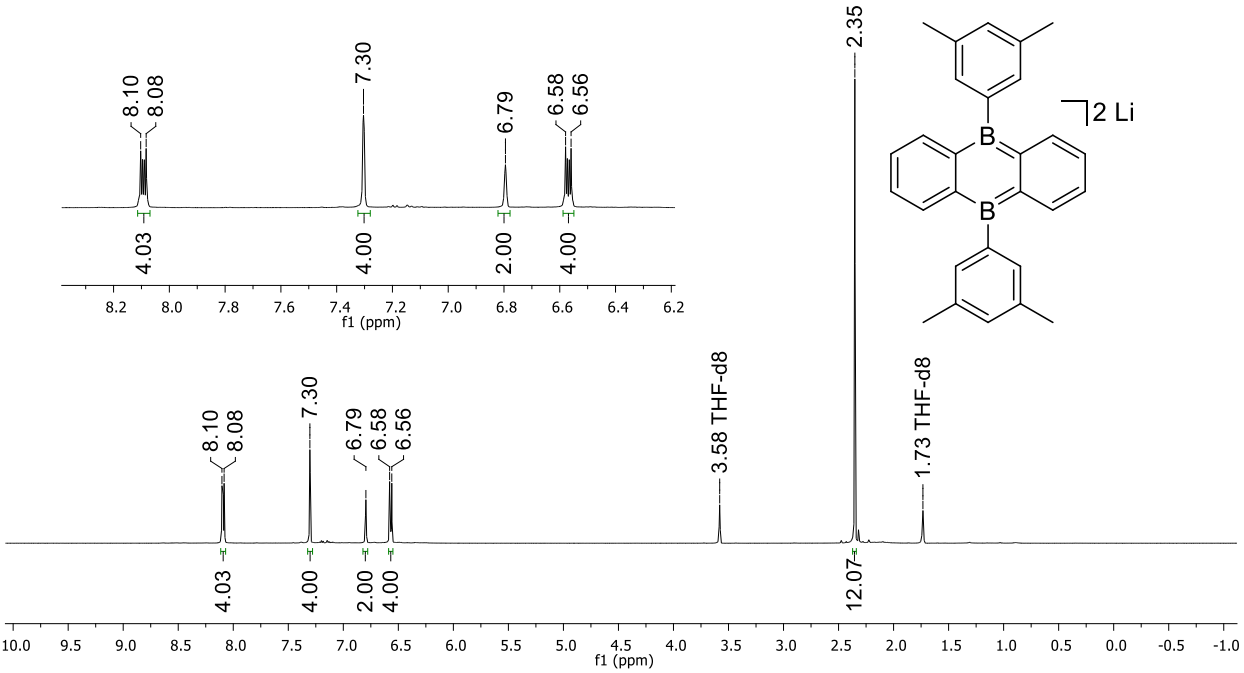

Figure S45. ^{1}H NMR spectrum of Li_2[**8**] (500.2 MHz, THF-d_8).

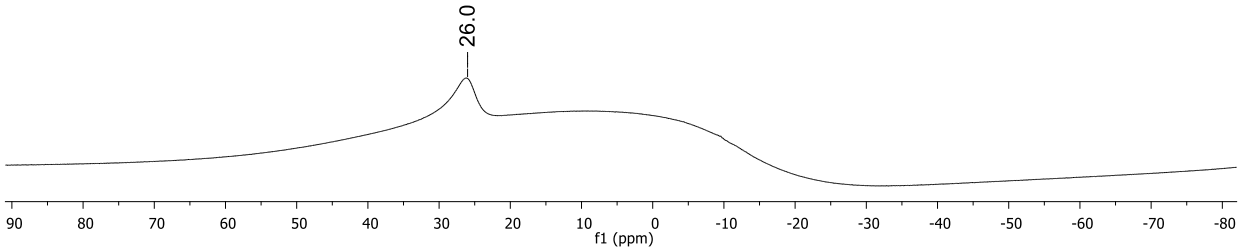

Figure S46. ^{11}B NMR spectrum of Li_2[**8**] (160.5 MHz, THF-d_8).

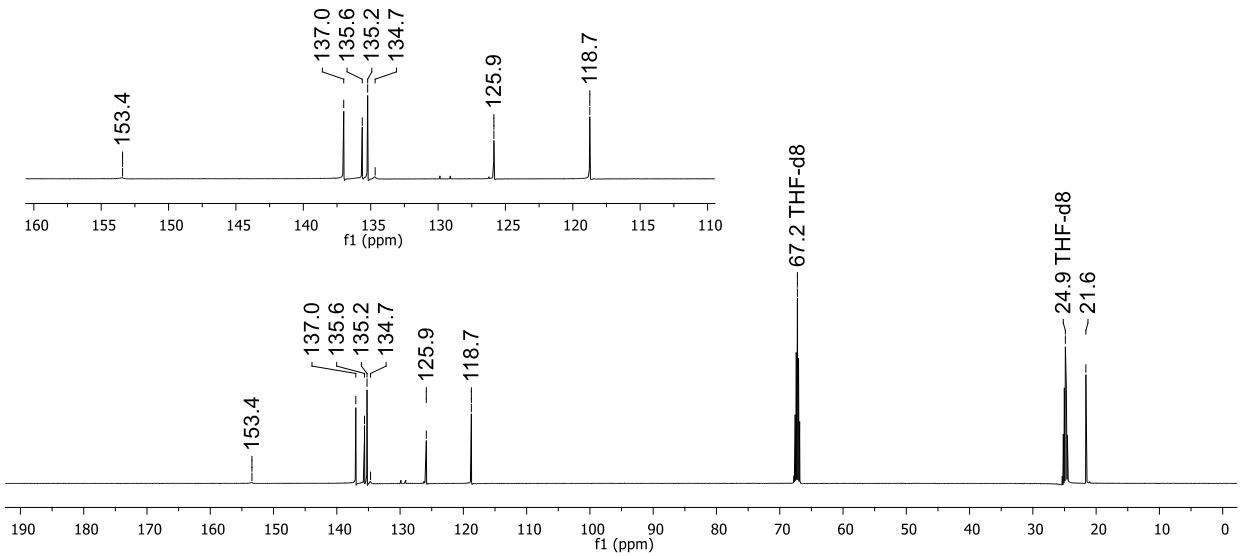

Figure S47. ^{13}C{^{1}H} NMR spectrum of Li_2[**8**] (125.8 MHz, THF-d_8).

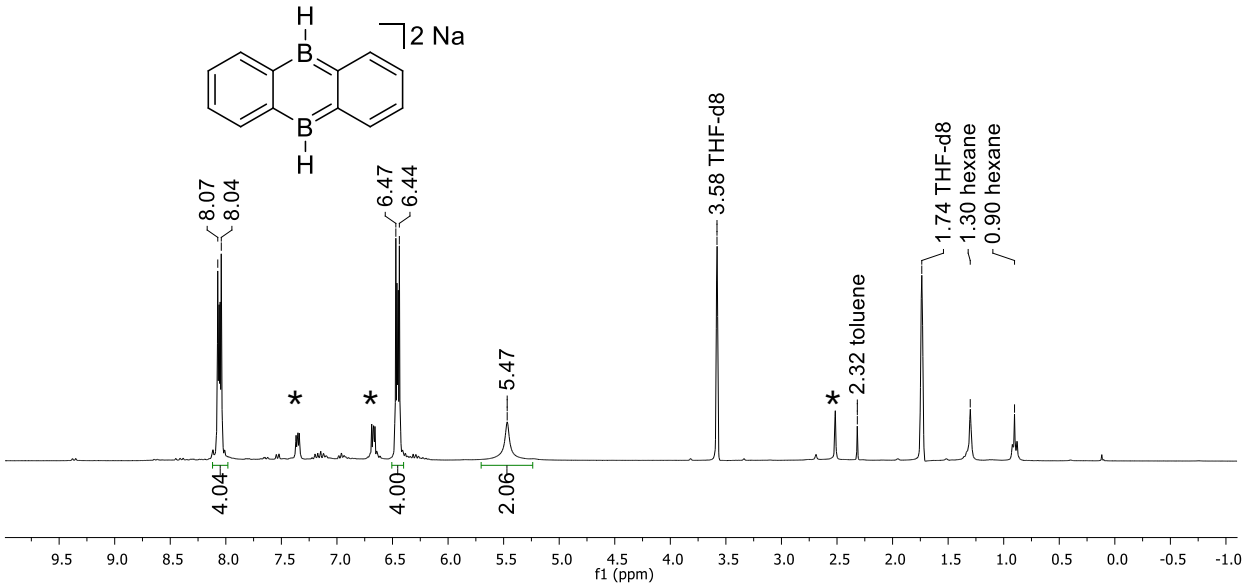

Figure S48. $^{1}H\{^{11}B\}$ NMR spectrum of Na_2[**1**] (300.0 MHz, THF-d_8). Asterisks mark resonances of Na_2[**1**-H_2] as a minor component; explanation of its derivation is provided in the SI of Ref. [4].

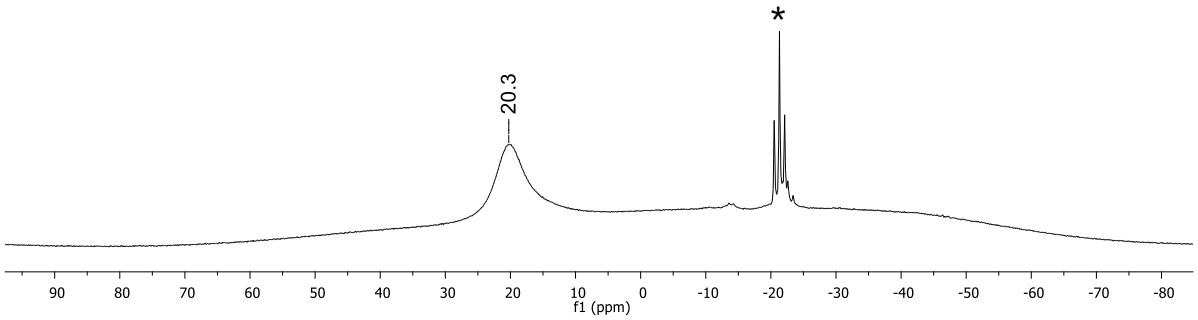

Figure S49. ^{11}B NMR spectrum of Na_2[**1**] (96.3 MHz, THF-d_8).

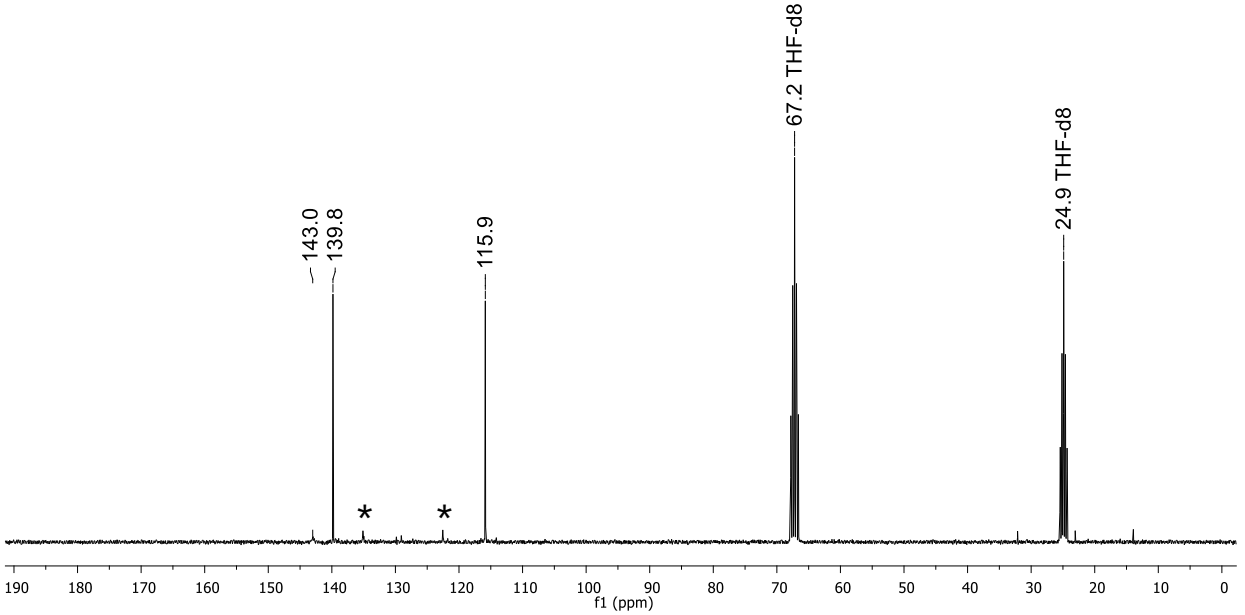

Figure S50. $^{13}C\{^{1}H\}$ NMR spectrum of Na_2[**1**] (75.4 MHz, THF-d_8).

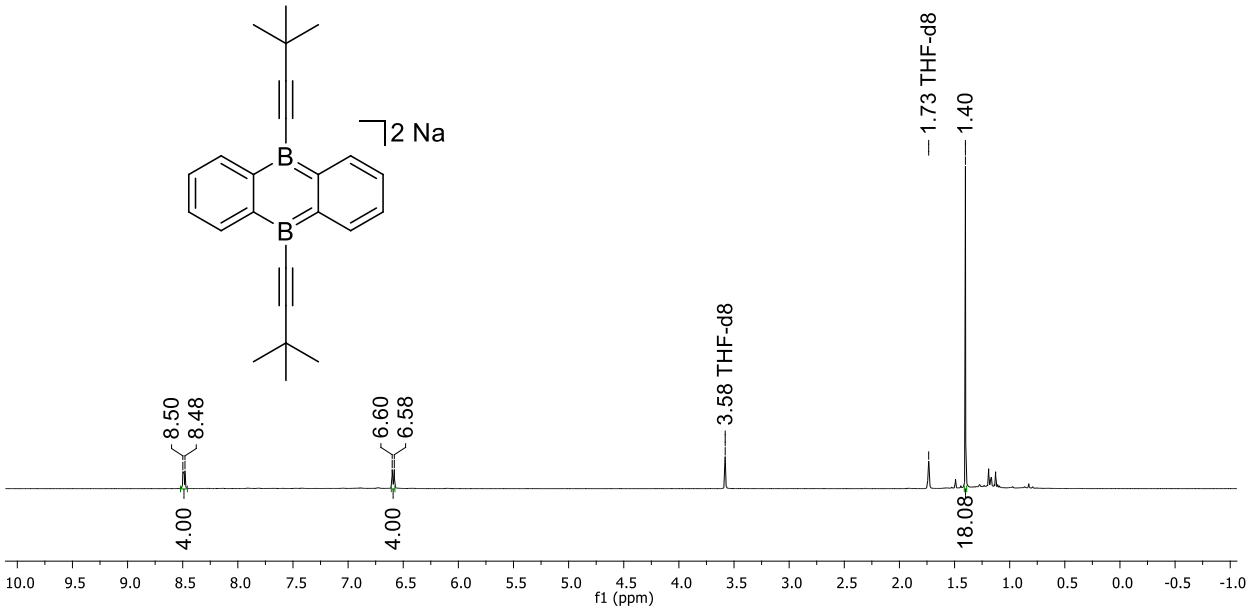

Figure S51. ^{1}H NMR spectrum of Na_2[**2**] (500.2 MHz, THF-d_8).

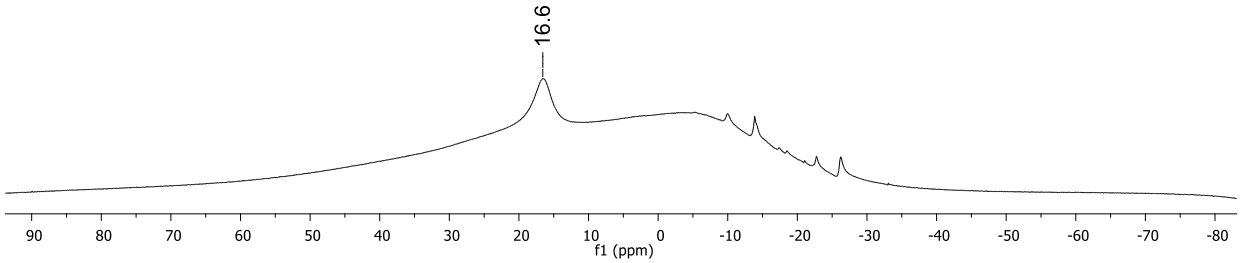

Figure S52. ^{11}B NMR spectrum of Na_2[**2**] (160.5 MHz, THF-d_8).

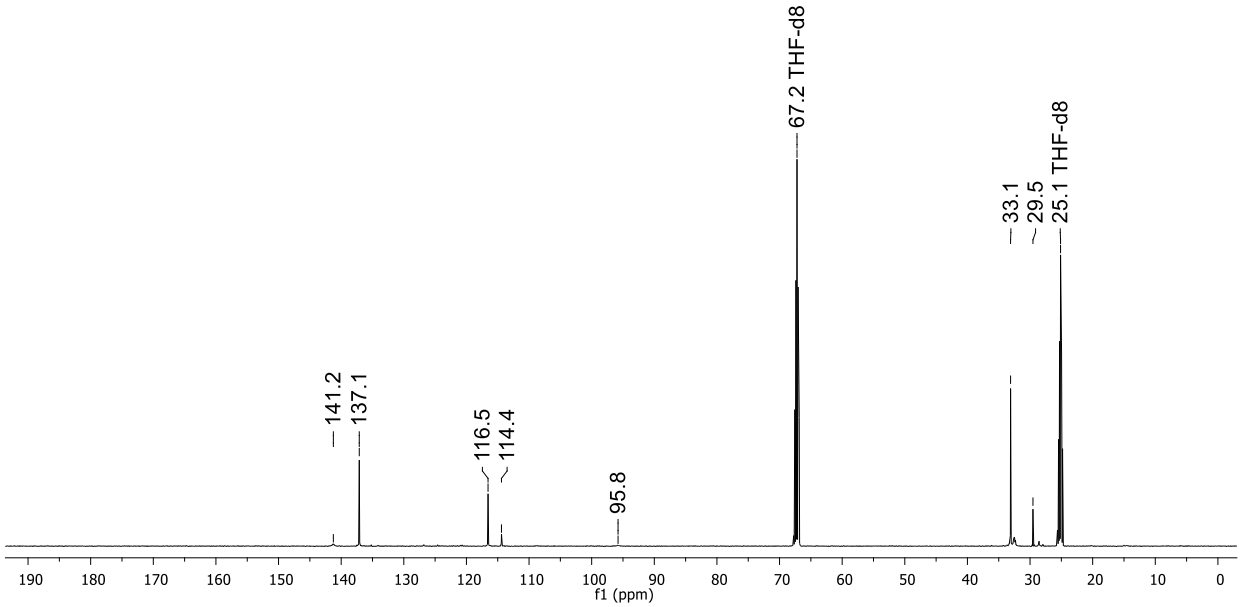

Figure S53. ^{13}C{^{1}H} NMR spectrum of Na_2[**2**] (125.8 MHz, THF-d_8).

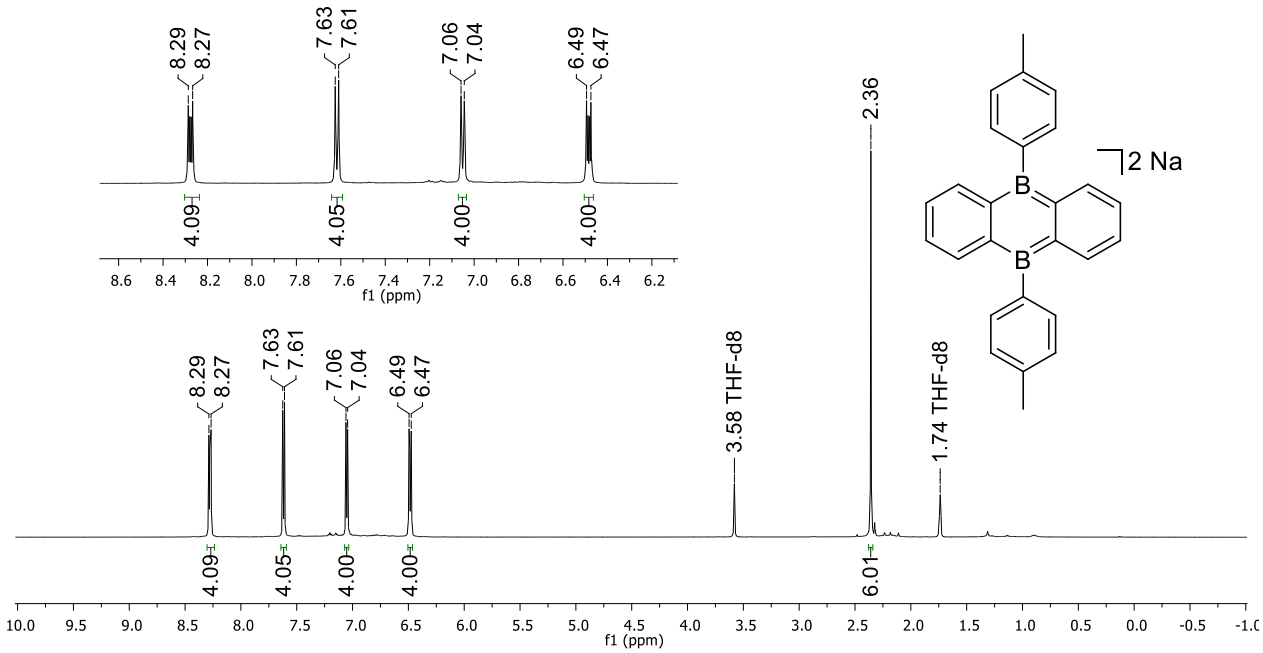

Figure S54. ^{1}H NMR spectrum of Na_2[**7**] (500.2 MHz, THF-d_8).

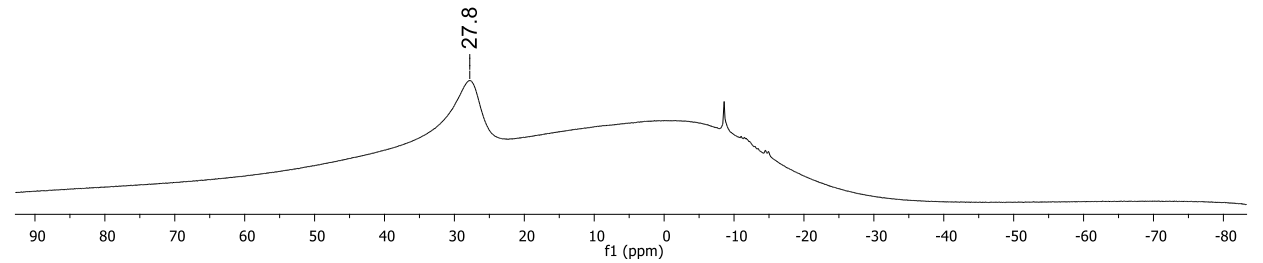

Figure S55. ^{11}B NMR spectrum of Na_2[**7**] (160.5 MHz, THF-d_8).

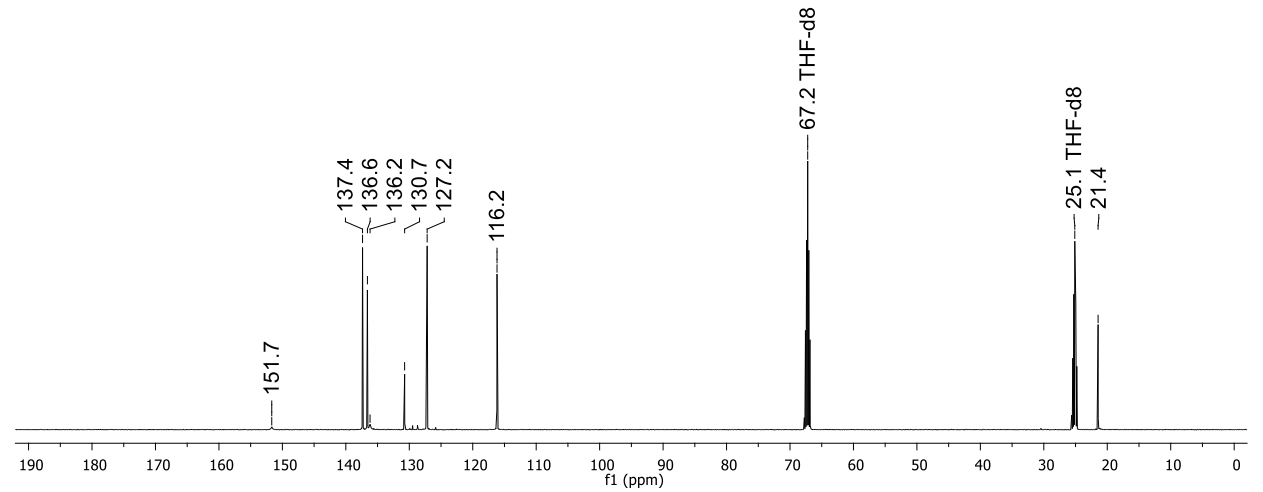

Figure S56. ^{13}C{^{1}H} NMR spectrum of Na_2[**7**] (125.8 MHz, THF-d_8).

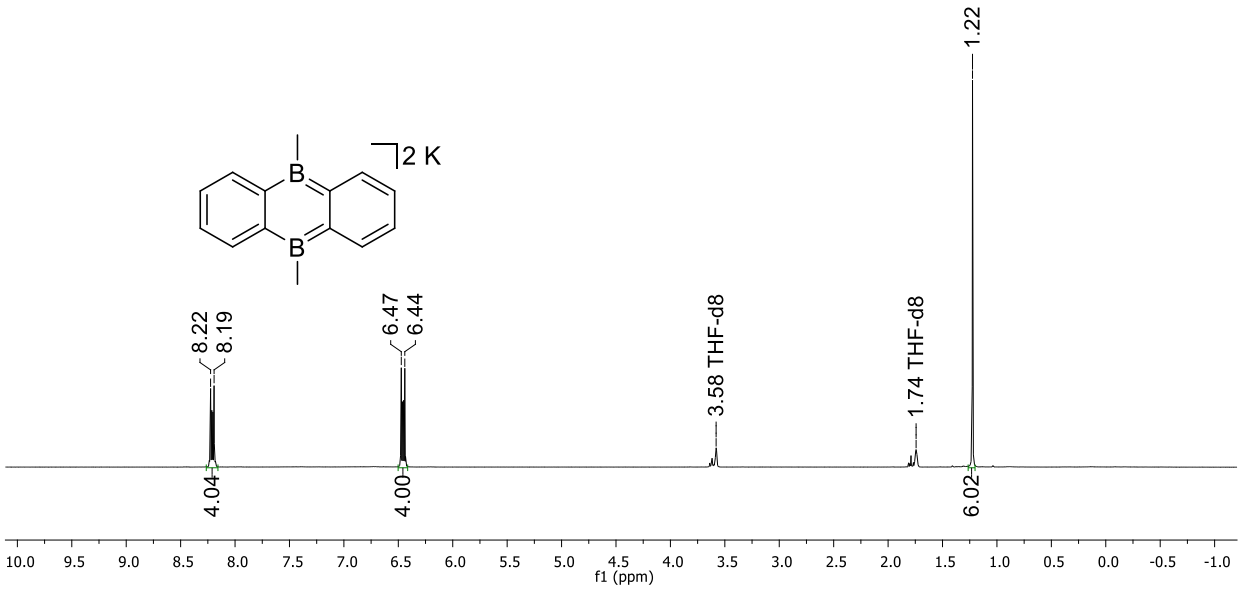

Figure S57. ^{1}H NMR spectrum of K_2[**4**] (300.0 MHz, THF-d_8).

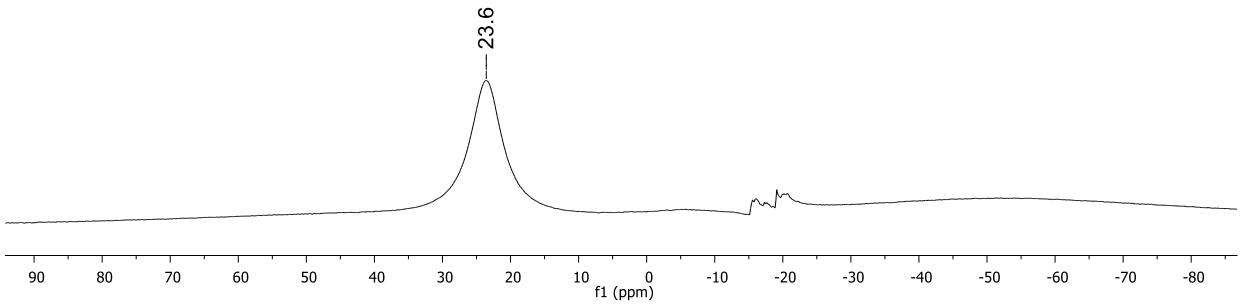

Figure S58. ^{11}B NMR spectrum of K_2[**4**] (96.3 MHz, THF-d_8).

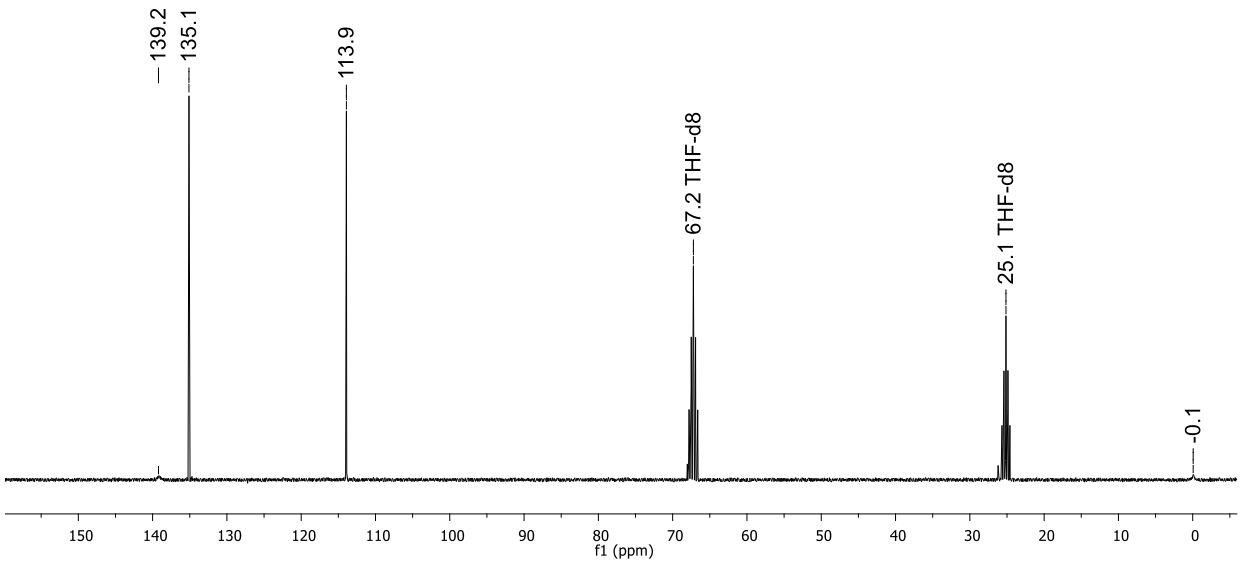

Figure S59. ^{13}C{^{1}H} NMR spectrum of K_2[**4**] (75.4 MHz, THF-d_8).

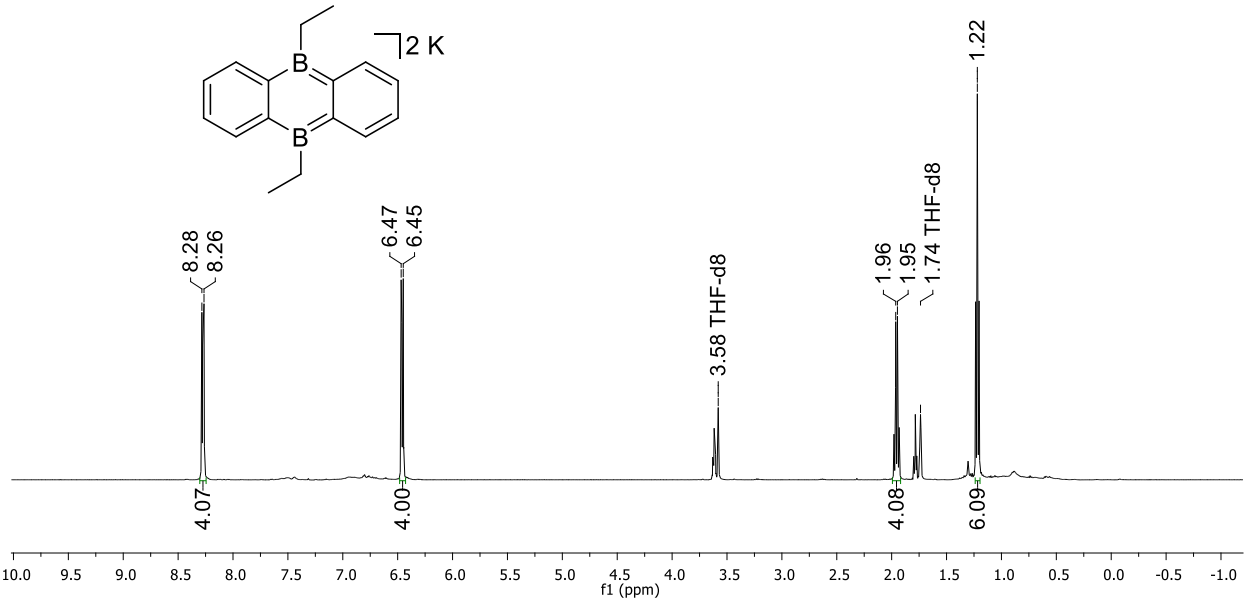

Figure S60. ^{1}H NMR spectrum of K_2[**5**] (500.2 MHz, THF-d_8).

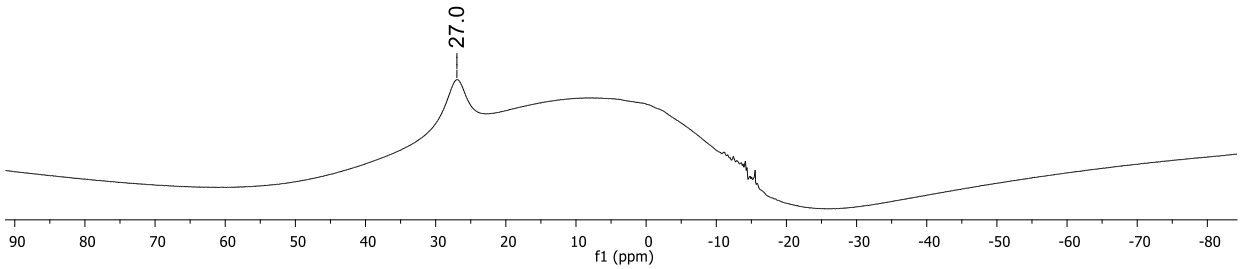

Figure S61. ^{11}B NMR spectrum of K_2[**5**] (160.5 MHz, THF-d_8).

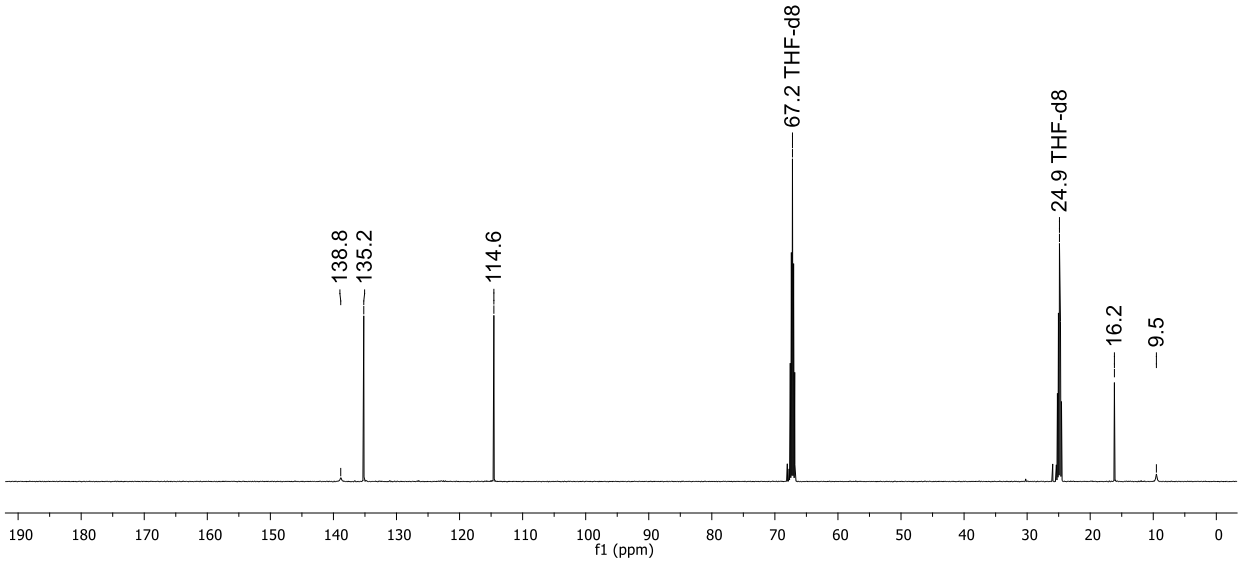

Figure S62. ^{13}C{^{1}H} NMR spectrum of K_2[**5**] (125.8 MHz, THF-d_8).

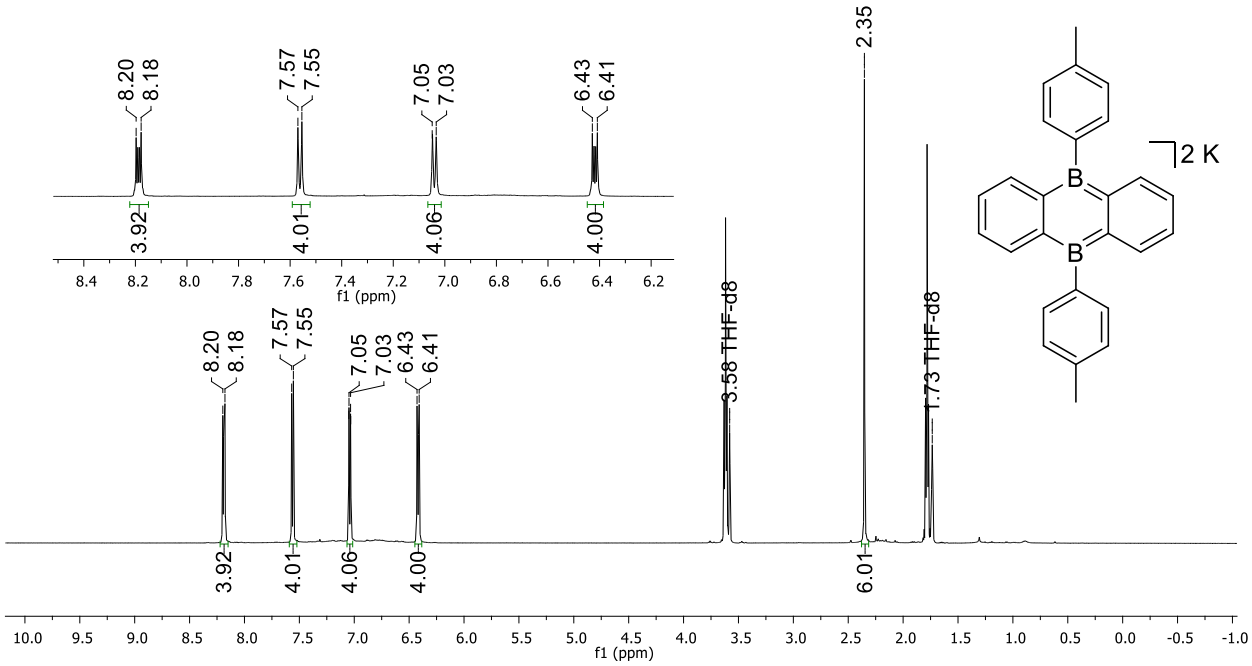

Figure S63. ^{1}H NMR spectrum of K_2[**7**] (500.2 MHz, THF-d_8).

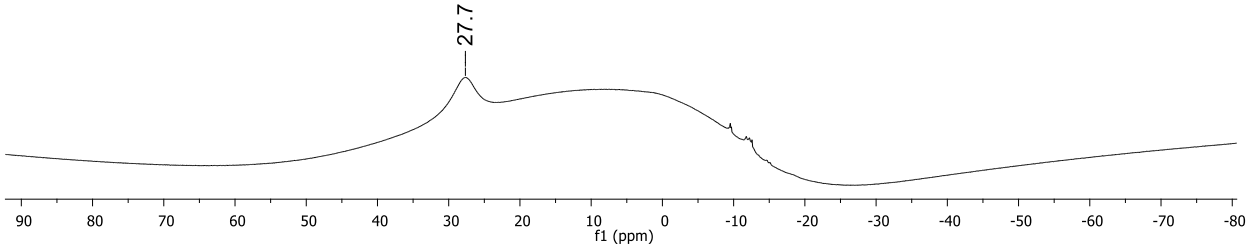

Figure S64. ^{11}B NMR spectrum of K_2[**7**] (160.5 MHz, THF-d_8).

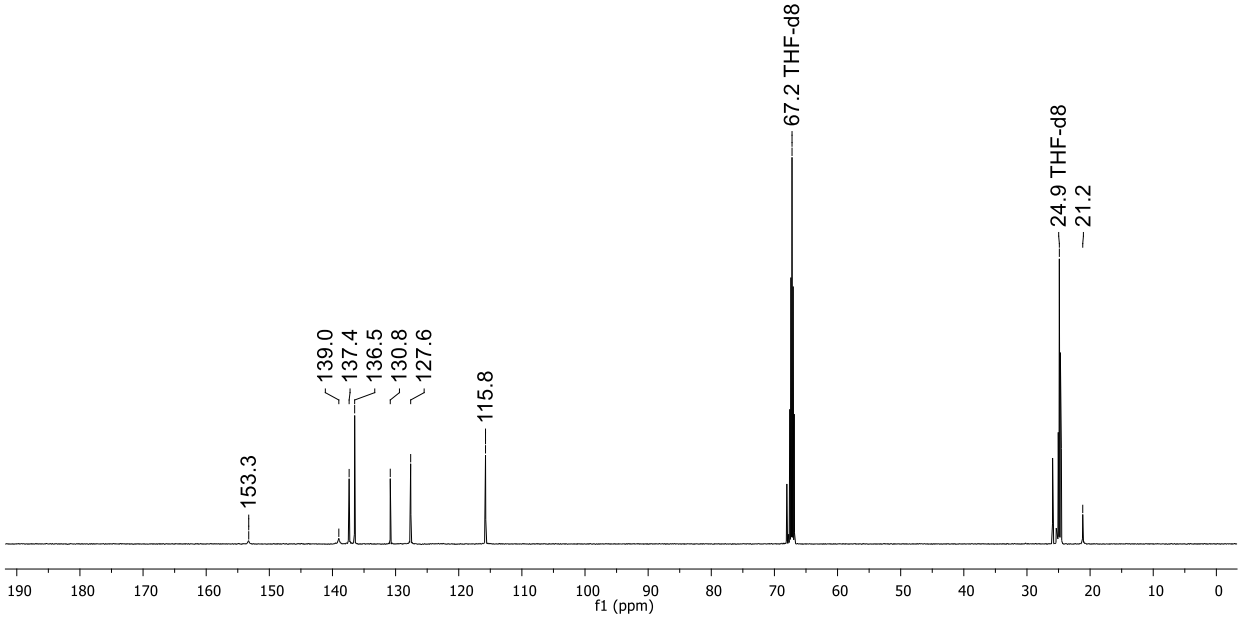

Figure S65. ^{13}C{^{1}H} NMR spectrum of K_2[**7**] (125.8 MHz, THF-d_8).

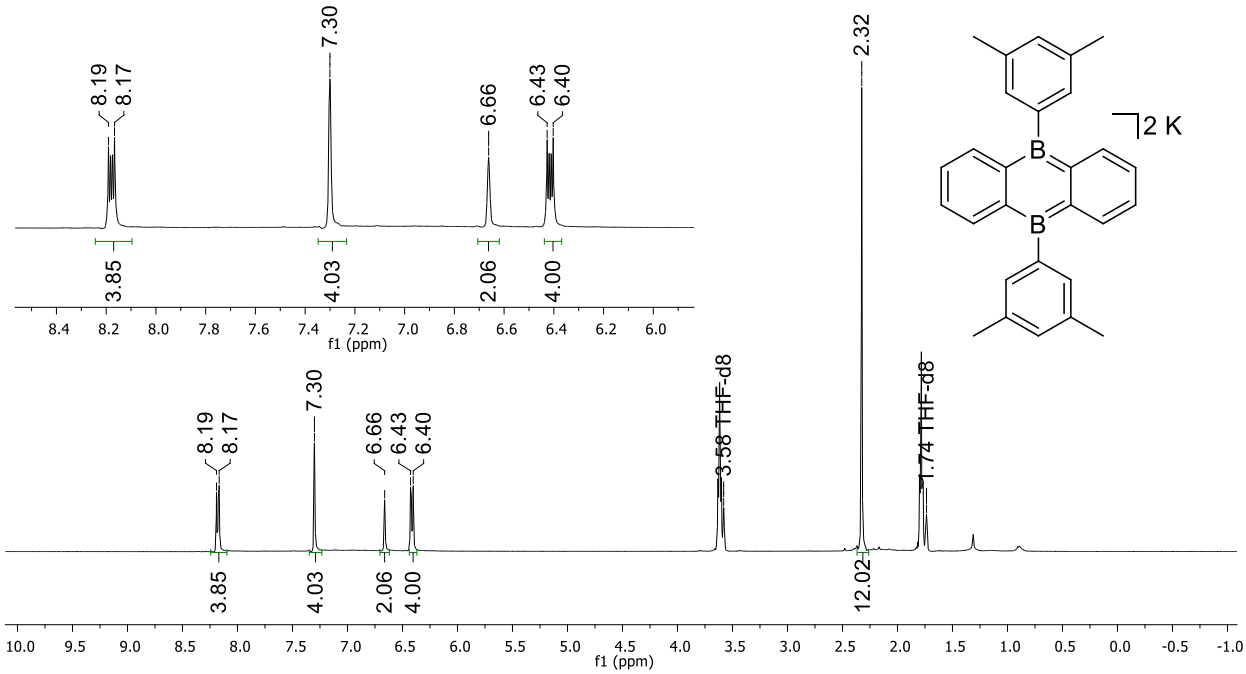

Figure S66. ^{1}H NMR spectrum of K_2[**8**] (400.1 MHz, THF-d_8).

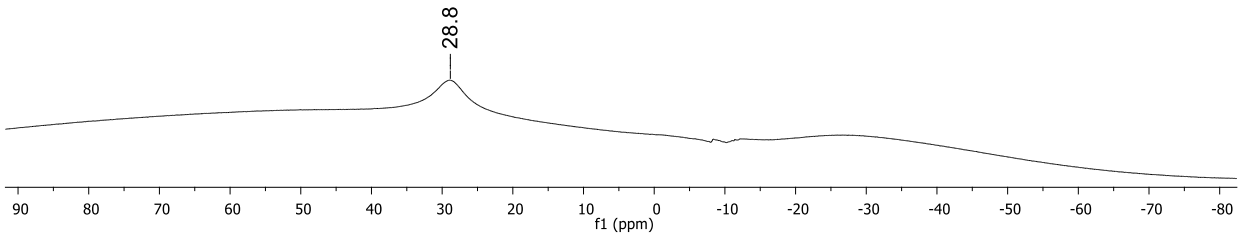

Figure S67. ^{11}B NMR spectrum of K_2[**8**] (128.4 MHz, THF-d_8).

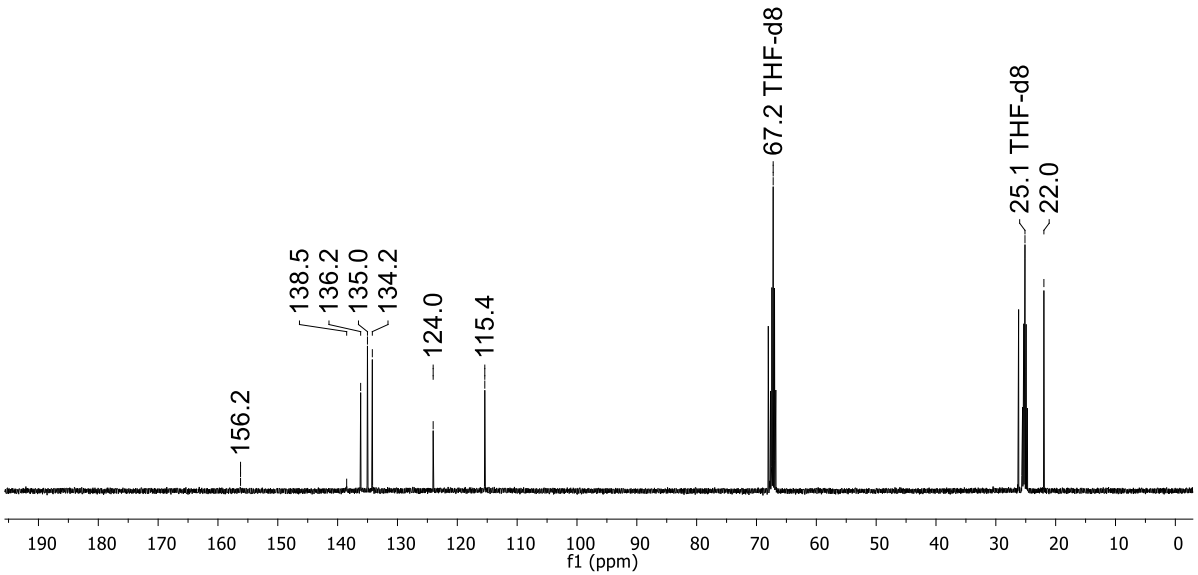

Figure S68. ^{13}C{^{1}H} NMR spectrum of K_2[**8**] (100.6 MHz, THF-d_8).

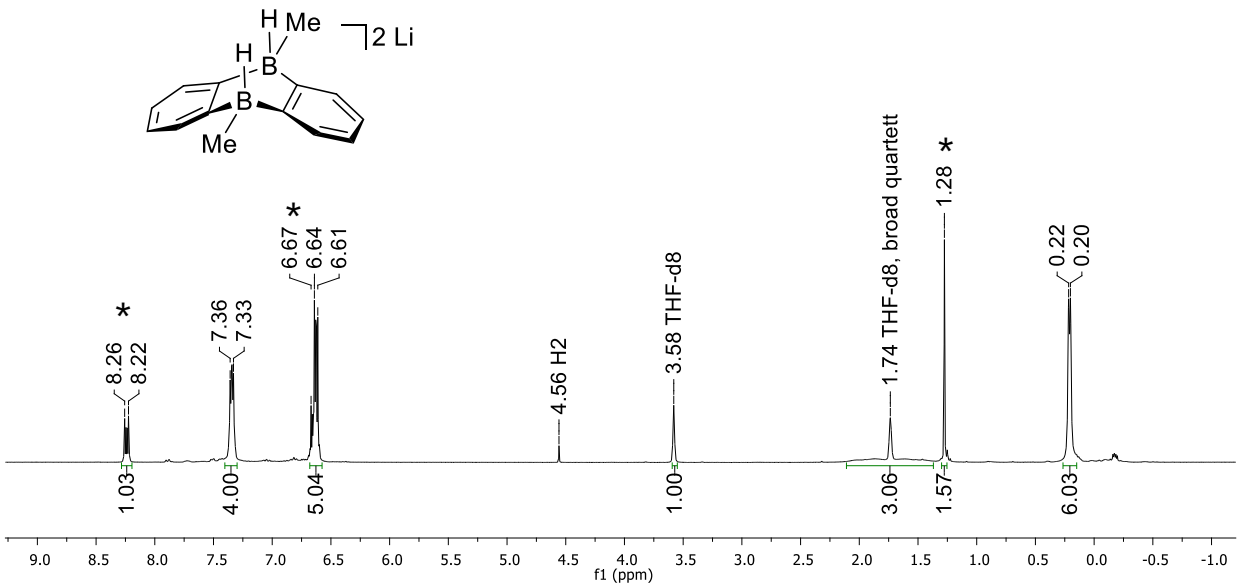

Figure S69. ^{1}H NMR spectrum of Li_2[**4**-H_2] (300.0 MHz, THF-d_8). Asterisks mark resonances of the starting material.

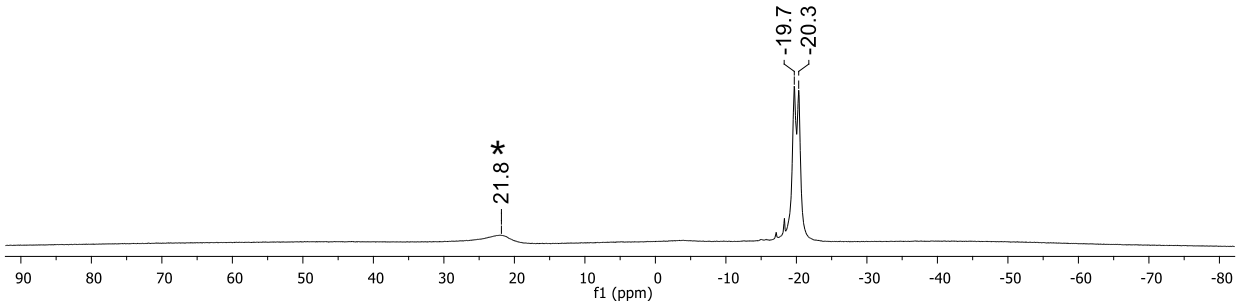

Figure S70. ^{11}B NMR spectrum of Li_2[**4**-H_2] (96.3 MHz, THF-d_8). Asterisk marks resonance of the starting material.

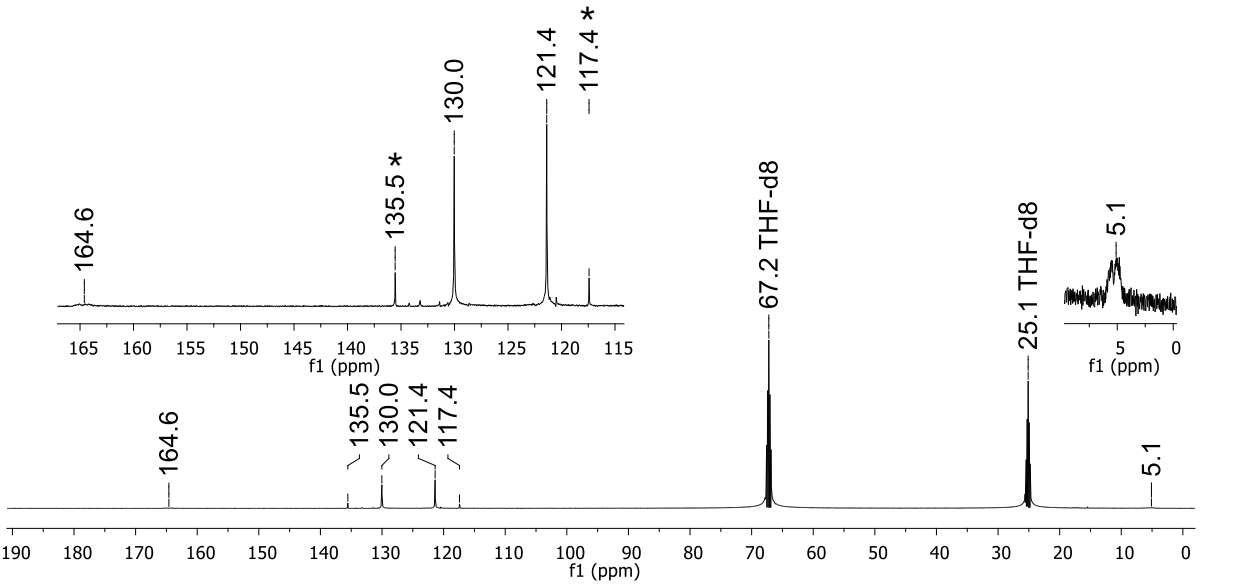

Figure S71. ^{13}C{^{1}H} NMR spectrum of Li_2[**4**-H_2] (125.8 MHz, THF-d_8). Asterisks mark resonances of the starting material.

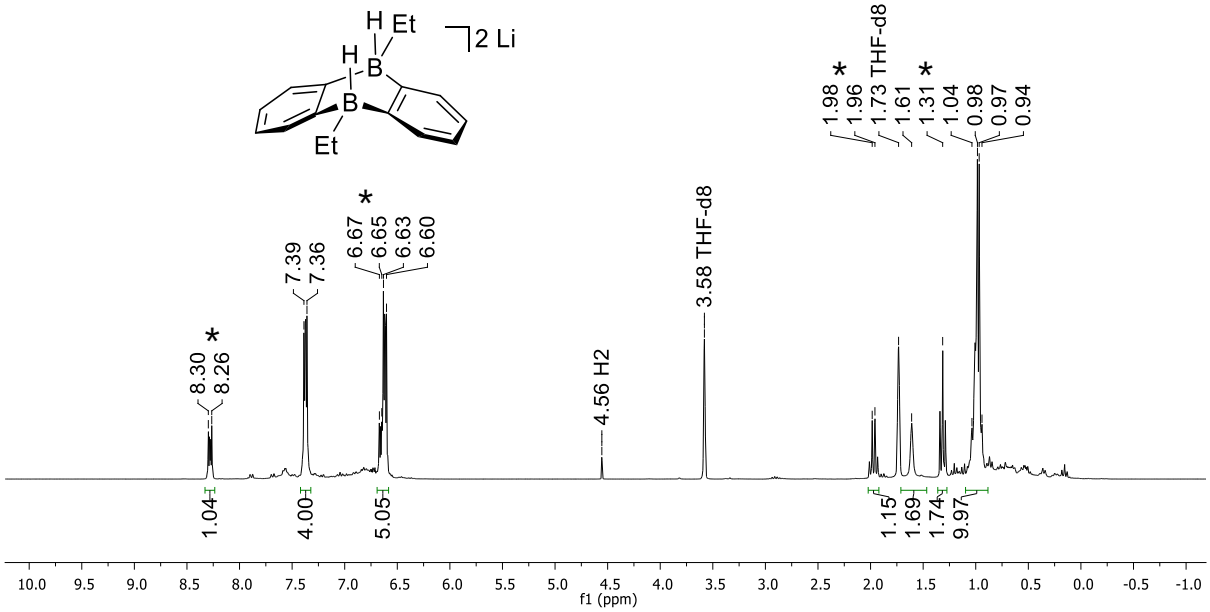

Figure S72. $^{1}H\{^{11}B\}$ NMR spectrum of Li_2[**5**-H_2] (300.0 MHz, THF-d_8). Asterisks mark resonances of the starting material.

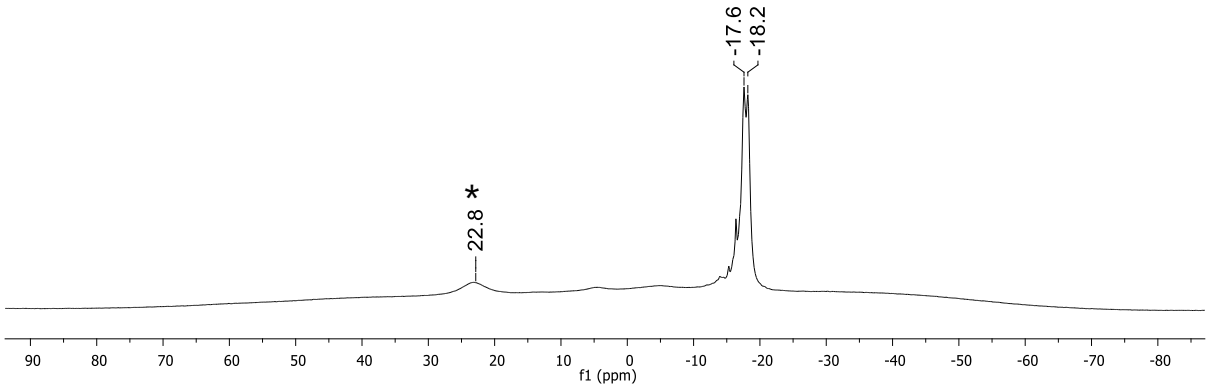

Figure S73. ^{11}B NMR spectrum of Li_2[**5**-H_2] (96.3 MHz, THF-d_8). Asterisk marks resonance of the starting material.

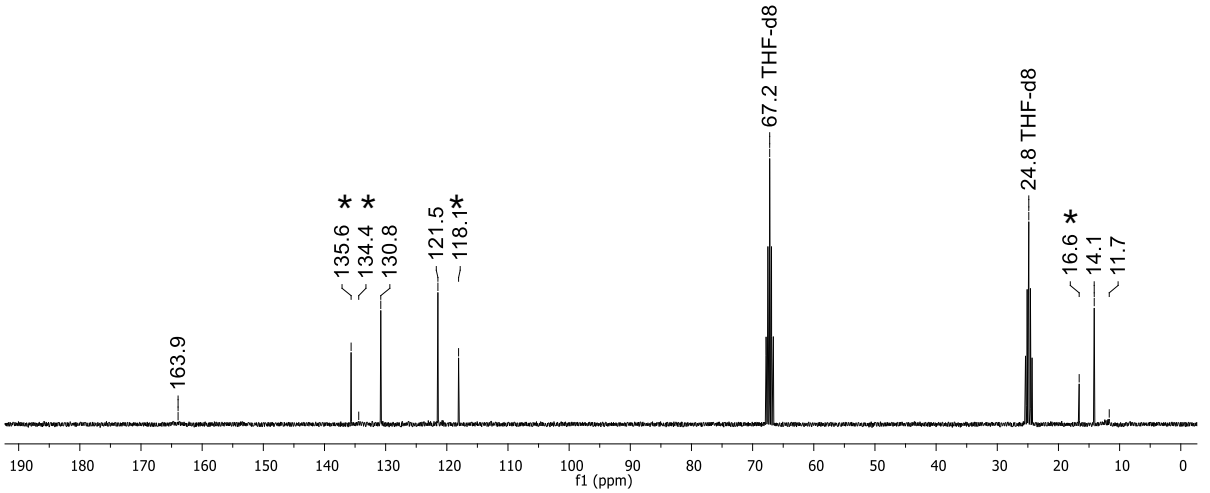

Figure S74. $^{13}C\{^{1}H\}$ NMR spectrum of Li_2[**5**-H_2] (75.4 MHz, THF-d_8). Asterisks mark resonances of the starting material.

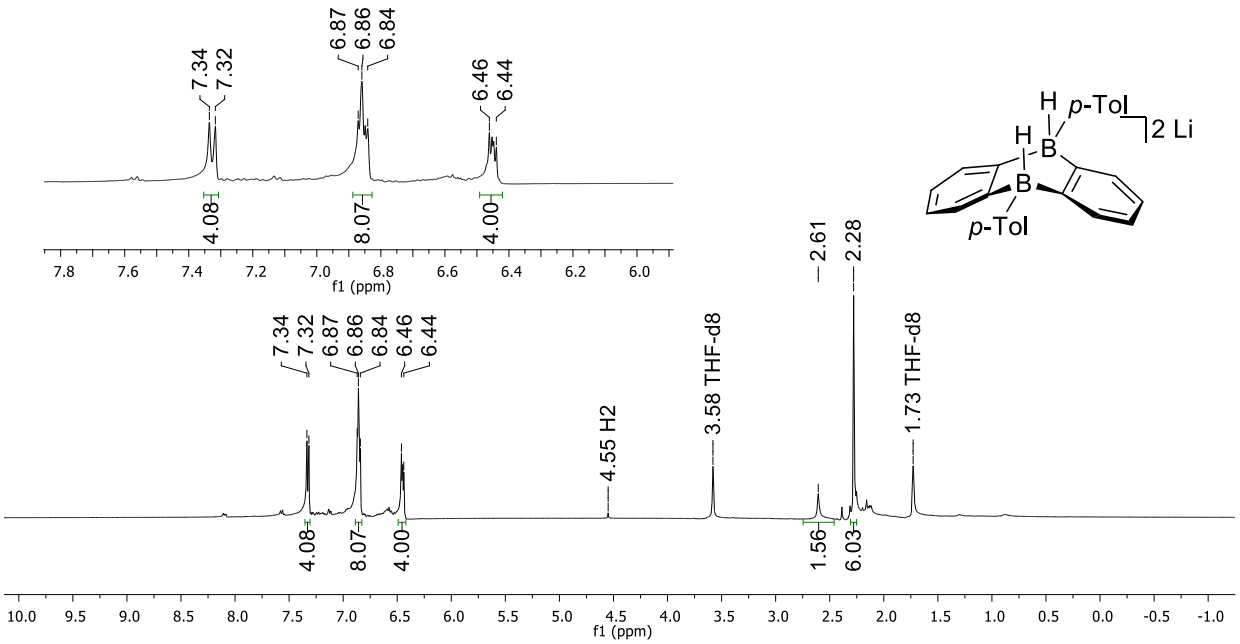

Figure S75. $^{1}H\{^{11}B\}$ NMR spectrum of Li_2[**7**-H_2] (400.1 MHz, THF-d_8).

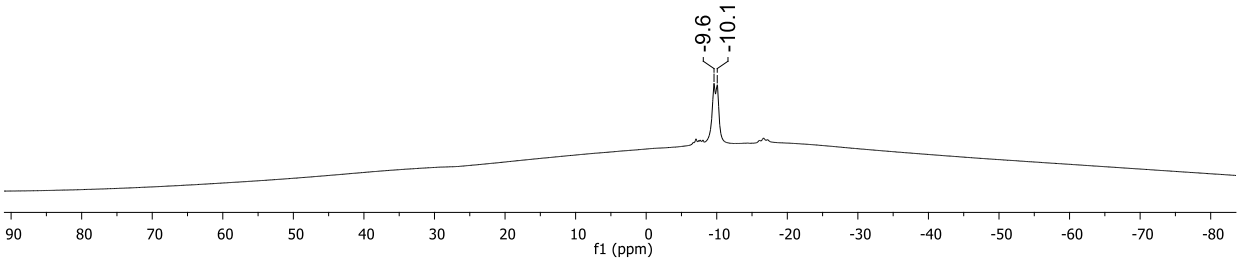

Figure S76. ^{11}B NMR spectrum of Li_2[**7**-H_2] (128.4 MHz, THF-d_8).

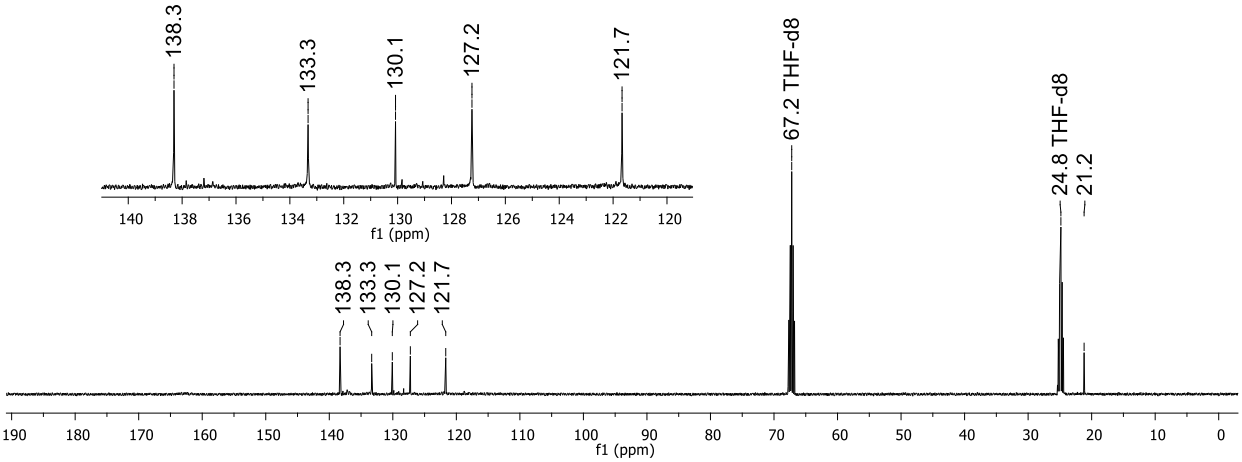

Figure S77. $^{13}C\{^{1}H\}$ NMR spectrum of Li_2[**7**-H_2] (100.6 MHz, THF-d_8).

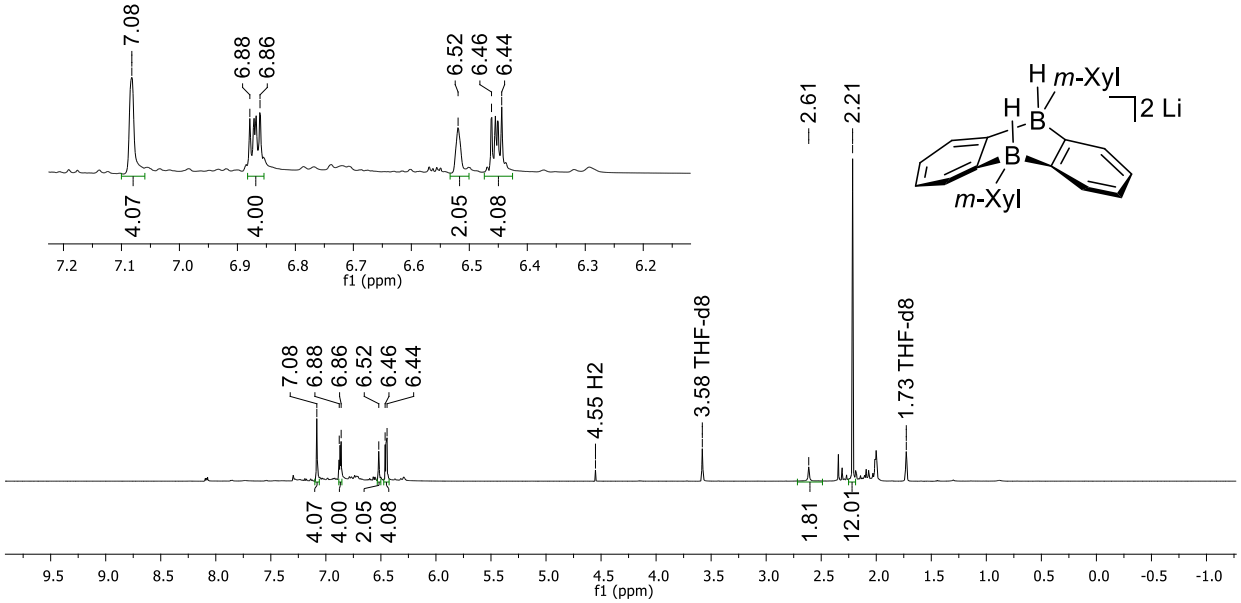

Figure S78. $^{1}H\{^{11}B\}$ NMR spectrum of Li_2[**8**-H_2] (500.2 MHz, THF-d_8).

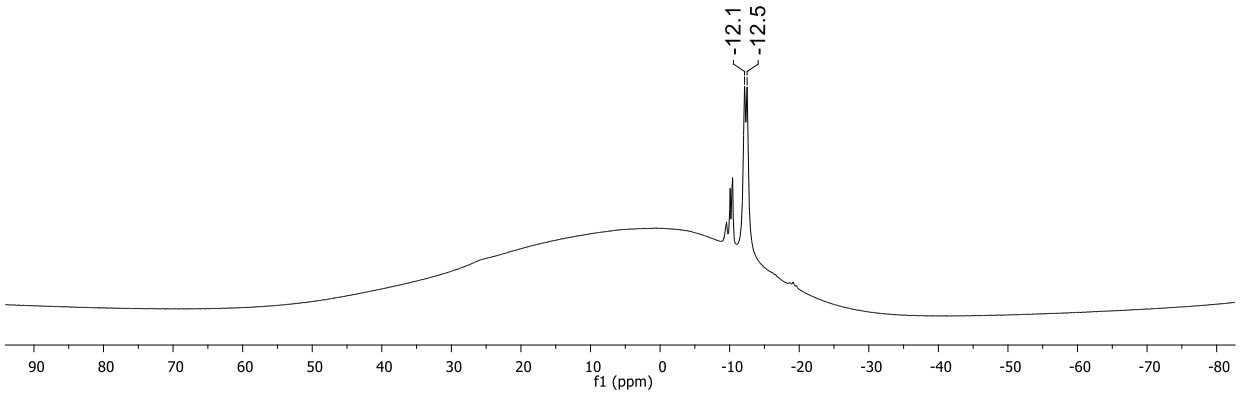

Figure S79. ^{11}B NMR spectrum of Li_2[**8**-H_2] (160.5 MHz, THF-d_8).

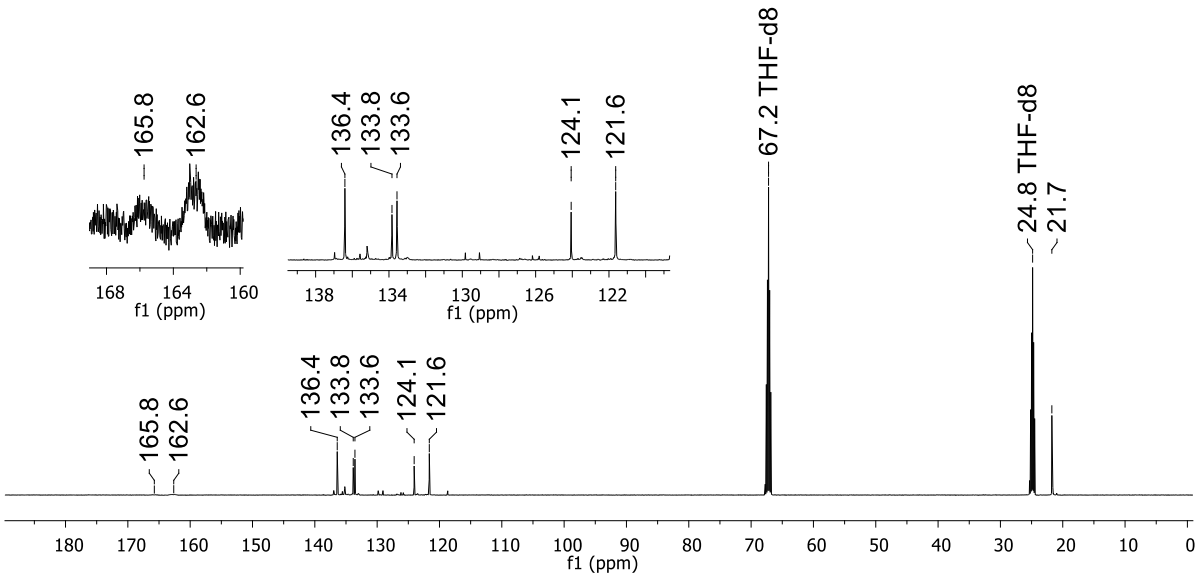

Figure S80. $^{13}C\{^{1}H\}$ NMR spectrum of Li_2[**8**-H_2] (125.8 MHz, THF-d_8).

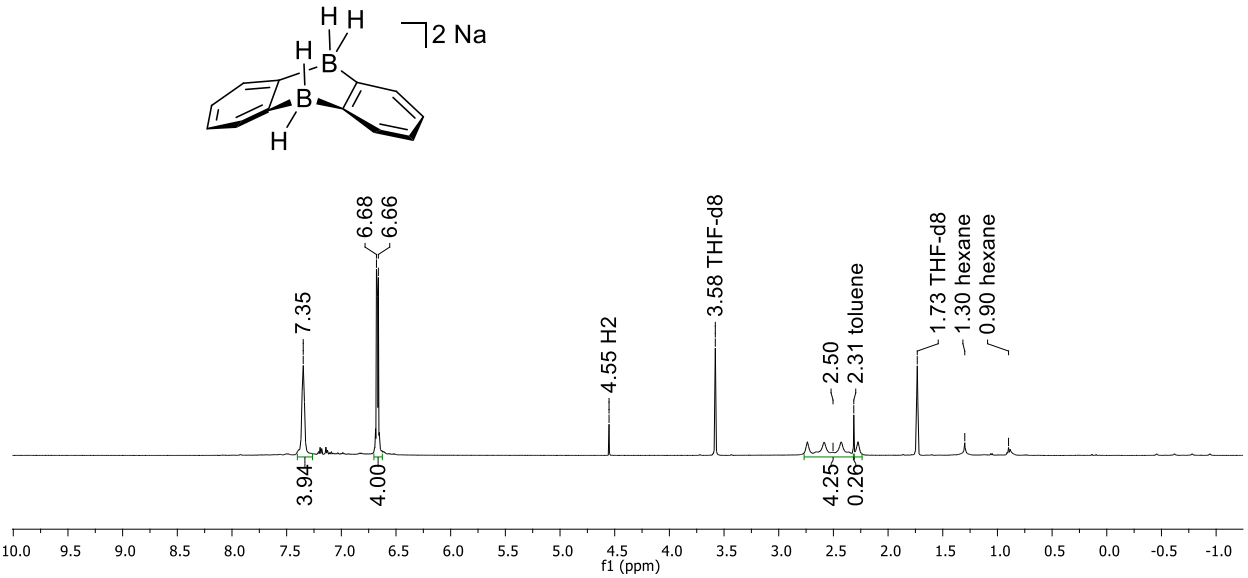

Figure S81. $^{1}H\{^{11}B\}$ NMR spectrum of Na_2[**1**-H_2] (500.2 MHz, THF-d_8).

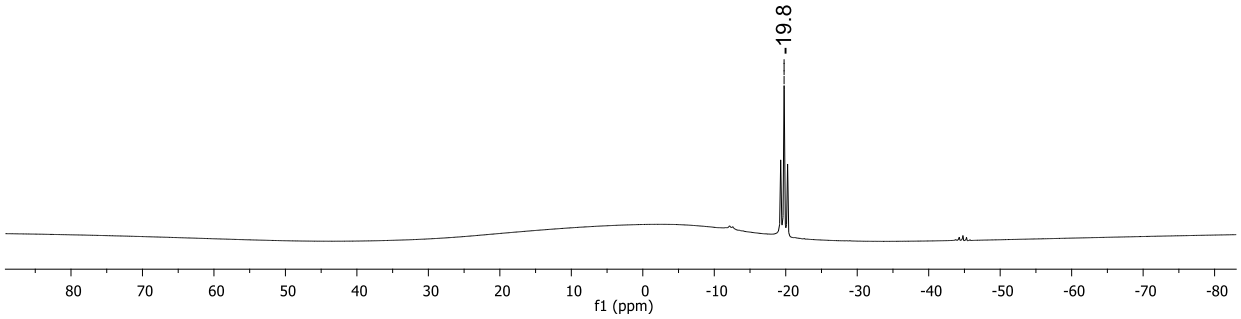

Figure S82. ^{11}B NMR spectrum of Na_2[**1**-H_2] (160.5 MHz, THF-d_8).

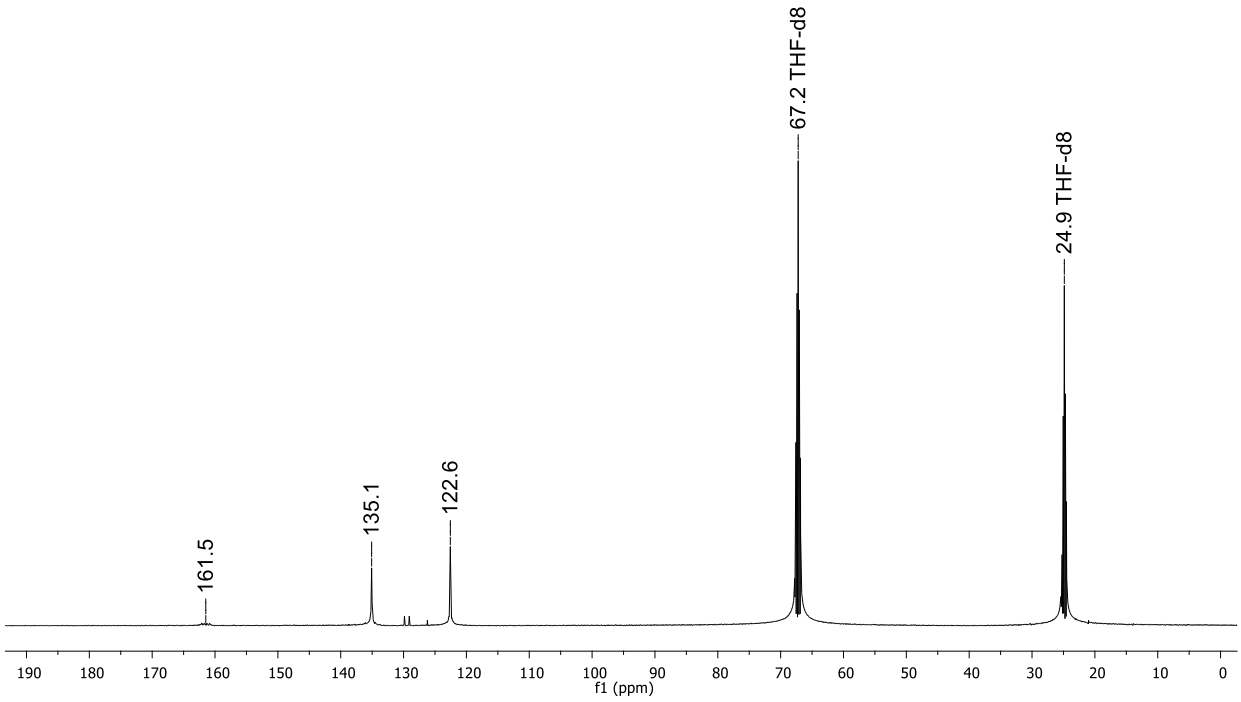

Figure S83. $^{13}C\{^{1}H\}$ NMR spectrum of Na_2[**1**-H_2] (125.8 MHz, THF-d_8).

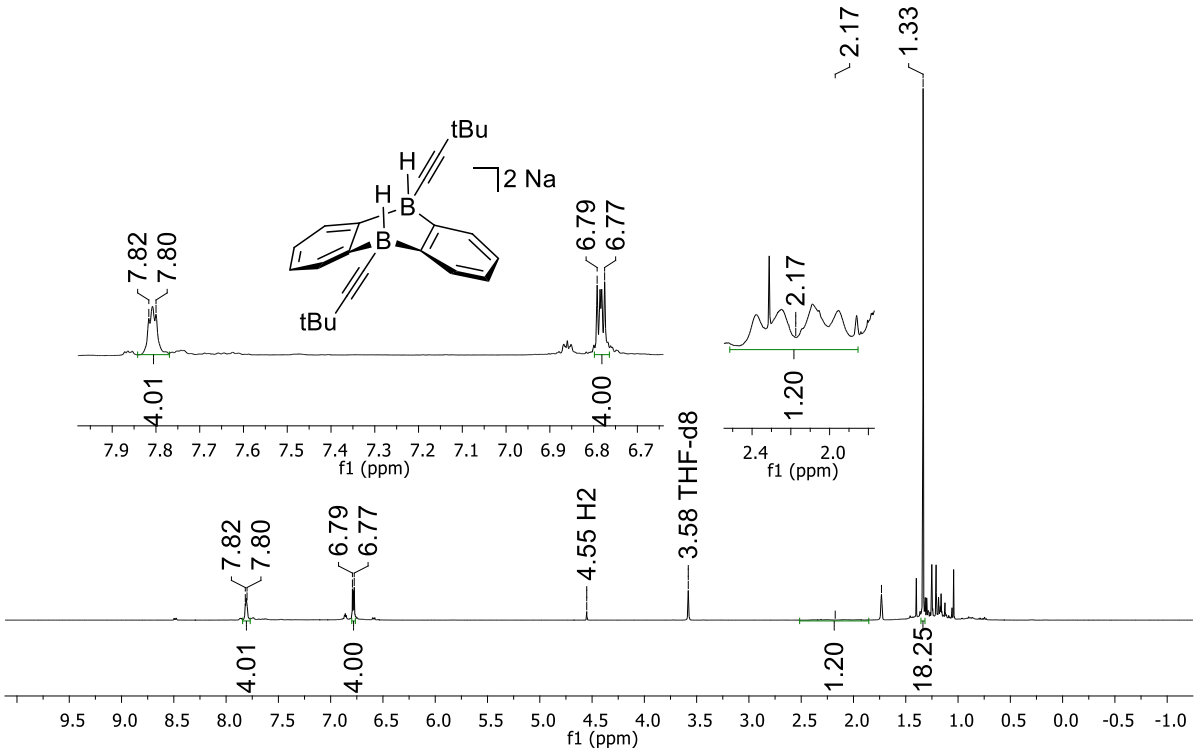

Figure S84. ^{1}H NMR spectrum of Na_2[**2**-H_2] (500.2 MHz, THF-d_8). Unpicked peaks are not specified decomposition products.

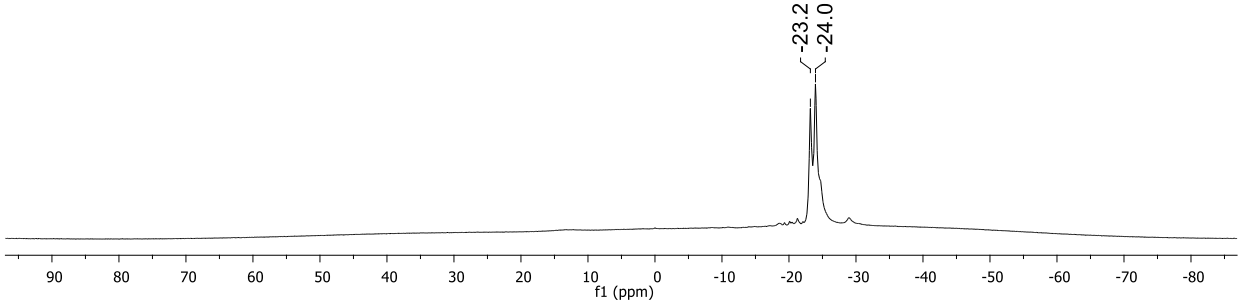

Figure S85. ^{11}B NMR spectrum of Na_2[**2**-H_2] (96.3 MHz, THF-d_8).

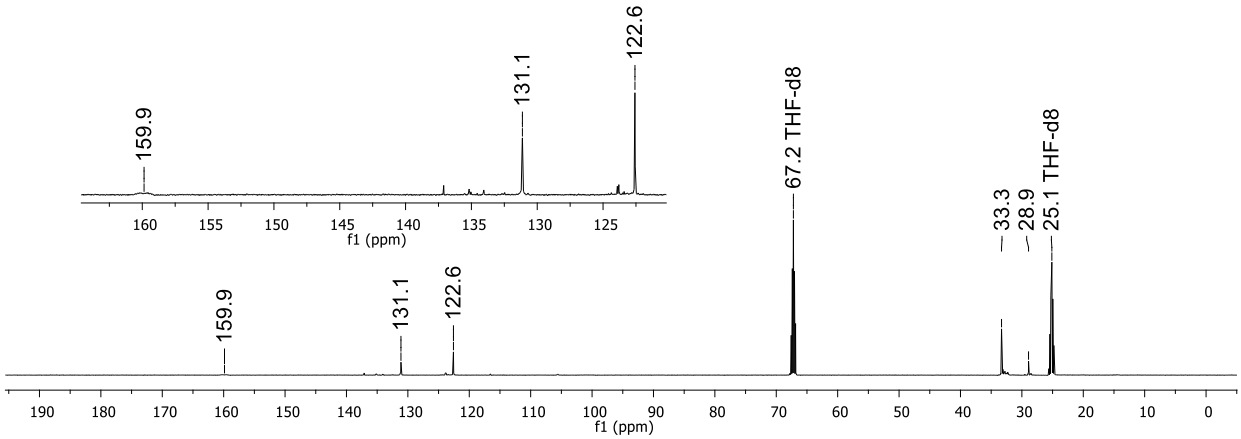

Figure S86. ^{13}C{^{1}H} NMR spectrum of Na_2[**2**-H_2] (125.8 MHz, THF-d_8).

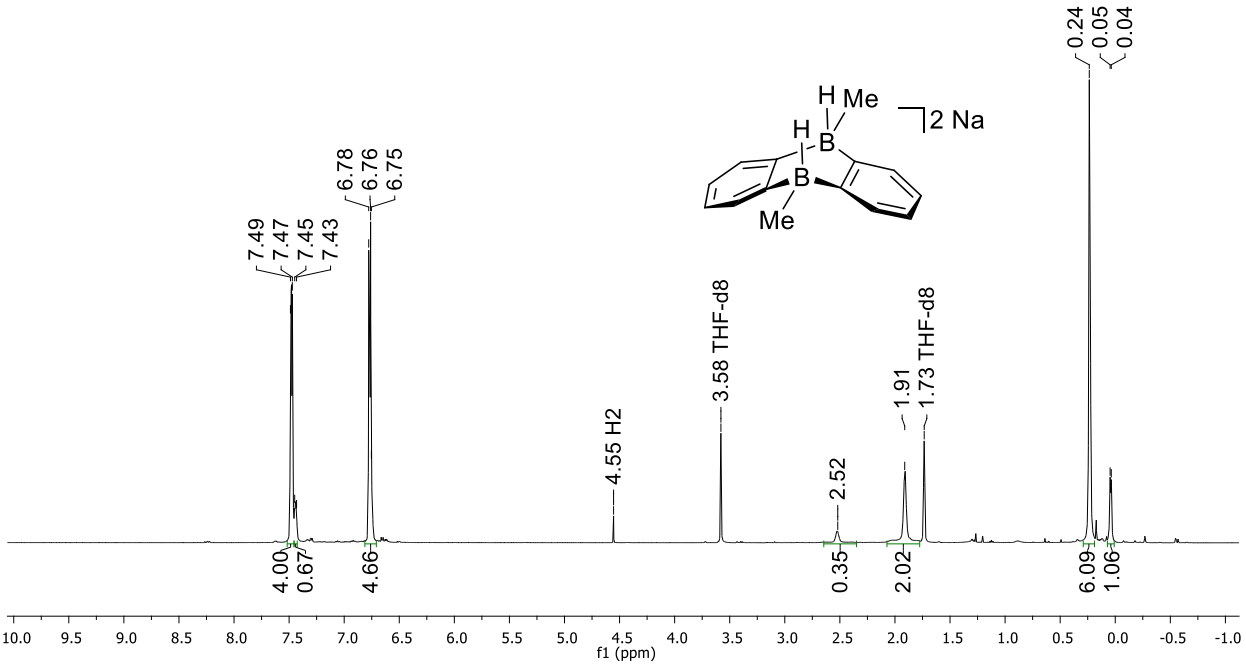

Figure S87. $^{1}H\{^{11}B\}$ NMR spectrum of Na_2[**4**-H_2] (500.2 MHz, THF-d_8).

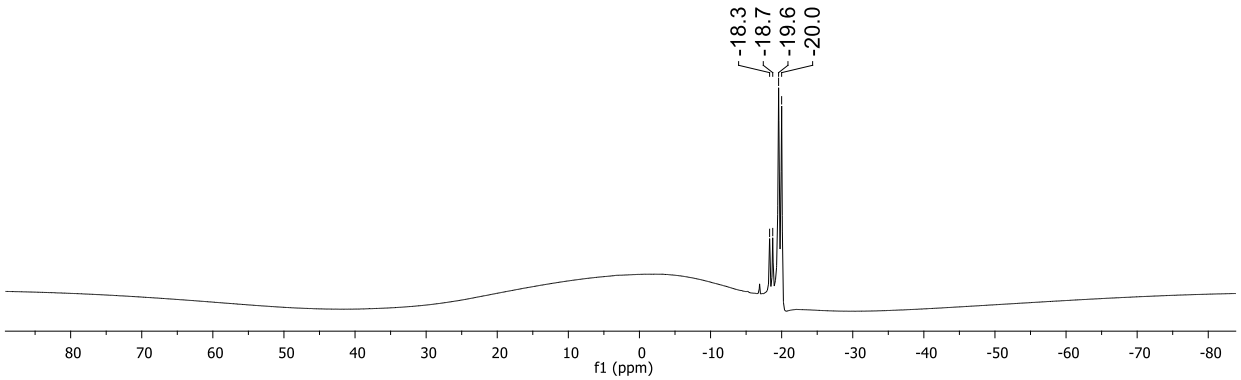

Figure S88. ^{11}B NMR spectrum of Na_2[**4**-H_2] (160.5 MHz, THF-d_8).

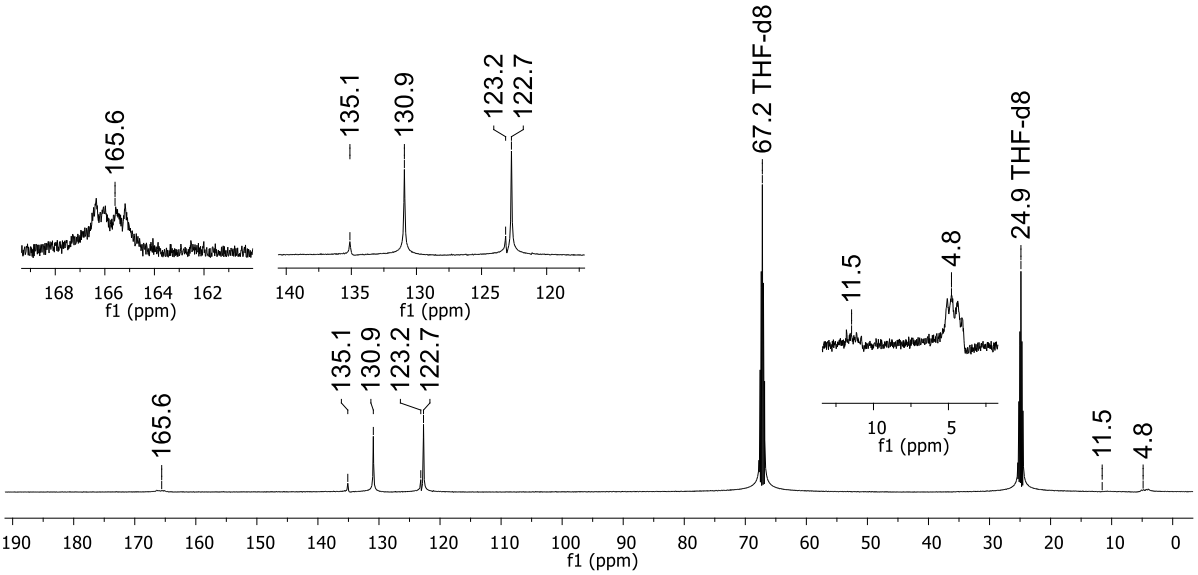

Figure S89. $^{13}C\{^{1}H\}$ NMR spectrum of Na_2[**4**-H_2] (125.8 MHz, THF-d_8).

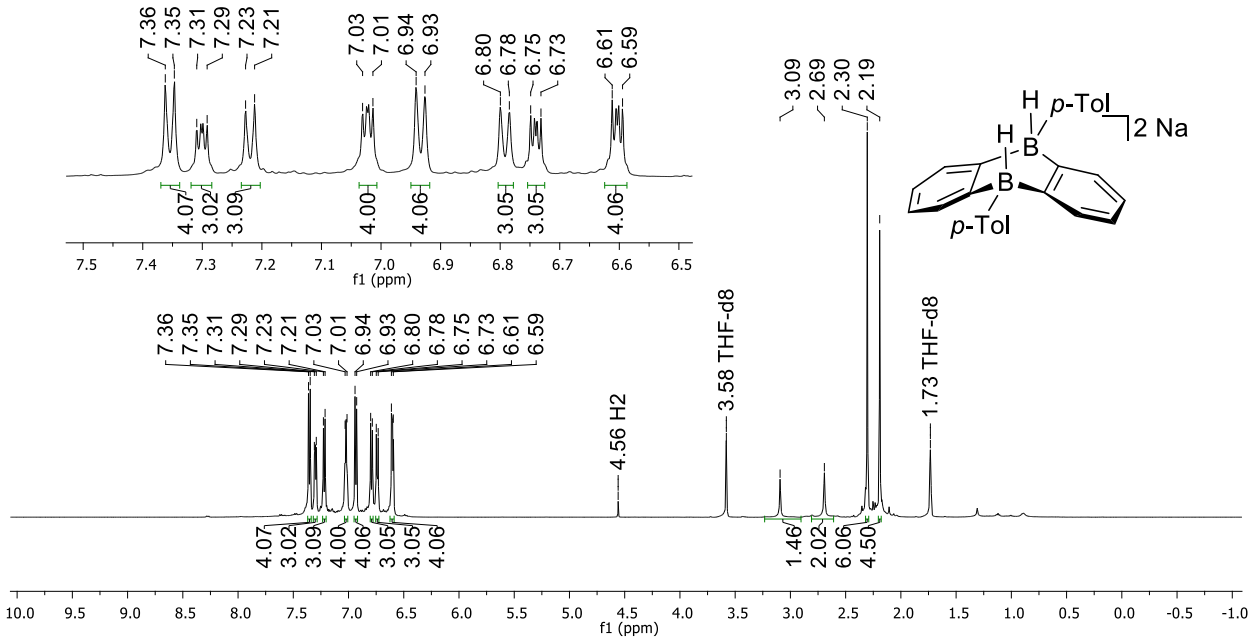

Figure S90. $^{1}H\{^{11}B\}$ NMR spectrum of Na_2[**7**-H_2] (500.2 MHz, THF-d_8).

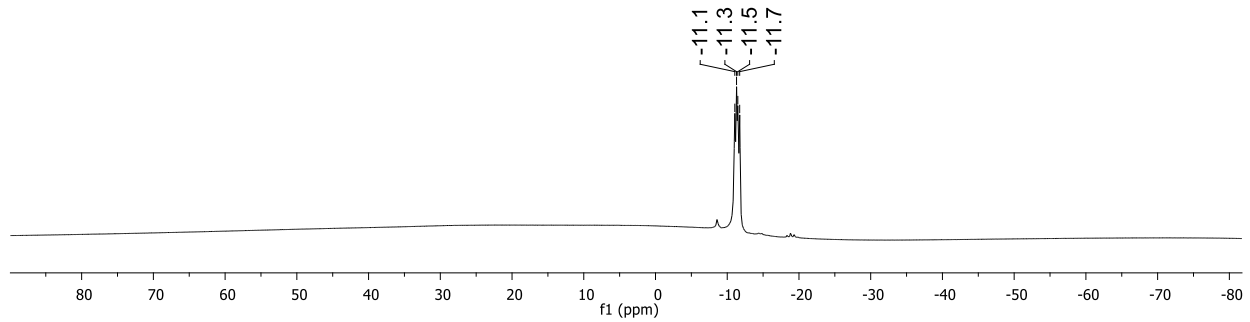

Figure S91. ^{11}B NMR spectrum of Na_2[**7**-H_2] (160.5 MHz, THF-d_8).

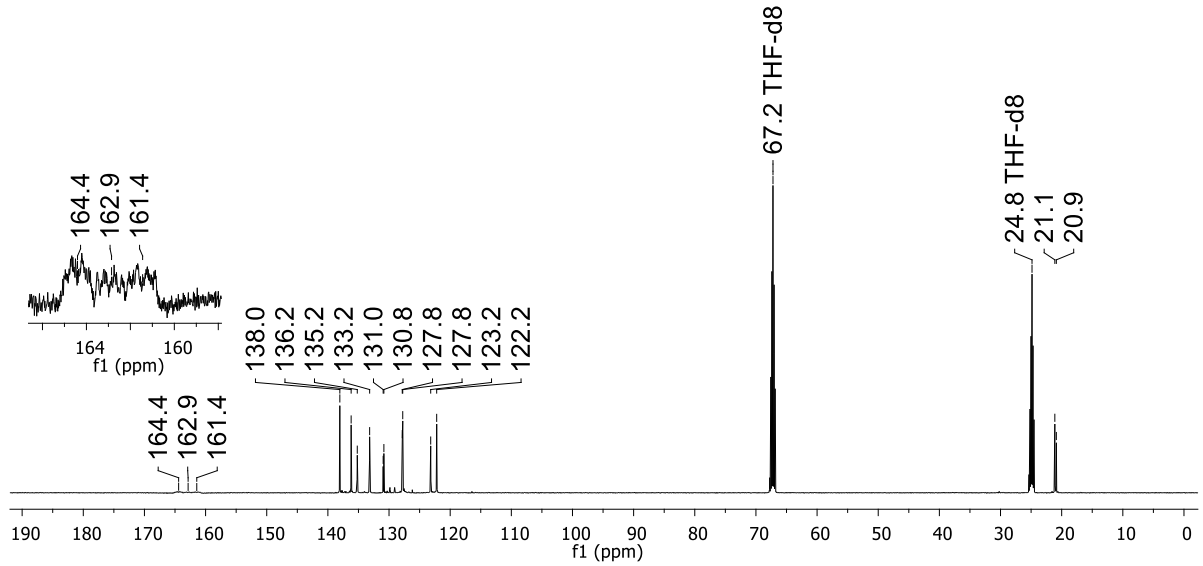

Figure S92. $^{13}C\{^{1}H\}$ NMR spectrum of Na_2[**7**-H_2] (125.8 MHz, THF-d_8).

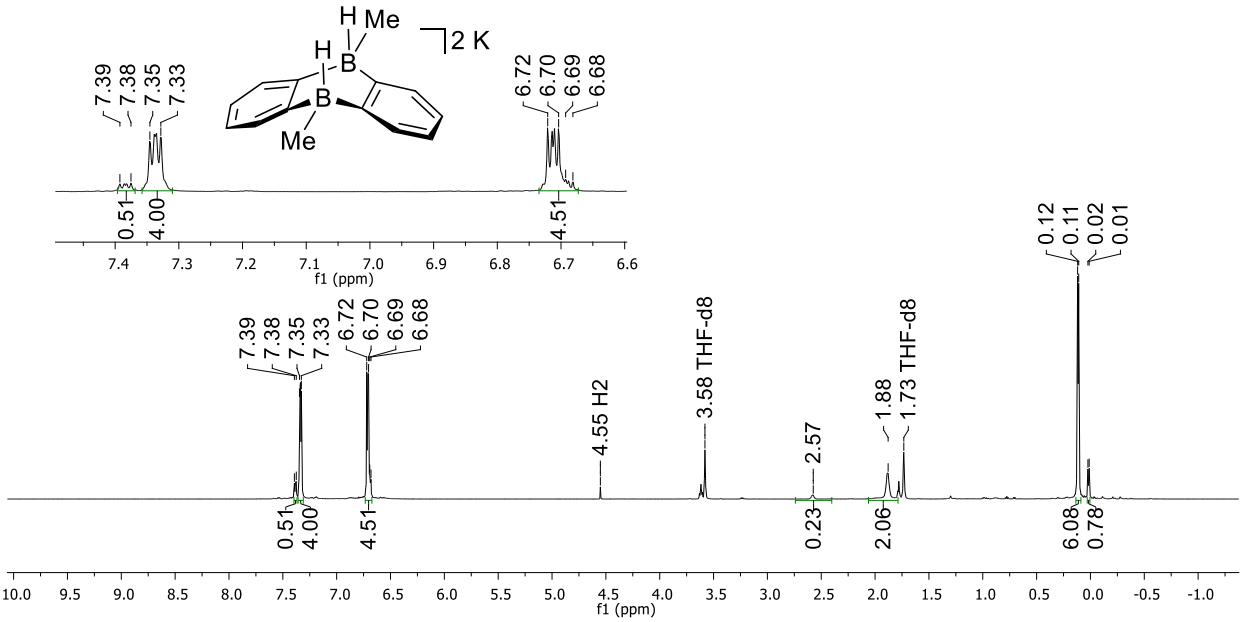

Figure S93. $^{1}H\{^{11}B\}$ NMR spectrum of K_2[**4**-H_2] (500.2 MHz, THF-d_8).

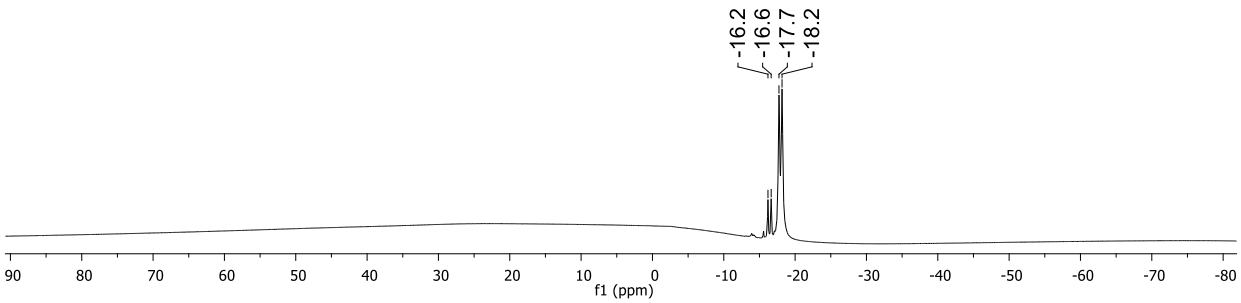

Figure S94. ^{11}B NMR spectrum of K_2[**4**-H_2] (160.5 MHz, THF-d_8).

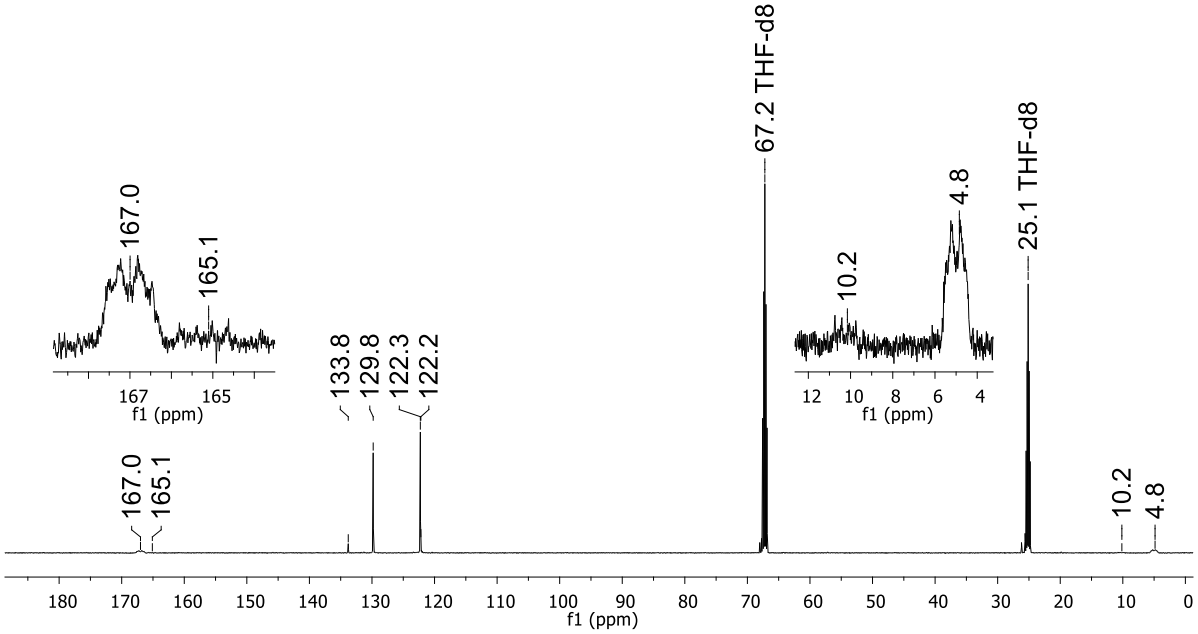

Figure S95. $^{13}C\{^{1}H\}$ NMR spectrum of K_2[**4**-H_2] (125.8 MHz, THF-d_8).

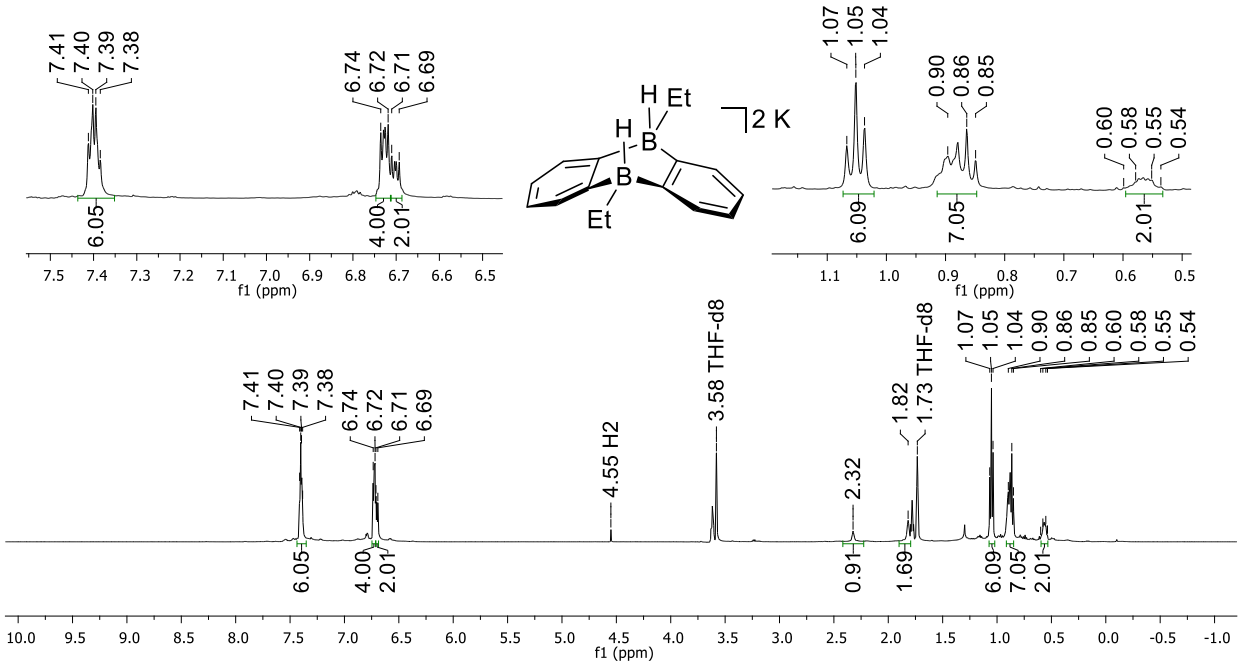

Figure S96. $^{1}H\{^{11}B\}$ NMR spectrum of K_2[**5**-H_2] (500.2 MHz, THF-d_8).

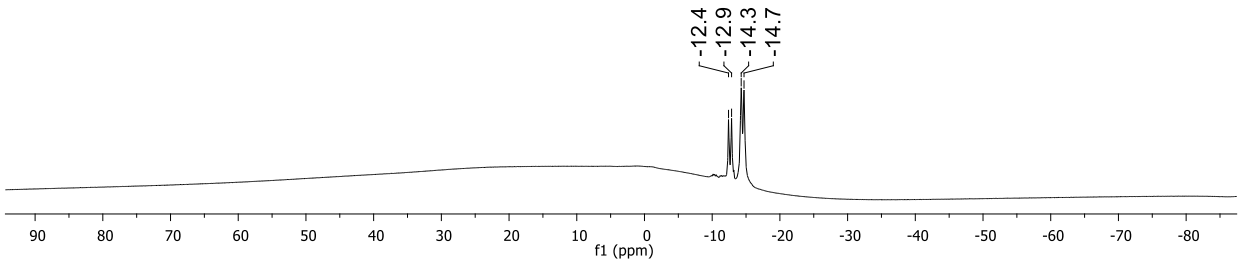

Figure S97. ^{11}B NMR spectrum of K_2[**5**-H_2] (160.5 MHz, THF-d_8).

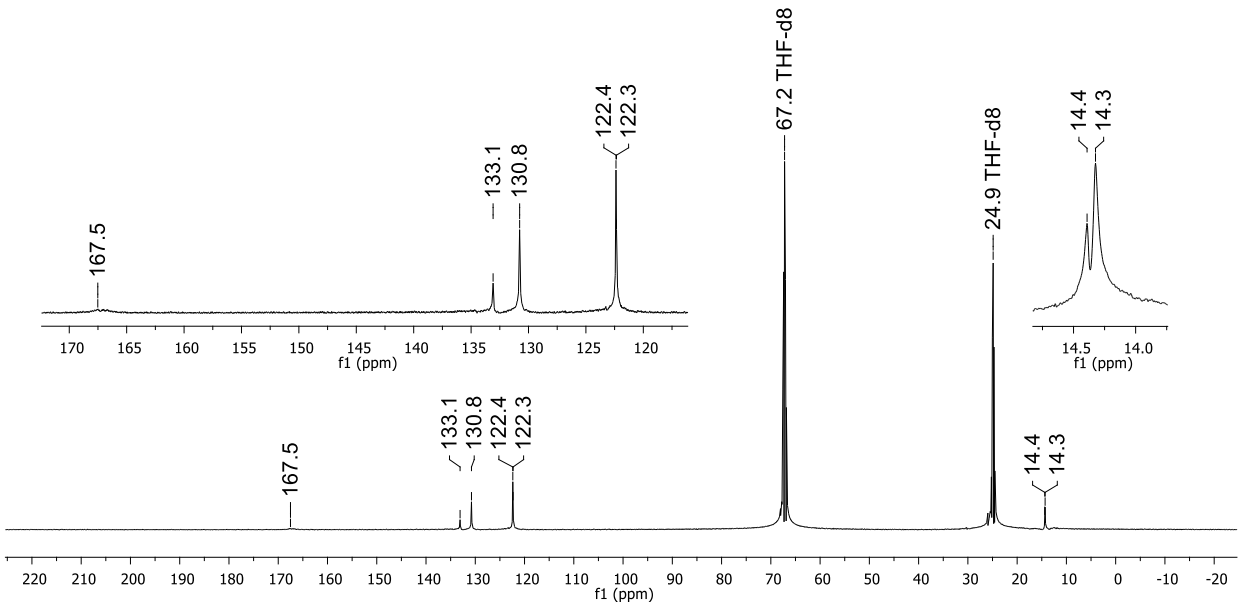

Figure S98. $^{13}C\{^{1}H\}$ NMR spectrum of K_2[**5**-H_2] (125.8 MHz, THF-d_8).

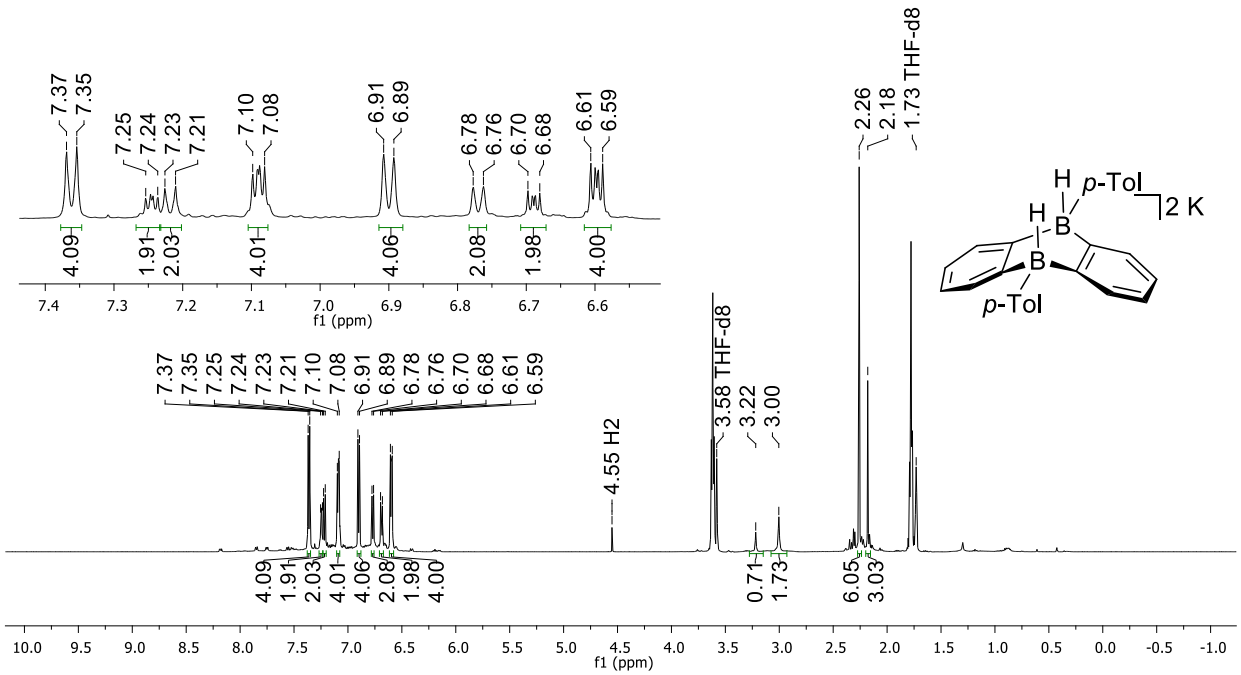

Figure S99. $^{1}H\{^{11}B\}$ NMR spectrum of K_2[**7**-H_2] (500.2 MHz, THF-d_8).

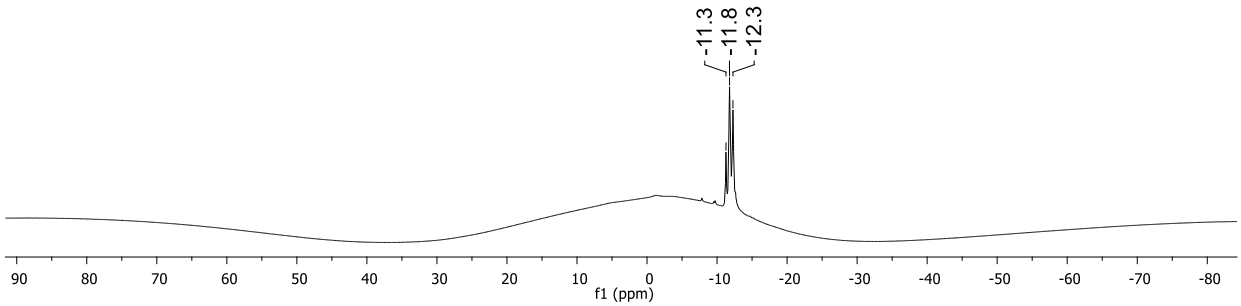

Figure S100. ^{11}B NMR spectrum of K_2[**7**-H_2] (160.5 MHz, THF-d_8).

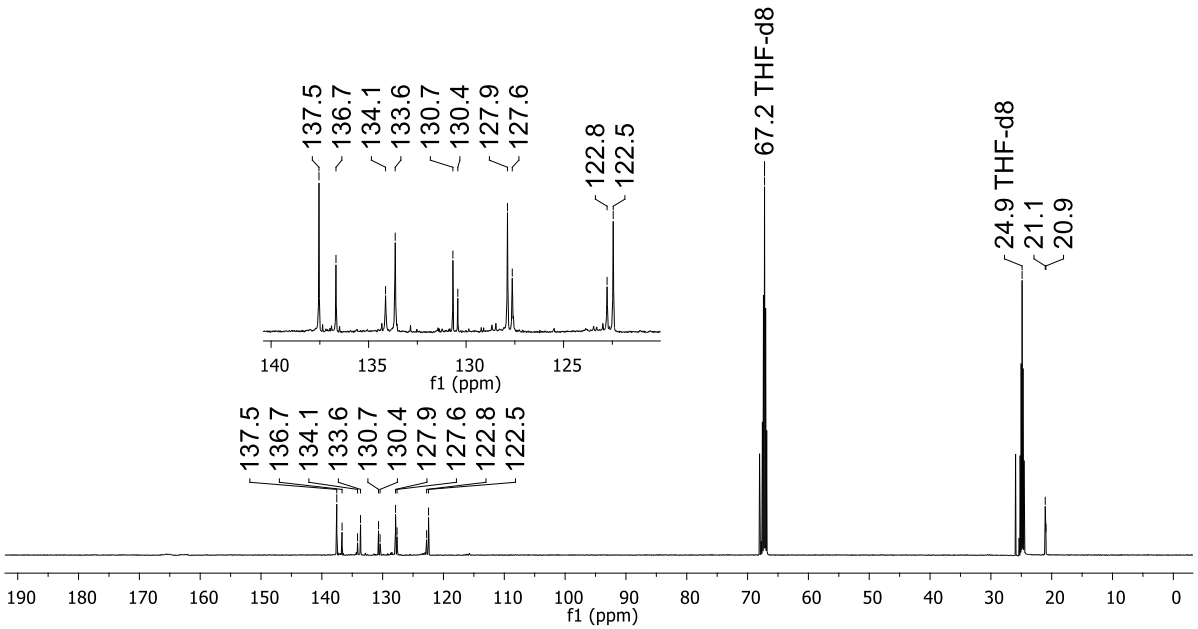

Figure S101. $^{13}C\{^{1}H\}$ NMR spectrum of K_2[**7**-H_2] (125.8 MHz, THF-d_8).

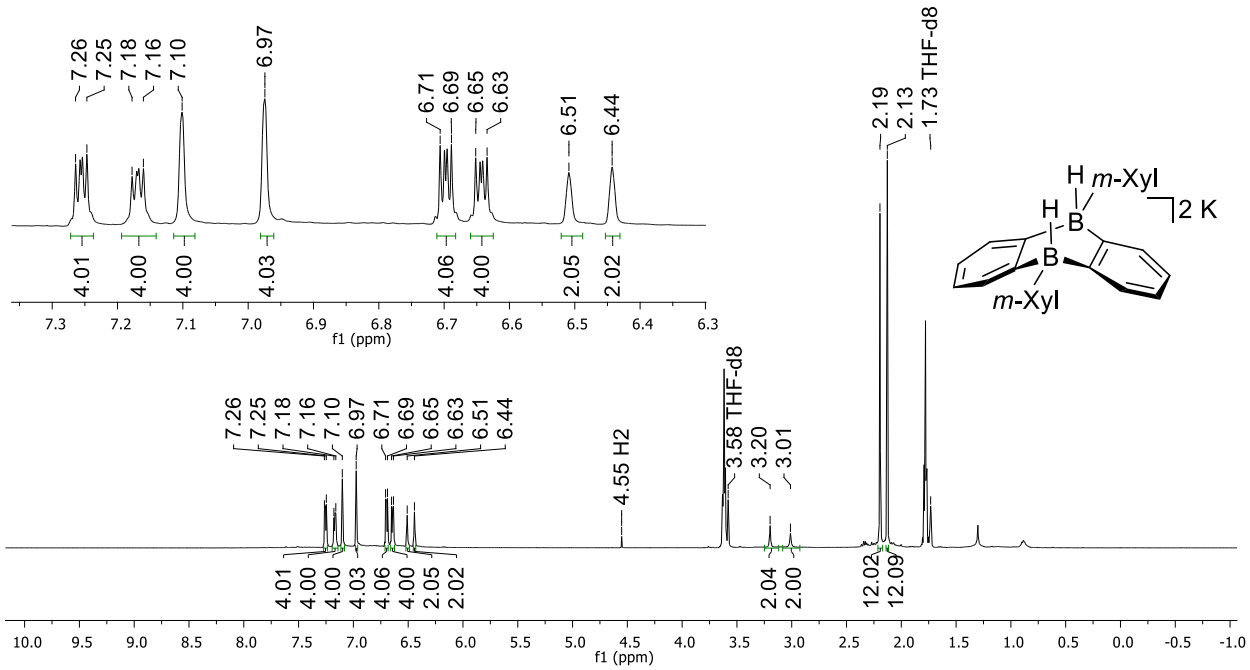

Figure S102. $^{1}H\{^{11}B\}$ NMR spectrum of K_2[**8**-H_2] (500.2 MHz, THF-d_8).

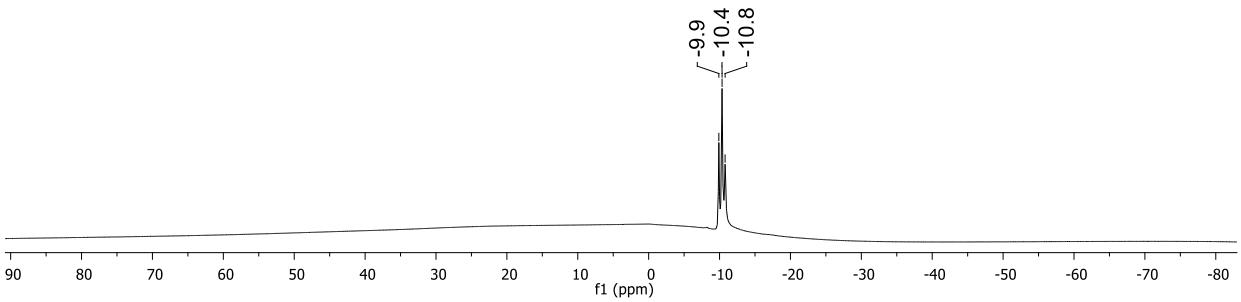

Figure S103. ^{11}B NMR spectrum of K_2[**8**-H_2] (160.5 MHz, THF-d_8).

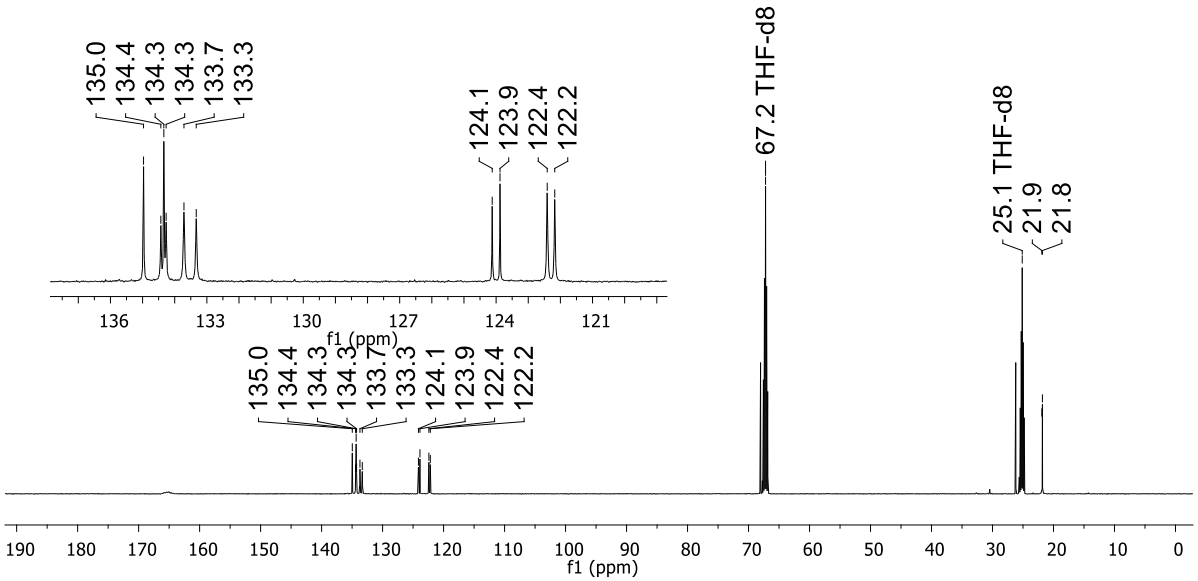

Figure S104. $^{13}C\{^{1}H\}$ NMR spectrum of K_2[**8**-H_2] (125.8 MHz, THF-d_8).

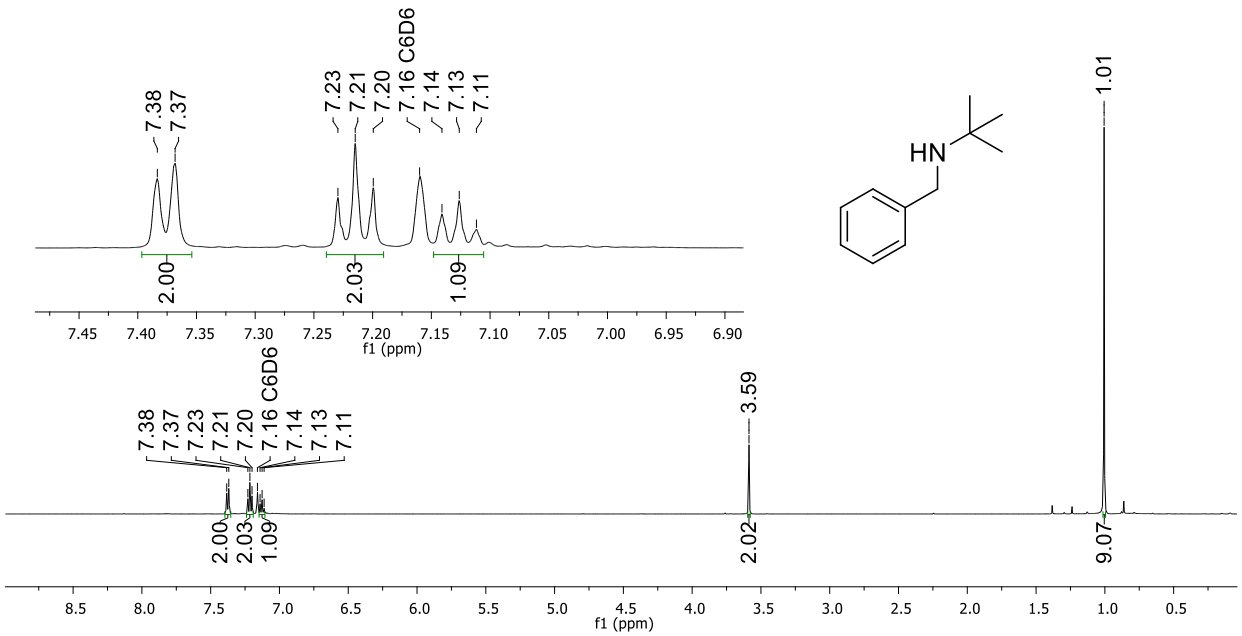

Figure S105. ^{1}H NMR spectrum of the amine Ph(H)$_2$C–N(H)*t*Bu from the autoclave reaction (500.2 MHz, C_6D_6).

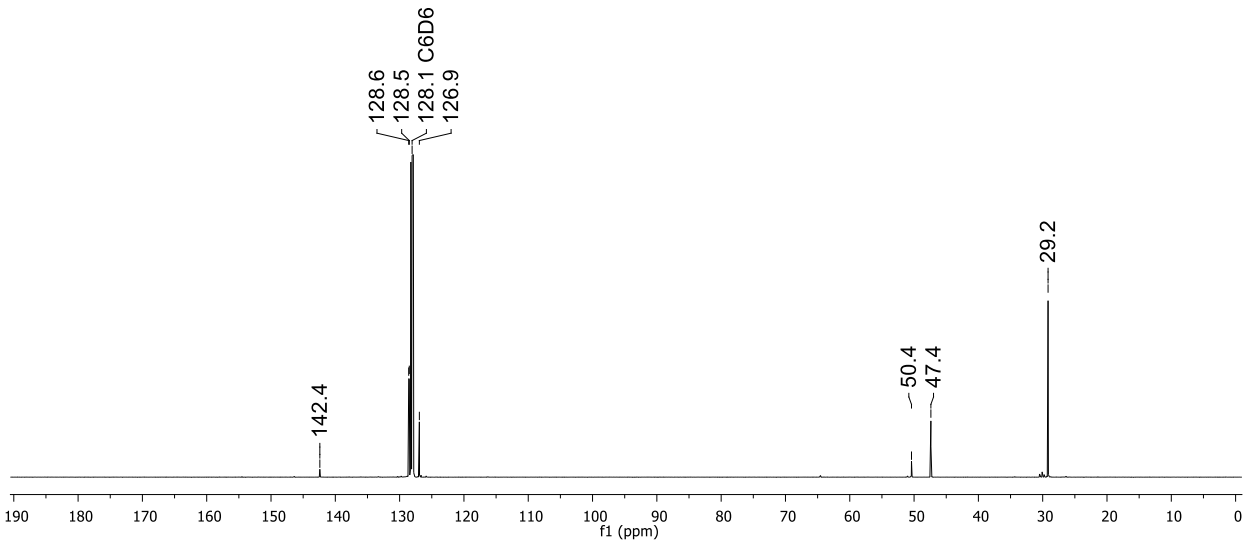

Figure S106. ^{13}C{^{1}H} NMR spectrum of the amine Ph(H)$_2$C–N(H)*t*Bu from the autoclave reaction (125.8 MHz, C_6D_6).

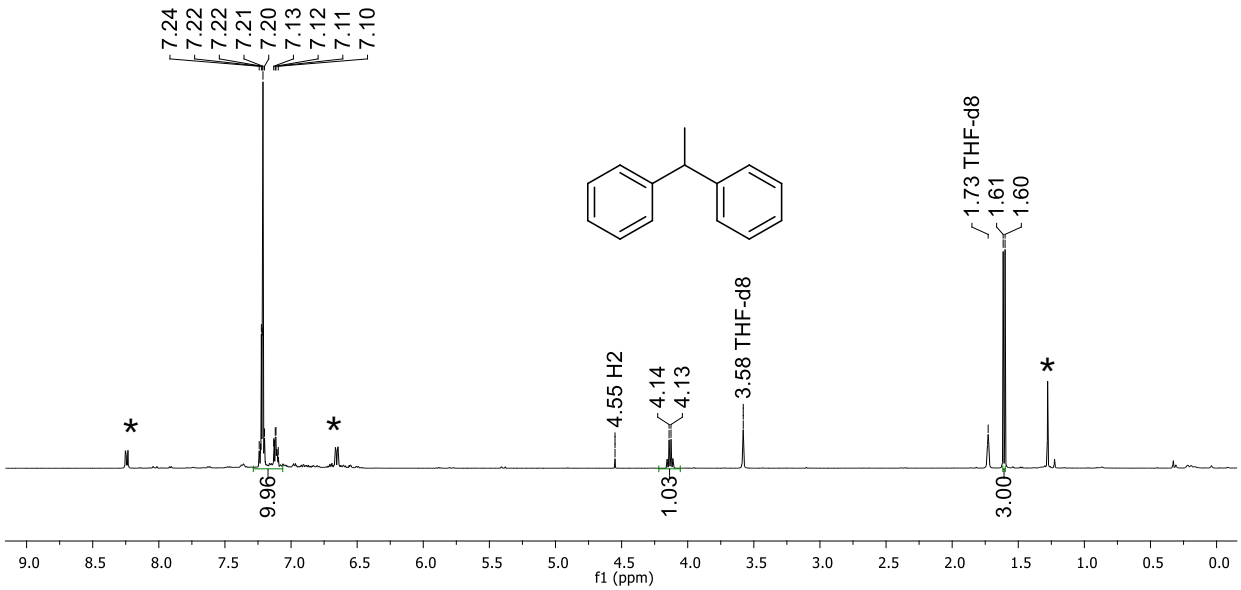

Figure S107. ^{1}H NMR spectrum of 1,1'-diphenylethane (500.2 MHz, THF-d_8). Asterisks mark resonances of the catalyst Li_2[**4**].

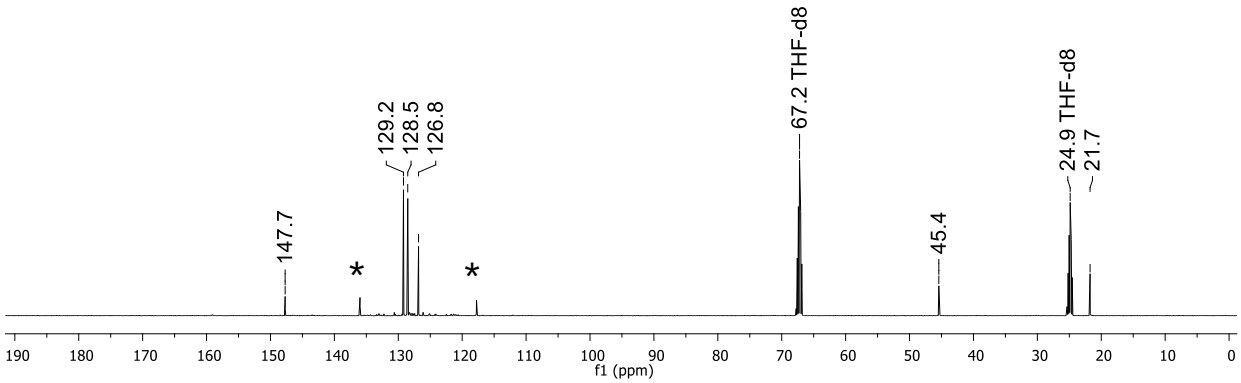

Figure S108. ^{13}C{^{1}H} NMR spectrum of 1,1'-diphenylethane (125.8 MHz, THF-d_8). Asterisks mark resonances of the catalyst Li_2[**4**].

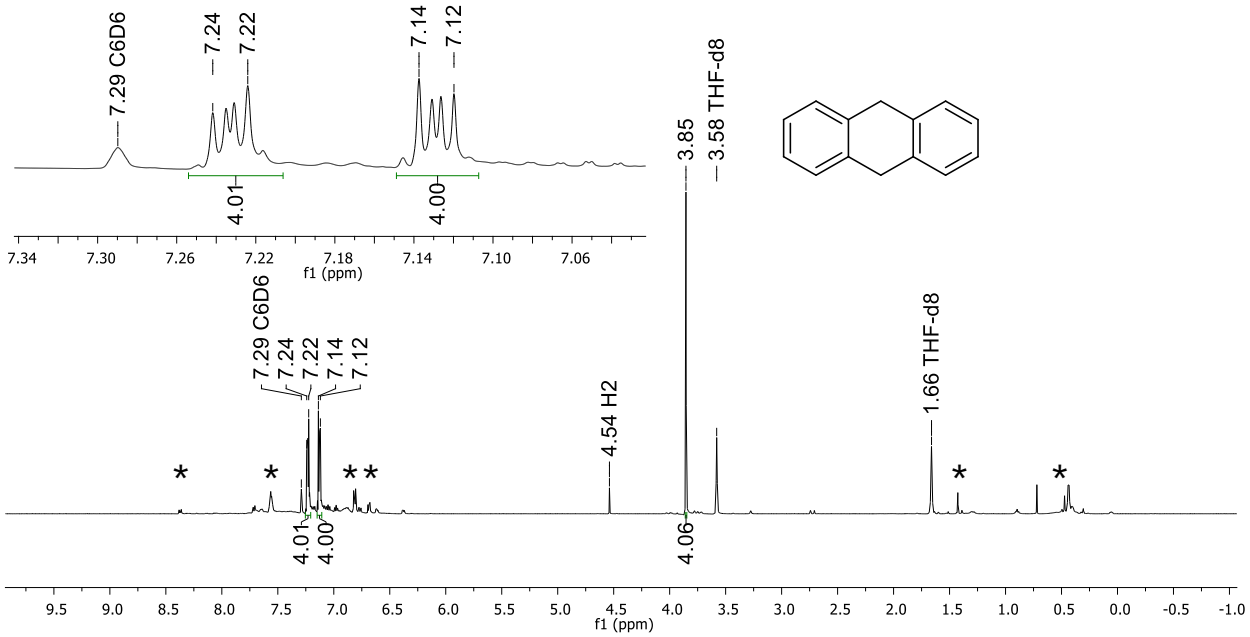

Figure S109. ^{1}H NMR spectrum of 9,10-dihydroanthracene (500.2 MHz, THF-d_8). Asterisks mark resonances of the catalyst Li_2[**4**] and its H_2 addition product.

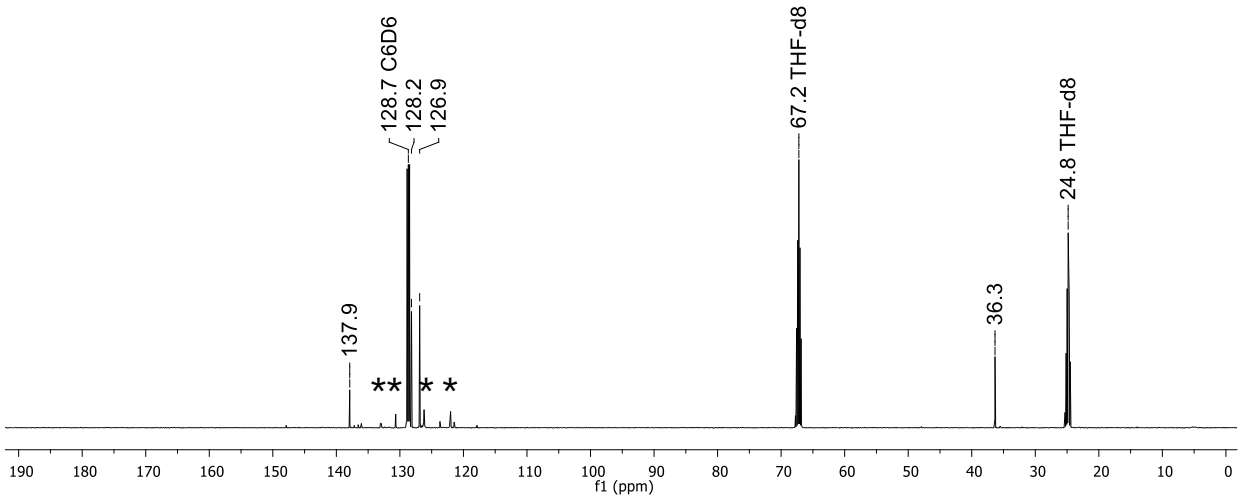

Figure S110. ^{13}C{^{1}H} NMR spectrum of 9,10-dihydroanthracene (125.8 MHz, THF-d_8). Asterisks mark resonances of the catalyst Li_2[**4**] and its H_2 addition product.

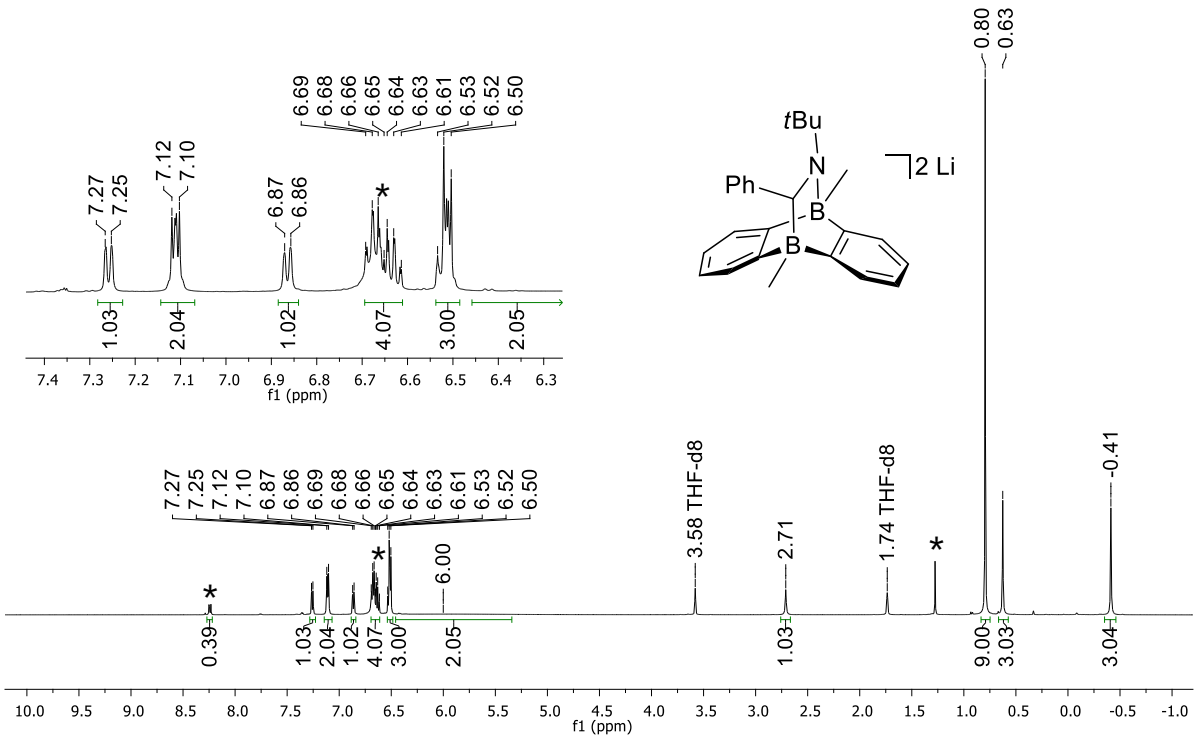

Figure S111. ^{1}H NMR spectrum of Li[**10**] (500.2 MHz, THF-d_8). Asterisks mark resonances of the starting material Li_2[**4**].

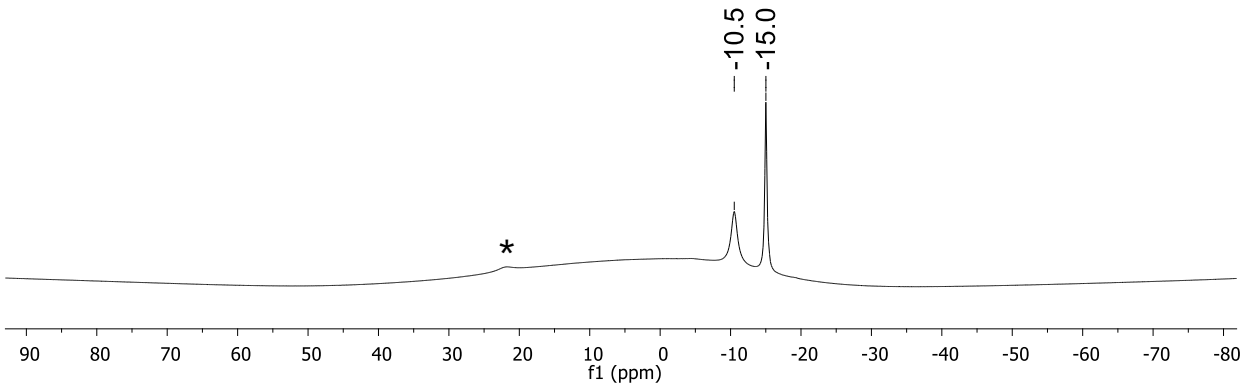

Figure S112. ^{11}B NMR spectrum of Li[**10**] (160.5 MHz, THF-d_8). Asterisk marks resonances of the starting material Li_2[**4**].

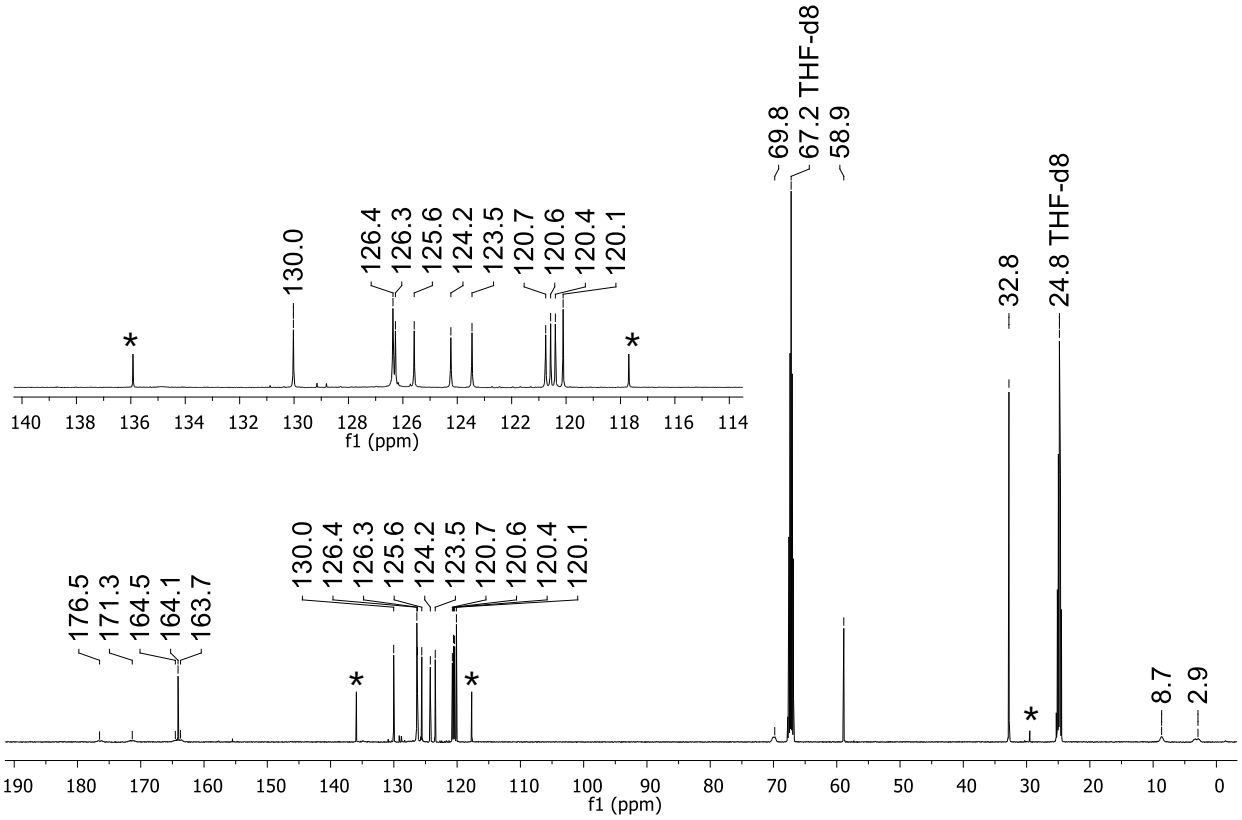

Figure S113. $^{13}C\{^{1}H\}$ NMR spectrum of Li[**10**] (125.8 MHz, THF-d_8). Asterisks mark resonances of the starting material Li_2[**4**].

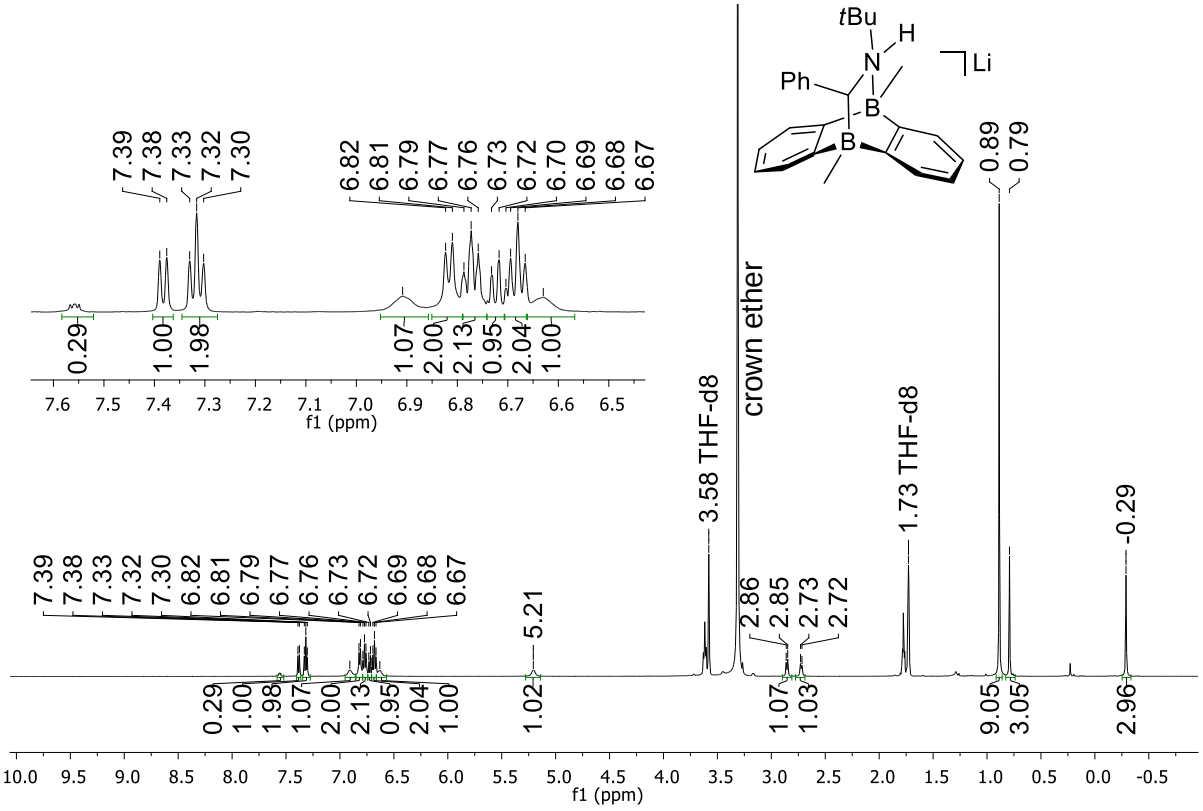

Figure S114. ^{1}H NMR spectrum of crystals of LiH[**10**] (500.2 MHz, THF-d_8).

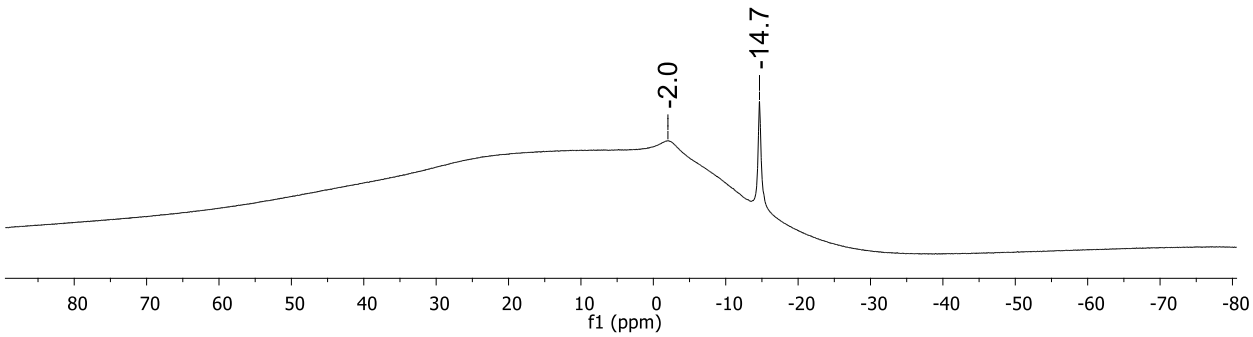

Figure S115. ^{11}B NMR spectrum of crystals of LiH[**10**] (160.5 MHz, THF-d_8).

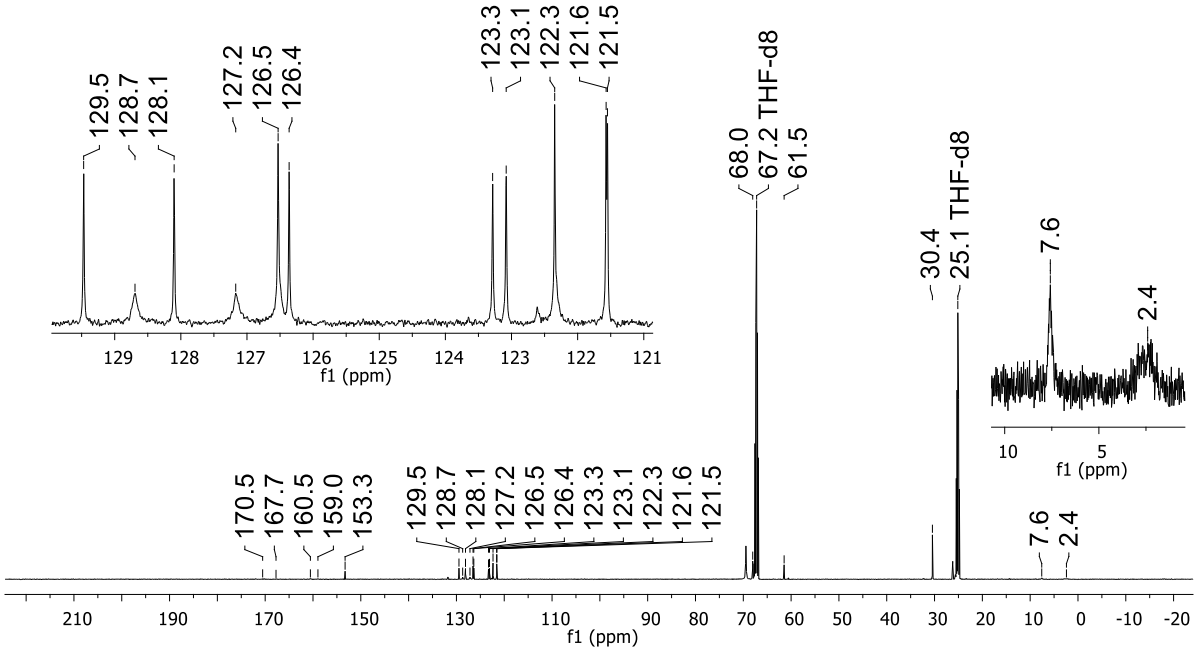

Figure S116. ^{13}C{^{1}H} NMR spectrum of crystals of LiH[**10**] (125.8 MHz, THF-d_8).

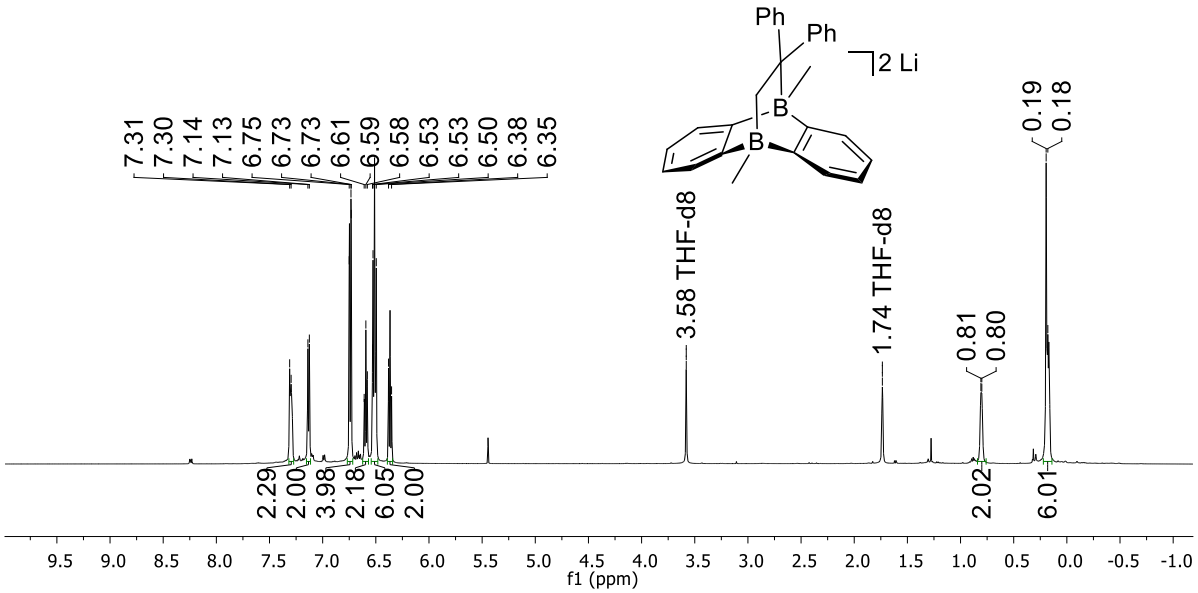

Figure S117. ^{1}H NMR spectrum of the cycloadduct of Li_2[**4**] with 1,1'-diphenylethylene (500.2 MHz, THF-d_8).

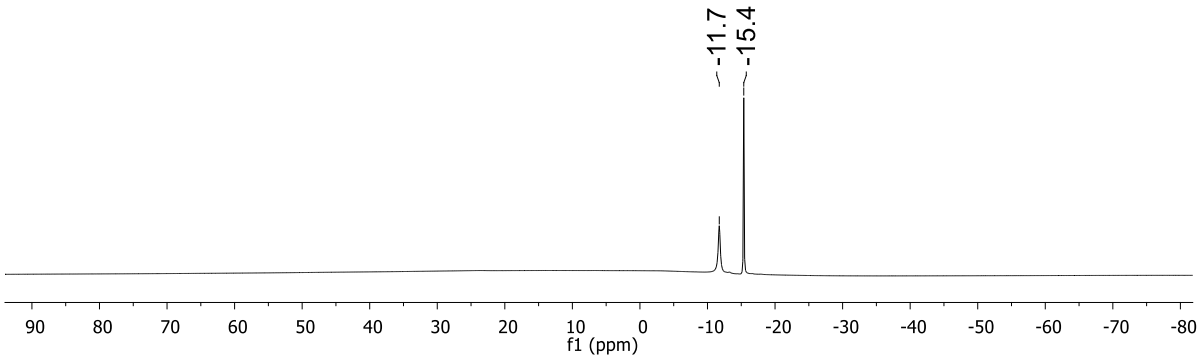

Figure S118. ^{11}B NMR spectrum of the cycloadduct of Li_2[**4**] with 1,1'-diphenylethylene (160.5 MHz, THF-d_8).

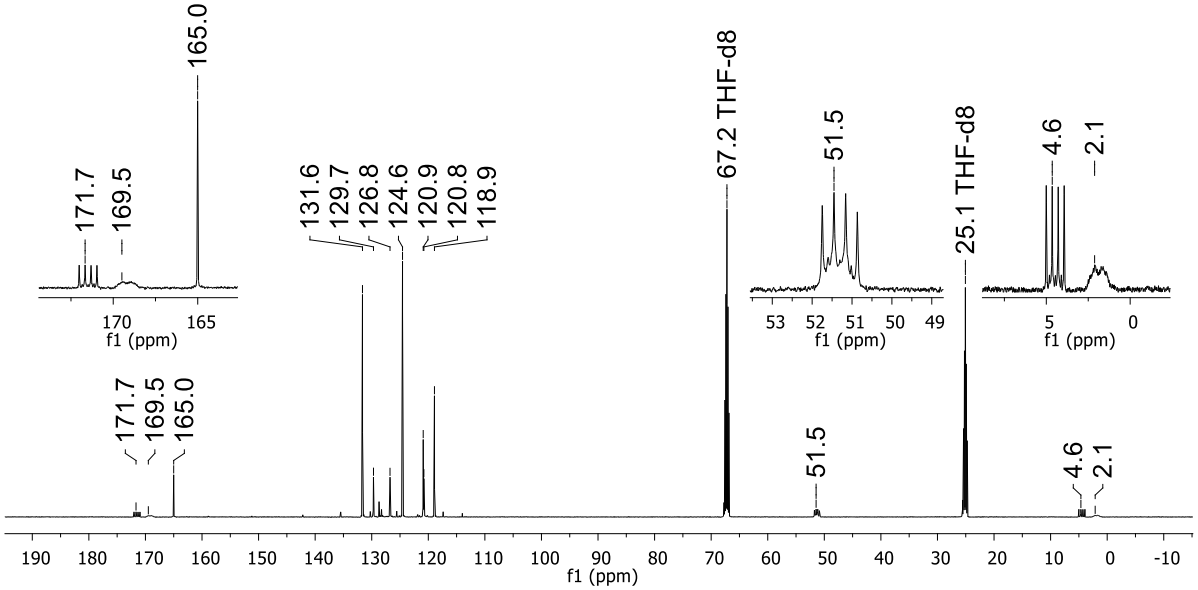

Figure S119. ^{13}C{^{1}H} NMR spectrum of the cycloadduct of Li_2[**4**] with 1,1'-diphenylethylene (125.8 MHz, THF-d_8).

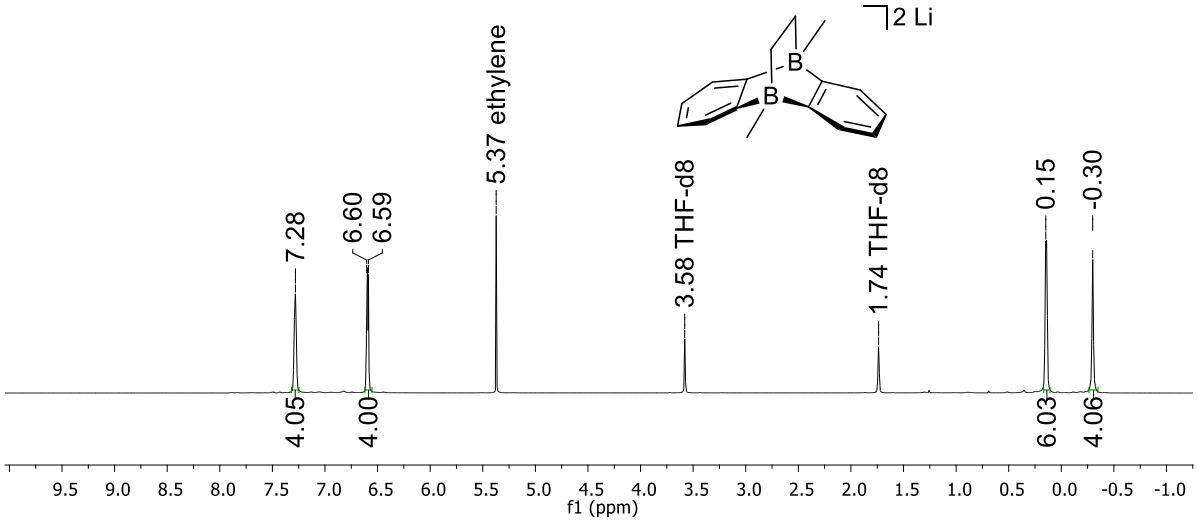

Figure S120. ^{1}H NMR spectrum of Li_2[**11**] (500.2 MHz, THF-d_8).

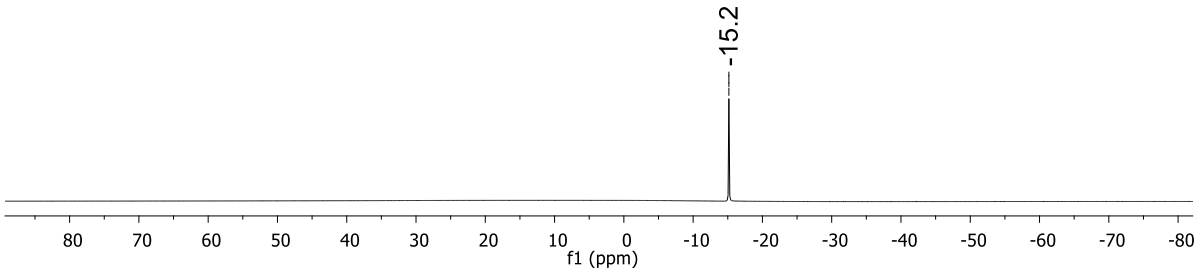

Figure S121. ^{11}B NMR spectrum of Li_2[**11**] (160.5 MHz, THF-d_8).

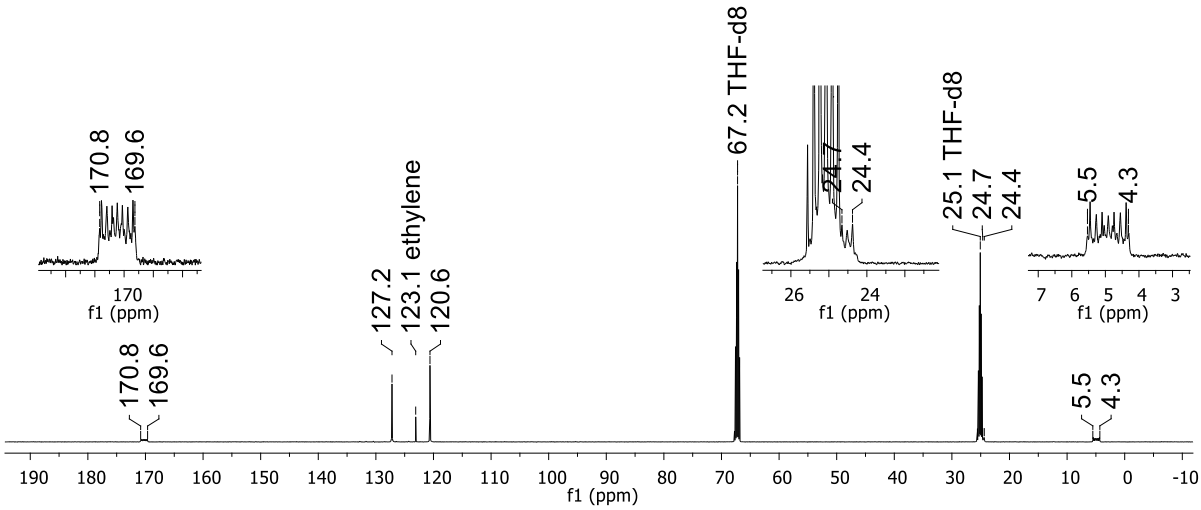

Figure S122. ^{13}C{^{1}H} NMR spectrum of Li_2[**11**] (125.8 MHz, THF-d_8).

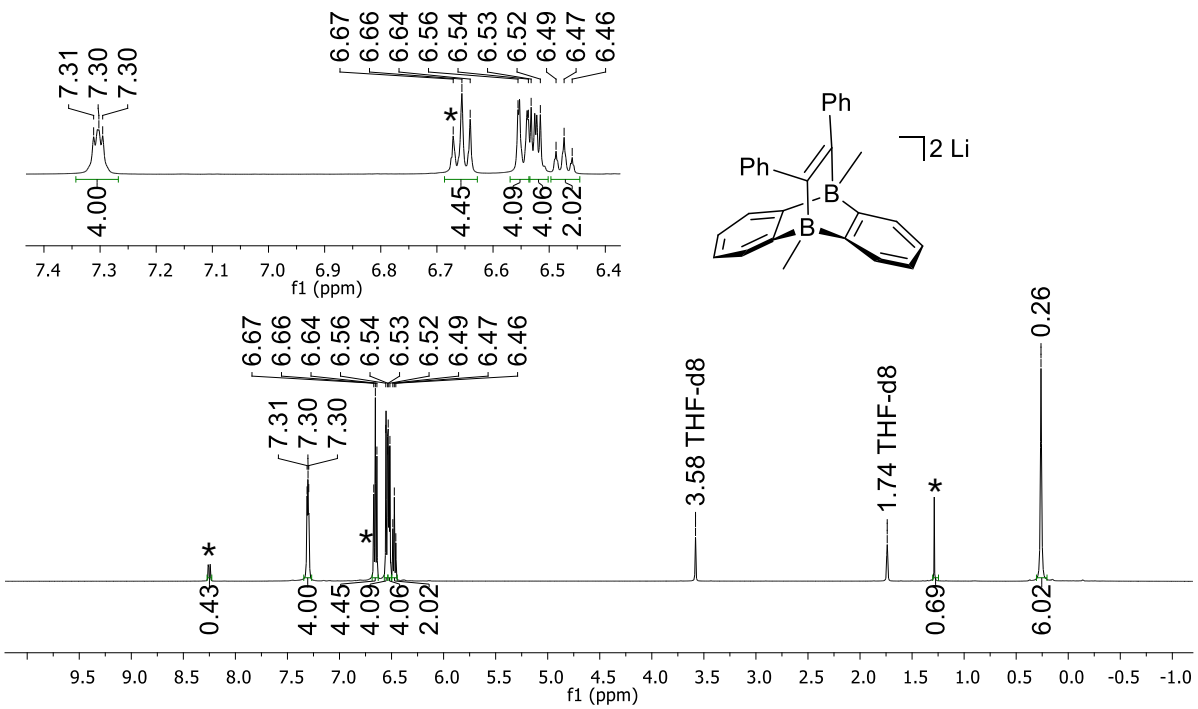

Figure S123. ^{1}H NMR spectrum of the cycloadduct of Li_2[**4**] with diphenylacetylene (500.2 MHz, THF-d_8). Asterisks mark resonances of the starting material Li_2[**4**].

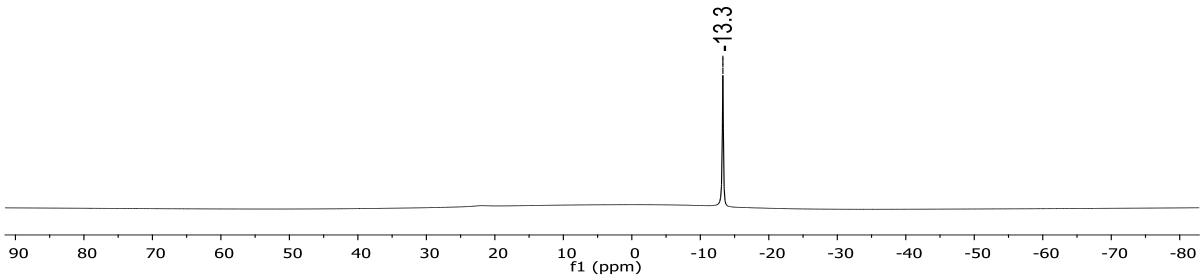

Figure S124. ^{11}B NMR spectrum of the cycloadduct of Li_2[**4**] with diphenylacetylene (160.5 MHz, THF-d_8).

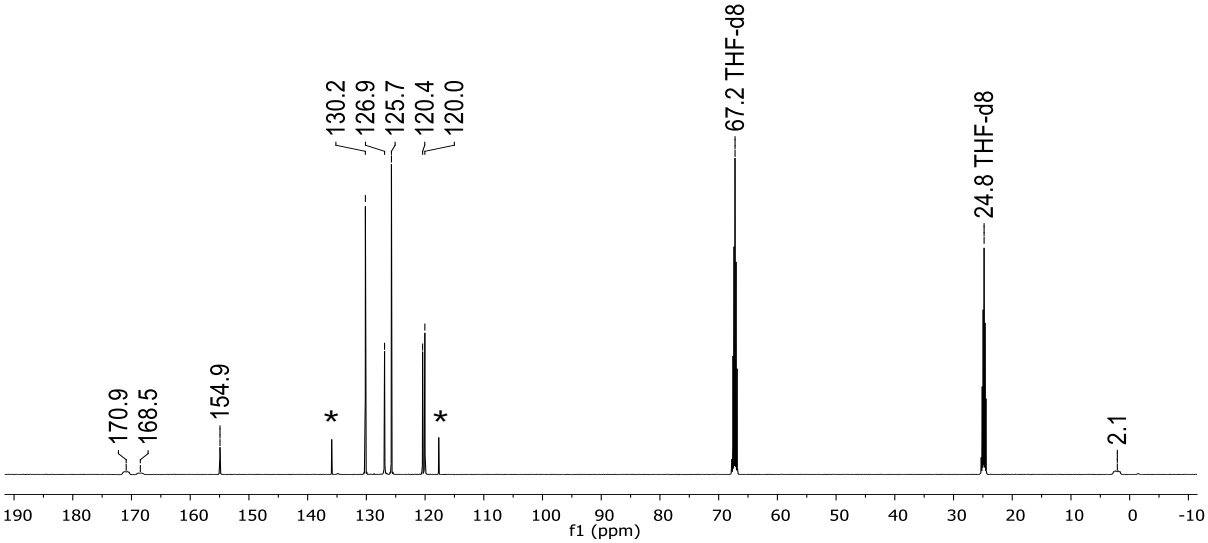

Figure S125. ^{13}C{^{1}H} NMR spectrum of the cycloadduct of Li_2[**4**] with diphenylacetylene (125.8 MHz, THF-d_8). Asterisks mark resonances of the starting material Li_2[**4**].

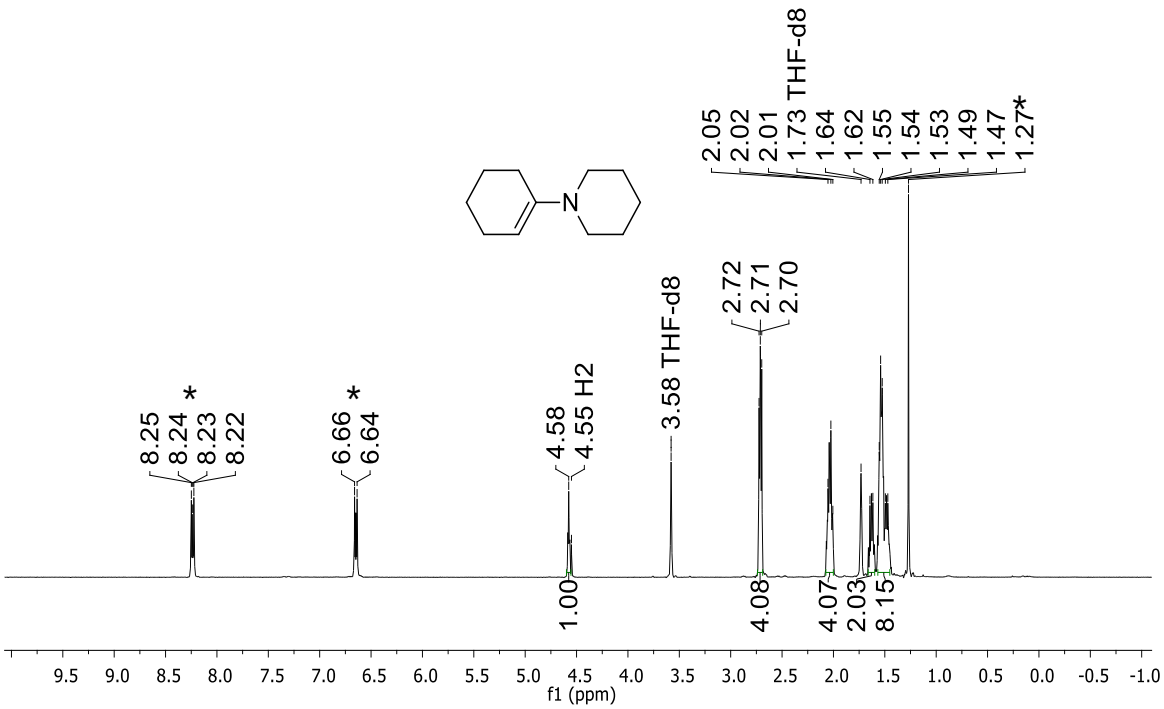

Figure S126. ^{1}H NMR spectrum of 1-(1-piperidinyl)cyclohexene beside Li_2[**4**] (400.1 MHz, THF-d_8).). Asterisks mark resonances of the starting material Li_2[**4**].

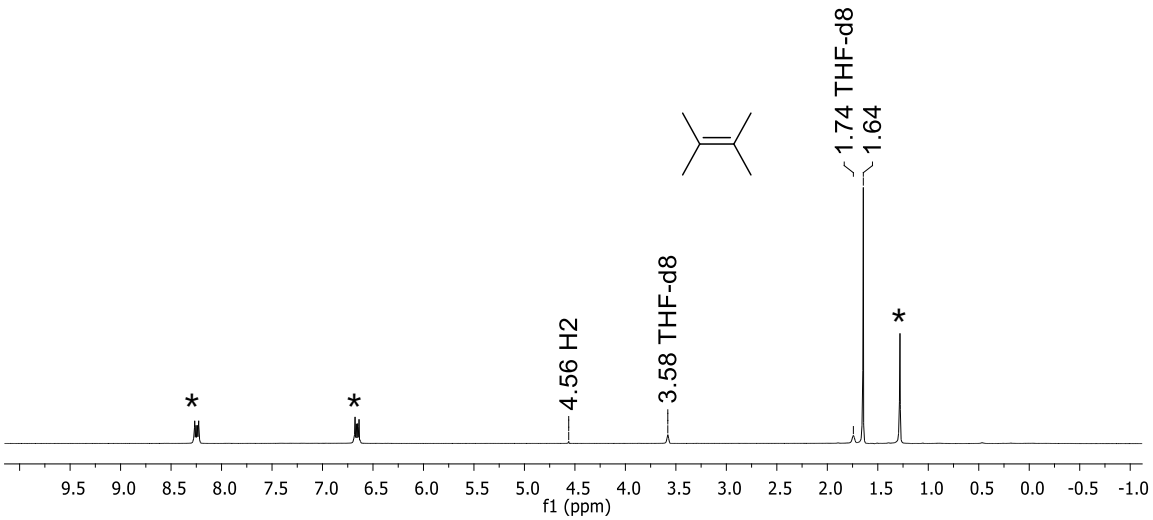

Figure S127. ^{1}H NMR spectrum of 2,3-dimethyl-2-butene beside Li_2[**4**] (250.1 MHz, THF-d_8). Asterisks mark resonances of the starting material Li_2[**4**].

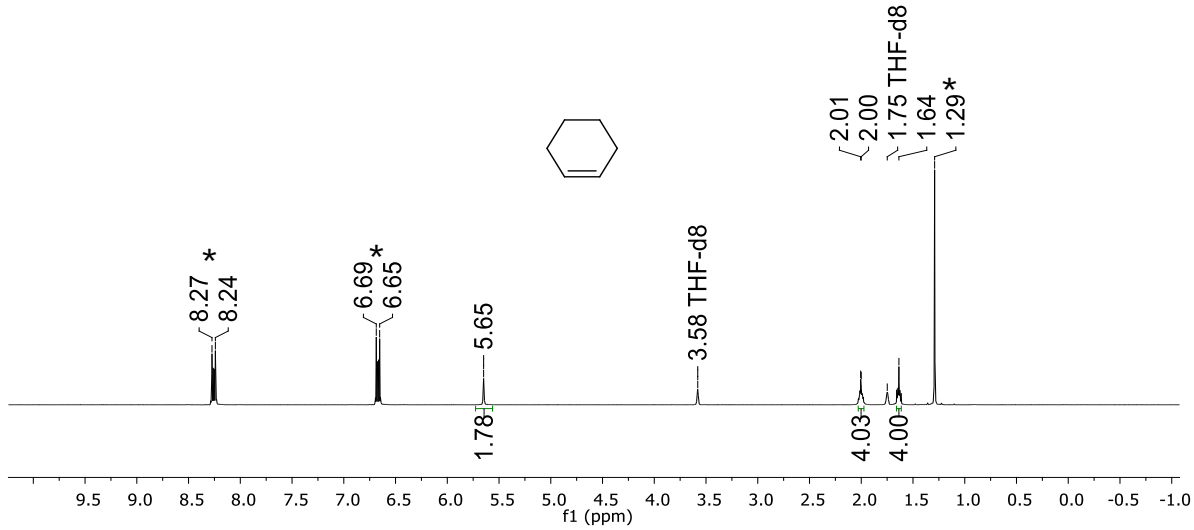

Figure S128. ^{1}H NMR spectrum of cyclohexene beside Li_2[**4**] (300.0 MHz, THF-d_8). Asterisks mark resonances of the starting material Li_2[**4**].

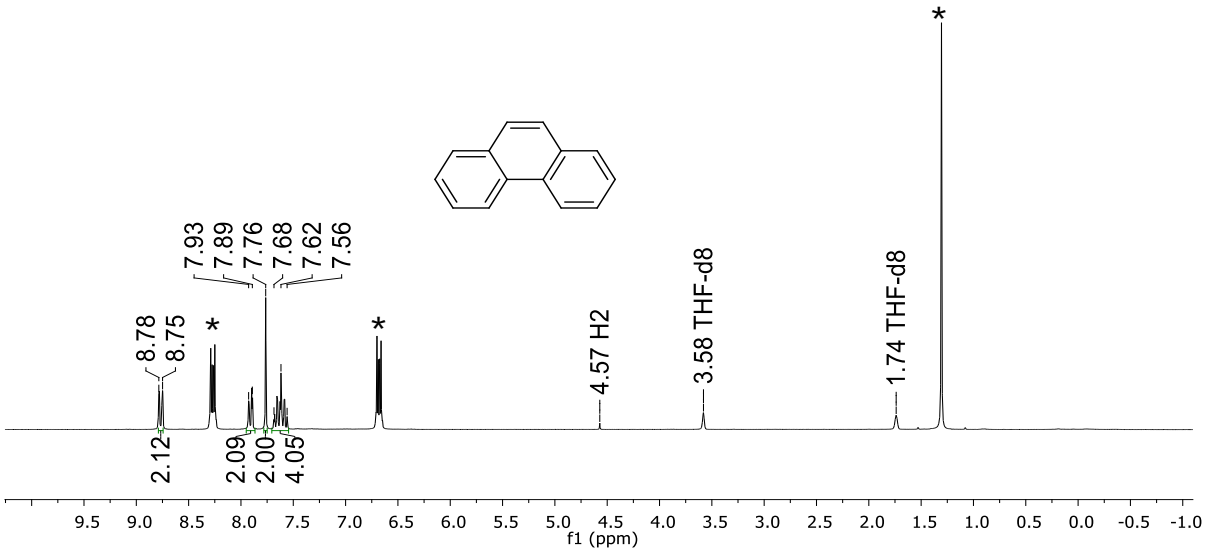

Figure S129. ^{1}H NMR spectrum of phenanthrene beside Li_2[**4**] (250.1 MHz, THF-d_8). Asterisks mark resonances of the starting material Li_2[**4**].

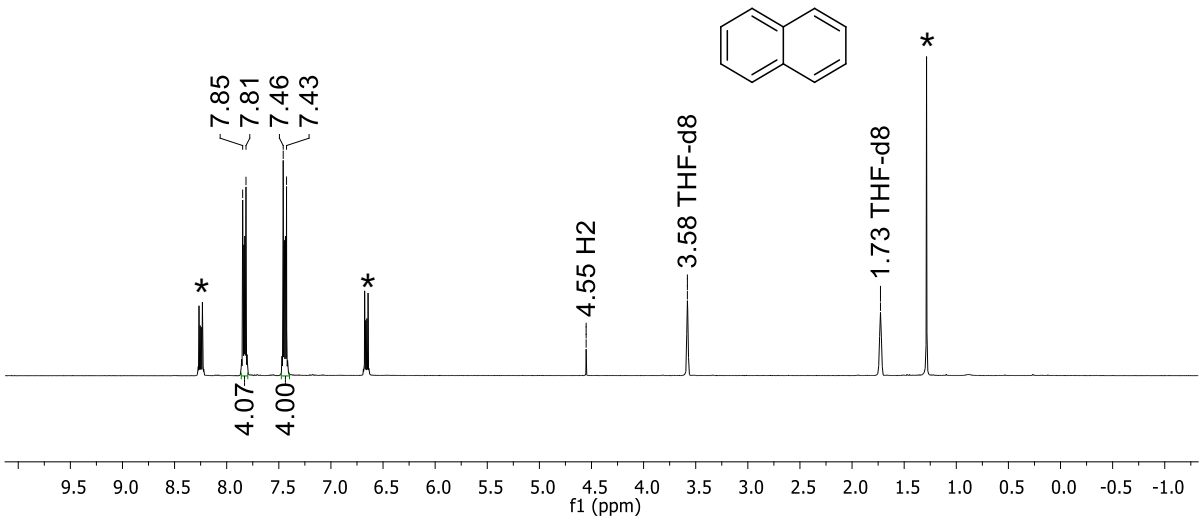

Figure S130. ^{1}H NMR spectrum of naphthalene beside Li_2[**4**] (300.0 MHz, THF-d_8). Asterisks mark resonances of the starting material Li_2[**4**].

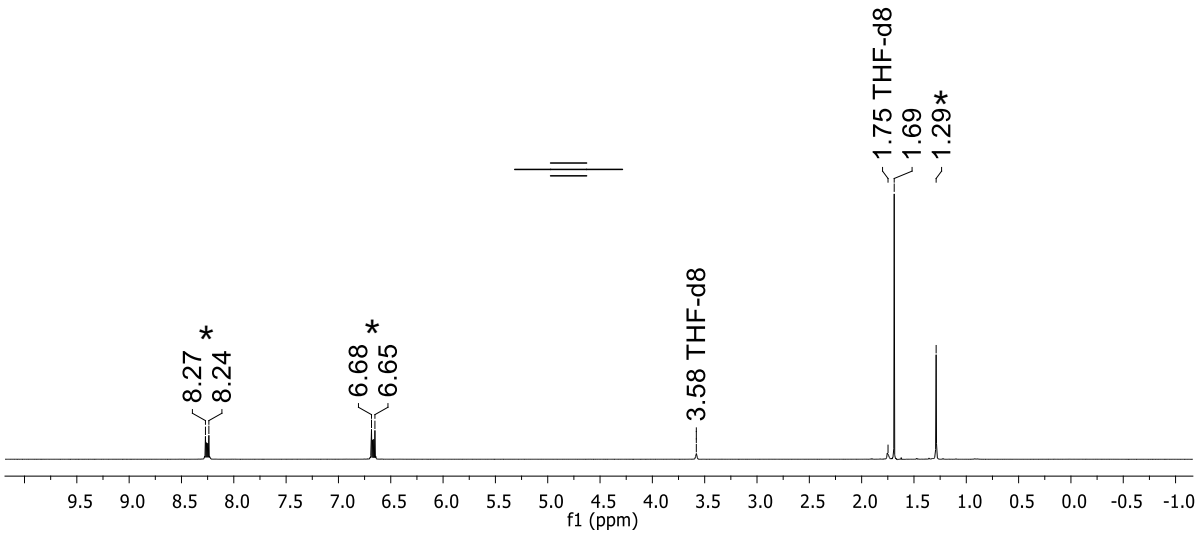

Figure S131. ^{1}H NMR spectrum of 2-butyne beside Li_2[**4**] (300.0 MHz, THF-d_8). Asterisks mark resonances of the starting material Li_2[**4**].

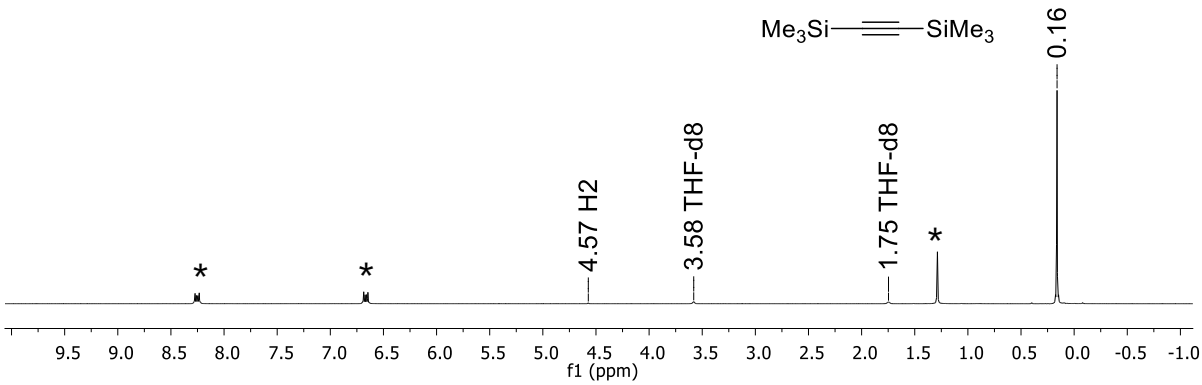

Figure S132. ^{1}H NMR spectrum of bis-(trimethylsilyl)acetylene beside Li_2[**4**] (250.1 MHz, THF-d_8). Asterisks mark resonances of the starting material Li_2[**4**].

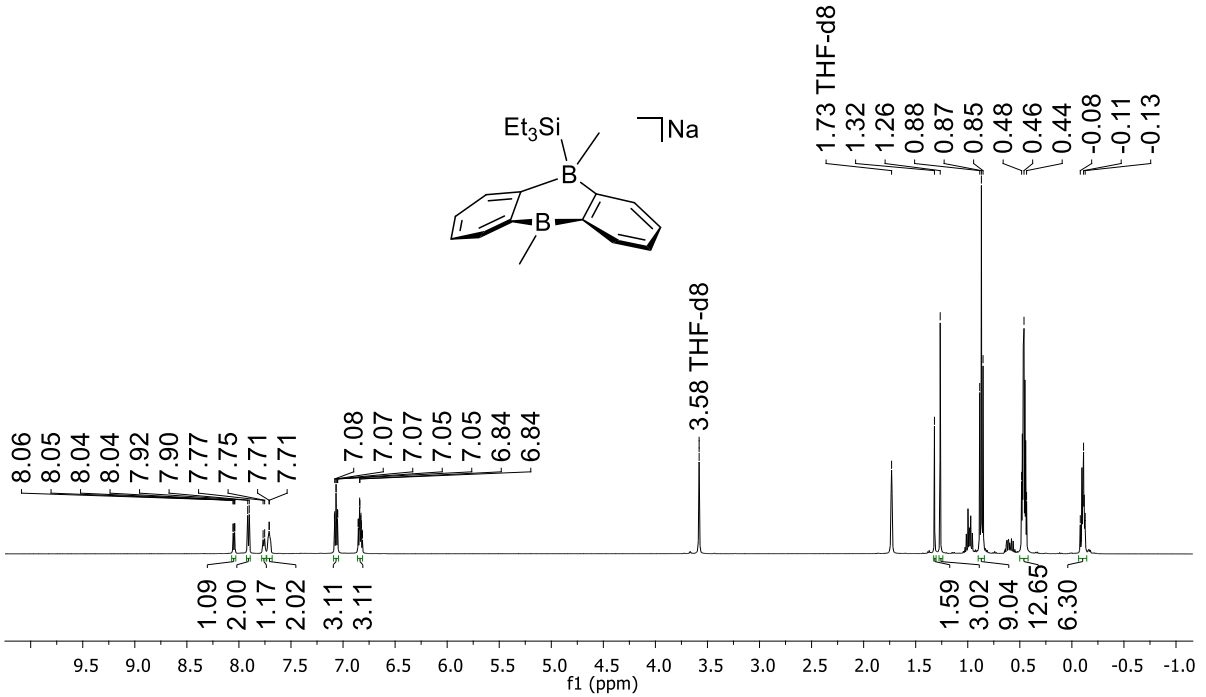

Figure S133. ^{1}H NMR spectrum (500.2 MHz, THF-d_8) recorded 2 d after the addition of Et_3SiCl to a solution of Na_2[**4**] (1:1).

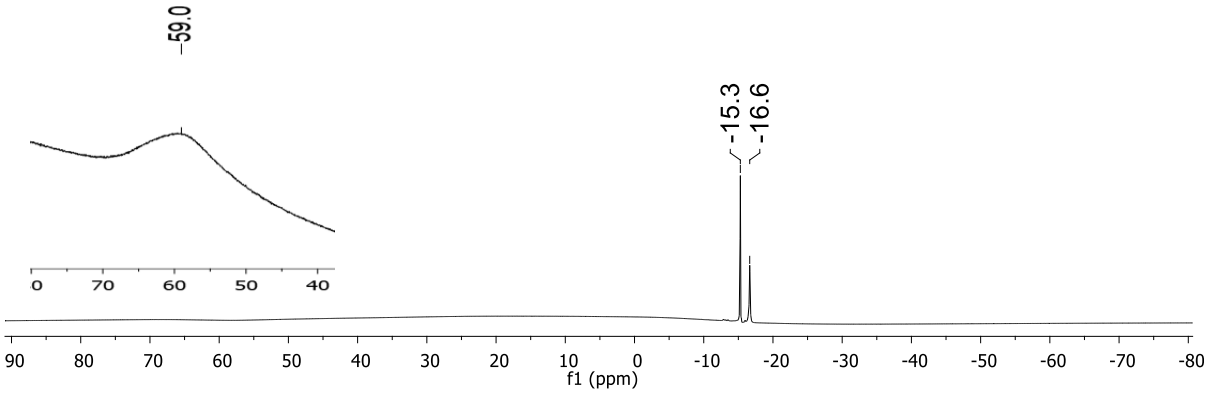

Figure S134. ^{11}B NMR spectrum (160.5 MHz, THF-d_8) recorded 2 d after the addition of Et_3SiCl to a solution of Na_2[**4**] (1:1).

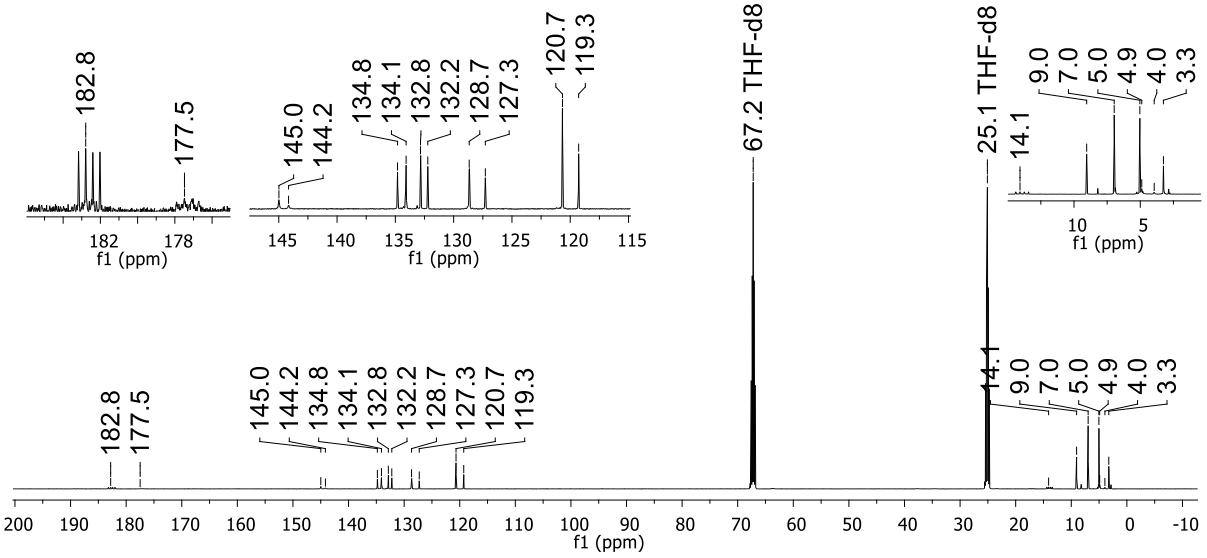

Figure S135. ^{13}C{^{1}H} NMR spectrum (125.8 MHz, THF-d_8) recorded 2 d after the addition of Et_3SiCl to a solution of Na_2[**4**] (1:1).

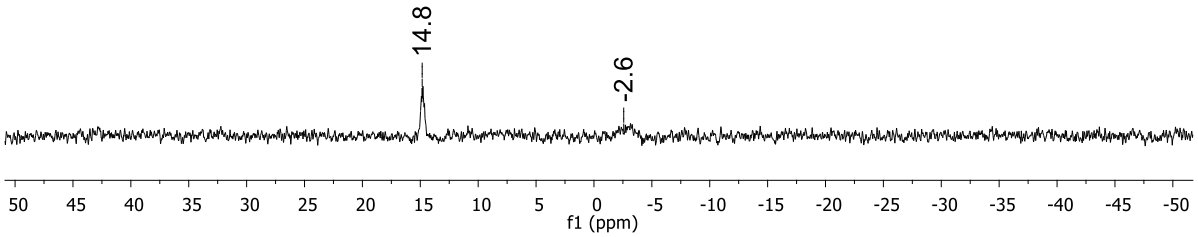

Figure S136. ^{29}Si NMR spectrum (99.4 MHz, THF-d_8) recorded 2 d after the addition of Et_3SiCl to a solution of Na_2[**4**] (1:1).

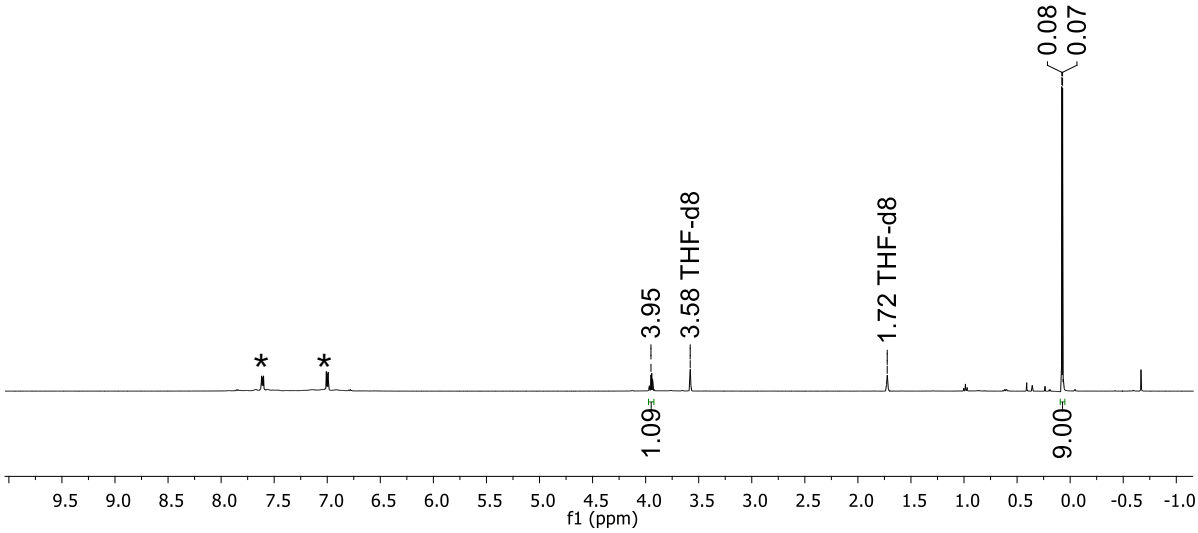

Figure S137. ^{1}H NMR spectrum of the reaction mixture Li_2[**1**-H_2]/Me_3SiCl (500.2 MHz, THF-d_8). Asterisks mark resonances of **1**.

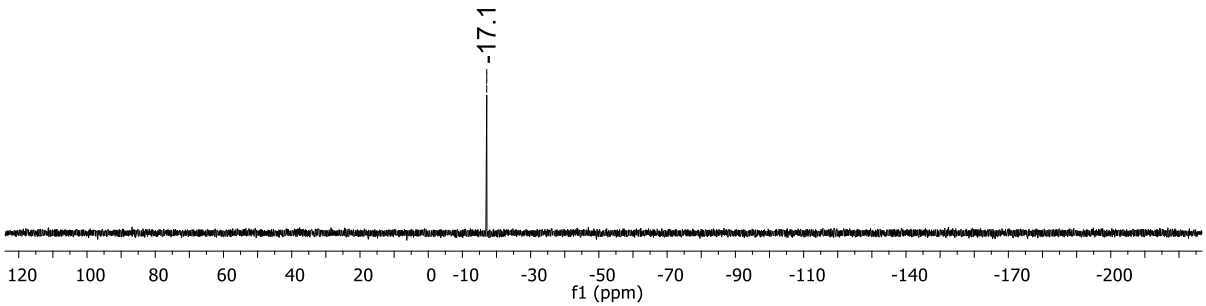

Figure S138. ^{29}Si-INEPT NMR spectrum of the reaction mixture Li_2[**1**-H_2]/Me_3SiCl (99.4 MHz, THF-d_8).

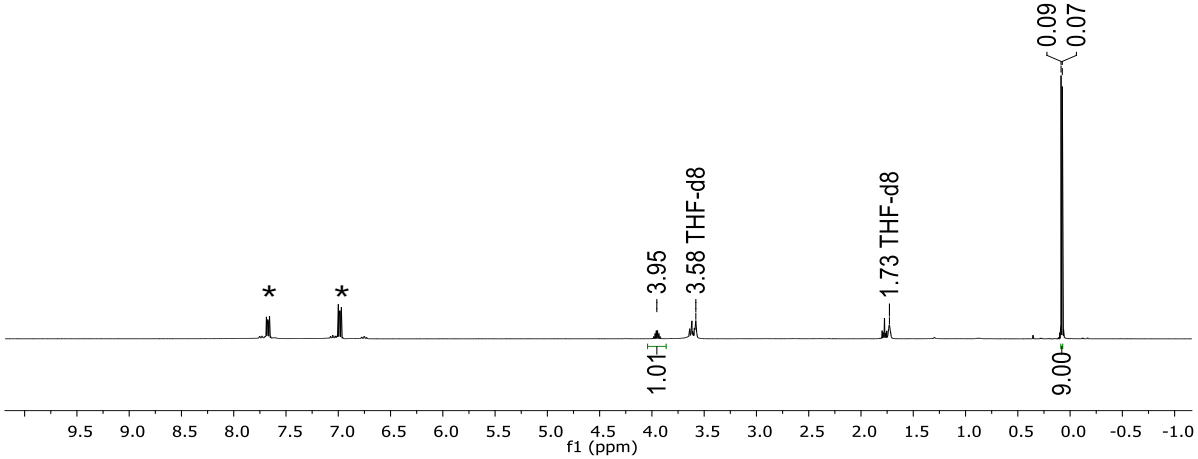

Figure S139. ^{1}H NMR spectrum of the reaction mixture K_2[**1**-H_2]/Me_3SiCl (300.0 MHz, THF-d_8). Asterisks mark resonances of **1**.

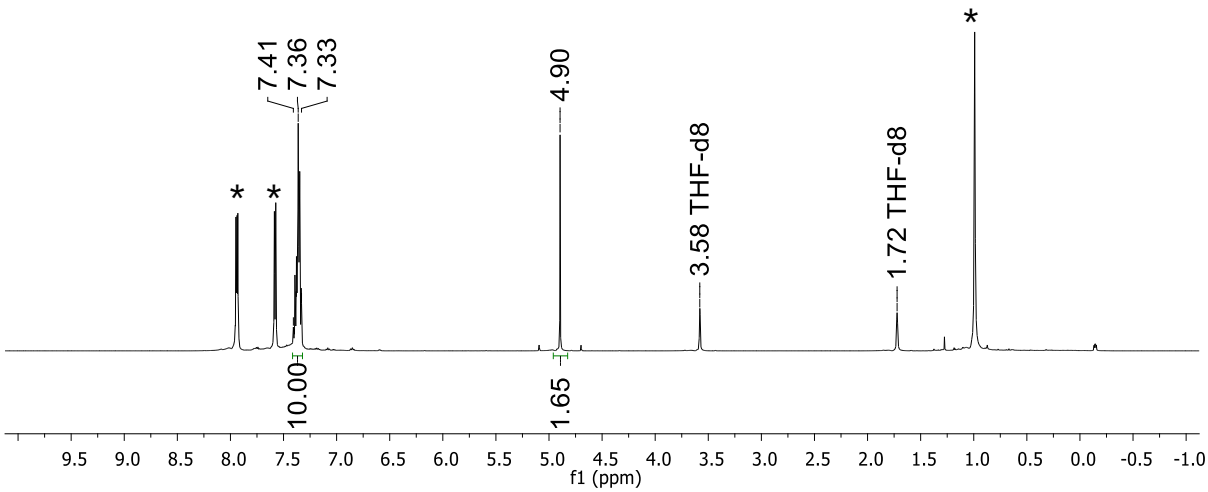

Figure S140. ^{1}H NMR spectrum of the reaction mixture Na_2[**4**-H_2]/Ph_2SiCl_2 (500.2 MHz, THF-d_8). Asterisks mark resonances of **4**.

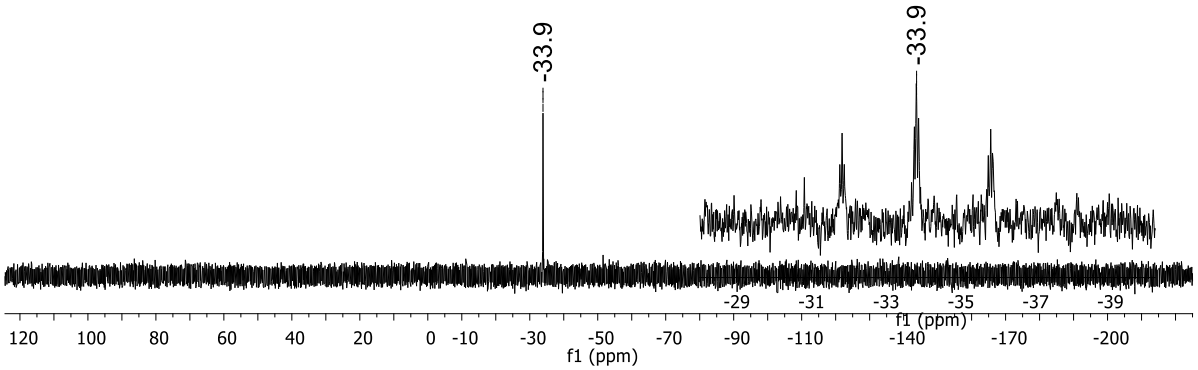

Figure S141. ^{29}Si{^{1}H} NMR spectrum of the reaction mixture Na_2[**4**-H_2]/Ph_2SiCl_2 (99.4 MHz, THF-d_8). The expansion shows the proton-coupled ^{29}Si NMR spectrum.

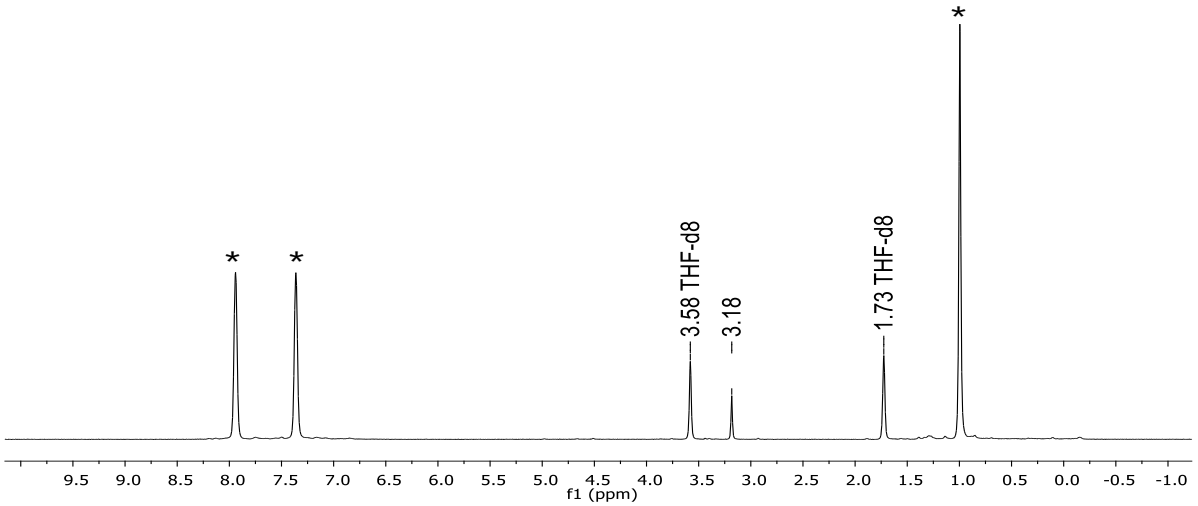

Figure S142. ^{1}H NMR spectrum of the reaction mixture Na_2[**4**-H_2]/$SiCl_4$ (400.1 MHz, THF-d_8). Asterisks mark resonances of **4**.

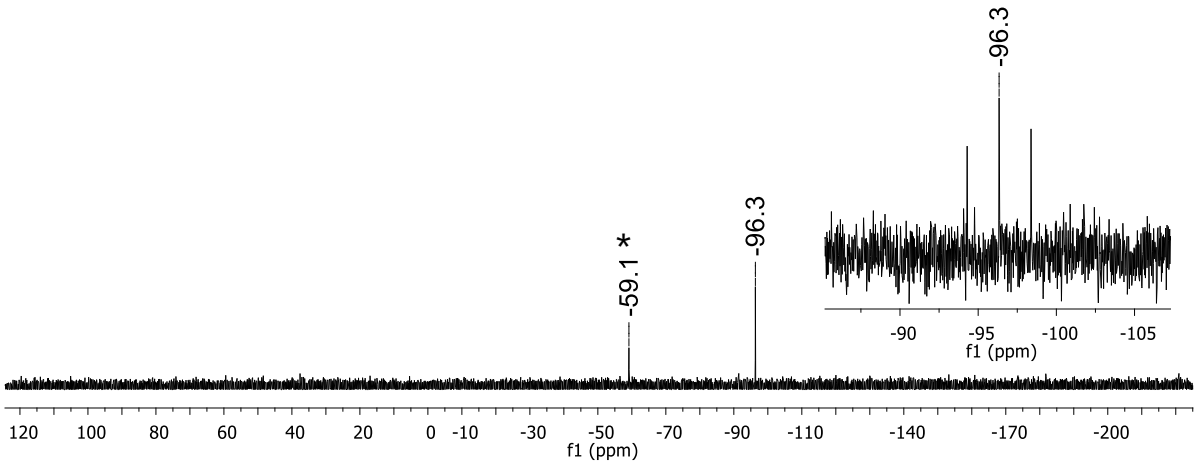

Figure S143. $^{29}Si\{^{1}H\}$ NMR spectrum of the reaction mixture Na_2[**4**-H_2]/$SiCl_4$ (99.4 MHz, THF-d_8). The NMR spectrum was measured several months after the initial reaction so that a second species formed which is marked with an asterisk. The expansion shows the proton-coupled ^{29}Si NMR spectrum.

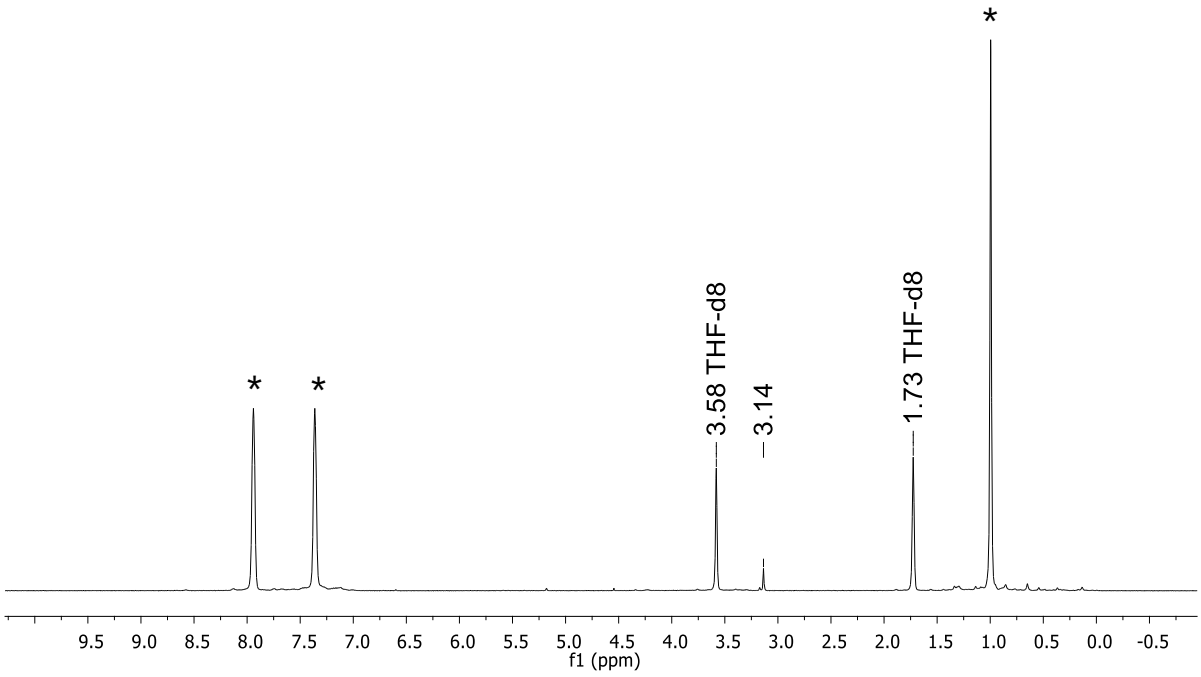

Figure S144. ^{1}H NMR spectrum of the reaction mixture Na_2[**4**-H_2]/$GeCl_4$ (400.1 MHz, THF-d_8). Asterisks mark resonances of **4**.

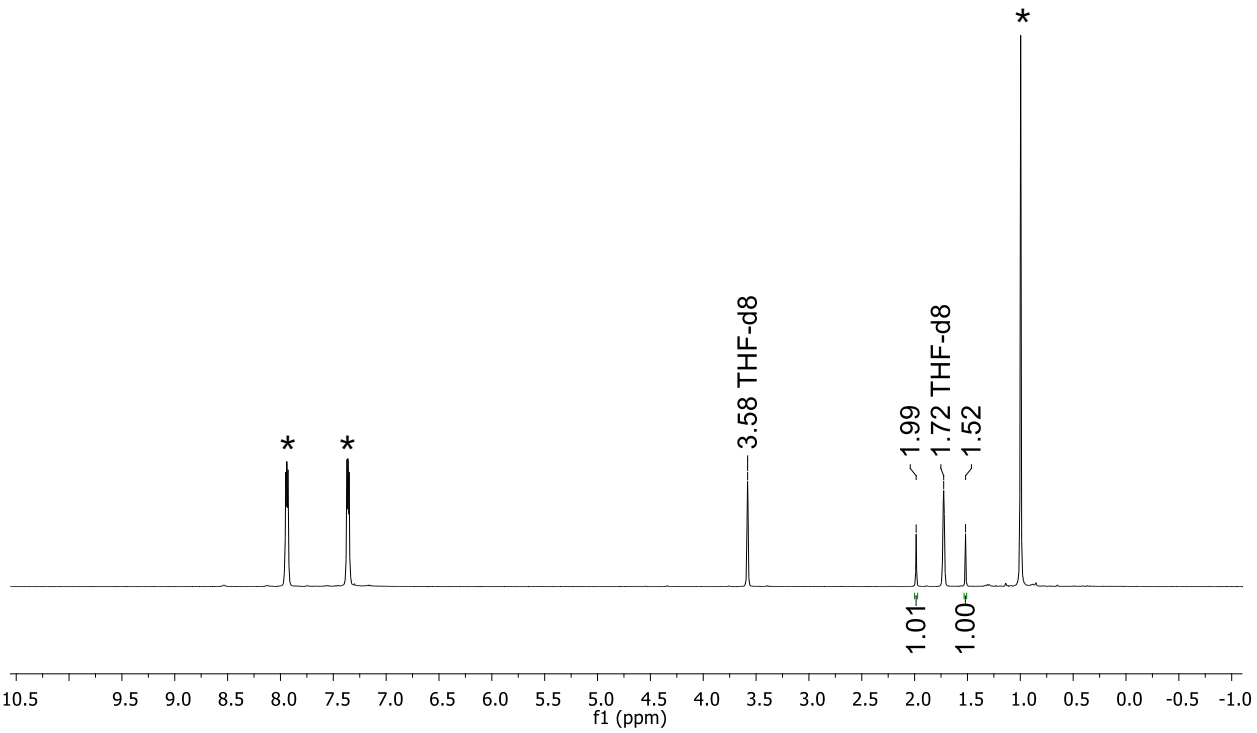

Figure S145. ^{1}H NMR spectrum of the reaction between Na_2[**4**-H_2] and PCl_3 (400.1 MHz, THF-d_8). Asterisks mark resonances of **4**.

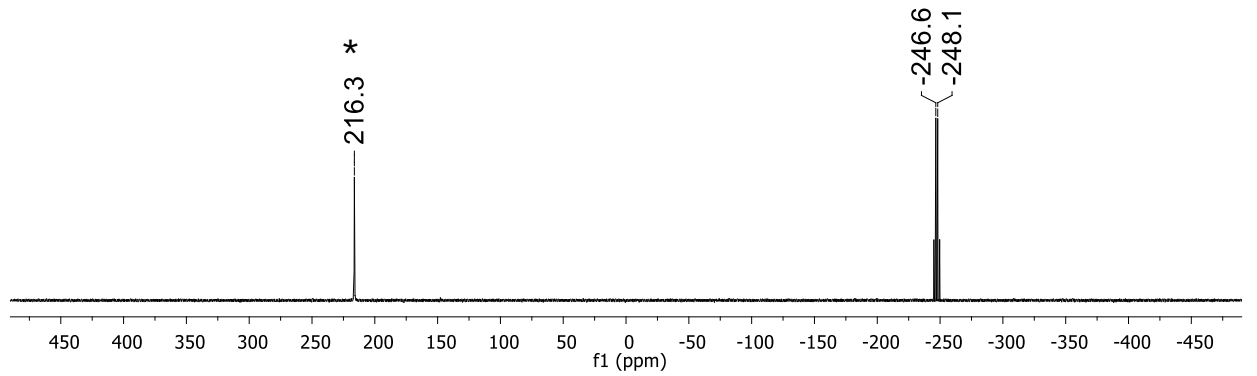

Figure S146. ^{31}P NMR spectrum of the reaction mixture Na$_2$[**4**-H_2]/PCl_3 (121.5 MHz, THF-d_8). Asterisk marks resonance of the starting material PCl_3 since the stoichiometry of the reaction matched not perfectly.

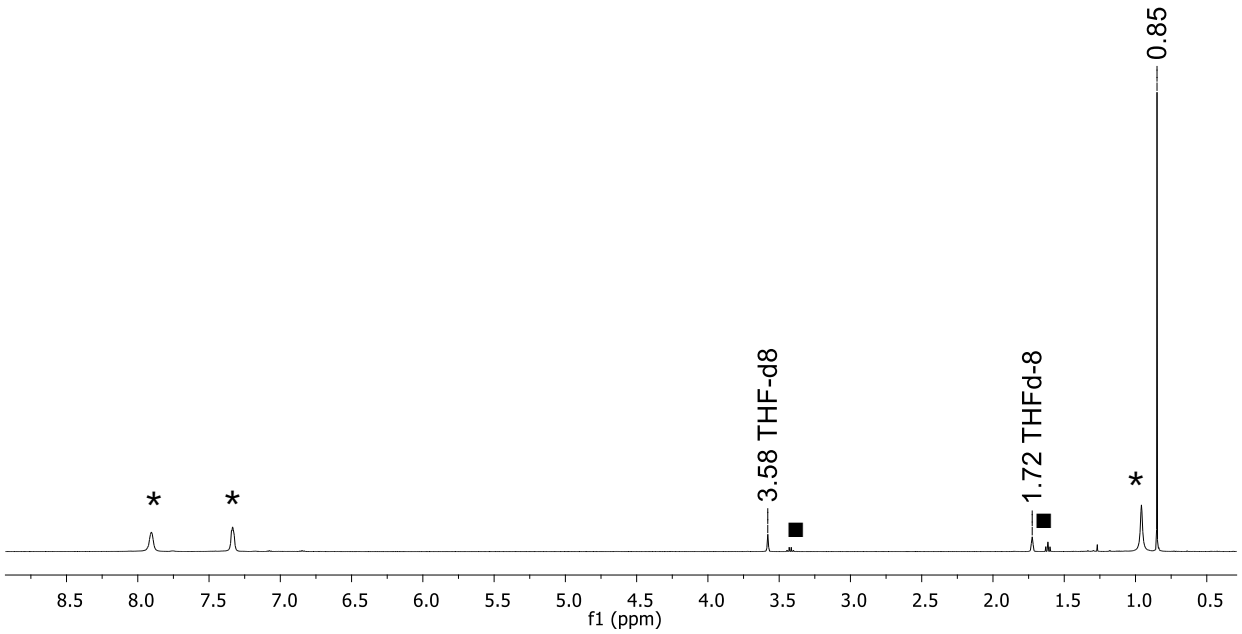

Figure S147. ^{1}H NMR spectrum of the reaction mixture Na_2[**4**-H_2]/EtBr (500.2 MHz, THF-d_8). Asterisks mark resonances of **4** and black squares mark resonances of C_2H_5Br.

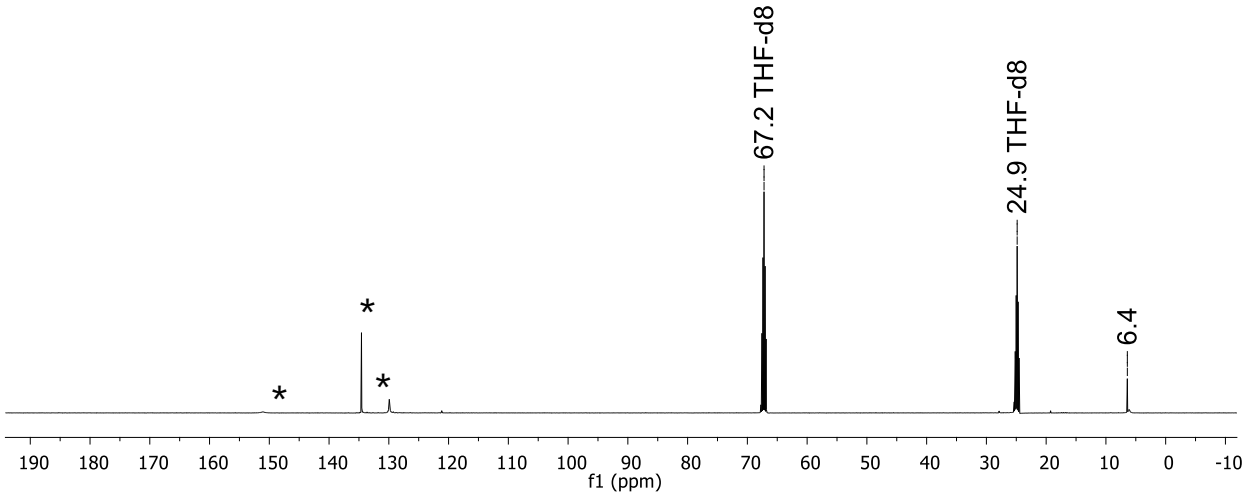

Figure S148. $^{13}C\{^{1}H\}$ NMR spectrum of the reaction mixture Na_2[**4**-H_2]/EtBr (125.8 MHz, THF-d_8). Asterisks mark resonances of **4**.

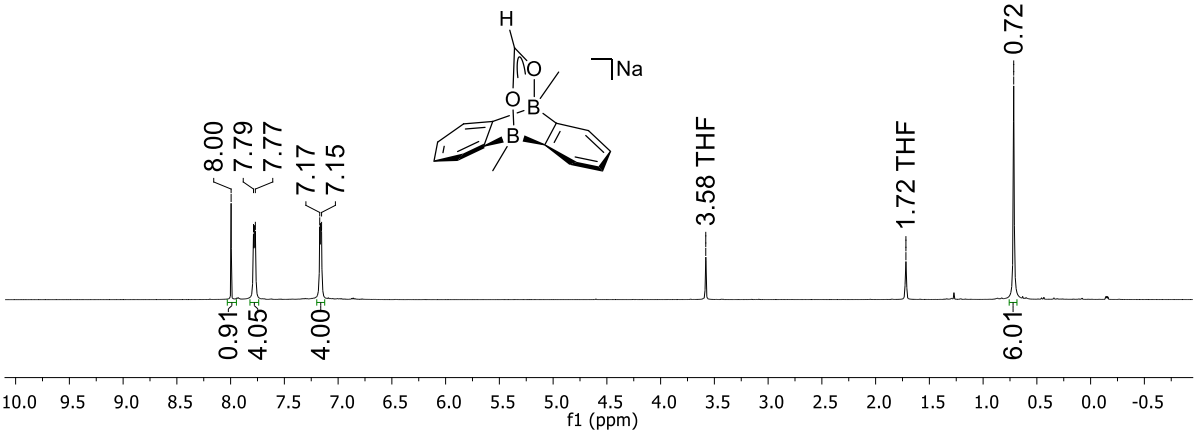

Figure S149. ^{1}H NMR spectrum of the reaction mixture Na_2[**4**-H_2]/CO_2 (500.2 MHz, THF-d_8).

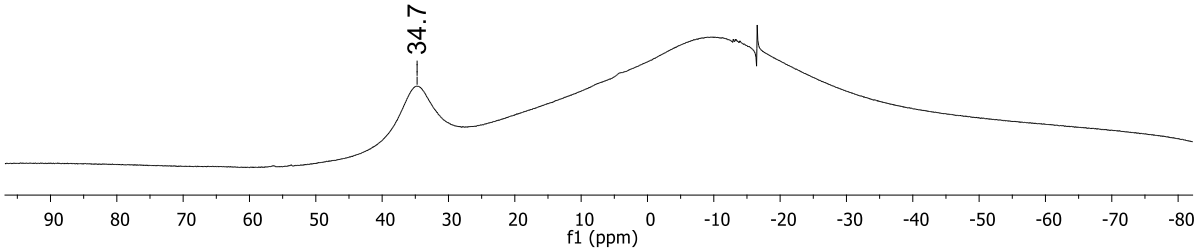

Figure S150. ^{11}B NMR spectrum of the reaction mixture Na_2[**4**-H_2]/CO_2 (160.5 MHz, THF-d_8).

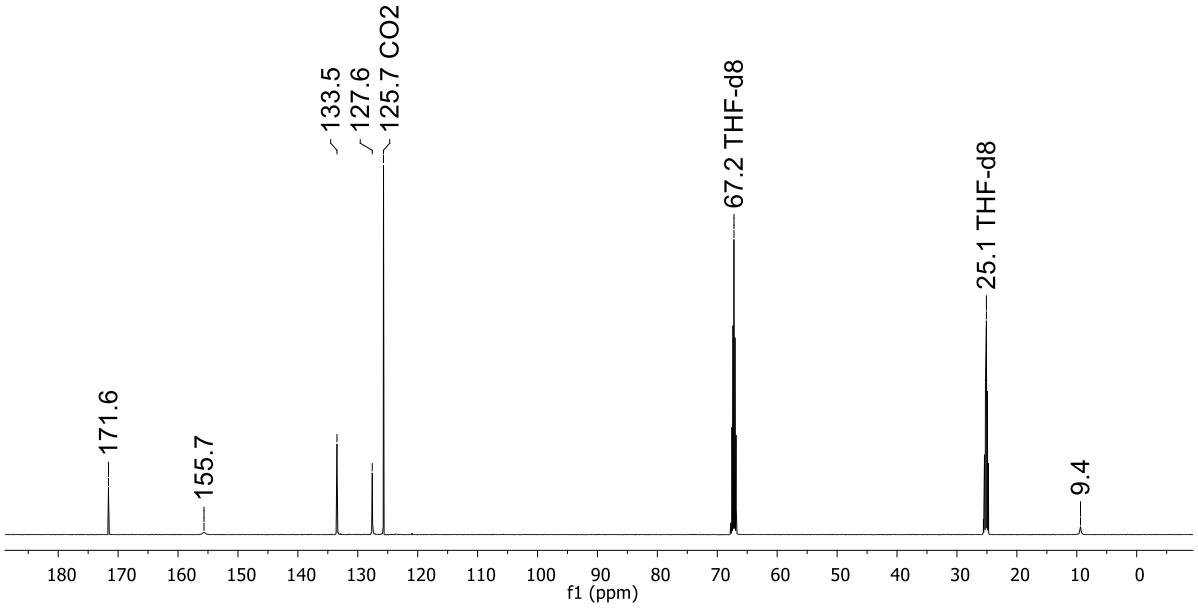

Figure S151. ^{13}C{^{1}H} NMR spectrum of the reaction mixture Na_2[**4**-H_2]/CO_2 (125.8 MHz, THF-d_8).

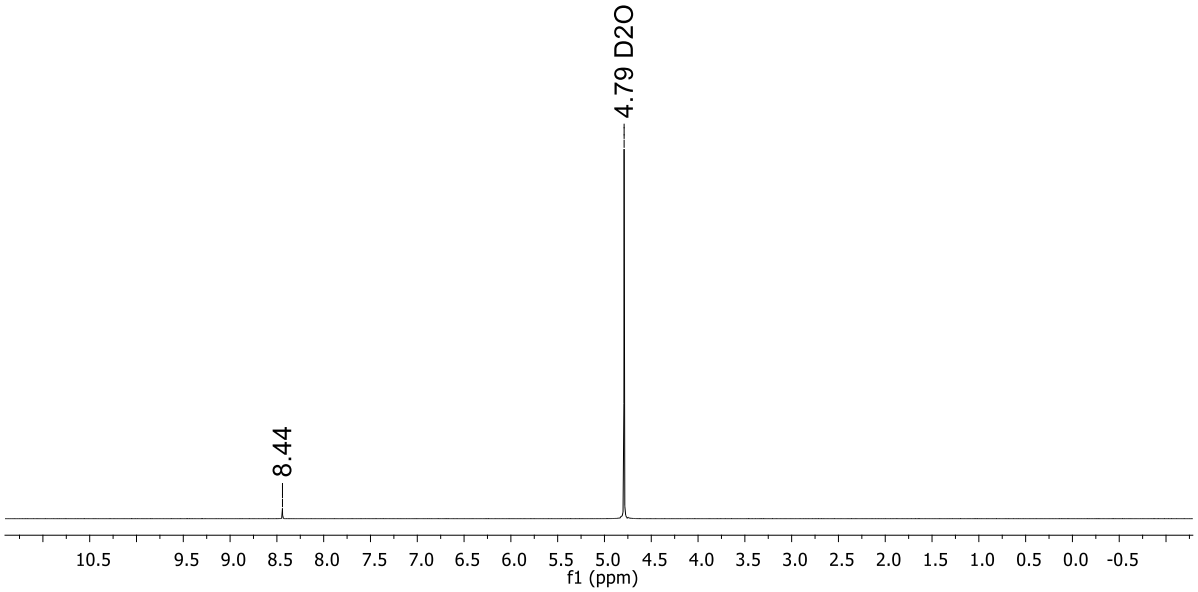

Figure S152. ^{1}H NMR spectrum of sodium formate of the reaction mixture Na_2[**4**-H_2]/CO_2 (500.2 MHz, D_2O).

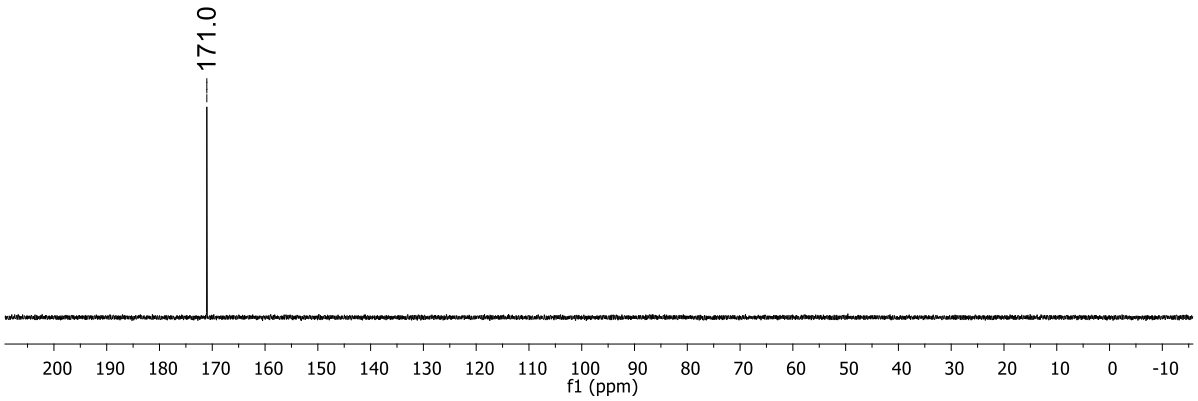

Figure S153. $^{13}C\{^{1}H\}$ NMR spectrum of sodium formate of the reaction mixture Na_2[**4**-H_2]/CO_2 (125.8 MHz, D_2O).

8. X-ray crystal structure analyses

Data for all structures were collected on a STOE IPDS II two-circle diffractometer with a Genix Microfocus tube with mirror optics using Mo*K*α radiation (λ = 0.71073 Å). The data were scaled using the frame-scaling procedure in the X-AREA program system.[23] The structures were solved by direct methods using the program SHELX and refined against F^2 with full-matrix least-squares techniques using the program SHELXL-97.[24]

In **8**, the H atoms of one methyl group in the asymmetric unit are disordered over two positions with a site occupation factor of 0.60(2) for the major occupied sites.

In $[Li(thf)_2]_2$[**7**], two methylene groups of one thf ligand in the asymmetric unit are disordered over two positions with a site occupation factor of 0.576(12) for the major occupied sites. The displacement ellipsoids of the disordered atoms were restrained to an isotropic behavior. The crystal was twinned with a fractional contribution of 0.7830(17) of the major domain.

In $[Na_2(thf)_3]$[**1**], one methylene group of one thf ligand in the asymmetric unit is disordered over two positions with a site occupation factor of 0.527(16) for the major occupied site. The H atom bonded to B was freely refined.

In $[K_2(thf)_4]$[**1**], two methylene groups of one thf ligand in the asymmetric unit are disordered over two positions with a site occupation factor of 0.55(2) for the major occupied sites. The displacement ellipsoids of all atoms of the disordered thf ligand were restrained to an isotropic behavior. The H atom bonded to B was freely refined.

In [Na][Na(thf)$_2$(18-c-6)][Na(thf)$_2$]$_2$(*n*-hexane)[**7**-H$_2$]$_2$, two methylene groups of two thf ligands in the asymmetric unit are disordered over two positions with a site occupation factor of 0.50(3) and 0.54(3), respectively, for the major occupied sites. In two thf ligands one methylene group is disordered over two positions with a site occupation factor of 0.65(3) and 0.63(3), respectively, for the major occupied sites. The displacement ellipsoids of the disordered atoms were restrained to an isotropic behavior. The H atoms bonded to B were freely refined. Bond lengths in the *n*-hexane molecule were restrained to 1.550(1) Å and 1-3 distances were restrained to 2.42(1) Å. The displacement ellipsoids of mutually bonded atoms of the *n*-hexane molecule were restrained to be similar.

In $[K(18\text{-c-}6)]_2[\mathbf{1}\text{-}H_2]$, the H atoms bonded to B were freely refined.
In $[K][K(thf)]_3[\mathbf{4}\text{-}H_2]_2$, two methylene groups of two thf ligands in the asymmetric unit are disordered over two positions with a site occupation factor of 0.664(15) and 0.548(13), respectively, for the major occupied sites. The displacement ellipsoids of all atoms in all thf molecules were restrained to an isotropic behavior. The H atoms bonded to B were freely refined.

In $[K]_2[K(18\text{-c-}6)][K(18\text{-c-}6)(thf)_2][\mathbf{7}\text{-}H_2]_2$, the H atoms bonded to B were freely refined.

In $[Li(12\text{-c-}4)_2](THF)[\mathbf{10}]$, two methylene groups of the co-crystallized THF molecule are disordered over two positions with a site occupation factor of 0.545(16) for the major occupied sites. The displacement ellipsoids of the disordered atoms were restrained to an isotropic behavior. The H atom bonded to N was freely refined.

In [Li(12-c-4)(thf)][Li(12-c-4)][**11**], two methylene groups of the thf ligand are disordered over two positions with a site occupation factor of 0.53(4) for the major occupied sites. One entire crown-ether ring is disordered over two positions with a site occupation factor of 0.697(8) for the major occupied sites. The lower occupied atoms of the disordered crown-ether ring and all disordered atoms of the thf molecule were isotropically refined. The displacement ellipsoids of the higher occupied sites of the disordered crown-ether ring were restrained to an isotropic behavior. The coordinates of the H atoms of the ethylene bridge between the B atoms were refined. Bond lengths and angles of the lower occupied crown-ether ring were restrained to be similar to those of a non-disordered crown-ether ring. Bond lengths and angles of the disordered thf ligand were restrained to be similar to those of a non-disordered thf ligand.

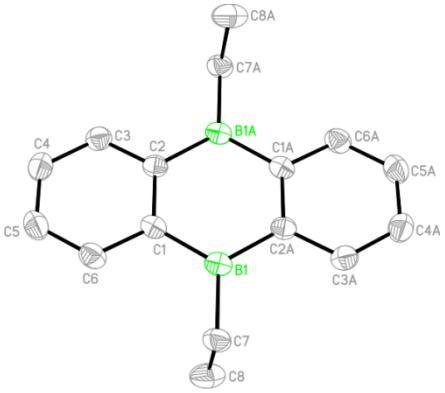

Figure S154. Molecular structure of **5** in the solid state. Displacement ellipsoids are drawn at the 50% probability level; hydrogen atoms are omitted for clarity. Selected bond lengths (Å) and bond angles (°): B1−C1 = 1.577(2), B1−C2A = 1.572(2), B1−C7 = 1.579(2), C1−C2 = 1.425(2), C1−C6 = 1.402(2), C2−C3 = 1.406(2), C3−C4 = 1.393(2), C4−C5 = 1.382(2), C5−C6 = 1.389(2), C7−C8 = 1.539(2); C1−B1−C2A = 118.6(1), C1−B1−C7 = 119.8(1), C2A−B1−C7 = 121.3(1). Symmetry transformation used to generate equivalent atoms: A: –x+1, –y+1, –z+2.

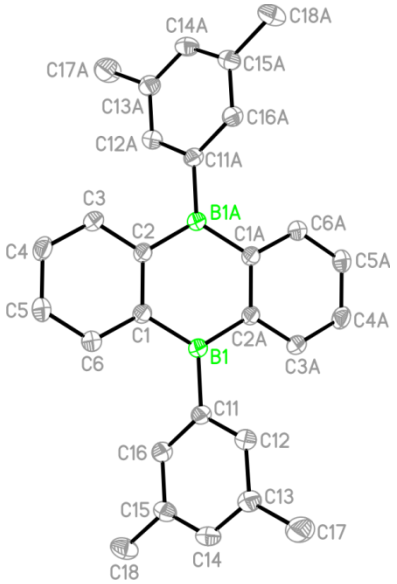

Figure S155. Molecular structure of **8** in the solid state. Displacement ellipsoids are drawn at the 50% probability level; hydrogen atoms are omitted for clarity. Selected bond lengths (Å), bond angles (°), and torsion angle (°): B1−C1 = 1.568(2), B1−C2A = 1.568(2), B1−C11 = 1.572(2), C1−C2 = 1.426(2), C1−C6 = 1.404(2), C2−C3 = 1.409(2), C3−C4 = 1.396(2), C4−C5 = 1.385(2), C5−C6 = 1.396(2); C1−B1−C2A = 119.29(9), C1−B1−C11 = 120.6(1), C2A−B1−C11 = 120.02(10); C1−B1−C11−C12 = −122.4(1). Symmetry transformation used to generate equivalent atoms: A: –x, –y, –z+1.

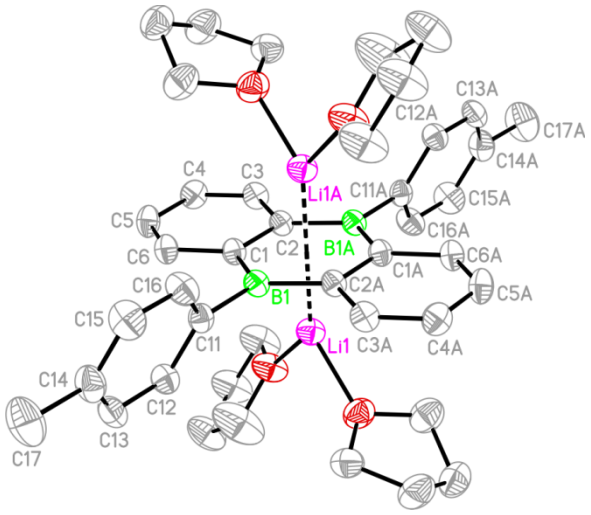

Figure S156. Molecular structure of $[Li(thf)_2]_2$[**7**] in the solid state. Displacement ellipsoids are drawn at the 50% probability level; hydrogen atoms are omitted for clarity. Selected bond lengths (Å), atom···COG distance (Å), bond angles (°), and torsion angle (°): B1−C1 = 1.538(3), B1−C2A = 1.534(3), B1−C11 = 1.605(3), C1−C2 = 1.473(2), C1−C6 = 1.447(3), C2−C3 = 1.447(3), C3−C4 = 1.368(3), C4−C5 = 1.423(3), C5−C6 = 1.366(3); Li···COG = 1.891(4); C1−B1−C2A = 117.4(2), C1−B1−C11 = 121.2(2), C2A−B1−C11 = 121.38(17); C1−B1−C11−C12 = 69.1(3). COG = centroid of the B_2C_4 ring. Symmetry transformation used to generate equivalent atoms: A: –x+1, –y+1, –z+1.

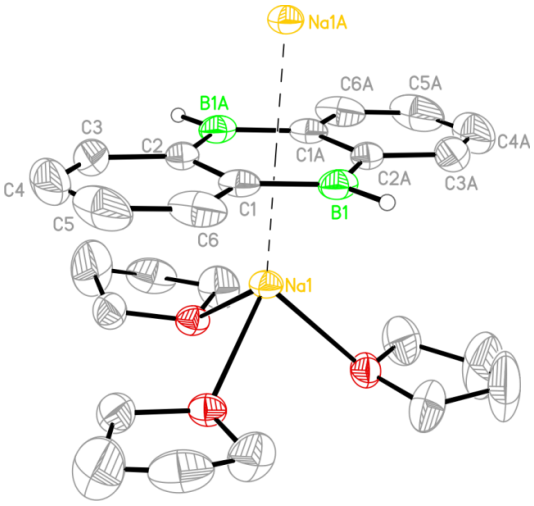

Figure S157. Molecular structure of $[Na_2(thf)_3][\mathbf{1}]$ in the solid state. Displacement ellipsoids are drawn at the 50% probability level; carbon-bonded hydrogen atoms are omitted for clarity. Selected bond lengths (Å), atom···COG distance (Å), and bond angles (°): B1−C1 = 1.527(3), B1−C2A = 1.522(3), B1−H1 = 1.12(3), C1−C2 = 1.468(3), C1−C6 = 1.432(3), C2−C3 = 1.435(3), C3−C4 = 1.354(4), C4−C5 = 1.397(4), C5−C6 = 1.369(4); Na···COG = 2.2394(7); C1−B1−C2A = 118.3(2). COG = centroid of the B_2C_4 ring. Symmetry transformation used to generate equivalent atoms: A: –x+1, –y+1, –z.

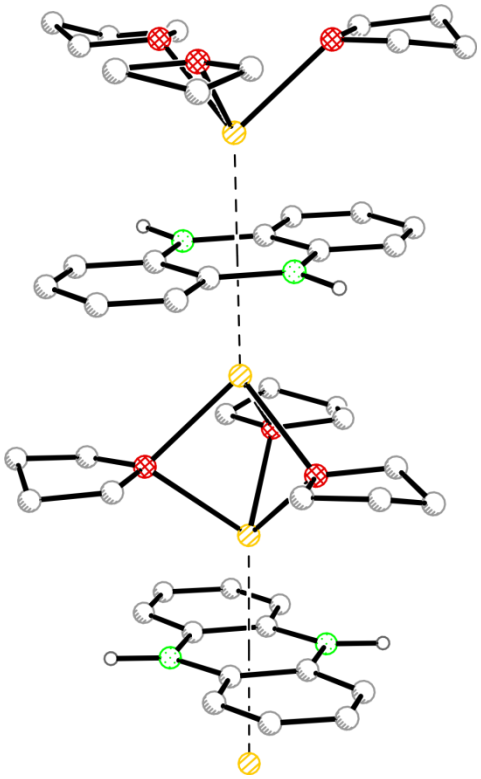

Figure S158. Description of the solid-state structure of $[Na_2(thf)_3][\mathbf{1}]$: Two Na^+ ions are located above and below the B_2C_4 ring. Three thf ligands connect two Na^+ ions of neighboring DBA fragments so that a coordination polymer is formed.

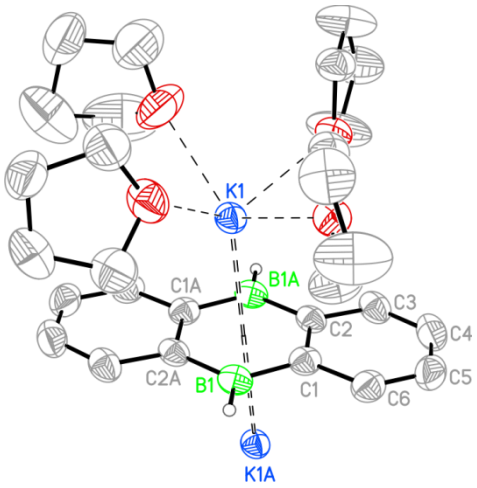

Figure S159. Molecular structure of one of the two crystallographically independent $[\mathbf{1}]^{2-}$ moieties of $[K_2(thf)_4][\mathbf{1}]$ in the solid state. Displacement ellipsoids are drawn at the 50% probability level; carbon-bonded hydrogen atoms are omitted for clarity. Selected bond lengths (Å), atom···COG distances (Å), and bond angles (°) of the two crystallographically independent dianions: B1−C1 = 1.523(4)/1.512(5), B1−C2A = 1.531(4)/1.509(6), B1−H1 = 1.14(3)/1.13(5), C1−C2 = 1.467(4)/1.463(5), C1−C6 = 1.444(4)/1.441(5), C2−C3 = 1.441(4)/1.435(5), C3−C4 = 1.368(5)/1.326(8), C4−C5 = 1.415(5)/1.391(8), C5−C6 = 1.382(5)/1.396(7); K1···COG = 2.7927(6)/2.7165(6); C1−B1−C2A = 118.7(3)/119.1(3). COG = centroid of the B_2C_4 ring. Symmetry transformation used to generate equivalent atoms: A: –x+1, –y+1, –z+1.

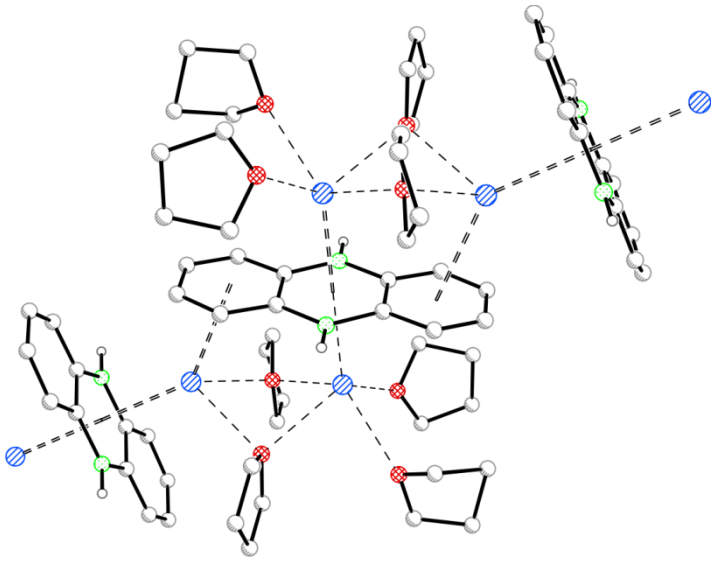

Figure S160. Description of the solid-state structure of $[K_2(thf)_4][\mathbf{1}]$: In the crystal lattice, coordination polymers are formed: Each K^+ ion coordinates one B_2C_4 ring in an η^6 mode, so that two K^+ ions are located above and below each B_2C_4 ring. Half of the K^+ ions connect two $[DBA]^{2-}$ ions because they also coordinate to one phenylene ring (in an η^3 fashion). Two thf ligands are located in bridging positions between two K^+ ions. The coordination sphere of one K^+ ion is completed by two additional thf ligands. Both $[DBA]^{2-}$ units form a dihedral angle of 63.71(9)°.

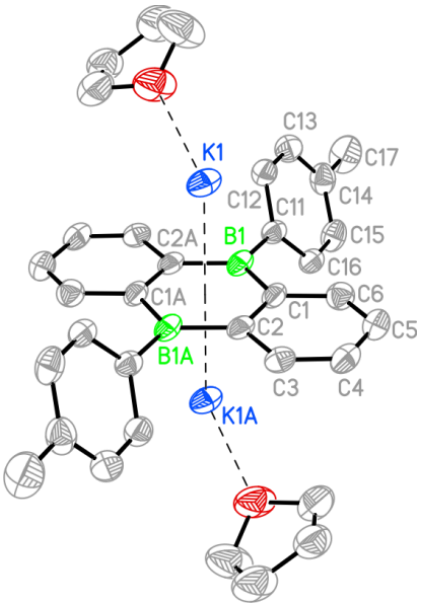

Figure S161. Molecular structure of [K(thf)]$_2$[**7**] in the solid state. Displacement ellipsoids are drawn at the 50% probability level; hydrogen atoms are omitted for clarity. Selected bond lengths (Å), atom···COG distances (Å), bond angles (°), and torsion angle (°): B1−C1 = 1.535(7), B1−C2A = 1.542(7), B1−C11 = 1.583(7), C1−C2 = 1.460(6), C1−C6 = 1.434(6), C2−C3 = 1.444(6), C3−C4 = 1.355(7), C4−C5 = 1.414(7), C5−C6 = 1.374(7); K1···COG = 2.702(1); C1−B1−C2A = 117.4(4), C1−B1−C11 = 122.1(4), C2A−B1−C11 = 120.5(4); C1−B1−C11−C12 = −124.6(5). COG = centroid of the B_2C_4 ring. Symmetry transformation used to generate equivalent atoms: A: –x+1, –y+1, –z+1.

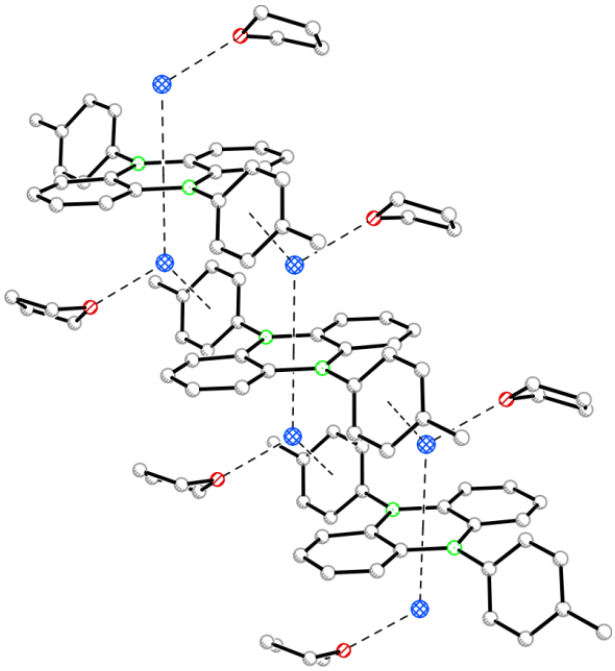

Figure S162. Description of the solid-state structure of [K(thf)]$_2$[**7**]: In the crystal lattice, coordination polymers are formed: Each K^+ ion coordinates one B_2C_4 ring in an η^6 mode, one tolyl ring of a neighboring $[DBA]^{2-}$ unit in an η^3 mode (K1···COG(C11-C16) = 3.201(2)). The coordination sphere is completed by one thf ligand. The $[DBA]^{2-}$ ions and the tolyl groups of the same polymer strand are oriented parallel to each other, respectively.

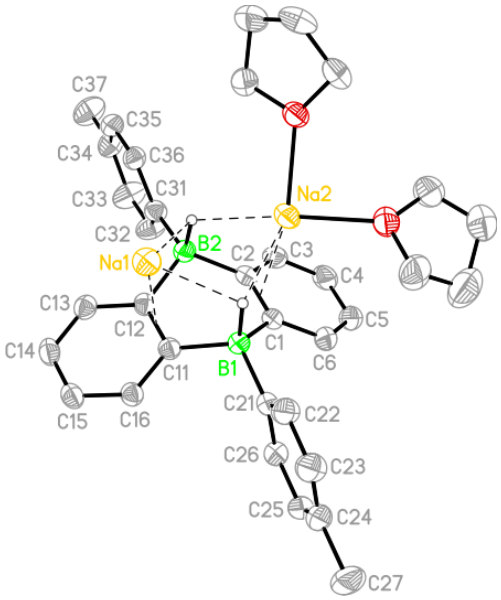

Figure S163. Molecular structure of one of the two crystallographically independent [**7**-H_2]$^{2-}$ moieties of [Na][Na(thf)$_2$(18-c-6)][Na(thf)$_2$]$_2$(*n*-hexane)[**7**-H_2]$_2$ in the solid state. Displacement ellipsoids are drawn at the 30% probability level; carbon-bonded hydrogen atoms, the [Na(thf)$_2$(18-c-6)]$^+$ ion, and the *n*-hexane molecule are omitted for clarity. Selected bond lengths (Å), atom···atom distances (Å), and bond angles (°) of the two crystallographically independent molecules: B1−C1 = 1.624(5)/1.626(5), B1−C11 = 1.620(5)/1.634(5), B1−C21 = 1.625(5)/1.610(5), B1−H1 = 1.26(3)/1.24(3), B2−C2 = 1.627(5)/1.623(5), B2−C12 = 1.630(5)/1.628(5), B2−C31 = 1.626(5)/1.614(4), B2−H2 = 1.27(3)/1.20(3), C1−C2 = 1.424(4)/1.424(4), C11−C12 = 1.424(4)/1.427(4); Na1···C11 = 2.542(3)/2.575(3), Na1···H1 = 2.31(3)/2.46(3), Na1···H2 = 2.29(3)/2.37(3), Na2···C1 = 2.741(3)/2.738(3), Na2···H1 = 2.35(3)/2.31(3), Na2···H2 = 2.28(3)/2.34(3); C1−B1−C11 = 109.1(2)/109.4(2), C2−B2−C12 = 108.7(3)/109.6(3).

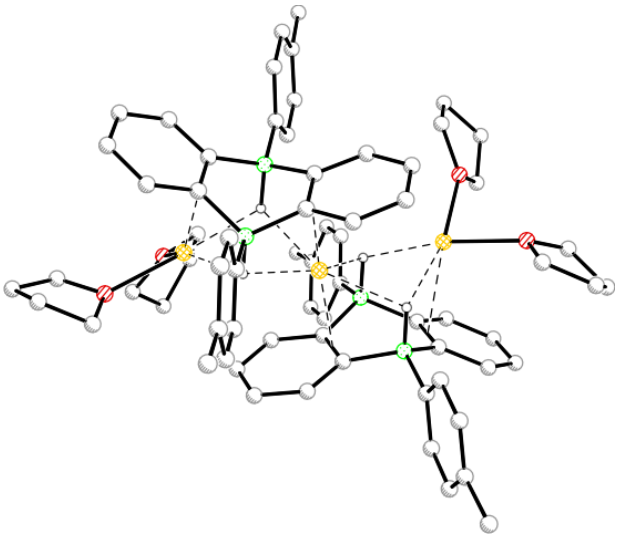

Figure S164. Description of the solid-state structure of [Na][Na(thf)$_2$(18-c-6)][Na(thf)$_2$]$_2$(*n*-hexane)[**7**-H_2]$_2$ (the discrete [Na(thf)$_2$(18-c-6)]$^+$ ion and the *n*-hexane molecule are omitted for clarity): The crystal lattice consists of dimers, in which two [DBA]$^{2-}$ entities are connected by one central Na^+ ion. This cation is coordinated in a chelating manner by the two axial B*H* substituents of each anionic fragment; the octahedral ligand sphere is completed by short contacts to two *trans*-positioned phenylene rings. Two other [Na(thf)$_2$]$^+$ ions are also coordinated in a chelating manner by two axial B*H* substituents of the same [**7**-H_2]$^{2-}$ fragment.

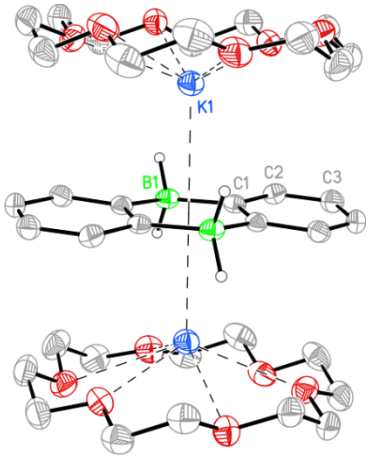

Figure S165: Molecular structure of one of the two crystallographically independent molecules of [K(18-c-6)]$_2$[**1**-H$_2$] in the solid state. Displacement ellipsoids are drawn at the 50% probability level; carbon-bonded hydrogen atoms are omitted for clarity. Selected bond lengths (Å), atom···COG distances (Å), and bond angles (°) of the two crystallographically independent molecules: B1−C1 = 1.619(3)/1.622(3), B1−H1A = 1.16(3)/1.20(3), B1−H1B = 1.13(3)/1.18(4), C1−C1(#1/#2) = 1.431(5)/1.434(4), C1−C2 = 1.408(4)/1.414(4), C2−C3 = 1.383(4)/1.378(4), C3−C3(#1/#2) = 1.399(5)/1.393(5); K1···COG = 2.9165(8)/2.9177(7); C1−B1−C1(#3/#4) = 115.7(3)/116.0(3). COG = centroid of the B_2C_4 ring. Symmetry transformation used to generate equivalent atoms: #1: –x+1, –y+2, z; #2: –x+1, –y+1, z; #3: x, y, –z+1; #4: x, y, –z.

The molecule possesses a high symmetry with a center of inversion, one mirror plane containing the two BH_2 fragments, and one C_2 axis perpendicular to the mirror plane.

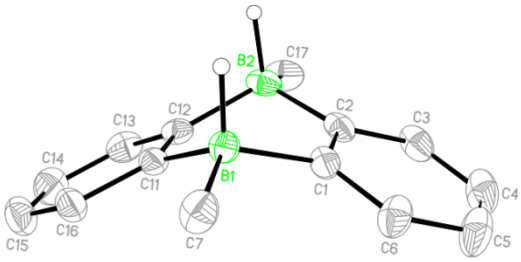

Figure S166. Molecular structure of one of the two crystallographically independent $[\mathbf{4}\text{-}H_2]^{2-}$ moieties of $[K][K(thf)]_3[\mathbf{4}\text{-}H_2]_2$ in the solid state. Displacement ellipsoids are drawn at the 30% probability level; carbon-bonded hydrogen atoms and all counter cations are omitted for clarity. Selected bond lengths (Å) and bond angles (°) of the two crystallographically independent molecules: B1−C1 = 1.625(3)/1.638(3), B1−C7 = 1.633(3)/1.645(3), B1−C11 = 1.632(3)/1.632(3), B1−H1 = 1.19(2)/1.18(2), B2−C2 = 1.631(4)/1.630(3), B2−C12 = 1.630(3)/1.628(3), B2−C17 = 1.642(3)/1.627(3), B2−H2 = 1.21(2)/1.220(18), C1−C2 = 1.425(3)/1.426(3), C11−C12 = 1.425(3)/1.432(3); C1−B1−C11 = 107.97(15)/107.15(15), C2−B2−C12 = 108.29(16)/105.87(15).

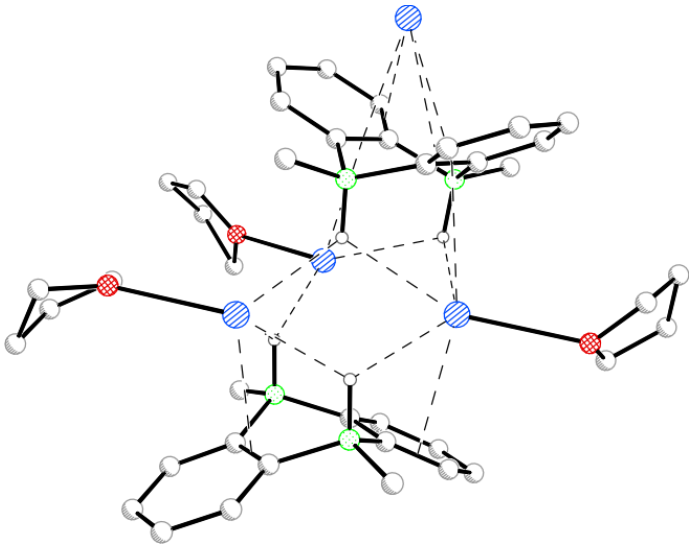

Figure S167. Description of the solid-state structure of $[K][K(thf)]_3[\mathbf{4}\text{-}H_2]_2$: In the crystal lattice, coordination polymers are formed. The repeating unit consists of two $[DBA]^{2-}$ entities, which are bridged by three $[K(thf)]^+$ ions, mainly via K···H interactions. The repeating units are connected by K^+ cations embedded between the concave sites of two $[\mathbf{4}\text{-}H_2]^{2-}$ units (contact ion pairs without additional thf ligands).

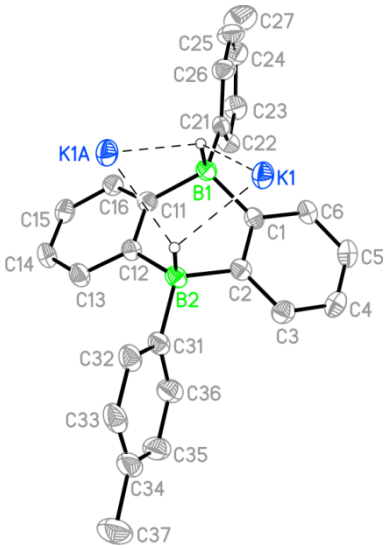

Figure S168. Molecular structure of one $[\mathbf{7}\text{-}H_2]^{2-}$ moiety of $[K]_2[K(18\text{-c-}6)][K(18\text{-c-}6)(thf)_2][\mathbf{7}\text{-}H_2]_2$ in the solid state. Displacement ellipsoids are drawn at the 50% probability level; carbon-bonded hydrogen atoms, the $[K(18\text{-c-}6)]^+$ ion, and the $[K(18\text{-c-}6)(thf)_2]^+$ ion are omitted for clarity. Selected bond lengths (Å), atom···atom distances (Å), and bond angles (°): B1−C1 = 1.628(2), B1−C11 = 1.636(2), B1−C21 = 1.626(2), B1−H1 = 1.217(17), B2−C2 = 1.641(2), B2−C12 = 1.634(2), B2−C31 = 1.631(2), B2−H2 = 1.22(2), C1−C2 = 1.426(2), C11−C12 = 1.427(2); K1···H1 = 2.655(18), $K1^+$···H2 = 2.622(19); C1−B1−C11 = 107.8(1), C2−B2−C12 = 108.3(1).

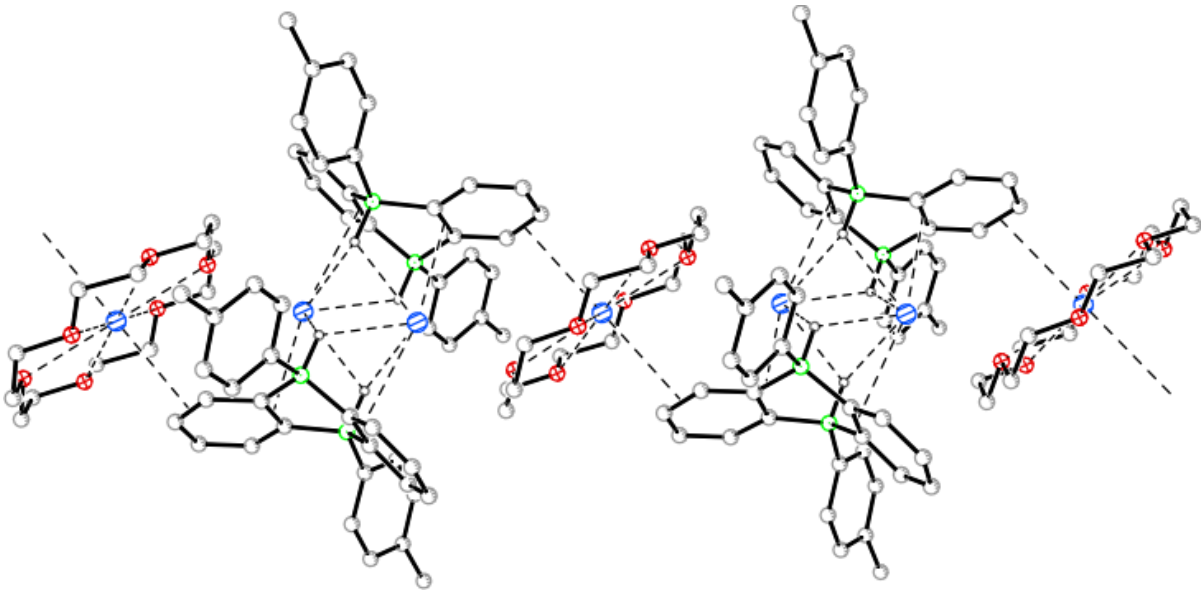

Figure S169. Description of the solid-state structure of $[K]_2[K(18\text{-c-}6)][K(18\text{-c-}6)(thf)_2][\mathbf{7}\text{-}H_2]_2$ (the discrete $[K(18\text{-c-}6)(thf)_2]^+$ ions are omitted for clarity): In the crystal lattice, coordination polymers are formed. The repeating unit consists of two $[\mathbf{7}\text{-}H_2]^{2-}$ entities, which are bridged by two K^+ ions. Each of these cations forms four K···H–B and two K···phenylene short contacts. The repeating units are connected by $[K(18\text{-c-}6)]^+$ ions via K···phenylene and O–K interactions.

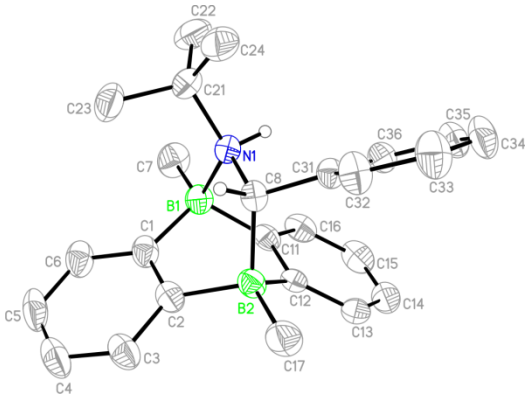

Figure S170. Molecular structure of [Li(12-c-4)$_2$](THF)[**10**] in the solid state. Displacement ellipsoids are drawn at the 50% probability level; carbon-bonded hydrogen atoms, the [Li(12-c-4)$_2$]$^+$ ion, and the co-crystallized THF molecule are omitted for clarity. Selected bond lengths (Å) and bond angles (°): B1−C1 = 1.616(3), B1−C7 = 1.624(3), B1−C11 = 1.629(3), B1−N1 = 1.737(3), B2−C2 = 1.622(3), B2−C8 = 1.693(3), B2−C12 = 1.613(3), B2−C17 = 1.623(3), C1−C2 = 1.408(3), C11−C12 = 1.411(3), C8−N1 = 1.537(3), N1−H1 = 0.90(2), N1−C21 = 1.535(3); C1−B1−C11 = 109.6(2), C2−B2−C12 = 108.3(2).

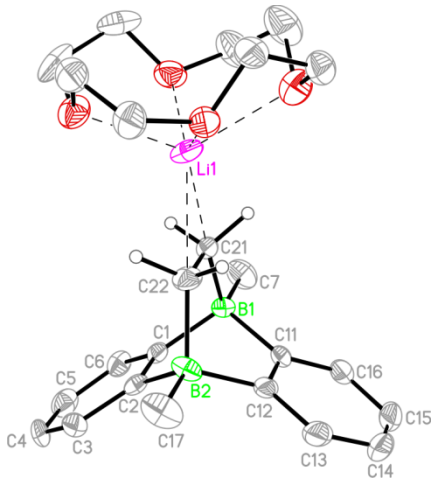

Figure S171. Molecular structure of one of the two crystallographically independent contact-ion pairs [Li(12-c-4)(thf)][Li(12-c-4)][**11**] in the solid state. Displacement ellipsoids are drawn at the 50% probability level; carbon-bonded hydrogen atoms of the DBA scaffold and the [Li(12-c-4)(thf)]$^+$ ion are omitted for clarity. Selected bond lengths (Å), atom···atom distances (Å), bond angles (°), and torsion angles (°) of the two crystallographically independent dianions: B1−C1 = 1.617(7)/1.632(8), B1−C7 = 1.632(8)/1.633(8), B1−C11 = 1.633(8)/1.623(8), B1−C21 = 1.684(7)/1.662(8), B2−C2 = 1.630(8)/1.611(8), B2−C12 = 1.623(9)/1.634(8), B2−C17 = 1.628(9)/1.643(8), B2−C22 = 1.677(8)/1.691(8), C1−C2 = 1.440(7)/1.428(8), C11−C12 = 1.423(8)/1.415(7), C21−C22 = 1.552(8)/1.551(8); Li1$^+$···C21 = 2.334(10)/2.309(11), Li1$^+$···C22 = 2.361(10)/2.420(10); C1−B1−C11 = 104.2(4)/103.5(4), C2−B2−C12 = 105.4(4)/104.3(4); B1−C21−C22−B2 = −1.4(6)/−1.9(6).

Table S6. Selected crystallographic data for **5**, **8**, and $[Li(thf)_2]_2$[**7**].

compound	**5**	**8**	$[Li(thf)_2]_2$[**7**]
CCDC	1888723	1888724	1888725
formula	$C_{16}H_{18}B_2$	$C_{28}H_{26}B_2$	$C_{42}H_{54}B_2Li_2O_4$
M_r	231.92	384.11	658.35
T (K)	173(2)	173(2)	173(2)
radiation, λ (Å)	Mo$K\alpha$, 0.71073	Mo$K\alpha$, 0.71073	Mo$K\alpha$, 0.71073
crystal system	triclinic	monoclinic	triclinic
space group	$P\,\bar{1}$	$P2_1/n$	$P\,\bar{1}$
a (Å)	5.1697(6)	10.3844(7)	9.1549(7)
b (Å)	7.5135(9)	8.6036(4)	9.8159(7)
c (Å)	9.1628(11)	12.5024(8)	11.6092(9)
α (°)	76.716(9)	90	69.862(6)
β (°)	74.826(9)	98.997(5)	79.949(6)
γ (°)	84.882(9)	90	81.811(6)
V (Å^3)	334.15(7)	1103.26(12)	960.60(13)
Z	1	2	1
D_{calcd} (g cm^{-3})	1.153	1.156	1.138
F (000)	124	408	354
μ (mm^{-1})	0.062	0.064	0.069
crystal size (mm)	0.28 × 0.21 × 0.05	0.28 × 0.26 × 0.25	0.19 × 0.18 × 0.09
crystal shape, color	colorless plate	yellow block	red plate
reflections collected	5472	19516	21740
independent reflections	1364	2812	21740
R_{int}	0.0193	0.0287	–
data/restraints/parameters	1364 / 0 / 82	2812 / 0 / 139	21740 / 24 / 247
R_1, wR_2 ($I > 2\,\sigma(I)$)	0.0473, 0.1360	0.0477, 0.1226	0.0604, 0.1410
R_1, wR_2 (all data)	0.0534, 0.1397	0.0562, 0.1282	0.0873, 0.1523
GOF on F^2	1.114	1.059	0.978
largest difference peak and hole (e Å^{-3})	0.265, –0.165	0.317, –0.191	0.243, –0.220

Table S7. Selected crystallographic data for $[Na_2(thf)_3][\mathbf{1}]$, $[K_2(thf)_4][\mathbf{1}]$, and $[K(thf)]_2[\mathbf{7}]$.

compound	$[Na_2(thf)_3][\mathbf{1}]$	$[K_2(thf)_4][\mathbf{1}]$	$[K(thf)]_2[\mathbf{7}]$
CCDC	1888726	1888727	1888728
formula	$C_{24}H_{34}B_2Na_2O_3$	$C_{28}H_{42}B_2K_2O_4$	$C_{34}H_{38}B_2K_2O_2$
M_r	438.11	542.43	578.46
T (K)	173(2)	173(2)	173(2)
radiation, λ (Å)	Mo$K\alpha$, 0.71073	Mo$K\alpha$, 0.71073	Mo$K\alpha$, 0.71073
crystal system	monoclinic	monoclinic	monoclinic
space group	$C2/c$	$P2_1/n$	$P2_1/c$
a (Å)	16.846(2)	14.6657(7)	6.3580(9)
b (Å)	10.2105(8)	10.0154(4)	12.581(2)
c (Å)	15.0325(17)	21.2355(10)	19.691(3)
α (°)	90	90	90
β (°)	106.425(9)	102.926(4)	90.278(12)
γ (°)	90	90	90
V (Å^3)	2480.2(5)	3040.1(2)	1575.1(4)
Z	4	4	2
D_{calcd} (g cm^{-3})	1.173	1.185	1.220
F (000)	936	1160	612
μ (mm^{-1})	0.103	0.341	0.329
crystal size (mm)	0.27 × 0.11 × 0.11	0.28 × 0.12 × 0.12	0.22 × 0.08 × 0.03
crystal shape, color	dark red needle	dark red needle	dark red needle
reflections collected	10625	41456	8870
independent reflections	2316	5727	2778
R_{int}	0.0479	0.0350	0.1002
data/restraints/parameters	2316 / 0 / 155	5727 / 42 / 352	2778 / 0 / 182
R_1, wR_2 ($I > 2\ \sigma(I)$)	0.0476, 0.1156	0.0597, 0.1597	0.0735, 0.1518
R_1, wR_2 (all data)	0.0689, 0.1238	0.0730, 0.1696	0.1380, 0.1750
GOF on F^2	1.043	1.021	0.971
largest difference peak and hole (e Å^{-3})	0.216, –0.185	0.745, –0.430	0.380, –0.358

Table S8. Selected crystallographic data for [Na][Na(thf)$_2$(18-c-6)][Na(thf)$_2$]$_2$(*n*-hexane)[**7**-H$_2$]$_2$, [K(18-c-6)]$_2$[**1**-H$_2$], and [K][K(thf)]$_3$[**4**-H$_2$]$_2$.

compound	[Na][Na(thf)$_2$(18-c-6)] [Na(thf)$_2$]$_2$(*n*-hexane) [**7**-H$_2$]$_2$	[K(18-c-6)]$_2$[**1**-H$_2$]	[K][K(thf)]$_3$[**4**-H$_2$]$_2$
CCDC	1888729	1888730	1888731
formula	$C_{94}H_{134}B_4Na_4O_{12}$	$C_{36}H_{60}B_2K_2O_{12}$	$C_{40}H_{56}B_4K_4O_3$
M_r	1591.20	784.66	784.48
T (K)	173(2)	173(2)	173(2)
radiation, λ (Å)	Mo$K\alpha$, 0.71073	Mo$K\alpha$, 0.71073	Mo$K\alpha$, 0.71073
crystal system	monoclinic	orthorhombic	monoclinic
space group	$P2_1/c$	*Pbam*	$P2_1/n$
a (Å)	16.0130(8)	22.959(2)	11.1111(3)
b (Å)	17.3067(6)	9.4933(8)	24.7167(5)
c (Å)	34.7821(19)	18.771(2)	16.6417(4)
α (°)	90	90	90
β (°)	101.572(4)	90	107.866(2)
γ (°)	90	90	90
V (Å^3)	9443.3(8)	4091.3(7)	4349.91(19)
Z	4	4	4
D_{calcd} (g cm^{-3})	1.119	1.274	1.198
F (000)	3432	1680	1664
μ (mm^{-1})	0.087	0.289	0.443
crystal size (mm)	0.21 × 0.11 × 0.02	0.17 × 0.17 × 0.08	0.29 × 0.28 × 0.23
crystal shape, color	colorless plate	colorless plate	colorless block
reflections collected	107613	13623	69817
independent reflections	17461	3949	8450
R_{int}	0.0924	0.0558	0.0284
data/restraints/parameters	17461 / 103 / 1105	3949 / 0 / 259	8450 / 90 / 509
R_1, wR_2 ($I > 2\ \sigma(I)$)	0.0682, 0.1531	0.0422, 0.0586	0.0441, 0.1148
R_1, wR_2 (all data)	0.1432, 0.1844	0.1055, 0.0699	0.0517, 0.1196
GOF on F^2	0.970	0.872	1.059
largest difference peak and hole (e Å^{-3})	0.287, –0.327	0.197, –0.211	0.668, –0.354

Table S9. Selected crystallographic data for and $[K]_2[K(18\text{-}c\text{-}6)][K(18\text{-}c\text{-}6)(thf)_2][\mathbf{7}\text{-}H_2]_2$, for $[Li(12\text{-}c\text{-}4)_2](THF)[\mathbf{10}]$ and [Li(12-c-4)(thf)][Li(12-c-4)][**11**].

compound	$[K]_2[K(18\text{-}c\text{-}6)][K(18\text{-}c\text{-}6)(thf)_2][\mathbf{7}\text{-}H_2]_2$	$[Li(12\text{-}c\text{-}4)_2]$ (THF)[**10**]	[Li(12-c-4)(thf)][Li(12-c-4)][**11**]
CCDC	1888732	1888733	1888734
formula	$C_{84}H_{112}B_4K_4O_{14}$	$C_{45}H_{70}B_2LiNO_9$	$C_{36}H_{58}B_2Li_2O_9$
M_r	1545.37	797.58	670.32
T (K)	173(2)	173(2)	173(2)
radiation, λ (Å)	Mo$K\alpha$, 0.71073	Mo$K\alpha$, 0.71073	Mo$K\alpha$, 0.71073
crystal system	triclinic	monoclinic	monoclinic
space group	$P\bar{1}$	$P2_1/c$	$P2_1$
a (Å)	11.9532(7)	13.8997(6)	14.3173(13)
b (Å)	12.6550(7)	13.1337(5)	12.8231(8)
c (Å)	15.2730(9)	25.5265(12)	20.9241(18)
α (°)	112.470(4)	90	90
β (°)	90.868(5)	104.454(4)	102.873(7)
γ (°)	100.044(5)	90	90
V (Å^3)	2093.7(2)	4512.5(3)	3744.9(5)
Z	1	4	4
D_{calcd} (g cm^{-3})	1.226	1.174	1.189
F (000)	824	1728	1448
μ (mm^{-1})	0.273	0.079	0.081
crystal size (mm)	0.27 × 0.27 × 0.13	0.29 × 0.27 × 0.11	0.14 × 0.11 × 0.04
crystal shape, color	colorless plate	colorless plate	colorless plate
reflections collected	26936	52297	29657
independent reflections	7828	8793	12967
R_{int}	0.0279	0.0622	0.0692
data/restraints/parameters	7828 / 0 / 491	8793 / 24 / 546	12967 / 236 / 955
R_1, wR_2 ($I > 2\ \sigma(I)$)	0.0367, 0.0902	0.0637, 0.1580	0.0678, 0.1387
R_1, wR_2 (all data)	0.0506, 0.0950	0.0955, 0.1734	0.1072, 0.1541
GOF on F^2	1.048	1.042	0.950
largest difference peak and hole (e Å^{-3})	0.315, –0.302	0.477, –0.183	0.453, –0.210

9. References

(1) Fulmer, G. R.; Miller, A. J. M.; Sherden, N. H.; Gottlieb, H. E.; Nudelman, A.; Stoltz, B. M.; Bercaw, J. E.; Goldberg, K. I., NMR Chemical Shifts of Trace Impurities: Common Laboratory Solvents, Organics, and Gases in Deuterated Solvents Relevant to the Organometallic Chemist. *Organometallics* **2010**, *29*, 2176.

(2) Januszewski, E.; Lorbach, A.; Grewal, R.; Bolte, M.; Bats, J. W.; Lerner, H.-W.; Wagner, M., Unsymmetrically Substituted 9,10-Dihydro-9,10-Diboraanthracenes as Versatile Building Blocks for Boron-Doped π-Conjugated Systems. *Chem. Eur. J.* **2011**, *17*, 12696.

(3) Lorbach, A.; Bolte, M.; Li, H.; Lerner, H.-W.; Holthausen, M. C.; Jäkle, F.; Wagner, M., 9,10-Dihydro-9,10-diboraanthracene: Supramolecular Structure and Use as a Building Block for Luminescent Conjugated Polymers. *Angew. Chem. Int. Ed.* **2009**, *48*, 4584.

(4) von Grotthuss, E.; Diefenbach, M.; Bolte, M.; Lerner, H.-W.; Holthausen, M. C.; Wagner, M., Reversible Dihydrogen Activation by Reduced Aryl Boranes as Main-Group Ambiphiles. *Angew. Chem. Int. Ed.* **2016**, *55*, 14067.

(5) Hoffend, C.; Diefenbach, M.; Januszewski, E.; Bolte, M.; Lerner, H.-W.; Holthausen, M. C.; Wagner, M., Effects of Boron Doping on the Structural and Optoelectronic Properties of 9,10-Diarylanthracenes. *Dalton Trans.* **2013**, *42*, 13826.

(6) Kessler, S. N.; Neuburger, M.; Wegner, H. A., Bidentate Lewis Acids for the Activation of 1,2-Diazines - a New Mode of Catalysis. *Eur. J. Org. Chem.* **2011**, 3238.

(7) von Grotthuss, E.; Prey, S. E.; Bolte, M.; Lerner, H.-W.; Wagner, M., Selective CO_2 Splitting by Doubly Reduced Aryl Boranes to Give CO and $[CO_3]^{2-}$. *Angew. Chem. Int. Ed.* **2018**, *57*, 16491.

(8) Lorbach, A.; Bolte, M.; Lerner, H.-W.; Wagner, M., Dilithio 9,10-Diborataanthracene: Molecular Structure and 1,4-Addition Reactions. *Organometallics* **2010**, *29*, 5762.

(9) Müller; P.; Huck, S. K., H.; Pritzkow, H.; Siebert, W., Synthesis and Structures of 9,10-Dihydro-9,10-diboraanthracene Derivatives. *Z. Naturforsch.* **1995**, *50b*, 1476.

(10) Brunner, E., Solubility of Hydrogen in 10 Organic Solvents at 298.15, 323.15, and 373.15 K. *J. Chem. Eng.Data* **1985**, *30*, 269.

(11) Eisch, J. J.; Kotowicz, B. W., Novel Organoborane Lewis Acids via Selective Boron-Tin Exchange Processes Steric Constraints to Electrophilic Initiation by the Boron Halide. *Eur. J. Inorg. Chem.* **1998**, 761.

(12) Spies, P.; Schwendemann, S.; Lange, S.; Kehr, G.; Fröhlich, R.; Erker, G., Metal-Free Catalytic Hydrogenation of Enamines, Imines, and Conjugated Phosphinoalkenylboranes. *Angew. Chem. Int. Ed.* **2008**, *47*, 7543.

(13) *NMR Basic Principles and Progress - Oxygen-17 and Silicon-29*; Diehl, P.; Fluck, E.; Kosfeld, R., Eds., 17th ed.; Springer-Verlag: Berlin Heidelberg, New York, **1981**.

(14) Thorshaug, K.; Swang, O.; Dahl, I. M.; Olafsen, A., An Experimental and Theoretical Study of Spin-Spin Coupling in Chlorosilanes. *J. Phys. Chem. A* **2006**, *110*, 9801.

(15) *Spectral Database for Organic Compounds (SDBS)*; ^{1}H spectrum; SDBS No.: 9419; RN 7782-65-2; https://sdbs.db.aist.go.jp/sdbs/ (accessed January 14, 2019).

(16) Ebsworth, E. A. V.; Sheldrick, G. M., N.M.R. Spectra of Phosphine, Arsine and Stibine. *Trans. Faraday Soc.* **1967**, *63*, 1071.

(17) *NMR-Spektroskopie von Nichtmetallen - 31P-NMR-Spektroskopie*; Berger, S.; Braun, S.; Kalinowski, H.-O., Eds., 3th ed.; Georg Thieme Verlag: Stuttgart New York, **1993**.

(18) Jana, A.; Tavcar, G.; Roesky, H. W.; John, M., Germanium(II) Hydride Mediated Reduction of Carbon Dioxide to Formic Acid and Methanol with Ammonia Borane as the Hydrogen Source. *Dalton Trans.* **2010**, *39*, 9487.

(19) *Spectral Database for Organic Compounds (SDBS)*; IR spectrum (KBr disc); SDBS No.: 2964; RN 141-53-7; https://sdbs.db.aist.go.jp/sdbs/ (accessed January 14, 2019).

(20) Frisch, M. J.; Trucks, G. W.; Schlegel, H. B.; Scuseria, G. E.; Robb, M. A.; Cheeseman, J. R.; Scalmani, G.; Barone, V.; Mennucci, B.; Petersson, G. A.; Nakatsuji, H.; Caricato, M.; Li, X.; Hratchian, H. P.; Izmaylov, A. F.; Bloino, J.; Zheng, G.; Sonnenberg, J. L.; Hada, M.; Ehara, M.; Toyota, K.; Fukuda, R.; Hasegawa, J.; Ishida, M.; Nakajima, T.; Honda, Y.; Kitao, O.;

Nakai, H.; Vreven, T.; Montgomery, J. A.; Peralta, Jr., J. E.; Ogliaro, F.; Bearpark, M.; Heyd, J. J.; Brothers, E.; Kudin, K. N.; Staroverov, V. N.; Kobayashi, R.; Normand, J.; Raghavachari, K.; Rendell, A.; Burant, J. C.; Iyengar, S. S.; Tomasi, J.; Cossi, M.; Rega, N.; Millam, J. M.; Klene, M.; Knox, J. E.; Cross, J. B.; Bakken, V.; Adamo, C.; Jaramillo, J.; Gomperts, R.; Stratmann, R. E.; Yazyev, O.; Austin, A. J.; Cammi, R.; Pomelli, C.; Ochterski, J. W.; Martin, R. L.; Morokuma, K.; Zakrzewski, V. G.; Voth, G. A.; Salvador, P.; Dannenberg, J. J.; Dapprich, S.; Daniels, A. D.; Farkas, Ö.; Foresman, J. B.; Ortiz, J. V.; Cioslowski J.; Fox, D. J. *Gaussian 09*, Revision D.01, Gaussian, Inc., Wallingford, CT, 2013; http://www.gaussian.com.

(21) Marenich, A. V.; Cramer, C. J.; Truhlar, D. G., Universal Solvation Model Based on Solute Electron Density and on a Continuum Model of the Solvent Defined by the Bulk Dielectric Constant and Atomic Surface Tensions. *J. Phys. Chem. B* **2009**, ***113***, 6378.

(22) Brend'amour, S.; Gilmer, J.; Bolte, M.; Lerner, H.-W.; Wagner, M., C-Halogenated 9,10-Diboraanthracenes: How the Halogen Load and Distribution Influences Key Optoelectronic Properties. *Chem. Eur. J.* **2018**, *24*, 16910.

(23) *X-AREA: Diffractometer Control Program System;* Stoe & Cie: Darmstadt, Germany, **2002**.

(24) Sheldrick, G. M., A Short History of *SHELX*. *Acta Crystallogr. Sect. A* **2008**, *64*, 112.